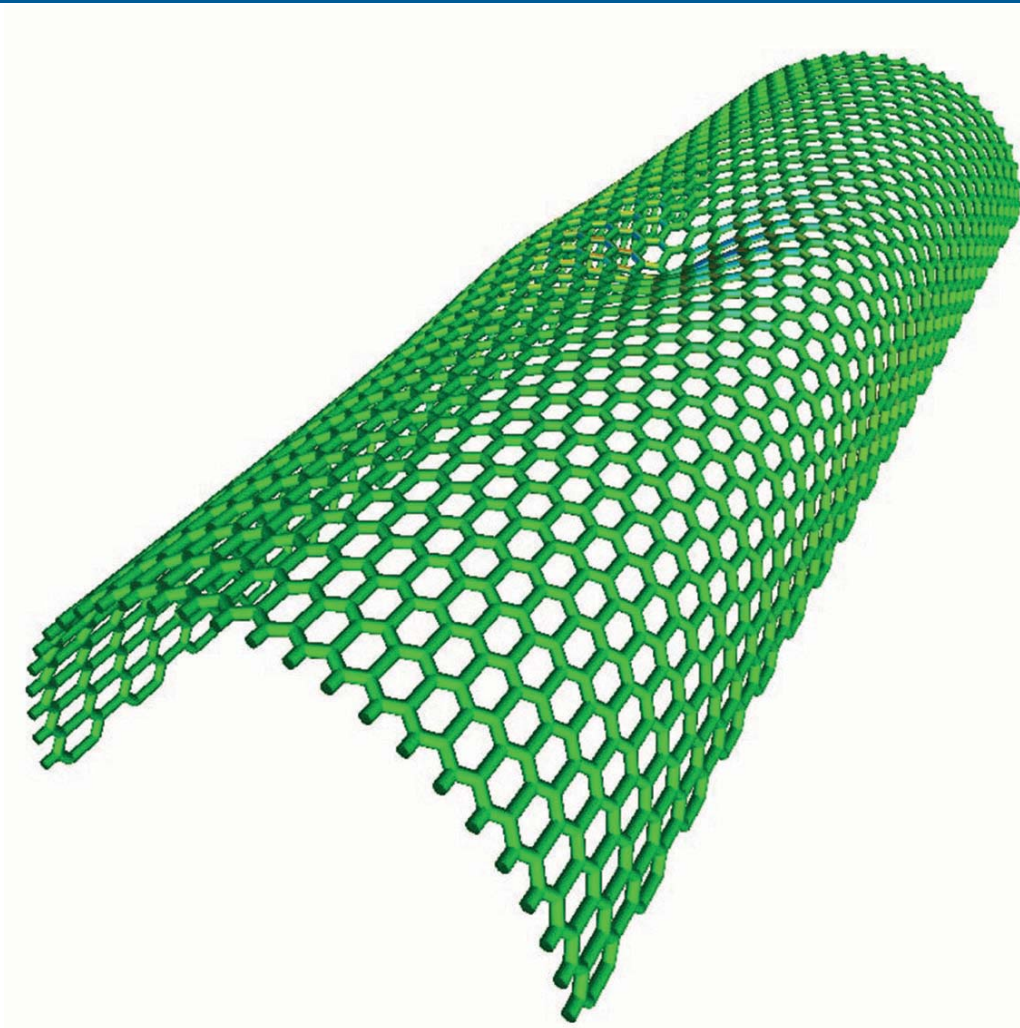


Michael Hauck

---

# Asymptotic Analysis and Design Optimization for Periodic Perforated Shells



Fraunhofer-Institut für  
Techno- und Wirtschaftsmathematik ITWM

# Asymptotic Analysis and Design Optimization for Periodic Perforated Shells

Michael Hauck

FRAUNHOFER VERLAG

**Kontakt:**

Fraunhofer-Institut für Techno- und Wirtschaftsmathematik ITWM  
Fraunhofer-Platz 1  
67663 Kaiserslautern  
Telefon +49 631/31600-0  
Fax +49 631/31600-1099  
E-Mail [info@itwm.fraunhofer.de](mailto:info@itwm.fraunhofer.de)  
URL [www.itwm.fraunhofer.de](http://www.itwm.fraunhofer.de)

**Bibliografische Information der Deutschen Nationalbibliothek**

Die Deutsche Nationalbibliothek verzeichnet diese Publikation in der Deutschen Nationalbibliografie; detaillierte bibliografische Daten sind im Internet über <http://dnb.d-nb.de> abrufbar.  
ISBN (Print): 978-3-8396-1569-0

**D 386**

Zugl.: Kaiserslautern, TU, Diss., 2019

Titelbild: © Michael Hauck

Druck: Mediendienstleistungen des  
Fraunhofer-Informationszentrum Raum und Bau IRB, Stuttgart

Für den Druck des Buches wurde chlor- und säurefreies Papier verwendet.

© by **FRAUNHOFER VERLAG**, 2020

Fraunhofer-Informationszentrum Raum und Bau IRB  
Postfach 80 04 69, 70504 Stuttgart  
Nobelstraße 12, 70569 Stuttgart  
Telefon 0711 970-2500  
Telefax 0711 970-2508  
E-Mail [verlag@fraunhofer.de](mailto:verlag@fraunhofer.de)  
URL <http://verlag.fraunhofer.de>

Alle Rechte vorbehalten

Dieses Werk ist einschließlich aller seiner Teile urheberrechtlich geschützt. Jede Verwertung, die über die engen Grenzen des Urheberrechtsgesetzes hinausgeht, ist ohne schriftliche Zustimmung des Verlages unzulässig und strafbar. Dies gilt insbesondere für Vervielfältigungen, Übersetzungen, Mikroverfilmungen sowie die Speicherung in elektronischen Systemen.

Die Wiedergabe von Warenbezeichnungen und Handelsnamen in diesem Buch berechtigt nicht zu der Annahme, dass solche Bezeichnungen im Sinne der Warenzeichen- und Markenschutz-Gesetzgebung als frei zu betrachten wären und deshalb von jedermann benutzt werden dürften. Soweit in diesem Werk direkt oder indirekt auf Gesetze, Vorschriften oder Richtlinien (z.B. DIN, VDI) Bezug genommen oder aus ihnen zitiert worden ist, kann der Verlag keine Gewähr für Richtigkeit, Vollständigkeit oder Aktualität übernehmen.

---

# Asymptotic Analysis and Design Optimization for Periodic Perforated Shells

---

Michael Hauck

*Vom Fachbereich Mathematik der Technischen Universität Kaiserslautern zur  
Verleihung des akademischen Grades Doktor der Naturwissenschaften (Doctor rerum  
naturalium, Dr. rer. nat.) genehmigte Dissertation*

*Gutachter*

Prof. Dr. Axel KLAR  
Technische Universität Kaiserslautern

Prof. Dr. Grigory PANASENKO  
Université de Saint-Etienne

*Datum der Disputation*  
03. Dezember 2019



---

# Danksagung

Eine Doktorarbeit zu verfassen ist eine der größten akademischen Herausforderungen, der man sich stellen kann. Auf diesem Wege habe ich von vielen Leuten Unterstützung erhalten, bei denen ich mich auch gebührend bedanken möchte.

Ich danke Herrn Prof. Dr. Axel Klar für die Betreuung meiner Arbeit und die regelmäßigen Rücksprachen zum Stand der Dissertation.

Mein besonderer Dank gilt Frau Dr. Julia Orlik, die mich während meiner über sechsjährigen Zeit am Fraunhofer-Institut für Techno- und Wirtschaftsmathematik ITWM betreut und unterstützt hat. Mit ihr zusammen wurden viele Projekte bearbeitet und besonders im Bereich der Homogenisierung neue Erkenntnisse und Resultate erlangt.

Des Weiteren danke ich Herrn Dr. Georges Griso für seine Diskussionen und Ratschläge bei der Anwendung des Unfolding Operators für die Homogenisierung. Die Zusammenarbeit mit ihm war für mich sehr lehrreich. Bei Herrn Dr. Viktor Levandovskyy bedanke ich mich für die Hilfe bei der Berechnung mit Singular. Ohne einen Algebraiker an meiner Seite wäre die symbolische Homogenisierung nicht so schön geworden.

Ich danke der Abteilung Strömungs- und Materialsimulation (SMS) am Fraunhofer ITWM für die Möglichkeit, meine Doktorarbeit in diesem Bereich anzufertigen. Allen Mitarbeitern und meinen Mitdoktoranden danke ich für die schöne Zeit. Für die gemeinsame Darstellung der ANSYS Simulationen bedanke ich mich bei Frau Dr. Olga Lykhashova.

Ich danke meinem Bürokollegen Stephan Wackerle für die Diskussionen, gemeinsame Unterstützung und das Korrekturlesen. Außerdem bedanke ich mich bei meinen weiteren Korrekturlesern und Freunden Simon Gottschalk, Thomas Jung, Matthias Andres, Marco Recktenwald und Fabian Fürchow.

Eine solche Arbeit wäre ohne die moralische Unterstützung meiner Familie nicht möglich gewesen. Dabei danke ich insbesondere meiner Freundin für ihren Rückhalt und Verpflegung an den Wochenenden, die für die Arbeit draufgingen. Meinen Eltern, meiner Schwester und meinen Großmüttern danke ich für ihre Unterstützung seit meiner Einschulung. Ihr wart immer an meiner Seite.



## Abstract

The core of this thesis lies in the task of structural optimization of periodic perforated cylindrical shells under a given point load. The analysis of the problem shows that it can be divided into three subcategories: Asymptotic analysis, macroscopic model and optimization.

First, we want to replace the heterogeneous shell with an equivalent and homogeneous 2D problem. This homogenization step together with dimensional reduction has already been considered for plates in the literature. However, there are no known papers that apply this complete analysis to a linear elastic shell. Most of them deal with either homogenization or dimensional reduction only. If a joint analysis takes place, then results are obtained as energy estimates. In this work we show a qualitative derivation, together with an algorithm for calculating the effective properties. We start with a decomposition of the applied displacements into a deformation of the middle surface and the corresponding rotation of the line segments, which are orthogonal to our middle surface. Using the Unfolding-Rescaling operator we can decouple the two small parameters, thickness and size of the periodicity cell. After that we utilize the beam-like structure of the perforated shell to calculate the effective properties. This algorithm is not only executed numerically, but also symbolically. The resulting solutions are therefore functions with respect to the parametrization of the periodicity cell. This symbolic approach requires special caution and has hardly been used in the case of homogenization. The solutions are to be regarded as exact.

In the next step we calculate the analytical solution of the derived limit equation. Here we use classical approaches from the PDE theory. The strategy is to separate the two variables of our 2D domain. The obtained functions depend either on the longitudinal coordinate or on the arc length. In the next step, we express the solution regarding the Fourier transformation and a Fourier series. Moreover, this function depends on the effective properties that we calculate with our symbolic algorithm. Therefore, it is possible to represent the displacements of our shell with respect to the design variables.

This allows us to approach optimization with simple methods. Since the function is given for the symbolic variables, we can perform the differentiation completely automatically with MATLAB's `diff` operator. We use the obtained gradient in a steepest descent procedure to find the minimum given certain objective functionals. This allows us to describe the optimal configuration with respect to our admissible design space.

Applied industrial problems can thus be effectively solved.



## Zusammenfassung

Der Kern dieser Arbeit liegt in der Aufgabe einer Strukturoptimierung von periodisch perforierten zylindrischen Schalen unter einer ebenen Punktlast. Bei der Analyse des Problems stellt man fest, dass es sich in drei Unterkategorien aufteilen lässt: Asymptotische Analyse, Makroskopisches Modell und Optimierung.

Als Erstes wollen wir die heterogene Schale durch ein äquivalentes und homogenes 2D Problem ersetzen. Dieser Homogenisierungsschritt zusammen mit der Dimensionsreduktion wurde in der Literatur schon vielfach für Platten behandelt. Jedoch gibt es keine uns bekannten Schriften, die diese vollständige Analyse bei einer linear elastischen Schale anwenden. Die meisten beschäftigen sich entweder nur mit der Homogenisierung oder Dimensionsreduktion. Aber falls doch eine gemeinsame Betrachtung stattfindet, dann erhält man die Ergebnisse nur in Bezug auf Energieabschätzungen. Wir zeigen hier eine qualitative Herleitung, zusammen mit einem Algorithmus zur Berechnung der effektiven Eigenschaften. Dabei starten wir mit einer Zerlegung der angewandten Verschiebungen in eine Verformung der Mittelfläche und der dazugehörigen Rotation der Liniensegmente, die orthogonal zu unserer Mittelfläche stehen. Mittels des Unfolding-Rescaling (Entfaltung und Umskalierung) Operators können wir die beiden kleinen Parameter, Dicke der Schale und Größe der Periodizitätszelle, entkoppelt betrachten. Danach nutzen wir die balkenähnliche Struktur der perforierten Schale aus, um die effektiven Eigenschaften computergestützt zu berechnen. Dieser Algorithmus wird nicht nur numerisch sondern auch symbolisch ausgeführt. Die dabei erhaltenen Lösungen sind deshalb Funktionen bezüglich der Parametrisierung der Periodizitätszelle. Diese symbolische Betrachtungsweise erfordert besondere Vorsicht und wurde im Fall der Homogenisierung bisher kaum eingesetzt. Die erhaltenen Ausdrücke sind dabei als exakt zu betrachten.

Anschließend berechnen wir die analytische Lösung der Limitgleichung. Wir nutzen hier klassische Herangehensweisen aus der Theorie der partiellen Differenzialgleichungen. Die Strategie besteht darin, die beiden Variablen des 2D Gebietes zu separieren. Die dadurch erhaltenen Funktionen hängen entweder von der längsverlaufenden Koordinate oder der Bogenlänge ab. Im nächsten Schritt stellen wir die Funktion bezüglich der Fouriertransformation und einer Fourierreihe dar. Die hergeleitete Lösung ist wiederum abhängig von den effektiven Eigenschaften, die wir mit unserem symbolischen Algorithmus berechnet haben. Deshalb ist es möglich, die Verschiebungen unserer Schale bezüglich der Designvariablen darzustellen.

Durch die vorher beschriebene Betrachtungsweise können wir die Optimierung mit einfachen Methoden angehen. Weil die Funktion bezüglich der symbolischen Variablen gegeben ist, können wir das Differenzieren vollkommen automatisch mit MATLABs `diff` Operator durchführen. Den erhaltenen Gradienten nutzen wir in einem Verfahren des steilsten Abstiegs, um das Minimum hinsichtlich gegebener Zielfunktionen zu finden. Dadurch gelingt es uns die optimale Konfiguration bezüglich unseres zulässigen Designraums zu beschreiben.

Angewandte Industrieprobleme können damit effektiv gelöst werden.

# Notations

## Abbreviations

<b>PDE</b>	partial differential equation
<b>FE</b>	finite element
<b>a.e.</b>	almost everywhere
<b>w.r.t.</b>	with respect to
<b>w.l.o.g</b>	without loss of generality
<b>s.t.</b>	subject to
<b>1D</b>	one dimensional
<b>2D</b>	two dimensional
<b>3D</b>	three dimensional
<b>4D</b>	four dimensional
<b>GSM</b>	global stiffness matrix
<b>BC</b>	boundary conditions
<b>I/O</b>	input/output

## Symbols

Symbol	Unit	Explanation
$\varepsilon$		small parameter; size of periodicity cell
$\delta$		small parameter; thickness of the shell
$\omega$		the reference domain
$s_1$	[m]	variable in the reference domain; shell's arc length
$s_2$	[m]	variable in the reference domain; shell's longitudinal direction
$a$	[m]	the shell's radius
$l$	[m]	the shell's length
$h$	[m]	fixed shell's thickness
$E$	$[\frac{\text{N}}{\text{m}^2}]$	Young's modulus
$G$	$[\frac{\text{N}}{\text{m}^2}]$	shear modulus
$\lambda, \mu$	$[\frac{\text{N}}{\text{m}^2}]$	Lamé parameters, $\mu = G$
$\nu_{12}, \nu_{21}$	[1]	orthotropic Poisson's ratio
$a_{\alpha\beta\alpha'\beta'}$	$[\frac{\text{N}}{\text{m}}]$	homogenized in-plane coefficients, $\alpha, \beta, \alpha', \beta' \in \{1, 2\}$
$c_{\alpha\beta\alpha'\beta'}$	[Nm]	homogenized bending coefficients, $\alpha, \beta, \alpha', \beta' \in \{1, 2\}$
$H$		ratio of effective orthotropic Young's moduli $E_1/E_2$
$r$	[m]	radius of a beam in lattice structure
$A$	[m <sup>2</sup> ]	area of the beam's cross-section
$I_{y,z}$	[m <sup>4</sup> ]	area moments of inertia of beam elements
$q$	$[\frac{\text{N}}{\text{m}^2}]$	load
$P$	[N]	point/pinching load
$\mathbf{x}$		symbolic variable

## Operators

### Scalar product

Given a Hilbert space  $X$ , we denote its scalar product with the bracket notation

$$\langle \cdot, \cdot \rangle_X : X \times X \mapsto \mathbb{R}.$$

### Cross product

Given two vectors  $a, b \in \mathbb{R}^3$  we define the cross product  $c$  as

$$c = a \wedge b = \begin{pmatrix} a_2 b_3 - a_3 b_2 \\ a_3 b_1 - a_1 b_3 \\ a_1 b_2 - a_2 b_1 \end{pmatrix}.$$

We then have the relation  $\langle c, a \rangle_{\mathbb{R}^3} = \langle c, b \rangle_{\mathbb{R}^3} = 0$ , w.r.t to the underlying scalar product  $\langle \cdot, \cdot \rangle_{\mathbb{R}^3}$  in  $\mathbb{R}^3$ .

### Gradient $\nabla$

Given a smooth function  $u : \mathbb{R}^m \mapsto \mathbb{R}$  and cartesian coordinate system  $(e_i)_{i=1,\dots,m}$ , where  $e_i$  is the  $i$ -th unit vector we define the gradient as

$$\nabla u = \sum_{i=1}^m \frac{\partial u}{\partial x_i} e_i.$$

### Frobenius scalar product

Given two matrices  $A, B \in \mathbb{R}^{m \times m}$  we denote the Frobenius scalar product as

$$A : B = \sum_{i=1}^m \sum_{j=1}^m A_{ij} B_{ij}.$$

### Strain tensor

Given a smooth function  $u : \mathbb{R}^3 \mapsto \mathbb{R}^3$  we define the strain tensor

$$e(u) = \frac{\nabla u + \nabla u^T}{2}.$$

# Contents

<b>Abstract</b>	<b>i</b>
<b>Notations</b>	<b>iii</b>
Abbreviations . . . . .	iii
Symbols . . . . .	iv
Operators . . . . .	v
<b>1 Introduction</b>	<b>1</b>
<b>2 Homogenization of Shells</b>	<b>5</b>
2.1 Introduction to shells and displacements . . . . .	5
2.1.1 Geometrical setting . . . . .	6
2.1.2 Decomposition of shell displacements . . . . .	8
2.2 The rescaling operator $\mathfrak{T}_\varepsilon$ . . . . .	12
2.3 Asymptotic behavior of the strain tensor . . . . .	13
2.4 Unfolding of the rescaled shell . . . . .	16
2.4.1 Limit of the rescaled-unfolded strain tensor . . . . .	19
2.5 Inextensional and extensional displacements . . . . .	21
2.5.1 Inextensional displacements . . . . .	21
2.5.2 Extensional displacements . . . . .	24
2.6 The linear elasticity problem . . . . .	29
2.6.1 Assumptions on the forces . . . . .	30
2.7 Unfolded limit problems . . . . .	33
2.8 Homogenization of the shell . . . . .	38
2.8.1 The limit problems in the shell's mid surface . . . . .	39
2.9 Different boundary conditions . . . . .	40
<b>3 Analytic Solution to Pinching a Homogeneous Shell</b>	<b>43</b>
3.1 Deriving the strong formulation . . . . .	43
3.2 Analytic solution to the pinched cylinder problem . . . . .	48
3.2.1 Examples . . . . .	56
3.3 Numerical models for pinching a cylinder . . . . .	64
3.3.1 Solving Koiter equation with FEniCS . . . . .	64
3.3.2 Numerical study of different boundary conditions . . . . .	65
<b>4 Calculating Effective Properties with Symbolic Parameters</b>	<b>69</b>
4.1 Algorithm for calculation of effective properties . . . . .	69
4.1.1 Reduction to 1D beam problems and stress interpolation . . . . .	70
4.2 Solving symbolic linear equations with Singular . . . . .	74
4.2.1 Preprocessing . . . . .	75
4.2.2 Calling Singular . . . . .	76

4.3	Examples . . . . .	77
4.3.1	Open grid structure . . . . .	77
4.3.2	Varying hexagon . . . . .	80
4.3.3	Varying cross sections . . . . .	83
4.3.4	Shifted beams . . . . .	85
4.3.5	Auxetic structure . . . . .	88
4.3.6	Summary . . . . .	89
4.4	Comparison symbolical and numerical homogenization . . . . .	91
<b>5</b>	<b>Optimization</b>	<b>95</b>
5.1	Objective functionals . . . . .	95
5.2	Examples for minimization . . . . .	97
5.2.1	Optimize: Open grid structure . . . . .	98
5.2.2	Optimize: Varying hexagon . . . . .	100
5.2.3	Optimize: Varying cross sections . . . . .	100
5.2.4	Optimize: Shifted beams . . . . .	102
5.2.5	Optimize: Auxetic structure . . . . .	102
<b>6</b>	<b>Conclusion</b>	<b>107</b>
	<b>Appendices</b>	<b>109</b>
<b>A</b>	<b>Important Results</b>	<b>111</b>
<b>B</b>	<b>Homogenization of Shell</b>	<b>113</b>
B.1	Proof of Proposition 2.1.1 . . . . .	113
B.2	Two lemmas . . . . .	114
<b>C</b>	<b>Analytic expressions of effective properties</b>	<b>119</b>
C.1	Varying Hexagon . . . . .	119
C.2	Varying cross section . . . . .	119
C.3	Vertical shift of beams . . . . .	119
C.4	Auxetic material . . . . .	120
	<b>Bibliography</b>	<b>121</b>



# 1 Introduction

In this thesis we want to investigate the effects of point loads on periodic perforated cylindrical shells. Such problems arise in various different industrial applications. For example in the case of clogged filter media, where the fluid goes through a small hole, which can be approximated by point loads. Another example can be found in the area of cosmetic applications. There we can observe that deflections of cylindrical shells have an immediate consequence on the quality.

The considered shell structures have all in common, that they consist of a certain periodic pattern of size  $\varepsilon$ . Moreover, we assume that the shells thickness is given by  $\delta$ , which is much smaller compared to its width and length. We are particularly interested in changing the design of these minimal cells in order to optimize their performance.

Of course it is in general possible to derive the solutions on the full heterogeneous domain. This computation can be quite time consuming and hence we want to follow a different strategy and simplify the underlying problem. Following the framework presented in figure 1.1 we have to consider three different steps in our analysis.

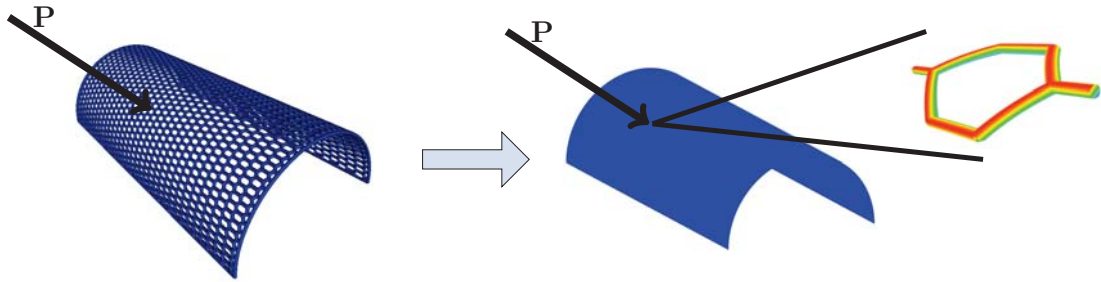


Figure 1.1: Description of Steps

- Homogenization and dimension reduction
- Macroscopic Model
- Optimization

Each step builds upon the previous one. We shortly want to discuss the mathematical backgrounds and give an outline.

## Homogenization and Dimension Reduction

We have mentioned that the investigated heterogeneous shells are assumed to be thin compared to their length and width scale, and periodically perforated. This perforation can be considered as a beam network spreading the shell's domain. In general we can identify the two small parameters  $\delta$ , for the shell's thickness, and  $\varepsilon$ , the size of the smallest periodicity cell. Starting from 3D linear elasticity we want to study the limit behavior of  $\varepsilon \rightarrow 0$ , which we call homogenization, and  $\delta \rightarrow 0$ , the dimension



reduction to obtain a 2D formulation. We want to emphasize that in this thesis the homogenization and dimension reduction will be performed simultaneously. Both problems have been investigated independently from each other in various different works. A complete study of 3D linear and non-linear elastic problems for homogeneous structures are given in [12, 13, 14]. In this series about mathematical elasticity the author starts with a general framework and applies his results first on the context of plates and then for shells. For a more mechanical perspective on this kind of problems we refer to [59], for the isotropic cases, and to [37], for anisotropic structures. It is important to note that the obtained limit models highly depend on the scaling of the linear elastic energy

$$\|e(u)\|_{L^2(Q_\delta)} \leq C\delta^\rho,$$

where  $C$  is a constant independent of  $\delta$ ,  $Q_\delta$  is the full shell domain and  $e(u)$  is the strain tensor of the deformation  $u$ . We refer here to [23], where a formal derivation of plate models from non-linear elasticity is presented. In this work we only consider the case  $\rho = \frac{3}{2}$ . Especially, for homogeneous shells we want to mention that the dimension reduction was analyzed in [11],[42] and [6]. For non-linear shells a membrane model was derived in [36].

There are various different techniques for the homogenization, as for example an asymptotic expansion ansatz presented in [4, 54] or via Gamma-convergence in [18]. Another variant is the so called two-scale convergence introduced in [47]. For non-linear behavior it was shown in [45] that homogenization and linearization commute. In general we note that the combined investigation of dimension reduction and homogenization for plates has already been studied in great detail in [50] and [16]. In our subsequent analysis we want to investigate the limit behavior via applying the rescaling and unfolding operator as applied in [15] or in the case of contact problems in [30]. This technique applied to linear elastic shells is new. We want to mention here, that the homogenization for piezoelectric perforated shells without dimension reduction was presented in [25]. Moreover, the dimension reduction and homogenization of a shell for the diffusion problem in the sense of two-scale convergence was presented in [46], where it was shown that the curvature does not enter the homogenized model. We show that the homogenization of a linear elastic shell is not affected by the curvature and is reduced to the one of a plate.

## Macroscopic Model

The obtained limit model from chapter 2 is then used to describe the effects of having a point load on the shell. There are already different shell models available, see [44], which have been solved numerically. However, our task is to get an analytic solution to this problem. For that reason we have to transform our weak formulation back to its strong form. Given the so obtained PDEs we can reduce them further to a single 8th order PDE. We further simplify this equation by asymptotic argumentations. We obtain our analytical solution by using Fourier transform and series. For some general remarks on PDEs we refer here to [21]. The Fourier series ansatz is important for capturing the boundary conditions. Hence, we also need to approximate the point load by some general loading on a small strip. Without the restrictions of the boundary conditions one can follow the results in [35]. The derived solution then depends on the homogenized coefficients and consequently on the respective design of the periodicity cells. In general we closely follow the approach presented in [33] for orthotropic shells. Later on we also provide a numerical solution to the full homogenized limit equation. We want

to investigate, which effects are missing in our approximate solution. We see that the maximal deflection is preserved, while the shell's arc length is diminished.

The next step is then to calculate the homogenized coefficients symbolically such that we can express the analytic solution w.r.t. our design variables.

## Optimization

The optimization via homogenization has already been considered for textile-like structures in [58] and for the optimization of dispersive coefficients in the wave equations in [1]. In both cases one obtains an optimization problem constrained by PDEs.

Anyhow, due to our efforts in getting an analytic solution and having symbolic expressions for our effective properties, which depend on the design parameters  $\mathbf{x} \in \mathbb{R}^m$ , we are left with a classical optimization task

$$\begin{aligned} \min_{\mathbf{x}} \quad & f(\mathbf{x}) \\ \text{s.t.} \quad & \mathbf{x} \in G \subset \mathbb{R}^m, \end{aligned}$$

where  $G$  is compact. To obtain a solution for this problem, we utilize the analytic expression given by the symbolic parameters. Using symbolic differentiation yields the gradient, which we use in a steepest descent approach.

With the presented steps we are able to fully analyze the periodic perforated shell and give qualitative answers to optimization problems in industrial applications. We want to highlight that such a combination of homogenization, analytic macroscopic solution and symbolic calculation has hardly been considered yet. The importance of this thesis lies in the drastic model reduction for a complex multi-scale problem of linear elasticity. Moreover, this yields a semi-analytic optimization problem and the practical usage of the underlying theoretical derivation. We underline that the homogenization and dimension reduction of a shell with holes and the analytic solution to the corresponding macroscopic problem are new.



## 2 Homogenization of Shells

### 2.1 Introduction to shells and displacements

In this section we consider a thin heterogeneous half-cylindrical shell with an in-plane periodic porous structure, where  $\varepsilon$  denotes the size of the periodicity cell and  $2\delta$  the shell's thickness. Both are of the same order. The parameters are small compared to its in-plane surface size. In the following we provide an analysis for homogenization and dimension reduction of the linear elastic shell. We want to point out that both tasks are performed simultaneously, where

$$\lim_{(\varepsilon, \delta) \rightarrow (0, 0)} \frac{\delta}{\varepsilon} \rightarrow \kappa \in (0, \infty).$$

This is necessary since homogenization and dimension reduction usually do not commute as it was shown in [9]. The presented approach via the rescaling-unfolding operator is closely related to the one given in [16, Chapter 11] for plates and for heterogeneous beams in [29], but new in the context of linear elastic shells.

In the analysis, we begin with a general extension technique (based on results developed in [27]) for displacements acting on a perforated shell, which is made up of a network of thin cylinders, to the full shell domain (see Proposition 2.1.1). The result is crucial for the subsequent analysis. We assume that the shell is fixed along the lateral boundary and continue with a decomposition approach for thin structures introduced in [27]. This allows us to represent any  $H^1$ -function in the thin domain through the one-to-one and onto map of the displacements and rotations of its middle surface together with a warping term, which takes into account the deformation of these small segments. With that approach we obtain Korn inequalities and estimates for each displacement field of the decomposition.

In section 2.2 - 2.4, the rescaling and unfolding operators are introduced and the strain tensor is considered on a reference domain. Furthermore, we decompose the shell's displacement fields into the two orthogonal complements of extensional and inextensional deformations, introduced in section 2.5. Such an approach has been considered for homogeneous thin shells in [6]. Section 2.6.1 presents assumptions on the forces and the detailed rescaling of the right-hand side.

At the end, the limit problem is discussed. Especially section 2.8.1 is important for applications, where the variational problem for an anisotropic homogenized shell is presented. Moreover, an analytic formula to compute its effective coefficients is shown, using the six auxiliary periodic problems on a rectangular parallelotop intersecting our structure with given perturbations. We highlight, that the anisotropic coefficient tensors coincide with those obtained in the homogenization of a plate in [16, Chapter 11]. In section 2.9 we focus on the important effects of the boundary conditions in our model. In particular, if we fix the shell's curved ends the limit problem is membrane dominated. In that case clamping the lateral boundary does not change the model. Those effects have been studied in [52] and [53], where the authors provide energy estimates for a homogeneous shell. All classical results mentioned in the following analysis are summarized in appendix A.

### 2.1.1 Geometrical setting

We start with describing the geometric properties of the perforated shell. We consider a cylindrical half-shell with a constant radius  $a$ . We assume that the shell consists of a periodic structure with a periodicity cell of size  $\varepsilon$  and thickness  $\delta = \kappa\varepsilon \in (0, \delta_0]$ , with  $\delta_0 = a/3$  and  $\kappa$  is a strictly positive fixed constant. We want to mention here that the limiting behavior of  $\frac{\delta}{\varepsilon} \in \{0, \infty\}$  are not considered in this thesis. The other two cases with  $\lim_{(\varepsilon, \delta) \rightarrow (0, 0)} \frac{\delta}{\varepsilon} \in \{0, \infty\}$  are not considered in this thesis.

Let  $Y'$  be a bounded domain in  $\mathbb{R}^2$  having the paving property with respect to an additive subgroup  $\mathbf{G} \doteq \mathbf{p}_1\mathbb{Z} \oplus \mathbf{p}_2\mathbb{Z}$  of  $\mathbb{R}^2$  of dimension 2 and let  $T$  be an open set such that  $\overline{T} \subset Y'$  (see Figure 2.1). We assume the boundary of  $T$  to be Lipschitz. For simplicity we also assume that  $T$  is connected. We define

$$Y \doteq Y' \times (-\kappa, \kappa), \quad Y'^* \doteq Y' \setminus \overline{T}, \quad Y^* \doteq Y'^* \times (-\kappa, \kappa).$$

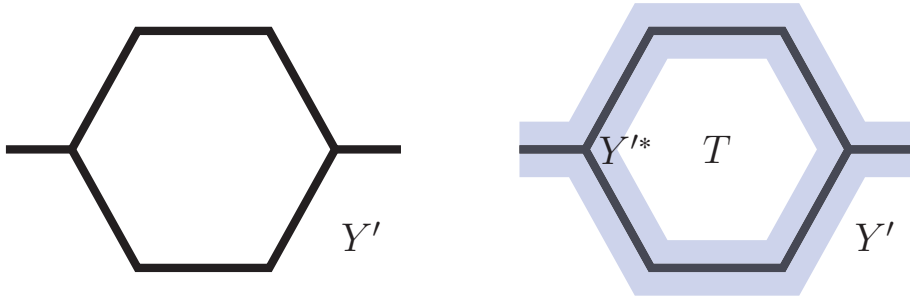


Figure 2.1: Cell  $Y'$  and the perforated domain  $Y'^*$

The asterisk denotes the material filled part of the periodicity cell. We introduce the reference domain with  $\omega \doteq (0, a\pi) \times (0, l)$ . In the periodic setting  $s' \in \mathbb{R}^2$  can be decomposed a.e. as

$$s' = \varepsilon \left[ \frac{s'}{\varepsilon} \right]_{Y'} + \varepsilon \left\{ \frac{s'}{\varepsilon} \right\}_{Y'}, \quad (2.1.1)$$

where  $[\cdot]_{Y'}$  belongs to  $\mathbf{G}$  and  $\{\cdot\}_{Y'}$  to  $Y'$ .

Set

$$\Xi_\varepsilon = \left\{ \xi \in \mathbf{G} \mid \varepsilon\xi + \varepsilon Y' \subset \omega \right\}, \quad \widehat{\omega}_\varepsilon = \text{interior} \left\{ \bigcup_{\xi \in \Xi_\varepsilon} (\varepsilon\xi + \varepsilon \overline{Y'}) \right\}, \quad \Lambda_\varepsilon = \omega \setminus \widehat{\omega}_\varepsilon,$$

where the set  $\Lambda_\varepsilon$  contains the parts of the cells intersecting the boundary  $\partial\omega$ . Let us also introduce the notations for the unions of all holes, the hole boundaries in  $\widehat{\omega}_\varepsilon$  and for the remaining structure of  $\widehat{\omega}_\varepsilon$ ,

$$T_\varepsilon \doteq \left\{ x \in \widehat{\omega}_\varepsilon \mid \left\{ \frac{x}{\varepsilon} \right\}_{Y'} \in T \right\}, \quad \partial T_\varepsilon \doteq \left\{ x \in \widehat{\omega}_\varepsilon \mid \left\{ \frac{x}{\varepsilon} \right\}_{Y'} \in \partial T \right\},$$

$$\omega_\varepsilon^* = \omega \setminus \overline{T}_\varepsilon, \quad \widehat{\omega}_\varepsilon^* = \widehat{\omega}_\varepsilon \setminus \overline{T}_\varepsilon.$$

In figure 2.2 we illustrate the underlying structure for the plane domain. There we see the perforated domain  $\omega^*$  with the blue cell being the reference periodicity cell. Given a point  $s'$ , represented by the black dot, we can decompose it into the position in the macroscopic domain  $\varepsilon \left[ \frac{s'}{\varepsilon} \right]_{Y'}$ , the green dot, and the location in the reference periodicity cell  $\varepsilon \left\{ \frac{s'}{\varepsilon} \right\}_{Y'}$ , the red dot.

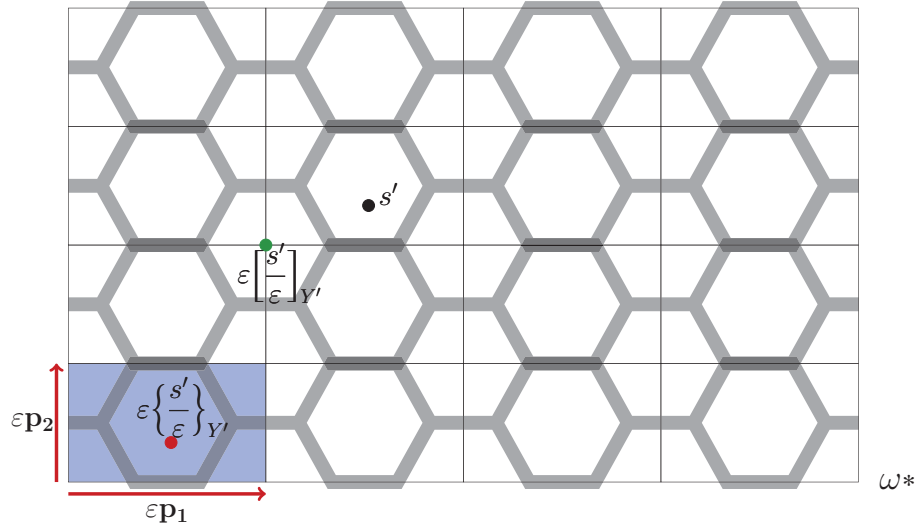


Figure 2.2: Perforated plane domain

Consider now the injective mapping  $\phi : \bar{\omega} \rightarrow \mathbb{R}^3$  defined as

$$\phi(s_1, s_2) = \begin{pmatrix} s_2 \\ a \cos\left(\frac{s_1}{a}\right) \\ a \sin\left(\frac{s_1}{a}\right) \end{pmatrix}, \quad (s_1, s_2) \in \bar{\omega}, \quad (2.1.2)$$

and denote by  $S = \phi(\bar{\omega})$  the mid-surface of the whole shell (without the holes). Furthermore, we introduce the vectors

$$\mathbf{t}_1 = \begin{pmatrix} 0 \\ -\sin\left(\frac{s_1}{a}\right) \\ \cos\left(\frac{s_1}{a}\right) \end{pmatrix}, \quad \mathbf{t}_2 = \begin{pmatrix} 1 \\ 0 \\ 0 \end{pmatrix}, \quad \mathbf{n} = \frac{\mathbf{t}_1 \wedge \mathbf{t}_2}{\|\mathbf{t}_1 \wedge \mathbf{t}_2\|_2} = \begin{pmatrix} 0 \\ \cos\left(\frac{s_1}{a}\right) \\ \sin\left(\frac{s_1}{a}\right) \end{pmatrix}. \quad (2.1.3)$$

Obviously,  $\mathbf{t}_1$  and  $\mathbf{t}_2$  are linearly independent and are tangential vectors to the surface  $S$ .

We denote

- $\Omega_\epsilon = \omega \times (-\kappa\epsilon, \kappa\epsilon)$ ,  $\Omega_\epsilon^* = \omega_\epsilon^* \times (-\kappa\epsilon, \kappa\epsilon)$ ,
- $\mathcal{Q}_\epsilon^* = \Phi(\Omega_\epsilon^*)$  the perforated shell,
- $\mathcal{Q}_\epsilon = \Phi(\Omega_\epsilon)$  the shell without the holes,

where  $\Phi : \bar{\Omega}_\epsilon \subset \mathbb{R}^3 \rightarrow \mathbb{R}^3$  is given by

$$\Phi(s) = \phi(s_1, s_2) + s_3 \mathbf{n}(s_1, s_2), \quad s = (s_1, s_2, s_3) \in \bar{\Omega}_\epsilon. \quad (2.1.4)$$

In figure 2.3 the transformation of the plane domain to the cylindrical shell is depicted. On the figure's left side we have the initial perforated domain and on the right side the cylindrical shell with holes. It is easy to check that for  $\delta = \kappa\epsilon \in (0, \delta_0]$  the map  $\Phi$  from  $\bar{\Omega}_\epsilon$  onto  $\bar{\mathcal{Q}}_\epsilon$  is a  $C^1$ -diffeomorphism. That means we have

$$c_0 \leq \|\nabla_s \Phi\|_{L^\infty(\Omega_\epsilon)^{3 \times 3}} \leq c_1 \quad \text{and} \quad c_0 \leq \|\nabla_x \Phi^{-1}\|_{L^\infty(\mathcal{Q}_\epsilon)^{3 \times 3}} \leq c_1, \quad (2.1.5)$$

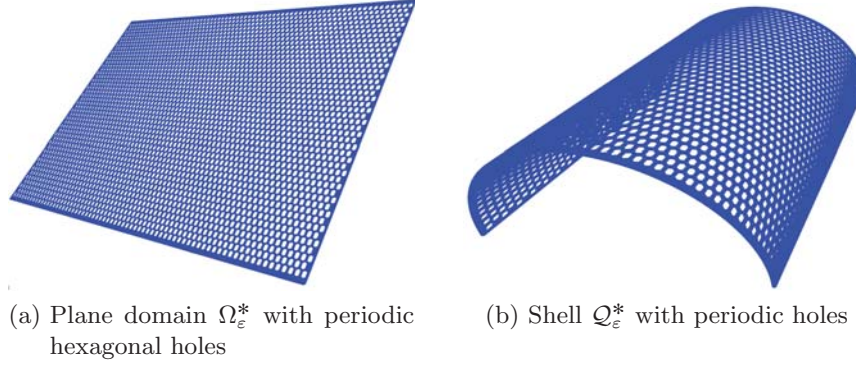


Figure 2.3: Periodic perforated plane domain transformed to a periodic shell

for some constants  $c_0, c_1 \in \mathbb{R}_+$ , which do not depend on  $\varepsilon$ .

We denote by  $x$  the running point of the shell while  $s$  is the running point in the reference domain, s.t.  $\Phi(s) = x$ .

**Proposition 2.1.1** *There exists an extension operator  $\mathcal{P}_\varepsilon$  from  $H^1(\mathcal{Q}_\varepsilon^*)^3$  into  $H^1(\mathcal{Q}_\varepsilon)^3$  satisfying for all  $u \in H^1(\mathcal{Q}_\varepsilon^*)^3$*

$$\begin{aligned} \mathcal{P}_\varepsilon(u)|_{\mathcal{Q}_\varepsilon^*} &= u, \\ \|e(\mathcal{P}_\varepsilon(u))\|_{L^2(\mathcal{Q}_\varepsilon)^{3 \times 3}} &\leq C \|e(u)\|_{L^2(\mathcal{Q}_\varepsilon^*)^{3 \times 3}}. \end{aligned} \quad (2.1.6)$$

The constant does not depend on  $\varepsilon$ .

*Proof.* The proof of Proposition 2.1.1 has been moved to the Appendix B.1.  $\square$

We omit from now on the explicit notation of the corresponding dimensions in the norms, if they can be concluded from the context.

Due to the properties of  $\Phi$ , we have for every  $u \in H^1(\mathcal{Q}_\varepsilon)$  (resp.  $H^1(\mathcal{Q}_\varepsilon^*)$ )

$$c\|u\|_{L^2(\mathcal{Q}_\varepsilon)} \leq \|u \circ \Phi\|_{L^2(\Omega_\varepsilon)} \leq C\|u\|_{L^2(\mathcal{Q}_\varepsilon)}, \quad (2.1.7)$$

$$c\|\nabla_x u\|_{L^2(\mathcal{Q}_\varepsilon)} \leq \|\nabla_s u\|_{L^2(\Omega_\varepsilon)} \leq C\|\nabla_x u\|_{L^2(\mathcal{Q}_\varepsilon)}. \quad (2.1.8)$$

Thus, we write henceforth indifferently  $u$  in place of  $u \circ \Phi \in H^1(\Omega_\varepsilon)$  (resp  $H^1(\Omega_\varepsilon^*)$ ). In the next step we discuss the boundary conditions. Therefore, we set  $\gamma_0 = \{0\} \times [0, l] \cup \{a\pi\} \times [0, l] \subset \partial\omega$ . The part  $\Gamma_{0,\varepsilon} = \Phi(\gamma_0 \times (-\kappa\varepsilon, \kappa\varepsilon))$  of the shell's lateral boundary is clamped. The complementary of  $\Gamma_{0,\varepsilon}$ , i.e., the shell's top and bottom part, is a free boundary. We will discuss in section 2.9 how a different choice of boundary conditions affects the resulting model.

**Remark 2.1.1** *From now on, any displacement  $u$  belonging to  $H^1(\mathcal{Q}_\varepsilon^*)^3$  will be extended to a displacement belonging to  $H^1(\mathcal{Q}_\varepsilon)^3$ . We will always denote by  $u$  the extended displacement, which satisfies (2.1.6).*

### 2.1.2 Decomposition of shell displacements

In the following part we introduce a decomposition for every displacement  $u$  of the shell  $\mathcal{Q}_\varepsilon$  as it was shown in [27, section 4]. This part is important to capture the effects of the thin domain. We want to decouple the mid-surface displacements from the effects caused

in the  $s_3$  direction. With that technique we can easily obtain Korn's type inequalities and study the convergence behavior for  $\varepsilon \rightarrow 0$ .

**Definition 2.1.1** *An elementary displacement  $U_e$  associated to  $u \in H^1(\Omega_\varepsilon; \mathbb{R}^3)$  is given by*

$$U_e = \mathcal{U}(s_1, s_2) + s_3 \mathcal{R}(s_1, s_2), \quad (2.1.9)$$

where  $(\alpha \in \{1, 2\})$

$$\begin{aligned} \mathcal{U} &= \frac{1}{2\kappa\varepsilon} \int_{-\kappa\varepsilon}^{\kappa\varepsilon} u(\cdot, s_3) ds_3, & \mathcal{R}_\alpha &= \frac{3}{2(\kappa\varepsilon)^3} \int_{-\kappa\varepsilon}^{\kappa\varepsilon} s_3 u(\cdot, s_3) \cdot \mathbf{t}_\alpha ds_3, \\ \mathcal{R}_3 &= 0, & \text{a.e. in } \omega. \end{aligned} \quad (2.1.10)$$

Moreover, we have that  $\mathcal{U} = (\mathcal{U}_1, \mathcal{U}_2, \mathcal{U}_3) \in H^1(\omega)^3$  and  $\mathcal{R} = (\mathcal{R}_1, \mathcal{R}_2) \in H^1(\omega)^2$ . Every displacement  $u$  is then decomposed as

$$u = U_e + \bar{u}, \quad (2.1.11)$$

where  $\bar{u} \in H^1(\Omega_\varepsilon)^3$  is a residual displacement called warping.

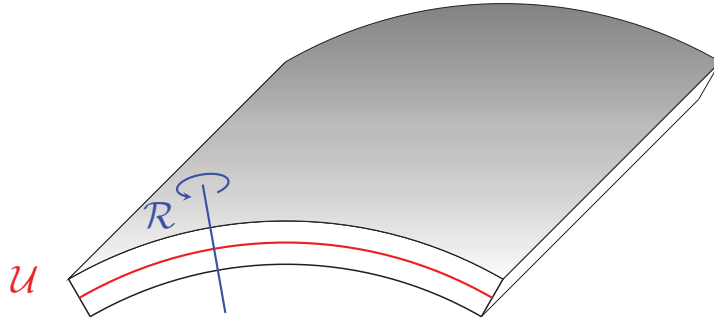


Figure 2.4: Decomposition of displacements.

Denote

$$\begin{aligned} V_\varepsilon &\doteq \{v \in H^1(\mathcal{Q}_\varepsilon)^3 \mid v = 0 \text{ on } \Gamma_{0,\varepsilon}\}, & V_\varepsilon^* &\doteq \{v \in H^1(\mathcal{Q}_\varepsilon^*)^3 \mid v = 0 \text{ on } \Gamma_{0,\varepsilon}\}, \\ H_{\Gamma_0}^1(\omega) &\doteq \{\Phi \in H^1(\omega) \mid \Phi = 0 \text{ on } \Gamma_0\}. \end{aligned}$$

Moreover, we have

$$\mathcal{U} \in H_{\Gamma_0}^1(\omega)^3, \quad \mathcal{R} \in H_{\Gamma_0}^1(\omega)^2, \quad \bar{u} \in V_\varepsilon,$$

due to the properties of  $u$  and the boundary conditions introduced in the previous section.

**Remark 2.1.2** *The warping  $\bar{u}$  fulfills the following properties*

$$\int_{-\kappa\varepsilon}^{\kappa\varepsilon} \bar{u}(\cdot, s_3) ds_3 = 0, \quad \int_{-\kappa\varepsilon}^{\kappa\varepsilon} s_3 \bar{u}(\cdot, s_3) \cdot \mathbf{t}_\alpha ds_3 = 0. \quad (2.1.12)$$

**Remark 2.1.3** *Given an elementary displacement  $U_e$  we have that  $\mathcal{U}$  describes the displacement of the red middle plane, as shown in figure 2.4. The field  $\mathcal{R}$  specifies the rotations of the segments  $\Phi(\{(s_1, s_2)\} \times [-\kappa\varepsilon, \kappa\varepsilon])$  perpendicular to the middle line, given in blue. The warping can be seen as a deformation of those perpendicular segments.*



For the functions  $\mathcal{U}$  and  $\mathcal{R}$  holds

$$\begin{aligned}\mathcal{U} &= \mathcal{U}_1 \mathbf{t}_1 + \mathcal{U}_2 \mathbf{t}_2 + \mathcal{U}_3 \mathbf{n}, \\ \mathcal{R} &= \mathcal{R}_1 \mathbf{t}_1 + \mathcal{R}_2 \mathbf{t}_2.\end{aligned}$$

In the next step we establish the strain tensor in the cylindrical coordinates. For that, the following identities are of great use:

$$\begin{aligned}\frac{\partial \mathbf{t}_1}{\partial s_1} &= -\frac{1}{a} \mathbf{n}, & \frac{\partial \mathbf{t}_2}{\partial s_1} &= 0, & \frac{\partial \mathbf{n}}{\partial s_1} &= \frac{1}{a} \mathbf{t}_1, \\ \frac{\partial \mathbf{t}_1}{\partial s_2} &= \frac{\partial \mathbf{t}_2}{\partial s_2} = \frac{\partial \mathbf{n}}{\partial s_2} &= 0.\end{aligned}$$

The derivatives of the elementary displacement  $U_e$  are calculated using

$$\begin{aligned}\frac{\partial \mathcal{U}}{\partial s_1} &= \frac{\partial \mathcal{U}_1}{\partial s_1} \mathbf{t}_1 - \frac{1}{a} \mathcal{U}_1 \mathbf{n} + \frac{\partial \mathcal{U}_2}{\partial s_1} \mathbf{t}_2 + \frac{\partial \mathcal{U}_3}{\partial s_1} \mathbf{n} + \frac{1}{a} \mathcal{U}_3 \mathbf{t}_1, \\ \frac{\partial \mathcal{U}}{\partial s_2} &= \frac{\partial \mathcal{U}_1}{\partial s_2} \mathbf{t}_1 + \frac{\partial \mathcal{U}_2}{\partial s_2} \mathbf{t}_2 + \frac{\partial \mathcal{U}_3}{\partial s_2} \mathbf{n},\end{aligned}\tag{2.1.13}$$

and

$$\begin{aligned}\frac{\partial \mathcal{R}}{\partial s_1} &= \frac{\partial \mathcal{R}_1}{\partial s_1} \mathbf{t}_1 - \frac{1}{a} \mathcal{R}_1 \mathbf{n} + \frac{\partial \mathcal{R}_2}{\partial s_1} \mathbf{t}_2, \\ \frac{\partial \mathcal{R}}{\partial s_2} &= \frac{\partial \mathcal{R}_1}{\partial s_2} \mathbf{t}_1 + \frac{\partial \mathcal{R}_2}{\partial s_2} \mathbf{t}_2.\end{aligned}\tag{2.1.14}$$

The strain tensor for a shell displacement  $u \in H^1(\mathcal{Q}_\varepsilon)$  is given by

$$e_x(u) = \frac{\nabla_x u + (\nabla_x u)^T}{2}.\tag{2.1.15}$$

A small computation yields, that  $\nabla_s u$  in the coordinates of the reference domain is given by

$$\nabla_s u = \nabla_x u \nabla \Phi.\tag{2.1.16}$$

Note that  $e_x(u)$  is in the shell configuration. Therefore, we consider the transformation matrix  $(\mathbf{t}_1 | \mathbf{t}_2 | \mathbf{n})$  and express our strain tensor in the reference domain by

$$(\mathbf{t}_1 | \mathbf{t}_2 | \mathbf{n})^T e_x(u) (\mathbf{t}_1 | \mathbf{t}_2 | \mathbf{n}).\tag{2.1.17}$$

**Definition 2.1.2** We define by  $e(u)$  the strain tensor in the coordinates of the reference domain by

$$e(u) = (\mathbf{t}_1 | \mathbf{t}_2 | \mathbf{n})^T \frac{\nabla_s u (\nabla \Phi)^{-1} + (\nabla_s u (\nabla \Phi)^{-1})^T}{2} (\mathbf{t}_1 | \mathbf{t}_2 | \mathbf{n}).\tag{2.1.18}$$

Hence, we obtain for the gradients

$$\begin{aligned}(\mathbf{t}_1 | \mathbf{t}_2 | \mathbf{n})^T \nabla_s u (\nabla \Phi)^{-1} (\mathbf{t}_1 | \mathbf{t}_2 | \mathbf{n}) &= (\mathbf{t}_1 | \mathbf{t}_2 | \mathbf{n})^T \nabla_s u \begin{pmatrix} \frac{a}{a+s_3} & 0 & 0 \\ 0 & 1 & 0 \\ 0 & 0 & 1 \end{pmatrix} \\ &= \begin{pmatrix} \frac{a}{a+s_3} \frac{\partial u}{\partial s_1} \mathbf{t}_1 & \frac{\partial u}{\partial s_2} \mathbf{t}_1 & \frac{\partial u}{\partial s_3} \mathbf{t}_1 \\ \frac{a}{a+s_3} \frac{\partial u}{\partial s_1} \mathbf{t}_2 & \frac{\partial u}{\partial s_2} \mathbf{t}_2 & \frac{\partial u}{\partial s_3} \mathbf{t}_2 \\ \frac{a}{a+s_3} \frac{\partial u}{\partial s_1} \mathbf{n} & \frac{\partial u}{\partial s_2} \mathbf{n} & \frac{\partial u}{\partial s_3} \mathbf{n} \end{pmatrix},\end{aligned}\tag{2.1.19}$$

where

$$\begin{aligned}\frac{\partial u}{\partial s_1} &= \left( \frac{\partial \mathcal{U}_1}{\partial s_1} + s_3 \frac{\partial \mathcal{R}_1}{\partial s_1} + \frac{\partial \bar{u}_1}{\partial s_1} + \frac{1}{a}(\mathcal{U}_3 + \bar{u}_3) \right) \mathbf{t}_1 + \left( \frac{\partial \mathcal{U}_2}{\partial s_1} + s_3 \frac{\partial \mathcal{R}_2}{\partial s_1} + \frac{\partial \bar{u}_2}{\partial s_1} \right) \mathbf{t}_2 \\ &\quad + \left( \frac{\partial \mathcal{U}_3}{\partial s_1} + \frac{\partial \bar{u}_3}{\partial s_1} - \frac{1}{a}(\mathcal{U}_1 + s_3 \mathcal{R}_1 + \bar{u}_1) \right) \mathbf{n}, \\ \frac{\partial u}{\partial s_2} &= \left( \frac{\partial \mathcal{U}_1}{\partial s_2} + s_3 \frac{\partial \mathcal{R}_1}{\partial s_2} + \frac{\partial \bar{u}_1}{\partial s_2} \right) \mathbf{t}_1 + \left( \frac{\partial \mathcal{U}_2}{\partial s_2} + s_3 \frac{\partial \mathcal{R}_2}{\partial s_2} + \frac{\partial \bar{u}_2}{\partial s_2} \right) \mathbf{t}_2 + \left( \frac{\partial \mathcal{U}_3}{\partial s_2} + \frac{\partial \bar{u}_3}{\partial s_2} \right) \mathbf{n}, \\ \frac{\partial u}{\partial s_3} &= \left( \mathcal{R}_1 + \frac{\partial \bar{u}_1}{\partial s_3} \right) \mathbf{t}_1 + \left( \mathcal{R}_2 + \frac{\partial \bar{u}_2}{\partial s_3} \right) \mathbf{t}_2 + \frac{\partial \bar{u}_3}{\partial s_3} \mathbf{n}.\end{aligned}$$

Then we get for the strain tensor  $e(u)$  of a displacement  $u \in V_\varepsilon$  the following components:

$$\begin{aligned}e_{11}(u) &= \frac{a}{a + s_3} \frac{\partial u}{\partial s_1} \mathbf{t}_1 = \frac{a}{a + s_3} \left[ \left( \frac{\partial \mathcal{U}_1}{\partial s_1} + \frac{1}{a} \mathcal{U}_3 \right) + s_3 \frac{\partial \mathcal{R}_1}{\partial s_1} + \frac{\partial \bar{u}_1}{\partial s_1} + \frac{1}{a} \bar{u}_3 \right], \\ e_{22}(u) &= \frac{\partial u}{\partial s_2} \mathbf{t}_2 = \frac{\partial \mathcal{U}_2}{\partial s_2} + s_3 \frac{\partial \mathcal{R}_2}{\partial s_2} + \frac{\partial \bar{u}_2}{\partial s_2}, \\ e_{12}(u) &= \frac{1}{2} \left\{ \frac{a}{a + s_3} \frac{\partial u}{\partial s_1} \mathbf{t}_2 + \frac{\partial u}{\partial s_2} \mathbf{t}_1 \right\}, \\ &= \frac{1}{2} \frac{a}{a + s_3} \left[ \left( \frac{\partial \mathcal{U}_2}{\partial s_1} + \frac{\partial \mathcal{U}_1}{\partial s_2} \right) + s_3 \left( \frac{\partial \mathcal{R}_2}{\partial s_1} + \frac{\partial \mathcal{R}_1}{\partial s_2} \right) + \frac{s_3}{a} \frac{\partial \mathcal{U}_1}{\partial s_2} + \frac{s_3^2}{a} \frac{\partial \mathcal{R}_1}{\partial s_2} \right. \\ &\quad \left. + \frac{\partial \bar{u}_2}{\partial s_1} + \left( 1 + \frac{s_3}{a} \right) \frac{\partial \bar{u}_1}{\partial s_2} \right], \\ e_{13}(u) &= \frac{1}{2} \left\{ \frac{a}{a + s_3} \frac{\partial u}{\partial s_1} \mathbf{n} + \frac{\partial u}{\partial s_3} \mathbf{t}_1 \right\} \\ &= \frac{1}{2} \frac{a}{a + s_3} \left[ \left( \frac{\partial \mathcal{U}_3}{\partial s_1} - \frac{1}{a} \mathcal{U}_1 + \mathcal{R}_1 \right) - \frac{1}{a} \bar{u}_1 + \frac{\partial \bar{u}_3}{\partial s_1} + \left( 1 + \frac{s_3}{a} \right) \frac{\partial \bar{u}_1}{\partial s_3} \right], \\ e_{23}(u) &= \frac{1}{2} \left\{ \frac{\partial u}{\partial s_2} \mathbf{n} + \frac{\partial u}{\partial s_3} \mathbf{t}_2 \right\} = \frac{1}{2} \left[ \left( \frac{\partial \mathcal{U}_3}{\partial s_2} + \mathcal{R}_2 \right) + \frac{\partial \bar{u}_3}{\partial s_2} + \frac{\partial \bar{u}_2}{\partial s_3} \right], \\ e_{33}(u) &= \frac{\partial u}{\partial s_3} \mathbf{n} = \frac{\partial \bar{u}_3}{\partial s_3}.\end{aligned}$$

**Theorem 2.1.1** *Let  $u \in H^1(\Omega_\varepsilon)^3$ ,  $(\mathcal{U}, \mathcal{R}, \bar{u})$  be its decomposition, then the following inequalities are satisfied:*

$$\|e(U_\varepsilon)\|_{L^2(\Omega_\varepsilon)} \leq C \|e(u)\|_{L^2(\Omega_\varepsilon^*)}, \quad (2.1.20)$$

$$\|\bar{u}\|_{L^2(\Omega_\varepsilon)^3} \leq C\varepsilon \|e(u)\|_{L^2(\Omega_\varepsilon^*)}, \quad (2.1.21)$$

$$\|\nabla \bar{u}\|_{L^2(\Omega_\varepsilon)} \leq C \|e(u)\|_{L^2(\Omega_\varepsilon^*)}. \quad (2.1.22)$$

*Proof.* The proof is given in [27, Theorem 4.1].  $\square$

From [27], we also obtain the full estimates of  $u$  and the components of the elementary displacement  $U_\varepsilon$ .

**Proposition 2.1.2** *For every  $u \in V_\varepsilon^*$*

$$\|u\|_{H^1(\Omega_\varepsilon)^3} \leq \frac{C}{\varepsilon} \|e(u)\|_{L^2(\Omega_\varepsilon^*)}, \quad (2.1.23)$$

$$\|\mathcal{R}\|_{H^1(\omega)^2} + \|\mathcal{U}\|_{H^1(\omega)^3} \leq \frac{C}{\varepsilon^{3/2}} \|e(u)\|_{L^2(\Omega_\varepsilon^*)}. \quad (2.1.24)$$

*The constants do not depend on  $\varepsilon$ .*

**Remark 2.1.4** Proposition 2.1.2 are the Korn inequalities for our shell domain. For a summary of the classical Korn inequalities we refer to [48, chapter 1, §2].

From the expression of the strain tensor  $e(u)$  one derives the following estimates.

**Lemma 2.1.1** One has also the following estimates  $((\alpha, \beta) \in \{1, 2\}^2)$ :

$$\begin{aligned} \left\| \frac{\partial \mathcal{U}}{\partial s_\alpha} \cdot \mathbf{t}_\beta + \frac{\partial \mathcal{U}}{\partial s_\beta} \cdot \mathbf{t}_\alpha \right\|_{L^2(\omega)} &\leq \frac{C}{\varepsilon^{1/2}} \|e(u)\|_{L^2(\Omega_\varepsilon^*)}, \\ \left\| \frac{\partial \mathcal{U}}{\partial s_\alpha} \cdot \mathbf{n} + \mathcal{R} \cdot \mathbf{t}_\alpha \right\|_{L^2(\omega)} &\leq \frac{C}{\varepsilon^{1/2}} \|e(u)\|_{L^2(\Omega_\varepsilon^*)}. \end{aligned} \quad (2.1.25)$$

The constant does not depend on  $\varepsilon$ .

*Proof.* We will only show that

$$\left\| \frac{\partial \mathcal{U}_2}{\partial s_1} + \frac{\partial \mathcal{U}_1}{\partial s_2} \right\|_{L^2(\omega)} \leq \frac{C}{\varepsilon^{1/2}} \|e(u)\|_{L^2(\Omega_\varepsilon^*)}, \quad (2.1.26)$$

since the other inequalities follow in the same way.

First observe that  $a/a+s_3$  is uniformly bounded. Then, we start with the expression of  $e_{12}(u)$  given by (2.1.20). Due to (2.1.21) and (2.1.22) we obtain

$$\int_{\Omega_\varepsilon} \left[ \left( \frac{\partial \mathcal{U}_2}{\partial s_1} + \frac{\partial \mathcal{U}_1}{\partial s_2} \right) + s_3 \left( \frac{\partial \mathcal{R}_2}{\partial s_1} + \frac{\partial \mathcal{R}_1}{\partial s_2} \right) + \frac{s_3}{a} \frac{\partial \mathcal{U}_1}{\partial s_2} + \frac{s_3^2}{a} \frac{\partial \mathcal{R}_1}{\partial s_2} \right]^2 ds \leq C \|e(u)\|_{L^2(\Omega_\varepsilon^*)}^2.$$

Hence, using the estimates (2.1.24)

$$\varepsilon \int_{\omega} \left( \frac{\partial \mathcal{U}_2}{\partial s_1} + \frac{\partial \mathcal{U}_1}{\partial s_2} \right)^2 ds \leq C \|e(u)\|_{L^2(\Omega_\varepsilon^*)}^2,$$

which proves the inequality (2.1.26).  $\square$

## 2.2 The rescaling operator $\mathfrak{T}_\varepsilon$

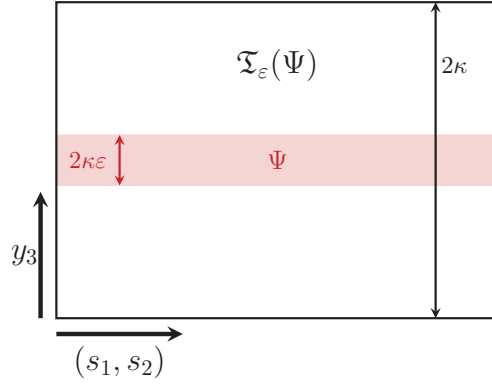
In this section we introduce an operator which transforms the initial domain such that the scaling of the thickness is no longer intrinsically given by  $s_3 \in \mathcal{O}(\varepsilon)$ . More precisely, we consider a variable  $y_3 \in \mathcal{O}(1)$  with the relation  $s_3 = \varepsilon y_3$ . Therefore, consider now the reference domain

$$\Omega = \omega \times (-\kappa, \kappa) \quad (2.2.1)$$

and rescale the shell in its  $s_3$  direction via the rescaling operator  $\mathfrak{T}_\varepsilon$ .

**Definition 2.2.1** Given a measurable function  $\Psi$  over  $\Omega_\varepsilon$ , we define the measurable function  $\mathfrak{T}_\varepsilon(\Psi)$  over  $\Omega$  as

$$\mathfrak{T}_\varepsilon(\Psi)(s_1, s_2, y_3) = \Psi(s_1, s_2, \varepsilon y_3), \quad \text{for a.e. } (s_1, s_2, y_3) \in \Omega. \quad (2.2.2)$$

Figure 2.5: Rescaling operator mapping  $\Psi$  onto the reference domain.

**Lemma 2.2.1** *One has for every  $\Psi \in L^2(\Omega_\varepsilon)$  and for the warping  $\bar{u}_\varepsilon$*

$$\begin{aligned}
 \|\mathfrak{T}_\varepsilon(\Psi)\|_{L^2(\Omega)} &\leq \varepsilon^{-1/2} \|\Psi\|_{L^2(\Omega_\varepsilon)}, \\
 \|\mathfrak{T}_\varepsilon(\bar{u}_\varepsilon)\|_{L^2(\Omega)^3} &\leq C\varepsilon^{1/2} \|e(u_\varepsilon)\|_{L^2(\Omega_\varepsilon)}, \\
 \left\| \frac{\partial \mathfrak{T}_\varepsilon(\bar{u}_\varepsilon)}{\partial s_\alpha} \right\|_{L^2(\Omega)^3} &\leq C\varepsilon^{-1/2} \|e(u_\varepsilon)\|_{L^2(\Omega_\varepsilon)}, \\
 \left\| \frac{\partial \mathfrak{T}_\varepsilon(\bar{u}_\varepsilon)}{\partial y_3} \right\|_{L^2(\Omega)^3} &\leq C\varepsilon^{1/2} \|e(u_\varepsilon)\|_{L^2(\Omega_\varepsilon)}.
 \end{aligned} \tag{2.2.3}$$

*Proof.* All estimates are obtained by using the transformation Theorem for integrals and especially for (2.2.3)<sub>2,3,4</sub> using the estimates (2.1.21) and (2.1.22).  $\square$

With this technique we can study in the subsequent section the asymptotics when the thickness tends to zero.

## 2.3 Asymptotic behavior of the strain tensor

**Lemma 2.3.1** *Let  $\{u_\varepsilon\}_\varepsilon$  be a sequence of displacements belonging to  $V_\varepsilon^*$  and satisfying*

$$\begin{aligned}
 \|e(u_\varepsilon)\|_{L^2(\Omega_\varepsilon^*)} &\leq C\varepsilon^{3/2}, \quad \text{or equivalently} \\
 \|e(u_\varepsilon)\|_{L^2(\Omega_\varepsilon)} &\leq C\varepsilon^{3/2}
 \end{aligned}$$

*with a constant independent of  $\varepsilon$ .*

*There exists a subsequence of  $\{\varepsilon\}$  (still denoted  $\varepsilon$ ) and  $\mathcal{U} \in H_{\Gamma_0}^1(\omega)^3$ ,  $\mathcal{R} \in H_{\Gamma_0}^1(\omega)^2$ ,  $\mathcal{Z}_{\alpha\beta} \in L^2(\omega)$ ,  $\mathcal{Z}_{\alpha 3} \in L^2(\omega)$  and  $\bar{u} \in L^2(\omega; H^1(-\kappa, \kappa))^3$  satisfying*

$$\int_{-\kappa}^{\kappa} \bar{u}(\cdot, y_3) dy_3 = 0, \quad \int_{-\kappa}^{\kappa} y_3 \bar{u}_\alpha(\cdot, y_3) dy_3 = 0, \quad \text{a.e. in } \omega, \tag{2.3.1}$$

such that

$$\begin{aligned}
\mathcal{U}_\varepsilon &\longrightarrow \mathcal{U} && \text{strongly in } H_{\Gamma_0}^1(\omega)^3, \\
\mathcal{R}_{\varepsilon,\alpha} &\rightharpoonup \mathcal{R}_\alpha && \text{weakly in } H_{\Gamma_0}^1(\omega), \\
\frac{1}{\varepsilon} \left( \frac{\partial \mathcal{U}_\varepsilon}{\partial s_\alpha} \cdot \mathbf{t}_\beta + \frac{\partial \mathcal{U}_\varepsilon}{\partial s_\beta} \cdot \mathbf{t}_\alpha \right) &\rightharpoonup \mathcal{Z}_{\alpha\beta} && \text{weakly in } L^2(\omega), \\
\frac{1}{\varepsilon} \left( \frac{\partial \mathcal{U}_\varepsilon}{\partial s_\alpha} \cdot \mathbf{n} + \mathcal{R}_\varepsilon \cdot \mathbf{t}_\alpha \right) &\rightharpoonup \mathcal{Z}_{\alpha 3} && \text{weakly in } L^2(\omega), \\
\frac{1}{\varepsilon^2} \mathfrak{T}_\varepsilon(\bar{u}_\varepsilon) &\rightharpoonup \bar{u} && \text{weakly in } L^2(\omega; H^1(-\kappa, \kappa))^3, \\
\frac{1}{\varepsilon} \mathfrak{T}_\varepsilon \left( \frac{\partial \bar{u}_\varepsilon}{\partial s_\alpha} \right) &= \frac{1}{\varepsilon} \frac{\partial}{\partial s_\alpha} \mathfrak{T}_\varepsilon(\bar{u}_\varepsilon) \rightharpoonup 0 && \text{weakly in } L^2(\omega \times (-\kappa, \kappa))^3, \\
\frac{1}{\varepsilon} \mathfrak{T}_\varepsilon(e(u_\varepsilon)) &\rightharpoonup \mathcal{E}(\mathcal{U}, \mathcal{Z}, \bar{u}) && \text{weakly in } L^2(\omega)^{3 \times 3}.
\end{aligned} \tag{2.3.2}$$

Moreover, one has

$$\frac{\partial \mathcal{U}_3}{\partial s_1} - \frac{1}{a} \mathcal{U}_1 + \mathcal{R}_1 = 0, \quad \frac{\partial \mathcal{U}_3}{\partial s_2} + \mathcal{R}_2 = 0.$$

*Proof.* We start with the weak limits. As a consequence of (2.1.24) we get that

$$\begin{aligned}
\mathcal{U}_\varepsilon &\rightharpoonup \mathcal{U} && \text{weakly in } H_{\Gamma_0}^1(\omega)^3, \\
\mathcal{R}_\varepsilon &\rightharpoonup \mathcal{R} && \text{weakly in } H_{\Gamma_0}^1(\omega)^2.
\end{aligned} \tag{2.3.3}$$

The results in (2.3.2)<sub>5,6</sub> follow from Lemma 2.2.1 and equation (2.1.21). Both convergences (2.3.2)<sub>3,4</sub> follow directly from Lemma 2.1.1.

Now we prove

$$\mathcal{U}_{\varepsilon,3} \longrightarrow \mathcal{U}_3 \quad \text{strongly in } H_{\Gamma_0}^1(\omega). \tag{2.3.4}$$

By the Sobolev embedding and the convergences (2.3.3), one has

$$\begin{aligned}
\mathcal{U}_\varepsilon &\longrightarrow \mathcal{U} && \text{strongly in } L^2(\omega)^3, \\
\mathcal{R}_\varepsilon &\longrightarrow \mathcal{R} && \text{strongly in } L^2(\omega)^2.
\end{aligned} \tag{2.3.5}$$

Besides, from estimate (2.1.25)<sub>2</sub>, one obtains

$$\begin{aligned}
\frac{\partial \mathcal{U}_{\varepsilon,3}}{\partial s_1} - \frac{1}{a} \mathcal{U}_{\varepsilon,1} + \mathcal{R}_{\varepsilon,1} &\longrightarrow 0 && \text{strongly in } L^2(\omega), \\
\frac{\partial \mathcal{U}_{\varepsilon,3}}{\partial s_2} + \mathcal{R}_{\varepsilon,2} &\longrightarrow 0 && \text{strongly in } L^2(\omega).
\end{aligned}$$

Hence,  $\nabla \mathcal{U}_{\varepsilon,3}$  strongly converges to its limit in  $L^2(\omega)^2$ , which ends the proof of (2.3.4). That also proves the last equalities of the Lemma.

Now, we want to prove the strong convergences

$$\mathcal{U}_{\varepsilon,\alpha} \longrightarrow \mathcal{U}_\alpha \quad \text{strongly in } H_{\Gamma_0}^1(\omega), \quad \alpha = 1, 2.$$

By estimates (2.1.25)<sub>1</sub> one immediately has

$$\begin{aligned}
\frac{\partial \mathcal{U}_{\varepsilon,1}}{\partial s_1} + \frac{1}{a} \mathcal{U}_{\varepsilon,3} &\longrightarrow 0 && \text{strongly in } L^2(\omega), \\
\frac{\partial \mathcal{U}_{\varepsilon,2}}{\partial s_2} &\longrightarrow 0 && \text{strongly in } L^2(\omega), \\
\frac{\partial \mathcal{U}_{\varepsilon,1}}{\partial s_2} + \frac{\partial \mathcal{U}_{\varepsilon,2}}{\partial s_1} &\longrightarrow 0 && \text{strongly in } L^2(\omega).
\end{aligned}$$

Furthermore, from (2.3.5) and the above strong convergences, one obtains the strong convergence of the strain tensor of the displacement  $(\mathcal{U}_{\varepsilon,1}, \mathcal{U}_{\varepsilon,2})$  in  $L^2(\omega)^2$ . Since  $\omega$  is a Lipschitz domain, this displacement strongly converges to its limit in  $H_{\Gamma_0}^1(\omega)^2$ . The elements of the limit strain tensor  $\mathcal{E}$  are then particularly given by

$$\begin{aligned}\frac{1}{\varepsilon}\mathfrak{T}_{\varepsilon}(e_{11}) &\rightharpoonup \mathcal{Z}_{11} + y_3 \frac{\partial \mathcal{R}_1}{\partial s_1}, \\ \frac{1}{\varepsilon}\mathfrak{T}_{\varepsilon}(e_{22}) &\rightharpoonup \mathcal{Z}_{22} + y_3 \frac{\partial \mathcal{R}_2}{\partial s_2}, \\ \frac{1}{\varepsilon}\mathfrak{T}_{\varepsilon}(e_{12}) &\rightharpoonup \frac{1}{2} \left\{ \mathcal{Z}_{12} + \frac{y_3}{a} \frac{\partial \mathcal{U}_1}{\partial s_2} + y_3 \frac{\partial \mathcal{R}_2}{\partial s_1} + y_3 \frac{\partial \mathcal{R}_1}{\partial s_2} \right\}, \\ \frac{1}{\varepsilon}\mathfrak{T}_{\varepsilon}(e_{13}) &\rightharpoonup \frac{1}{2} \left\{ \mathcal{Z}_{13} + \frac{\partial \bar{u}_1}{\partial y_3} \right\}, \\ \frac{1}{\varepsilon}\mathfrak{T}_{\varepsilon}(e_{23}) &\rightharpoonup \frac{1}{2} \left\{ \mathcal{Z}_{23} + \frac{\partial \bar{u}_2}{\partial y_3} \right\}, \\ \frac{1}{\varepsilon}\mathfrak{T}_{\varepsilon}(e_{33}) &\rightharpoonup \frac{\partial \bar{u}_3}{\partial y_3}.\end{aligned}$$

Putting everything together yields the symmetric tensor

$$\mathcal{E}(\mathcal{U}, \mathcal{Z}, \bar{u}) = \begin{pmatrix} \mathcal{Z}_{11} + \frac{y_3}{a} \frac{\partial \mathcal{U}_1}{\partial s_1} - y_3 \frac{\partial^2 \mathcal{U}_3}{\partial s_1^2} & \frac{1}{2} \mathcal{Z}_{12} + \frac{y_3}{a} \frac{\partial \mathcal{U}_1}{\partial s_2} - y_3 \frac{\partial^2 \mathcal{U}_3}{\partial s_1 \partial s_2} & \frac{1}{2} \left( \mathcal{Z}_{13} + \frac{\partial \bar{u}_1}{\partial y_3} \right) \\ * & \mathcal{Z}_{22} - y_3 \frac{\partial^2 \mathcal{U}_3}{\partial s_2^2} & \frac{1}{2} \left( \mathcal{Z}_{23} + \frac{\partial \bar{u}_2}{\partial y_3} \right) \\ * & * & \frac{\partial \bar{u}_3}{\partial y_3} \end{pmatrix},$$

which ends the proof of the Lemma.  $\square$

As a consequence of the estimates in Lemma 2.1.1 and the above Lemma, one has a.e. in  $\omega$

$$\frac{\partial \mathcal{U}}{\partial s_{\alpha}} \cdot \mathbf{t}_{\beta} + \frac{\partial \mathcal{U}}{\partial s_{\beta}} \cdot \mathbf{t}_{\alpha} = 0, \quad \mathcal{U}_i \in H_{\Gamma_0}^1(\omega), \quad (2.3.6)$$

$$\frac{\partial \mathcal{U}}{\partial s_{\alpha}} \cdot \mathbf{n} + \mathcal{R} \cdot \mathbf{t}_{\alpha} = 0, \quad \mathcal{R}_{\alpha} \in H_{\Gamma_0}^1(\omega). \quad (2.3.7)$$

From the equation (2.3.6) we obtain for  $\alpha = \beta = 2$  that

$$\frac{\partial \mathcal{U}_2}{\partial s_2} = 0.$$

Hence,  $\mathcal{U}_2$  does not depend on  $s_2$  and we get that  $\mathcal{U}_2 = U_2(s_1)$  and due to the boundary conditions, one has  $U_2 \in H_0^1(0, a\pi)$ .

With that we conclude for  $\alpha = 1$  and  $\beta = 2$  that

$$\frac{dU_2(s_1)}{ds_1} + \frac{\partial \mathcal{U}_1(s_1, s_2)}{\partial s_2} = 0 \quad \Longleftrightarrow \quad \mathcal{U}_1(s_1, s_2) = -s_2 \frac{dU_2}{ds_1}(s_1) + U_1(s_1).$$

Since  $\mathcal{U}_1$  belongs to  $H_{\Gamma_0}^1(\omega)$ , this yields  $U_2 \in H_0^2(0, a\pi)$  and  $U_1 \in H_0^1(0, a\pi)$ .

For the last case,  $\alpha = \beta = 1$ , then follows that

$$\begin{aligned}\frac{\partial \mathcal{U}_1}{\partial s_1} + \frac{1}{a} \mathcal{U}_3 &= 0 \quad \Longleftrightarrow \quad -\frac{d}{ds_1} \left( -s_2 \frac{dU_2}{ds_1}(s_1) + U_1(s_1) \right) = \frac{1}{a} \mathcal{U}_3 \\ &\Longleftrightarrow \quad \mathcal{U}_3(s_1, s_2) = a s_2 \frac{d^2 U_2}{ds_1^2} - a \frac{dU_1}{ds_1}(s_1).\end{aligned}$$

Since  $\mathcal{U}_3$  belongs to  $H_{\Gamma_0}^1(\omega)$ , this implies

$$\begin{aligned} U_2 &\in H_0^3(0, a\pi), \quad U_1 \in H_0^2(0, a\pi), \quad \text{and} \\ \mathcal{U}(s_1, s_2) &= \left( -s_2 \frac{dU_2}{ds_1}(s_1) + U_1(s_1), U_2(s_1), as_2 \frac{d^2U_2}{ds_1^2} - a \frac{dU_1}{ds_1}(s_1) \right)^T. \end{aligned} \quad (2.3.8)$$

Now focus on the equality given by (2.3.7). For the case  $\alpha = 1$  we obtain with our expression for  $\mathcal{U}$

$$\begin{aligned} \frac{\partial \mathcal{U}_3}{\partial s_1} - \frac{1}{a} \mathcal{U}_1 + \mathcal{R}_1 &= 0 \quad \Longleftrightarrow \\ \mathcal{R}_1(s_1, s_2) &= -s_2 \left( \frac{1}{a} \frac{dU_2}{ds_1}(s_1) + a \frac{d^3U_2}{ds_1^3}(s_1) \right) + \frac{1}{a} U_1(s_1) + a \frac{d^2U_1}{ds_1^2}(s_1). \end{aligned}$$

Moreover, we get for  $\alpha = 2$

$$\frac{\partial \mathcal{U}_3}{\partial s_2} + \mathcal{R}_2 = 0 \quad \Longleftrightarrow \quad \mathcal{R}_2(s_1, s_2) = -a \frac{d^2U_2}{ds_1^2}(s_1).$$

Observe that due to the above conditions on  $U_2$ ,  $\mathcal{R}_2$  belongs to  $H_{\Gamma_0}^1(\omega)$ . Now, since  $\mathcal{R}_1$  also belongs to  $H_{\Gamma_0}^1(\omega)$ , we finally obtain

$$U_2 \in H_0^4(0, a\pi), \quad U_1 \in H_0^3(0, a\pi).$$

Thus,

$$\begin{aligned} \mathcal{R}_1 &\in H_{\Gamma_0}^1(\omega), \quad \mathcal{R}_2 \in H^2(\omega) \cap H_{\Gamma_0}^1(\omega), \\ \mathcal{U}_1 &\in H^3(\omega) \cap H_{\Gamma_0}^1(\omega), \quad \mathcal{U}_2 \in H^4(\omega) \cap H_{\Gamma_0}^1(\omega), \quad \mathcal{U}_3 \in H^2(\omega) \cap H_{\Gamma_0}^1(\omega) \end{aligned}$$

and

$$\begin{aligned} \mathcal{R}_1 &= -s_2 \left( \frac{1}{a} \frac{dU_2}{ds_1}(s_1) + a \frac{d^3U_2}{ds_1^3}(s_1) \right) + \frac{1}{a} U_1(s_1) + a \frac{d^2U_1}{ds_1^2}(s_1), \\ \mathcal{R}_2 &= -a \frac{d^2U_2}{ds_1^2}(s_1). \end{aligned}$$

## 2.4 Unfolding of the rescaled shell

With the rescaling operator we could successfully analyze the limit behavior, where the thickness tends to zero. However, there is a second small parameter describing the microscopic periodic pattern of our structure. For that reason we need to introduce the unfolding operator. This operator decouples the macroscopic and microscopic scales and introduces a new set of variables solely acting in the reference periodicity cell.

**Definition 2.4.1** *The unfolding  $\mathcal{T}_\varepsilon(\psi')$  (resp.  $\mathcal{T}_\varepsilon(\psi)$ ) of a measurable function  $\psi'$  (resp.  $\psi$ ) defined on  $\omega$  (resp.  $\Omega$ ) is measurable on  $\omega \times Y'$  (resp.  $\Omega \times Y'$ ) and given by*

$$\begin{aligned} \mathcal{T}_\varepsilon(\psi')(s', y') &= \psi' \left( \varepsilon \left[ \frac{s'}{\varepsilon} \right] + \varepsilon y' \right), \quad \text{for a.e. } (s', y') \in \hat{\omega}_\varepsilon \times Y', \\ \mathcal{T}_\varepsilon(\psi)(s', y') &= 0, \quad \text{for a.e. } (s', y') \in \Lambda_\varepsilon \times Y', \end{aligned}$$

and

$$\begin{aligned} \mathcal{T}_\varepsilon(\psi)(s', y', y_3) &= \psi \left( \varepsilon \left[ \frac{s'}{\varepsilon} \right] + \varepsilon y', y_3 \right), \quad \text{for a.e. } (s', y', y_3) \in \hat{\omega}_\varepsilon \times Y, \\ \mathcal{T}_\varepsilon(\psi)(s', y', y_3) &= 0, \quad \text{for a.e. } (s', y', y_3) \in \Lambda_\varepsilon \times Y. \end{aligned}$$

As shown in [15], for every  $\psi' \in L^2(\omega)$  we have

$$\|\mathcal{T}_\varepsilon(\psi')\|_{L^2(\omega \times Y')} \leq \|\psi'\|_{L^2(\omega)}. \quad (2.4.1)$$

**Remark 2.4.1** We consider the function  $f_\varepsilon(x) = \frac{1}{4} \sin(2\pi \frac{x}{\varepsilon}) + x$ , with  $\varepsilon = \frac{1}{6}$  as presented in [15]. In figure 2.6 we have plotted the original function on the top. On the bottom we can find the unfolded function  $\mathcal{T}_\varepsilon(f_\varepsilon)$ .

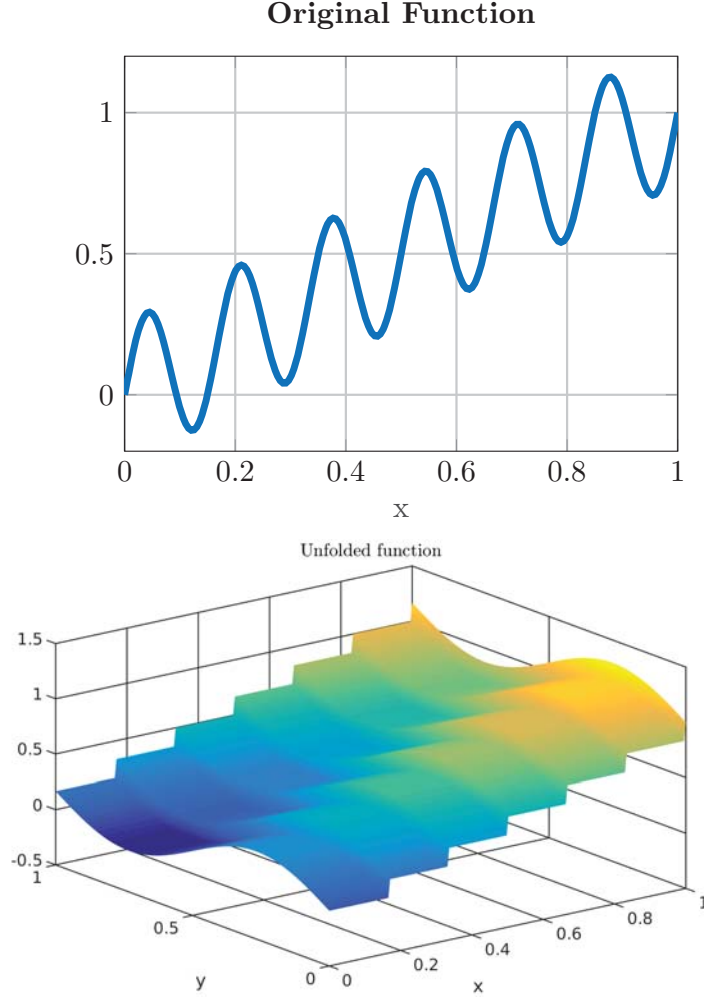


Figure 2.6: Original and unfolded function from remark 2.4.1.

**Definition 2.4.2** The rescaling-unfolding operator is defined by

$$\Pi_\varepsilon = \mathcal{T}_\varepsilon \circ \mathfrak{T}_\varepsilon.$$

Given a measurable function  $\psi$  over  $\Omega_\varepsilon$  then  $\Pi_\varepsilon(\psi)$  is a measurable function on  $\omega \times Y$ .

**Lemma 2.4.1** We obtain the following estimate for the warping:

$$\|\Pi_\varepsilon(\bar{u}_\varepsilon)\|_{L^2(\omega; H^1(Y))} \leq C\varepsilon^{1/2} \|e(u_\varepsilon)\|_{L^2(\Omega_\varepsilon^*)}. \quad (2.4.2)$$

We denote by  $H_{per}^1(Y')$  (respectively  $H_{per}^1(Y)$ ) the subspace of  $H_{loc}^1(\mathbb{R}^2)$  (respectively  $H_{loc}^1(\mathbb{R}^2 \times (-\kappa, \kappa)) \cap H^1(Y)$ ) containing the  $\mathbf{G}$  periodic functions and

$$\widehat{\mathcal{W}} \doteq \left\{ \widehat{\pi} \in H_{per}^1(Y)^3 \mid \int_{-\kappa}^{\kappa} \widehat{\pi}(\cdot, y_3) dy_3 = 0, \int_{-\kappa}^{\kappa} y_3 \widehat{\pi}_\alpha(\cdot, y_3) dy_3 = 0 \text{ a.e. in } \omega \times Y' \right\}.$$



**Theorem 2.4.1** *There exists a subsequence of  $\{\varepsilon\}$  (still denoted  $\{\varepsilon\}$ ) and  $\widehat{\mathcal{U}} \in L^2(\omega; H_{per}^1(Y'))^3$ ,  $\widehat{\mathcal{R}} \in L^2(\omega; H_{per}^1(Y'))^2$  and  $\widehat{\bar{u}} \in L^2(\omega; \widehat{\mathcal{W}})$  such that*

$$\begin{aligned} \mathcal{T}_\varepsilon(\mathcal{U}_\varepsilon) &\longrightarrow \mathcal{U} && \text{strongly in } L^2(\omega; H^1(Y'))^3, \\ \mathcal{T}_\varepsilon(\mathcal{R}_\varepsilon) &\longrightarrow \mathcal{R} && \text{strongly in } L^2(\omega; H^1(Y'))^2, \\ \mathcal{T}_\varepsilon\left(\frac{\partial \mathcal{U}_\varepsilon}{\partial s_\alpha}\right) &\longrightarrow \frac{\partial \mathcal{U}}{\partial s_\alpha} && \text{strongly in } L^2(\omega \times Y')^3, \\ \mathcal{T}_\varepsilon\left(\frac{\partial \mathcal{R}_\varepsilon}{\partial s_\alpha}\right) &\rightharpoonup \frac{\partial \mathcal{R}}{\partial s_\alpha} + \frac{\partial \widehat{\mathcal{R}}}{\partial y_\alpha} && \text{weakly in } L^2(\omega \times Y')^2, \\ \frac{1}{\varepsilon^2} \Pi_\varepsilon(\bar{u}_\varepsilon) &\rightharpoonup \widehat{\bar{u}} && \text{weakly in } L^2(\omega; H^1(Y))^3. \end{aligned} \quad (2.4.3)$$

One has

$$\bar{u}(s_1, s_2, y_3) = \frac{1}{|Y'|} \int_{Y'} \widehat{\bar{u}}(s_1, s_2, y_1, y_2, y_3) dy_1 dy_2, \quad \text{for a.e. } (s_1, s_2, y_3) \in \Omega.$$

Moreover,

$$\begin{aligned} \frac{1}{\varepsilon} \mathcal{T}_\varepsilon\left(\frac{\partial \mathcal{U}_\varepsilon}{\partial s_\alpha} \cdot \mathbf{n} + \mathcal{R}_\varepsilon \cdot \mathbf{t}_\alpha\right) &\rightharpoonup \mathcal{Z}_{\alpha 3} + \widehat{Z}_{\alpha 3} && \text{weakly in } L^2(\omega; H^1(Y')), \\ \frac{1}{\varepsilon} \mathcal{T}_\varepsilon\left(\frac{\partial \mathcal{U}_\varepsilon}{\partial s_\alpha} \cdot \mathbf{t}_\beta + \frac{\partial \mathcal{U}_\varepsilon}{\partial s_\beta} \cdot \mathbf{t}_\alpha\right) &\rightharpoonup \mathcal{Z}_{\alpha\beta} + \widehat{Z}_{\alpha\beta} && \text{weakly in } L^2(\omega; H^1(Y')), \end{aligned} \quad (2.4.4)$$

where

$$\widehat{Z}_{13} = \frac{\partial \widehat{\mathcal{U}}_3}{\partial y_1} + \widehat{\mathcal{R}}_1, \quad \widehat{Z}_{23} = \frac{\partial \widehat{\mathcal{U}}_3}{\partial y_2} + \widehat{\mathcal{R}}_2, \quad \widehat{Z}_{\alpha\beta} = e_{y,\alpha\beta}(\widehat{\mathcal{U}}). \quad (2.4.5)$$

*Proof.* The strong convergences of (2.4.3)<sub>1,2,3</sub> follow from (2.3.2)<sub>1,2</sub> and [15, Propostion 3.4]. Convergences (2.4.3)<sub>4</sub> and (2.4.3)<sub>5</sub> are the consequence of [15, Theorem 3.5] and [15, Corollary 3.2], respectively.

The convergences of (2.4.4)<sub>1,2</sub> follow from Lemma 2.3.1 and [15, Theorem 3.5]. With Lemma B.2.1 we then obtain the expressions for  $\widehat{Z}_{\alpha 3}$  in (2.4.5) and Lemma B.2.2 yields the expressions  $\widehat{Z}_{\alpha\beta}$ .

Indeed, we first need to identify the different fields appearing in Lemma B.2.1 with

$$u_\varepsilon \longleftrightarrow \mathcal{U}_{\varepsilon,3}, \quad v_\varepsilon \longleftrightarrow \begin{pmatrix} -\frac{1}{a}\mathcal{U}_{\varepsilon,1} + \mathcal{R}_{\varepsilon,1} \\ \mathcal{R}_{\varepsilon,2} \end{pmatrix}.$$

From (2.3.2)<sub>1,4</sub>, one has

$$\begin{aligned} \frac{1}{\varepsilon} \left( \nabla \mathcal{U}_{\varepsilon,3} + \begin{pmatrix} -\frac{1}{a}\mathcal{U}_{\varepsilon,1} + \mathcal{R}_{\varepsilon,1} \\ \mathcal{R}_{\varepsilon,2} \end{pmatrix} \right) &\rightharpoonup \begin{pmatrix} \mathcal{Z}_{13} \\ \mathcal{Z}_{23} \end{pmatrix} && \text{weakly in } L^2(\omega)^2, \\ \mathcal{T}_\varepsilon \left[ \nabla \begin{pmatrix} -\frac{1}{a}\mathcal{U}_{\varepsilon,1} + \mathcal{R}_{\varepsilon,1} \\ \mathcal{R}_{\varepsilon,2} \end{pmatrix} \right] &\rightharpoonup \nabla \begin{pmatrix} -\frac{1}{a}\mathcal{U}_1 + \mathcal{R}_1 \\ \mathcal{R}_2 \end{pmatrix} + \nabla_y \begin{pmatrix} \widehat{\mathcal{R}}_1 \\ \widehat{\mathcal{R}}_2 \end{pmatrix} && \text{weakly in } L^2(\omega \times Y')^2. \end{aligned}$$

Moreover, we set

$$v = \begin{pmatrix} -\frac{1}{a}\mathcal{U}_1 + \mathcal{R}_1 \\ \mathcal{R}_2 \end{pmatrix}, \quad \widehat{v} = \begin{pmatrix} \widehat{\mathcal{R}}_1 \\ \widehat{\mathcal{R}}_2 \end{pmatrix}.$$

Then, one can apply Lemma B.2.1. The function  $\mathbf{u}$  is in the following defined as  $\widehat{\mathcal{U}}_3$ . To determine the  $\widehat{Z}_{\alpha\beta}$ , let us identify

$$u_\varepsilon \longleftrightarrow \begin{pmatrix} \mathcal{U}_{\varepsilon,1} \\ \mathcal{U}_{\varepsilon,2} \end{pmatrix}, \quad v_\varepsilon \longleftrightarrow \begin{pmatrix} \frac{1}{a}\mathcal{U}_{\varepsilon,3} & 0 \\ 0 & 0 \end{pmatrix}.$$

Together with

$$e_{\alpha\beta}(u_\varepsilon) = \frac{1}{2} \left( \frac{\partial u_{\beta,\varepsilon}}{\partial s_\alpha} + \frac{\partial u_{\alpha,\varepsilon}}{\partial s_\beta} \right)$$

we then obtain

$$e(u_\varepsilon) = \begin{pmatrix} \frac{\partial \mathcal{U}_{\varepsilon,1}}{\partial s_1} & \frac{1}{2} \left( \frac{\partial \mathcal{U}_{\varepsilon,1}}{\partial s_2} + \frac{\partial \mathcal{U}_{\varepsilon,2}}{\partial s_1} \right) \\ \frac{1}{2} \left( \frac{\partial \mathcal{U}_{\varepsilon,1}}{\partial s_2} + \frac{\partial \mathcal{U}_{\varepsilon,2}}{\partial s_1} \right) & \frac{\partial \mathcal{U}_{\varepsilon,2}}{\partial s_2} \end{pmatrix}.$$

Hence, by (2.3.2)<sub>1,3</sub>

$$\frac{1}{\varepsilon} (e(u_\varepsilon) + v_\varepsilon) \rightharpoonup \mathcal{X},$$

and

$$\mathcal{T}_\varepsilon(\nabla v_\varepsilon) \rightharpoonup \nabla v + \nabla_y \widehat{v}.$$

In our case we have that  $\widehat{v} = 0$ . The field  $(\mathbf{u}_1, \mathbf{u}_2)$  given by Lemma B.2.2 is denoted  $(\widehat{\mathcal{U}}_1, \widehat{\mathcal{U}}_2)$ .  $\square$

### 2.4.1 Limit of the rescaled-unfolded strain tensor

**Proposition 2.4.1** *Under the assumptions and the results of Theorem 2.4.1 we obtain the following weak convergences in  $L^2(\omega \times Y)$ :*

$$\begin{aligned} \frac{1}{\varepsilon} \Pi_\varepsilon(e_{11}(u_\varepsilon)) &\rightharpoonup \mathcal{Z}_{11} + e_{y,11}(\widehat{\mathcal{U}}) + y_3 \left( \frac{\partial \mathcal{R}_1}{\partial s_1} + \frac{\partial \widehat{\mathcal{R}}_1}{\partial y_1} \right) + \frac{\partial \widehat{u}_1}{\partial y_1}, \\ \frac{1}{\varepsilon} \Pi_\varepsilon(e_{22}(u_\varepsilon)) &\rightharpoonup \mathcal{Z}_{22} + e_{y,22}(\widehat{\mathcal{U}}) + y_3 \left( \frac{\partial \mathcal{R}_2}{\partial s_2} + \frac{\partial \widehat{\mathcal{R}}_2}{\partial y_2} \right) + \frac{\partial \widehat{u}_2}{\partial y_2}, \\ \frac{1}{\varepsilon} \Pi_\varepsilon(e_{12}(u_\varepsilon)) &\rightharpoonup \frac{1}{2} \left( \mathcal{Z}_{12} + 2e_{y,22}(\widehat{\mathcal{U}}) + y_3 \left( \frac{\partial \mathcal{R}_1}{\partial s_2} + \frac{\partial \widehat{\mathcal{R}}_1}{\partial y_2} + \frac{\partial \mathcal{R}_2}{\partial s_1} + \frac{\partial \widehat{\mathcal{R}}_2}{\partial y_1} \right) + \frac{\partial \widehat{u}_1}{\partial y_2} + \frac{\partial \widehat{u}_2}{\partial y_1} \right), \\ \frac{1}{\varepsilon} \Pi_\varepsilon(e_{13}(u_\varepsilon)) &\rightharpoonup \frac{1}{2} \left( \mathcal{Z}_{13} + \frac{\partial \widehat{\mathcal{U}}_3}{\partial y_1} + \widehat{\mathcal{R}}_1 + \frac{\partial \widehat{u}_1}{\partial y_3} + \frac{\partial \widehat{u}_3}{\partial y_1} \right), \\ \frac{1}{\varepsilon} \Pi_\varepsilon(e_{23}(u_\varepsilon)) &\rightharpoonup \frac{1}{2} \left( \mathcal{Z}_{23} + \frac{\partial \widehat{\mathcal{U}}_3}{\partial y_2} + \widehat{\mathcal{R}}_2 + \frac{\partial \widehat{u}_2}{\partial y_3} + \frac{\partial \widehat{u}_3}{\partial y_2} \right), \\ \frac{1}{\varepsilon} \Pi_\varepsilon(e_{33}(u_\varepsilon)) &\rightharpoonup \frac{\partial \widehat{u}_3}{\partial y_3}. \end{aligned}$$

*Proof.* First, note that the function  $y_3 \longrightarrow \frac{a}{a + \varepsilon y_3}$  converges uniformly to 1 in  $\omega \times Y$ . Below, we give the limits for  $\frac{1}{\varepsilon} \Pi_\varepsilon(e_{11}(u_\varepsilon))$  and  $\frac{1}{\varepsilon} \Pi_\varepsilon(e_{13}(u_\varepsilon))$ , since the other cases follow

analogously. For the calculation we combine the results obtained in Lemma 2.3.1 and Theorem 2.4.1. We have,

$$\begin{aligned} \frac{1}{\varepsilon} \Pi_\varepsilon(e_{11}(u_\varepsilon)) &= \frac{1}{\varepsilon} \frac{a}{a + \varepsilon y_3} \left[ \mathcal{T}_\varepsilon \left( \frac{\partial \mathcal{U}_{\varepsilon,1}}{\partial s_1} + \frac{1}{a} \mathcal{U}_{\varepsilon,3} \right) \right. \\ &\quad \left. + \varepsilon y_3 \mathcal{T}_\varepsilon \left( \frac{\partial \mathcal{R}_{\varepsilon,1}}{\partial s_1} \right) + \Pi_\varepsilon \left( \frac{\partial \bar{u}_{\varepsilon,1}}{\partial s_1} \right) + \frac{1}{a} \Pi_\varepsilon(\bar{u}_{\varepsilon,3}) \right]. \end{aligned}$$

Therefore, we get for each term in the limit

$$\begin{aligned} \frac{1}{\varepsilon} \mathcal{T}_\varepsilon \left( \frac{\partial \mathcal{U}_{\varepsilon,1}}{\partial s_1} + \frac{1}{a} \mathcal{U}_{\varepsilon,3} \right) &\rightharpoonup \mathcal{Z}_{11} + e_{y,11}(\hat{\mathcal{U}}) \quad \text{weakly in } L^2(\omega \times Y'), \\ \mathcal{T}_\varepsilon \left( \frac{\partial \mathcal{R}_{\varepsilon,1}}{\partial s_1} \right) &\rightharpoonup \frac{\partial \mathcal{R}_1}{\partial s_1} + \frac{\partial \hat{\mathcal{R}}_1}{\partial y_1} \quad \text{weakly in } L^2(\omega \times Y'), \\ \frac{1}{\varepsilon} \Pi_\varepsilon \left( \frac{\partial \bar{u}_{\varepsilon,1}}{\partial s_1} \right) &= \frac{1}{\varepsilon^2} \frac{\partial \Pi_\varepsilon(\bar{u}_{\varepsilon,1})}{\partial y_1} \rightharpoonup \frac{\partial \hat{u}_1}{\partial y_1} \quad \text{weakly in } L^2(\omega \times Y), \\ \frac{1}{\varepsilon} \Pi_\varepsilon(\bar{u}_{\varepsilon,3}) &\rightharpoonup 0 \quad \text{weakly in } L^2(\omega \times Y), \end{aligned}$$

and hence

$$\frac{1}{\varepsilon} \Pi_\varepsilon(e_{11}(u_\varepsilon)) \rightharpoonup \mathcal{Z}_{11} + e_{y,11}(\hat{\mathcal{U}}) + y_3 \left( \frac{\partial \mathcal{R}_1}{\partial s_1} + \frac{\partial \hat{\mathcal{R}}_1}{\partial y_1} \right) + \frac{\partial \hat{u}_1}{\partial y_1} \quad \text{weakly in } L^2(\omega \times Y).$$

Now consider

$$\begin{aligned} \frac{1}{\varepsilon} \Pi_\varepsilon(e_{13}(u_\varepsilon)) &= \frac{1}{\varepsilon} \frac{a}{2(a + \varepsilon y_3)} \left[ \mathcal{T}_\varepsilon \left( \frac{\partial \mathcal{U}_{\varepsilon,3}}{\partial s_1} - \frac{1}{a} \mathcal{U}_{\varepsilon,1} + \mathcal{R}_{\varepsilon,1} \right) \right. \\ &\quad \left. - \frac{1}{a} \Pi_\varepsilon(\bar{u}_{\varepsilon,1}) + \Pi_\varepsilon \left( \frac{\partial \bar{u}_{\varepsilon,3}}{\partial s_1} \right) + \left( 1 + \frac{\varepsilon y_3}{a} \right) \Pi_\varepsilon \left( \frac{\partial \bar{u}_{\varepsilon,1}}{\partial s_3} \right) \right]. \end{aligned}$$

Similar to the previous case we investigate the limits of each component, obtaining

$$\begin{aligned} \frac{1}{\varepsilon} \mathcal{T}_\varepsilon \left( \frac{\partial \mathcal{U}_{\varepsilon,3}}{\partial s_1} - \frac{1}{a} \mathcal{U}_{\varepsilon,1} + \mathcal{R}_{\varepsilon,1} \right) &\rightharpoonup \mathcal{Z}_{13} + \frac{\partial \hat{\mathcal{U}}_3}{\partial y_1} + \hat{\mathcal{R}}_1 \quad \text{weakly in } L^2(\omega \times Y'), \\ \frac{1}{\varepsilon} \Pi_\varepsilon(\bar{u}_{\varepsilon,1}) &\rightharpoonup 0 \quad \text{weakly in } L^2(\omega \times Y), \\ \frac{1}{\varepsilon} \Pi_\varepsilon \left( \frac{\partial \bar{u}_{\varepsilon,3}}{\partial s_1} \right) &= \frac{1}{\varepsilon^2} \frac{\partial \Pi_\varepsilon(\bar{u}_{\varepsilon,3})}{\partial y_1} \rightharpoonup \frac{\partial \hat{u}_3}{\partial y_1} \quad \text{weakly in } L^2(\omega \times Y), \\ \frac{1}{\varepsilon^2} \frac{\partial \Pi_\varepsilon(\bar{u}_{\varepsilon,1})}{\partial y_3} &\rightharpoonup \frac{\partial \hat{u}_1}{\partial y_3} \quad \text{weakly in } L^2(\omega \times Y). \end{aligned}$$

Therefore,

$$\frac{1}{\varepsilon} \Pi_\varepsilon(e_{13}(u_\varepsilon)) \rightharpoonup \frac{1}{2} \left( \mathcal{Z}_{13} + \frac{\partial \hat{\mathcal{U}}_3}{\partial y_1} + \hat{\mathcal{R}}_1 + \frac{\partial \hat{u}_3}{\partial y_1} + \frac{\partial \hat{u}_1}{\partial y_3} \right) \quad \text{weakly in } L^2(\omega \times Y).$$

□

Define the displacement  $\hat{u}$  belonging to  $L^2(\omega; H_{per}^1(Y))^3$  by

$$\begin{aligned} \hat{u}(\cdot, y) &= \hat{\mathcal{U}}(\cdot, y_1, y_2) + y_3 \hat{\mathcal{R}}(\cdot, y_1, y_2) + (y_3(\mathcal{Z}_{13} \mathbf{t}_1 + \mathcal{Z}_{23} \mathbf{t}_2) + \hat{u}(\cdot, y)), \\ &\quad \text{for a.e. } y \in Y^* \text{ and a.e. in } \omega. \end{aligned}$$

Hence, one obtains

$$\frac{1}{\varepsilon} \Pi_\varepsilon(e(u_\varepsilon)) \rightharpoonup \begin{pmatrix} \mathcal{Z}_{11} + \frac{y_3}{a} \frac{\partial \mathcal{U}_1}{\partial s_1} - y_3 \frac{\partial^2 \mathcal{U}_3}{\partial s_1^2} & \frac{1}{2} \mathcal{Z}_{12} + \frac{y_3}{a} \frac{\partial \mathcal{U}_1}{\partial s_2} - y_3 \frac{\partial^2 \mathcal{U}_3}{\partial s_1 \partial s_2} & 0 \\ * & \mathcal{Z}_{22} - y_3 \frac{\partial^2 \mathcal{U}_3}{\partial s_2^2} & 0 \\ * & * & 0 \end{pmatrix} + \mathcal{E}_y(\hat{u}) \quad \text{weakly in } L^2(\omega \times Y)^{3 \times 3},$$

where  $\mathcal{E}_y(\hat{u})$  is the symmetric tensor whose components are the  $e_{y,ij}(\hat{u})$ 's. We want to note here that we obtain the same kind of result as in [29].

**Remark 2.4.2** *If we compare our results with [16, Proposition 11.13], we see that*

$$\mathcal{E}_y(\hat{u}) = E_w(\hat{u}) + \mathcal{E}_y^1(\hat{u}),$$

where the terms on the right hand side follow from the given definitions in [16].

The aim of the following section is to determine the  $\mathcal{Z}_{\alpha\beta}$  by decomposing the displacements into two disjoint sets.

## 2.5 Inextensional and extensional displacements

### 2.5.1 Inextensional displacements

Denote  $\mathbb{H} \doteq [H_{\Gamma_0}^1(\omega)]^2 \times L^2(\omega)$ . We equip  $\mathbb{H}$  with the scalar product

$$\langle \mathcal{U}, \mathcal{V} \rangle_{\mathbb{H}} = \int_{\omega} \left[ \frac{1}{2} \left( \frac{\partial \mathcal{U}_1}{\partial s_1} + \frac{1}{a} \mathcal{U}_3 \right) \left( \frac{\partial \mathcal{V}_1}{\partial s_1} + \frac{1}{a} \mathcal{V}_3 \right) + \frac{\partial \mathcal{U}_2}{\partial s_2} \frac{\partial \mathcal{V}_2}{\partial s_2} + \frac{1}{2} \left( \frac{\partial \mathcal{U}_1}{\partial s_2} + \frac{\partial \mathcal{U}_2}{\partial s_1} \right) \left( \frac{\partial \mathcal{V}_1}{\partial s_2} + \frac{\partial \mathcal{V}_2}{\partial s_1} \right) + \mathcal{U}_3 \mathcal{V}_3 \right] ds_1 ds_2.$$

The associated norm is equivalent to the usual product norm of  $[H_{\Gamma_0}^1(\omega)]^2 \times L^2(\omega)$ . Denote  $D_I$  the space of inextensional displacements

$$D_I \doteq \left\{ \Phi \in \mathbb{H} \mid \frac{\partial \Phi_1}{\partial s_1} + \frac{1}{a} \Phi_3 = 0, \quad \frac{\partial \Phi_2}{\partial s_2} = 0, \quad \frac{\partial \Phi_1}{\partial s_2} + \frac{\partial \Phi_2}{\partial s_1} = 0 \right\}.$$

We define the spaces

$$H_0^1(0, a\pi) = \{\psi \in H^1([0, a\pi], \mathbb{R}) \mid \psi(0) = \psi(a\pi) = 0\}$$

and  $H_0^2(0, a\pi)$ , respectively. Moreover, we set

$$s_1^c = s_1 - \frac{a\pi}{2}, \quad s_2^c = s_2 - \frac{l}{2}.$$

A displacement  $\mathcal{V}$  belongs to  $D_I$  if and only if there exists  $(V_1, V_2) \in H_0^1(0, a\pi) \times H_0^2(0, a\pi)$  such that for a.e.  $(s_1, s_2) \in \omega$

$$\begin{aligned} \mathcal{V}_1(s_1, s_2) &= -s_2^c V_2'(s_1) + V_1(s_1), \\ \mathcal{V}_2(s_1, s_2) &= V_2(s_1), \\ \mathcal{V}_3(s_1, s_2) &= a(s_2^c V_2''(s_1) - V_1'(s_1)), \end{aligned} \tag{2.5.1}$$

where the prime denotes the differentiation w.r.t.  $s_1$ . The map  $\mathcal{V} \in D_I \mapsto (V_1, V_2) \in H_0^1(0, a\pi) \times H_0^2(0, a\pi)$  is one to one and onto.

Denote

$$\mathbb{D}_I = D_I \cap ([H_{\Gamma_0}^1(\omega)]^2 \times H_{\Gamma_0}^2(\omega)).$$

Note that the limit of the mid-surface displacement of the shell  $\mathcal{U}$  belongs to  $\mathbb{D}_I$ .

We equip  $D_I$  (resp.  $\mathbb{D}_I$ ) with the semi-norm

$$\|\mathcal{V}\|_{D_I} = \|\mathcal{V}_3\|_{L^2(\omega)}, \quad (\text{resp. } \|\mathcal{V}\|_{\mathbb{D}_I} = \|\mathcal{V}_3\|_{H^2(\omega)}).$$

**Lemma 2.5.1** *The semi-norm  $\|\cdot\|_{D_I}$  (resp.  $\|\cdot\|_{\mathbb{D}_I}$ ) is a norm equivalent to the norm of the product space  $[H^1(\omega)]^2 \times L^2(\omega)$  (resp.  $[H^1(\omega)]^2 \times H^2(\omega)$ ).*

*Moreover, there exist two constants  $c, C$  such that for every  $\mathcal{V} \in D_I$  (resp.  $\mathcal{V} \in \mathbb{D}_I$ ) one has*

$$\begin{aligned} c(\|V_1\|_{H_0^1(0, a\pi)}^2 + \|V_2\|_{H_0^2(0, a\pi)}^2) &\leq \|\mathcal{V}\|_{D_I}^2 \leq C(\|V_1\|_{H_0^1(0, a\pi)}^2 + \|V_2\|_{H_0^2(0, a\pi)}^2), \\ (c(\|V_1\|_{H_0^3(0, a\pi)}^2 + \|V_2\|_{H_0^4(0, a\pi)}^2) &\leq \|\mathcal{V}\|_{\mathbb{D}_I}^2 \leq C(\|V_1\|_{H_0^3(0, a\pi)}^2 + \|V_2\|_{H_0^4(0, a\pi)}^2)) \end{aligned} \quad (2.5.2)$$

where  $(V_1, V_2)$  are associated to  $\mathcal{V}$  by expression (2.5.1).

*Proof.* Step 1. We start by showing the norm equivalences.

Take  $\mathcal{V} \in D_I$  (resp.  $\mathbb{D}_I$ ), then one has

$$e_{11}(\mathcal{V}) = -\frac{1}{a}\mathcal{V}_3, \quad e_{12}(\mathcal{V}) = e_{22}(\mathcal{V}) = 0.$$

Now, the 2D-Korn inequality gives (recall that  $\mathcal{V}_1 = \mathcal{V}_2 = 0$  on  $\Gamma_0$ )

$$\|\mathcal{V}_1\|_{H^1(\omega)}^2 + \|\mathcal{V}_2\|_{H^1(\omega)}^2 \leq C\|\mathcal{V}_3\|_{L^2(\omega)}^2.$$

Hence, we obtain

$$\|\mathcal{V}\|_{[H^1(\omega)]^2 \times L^2(\omega)}^2 = \|\mathcal{V}_1\|_{H^1(\omega)}^2 + \|\mathcal{V}_2\|_{H^1(\omega)}^2 + \|\mathcal{V}_3\|_{L^2(\omega)}^2 \leq C\|\mathcal{V}_3\|_{L^2(\omega)}^2 = C\|\mathcal{V}\|_{D_I}^2.$$

On the contrary, to estimate  $\|\cdot\|_{D_I}$  by  $\|\cdot\|_{[H^1(\omega)]^2 \times L^2(\omega)}$  from above, we can use Young's inequality such that

$$\begin{aligned} \|\mathcal{V}\|_{D_I}^2 &= \|\mathcal{V}_3\|_{L^2(\omega)}^2 = \int_{\omega} \mathcal{V}_3^2 ds' \\ &= \int_{\omega} \left[ \frac{1}{2} \left( \frac{\partial \mathcal{V}_1}{\partial s_1} + \frac{1}{a} \mathcal{V}_3 \right)^2 + \left( \frac{\partial \mathcal{V}_2}{\partial s_2} \right)^2 + \frac{1}{2} \left( \frac{\partial \mathcal{V}_1}{\partial s_2} + \frac{\partial \mathcal{V}_2}{\partial s_1} \right)^2 + \mathcal{V}_3^2 \right] ds' \\ &\leq \int_{\omega} \left[ \left( \frac{\partial \mathcal{V}_1}{\partial s_1} \right)^2 + \frac{1}{a^2} \mathcal{V}_3^2 + \left( \frac{\partial \mathcal{V}_2}{\partial s_2} \right)^2 + \left( \frac{\partial \mathcal{V}_1}{\partial s_2} \right)^2 + \left( \frac{\partial \mathcal{V}_2}{\partial s_1} \right)^2 + \mathcal{V}_3^2 \right] ds' \\ &\leq C \left( \|\mathcal{V}_1\|_{H^1(\omega)}^2 + \|\mathcal{V}_2\|_{H^1(\omega)}^2 + \|\mathcal{V}_3\|_{L^2(\omega)}^2 \right) \\ &= C\|\mathcal{V}\|_{[H^1(\omega)]^2 \times L^2(\omega)}^2. \end{aligned}$$

For the equivalence of the norm  $\|\cdot\|_{\mathbb{D}_I}$  we use the same argumentation as above. The 2D-Korn inequality yields

$$\|\mathcal{V}\|_{[H^1(\omega)]^2 \times H^2(\omega)}^2 = \|\mathcal{V}_1\|_{H^1(\omega)}^2 + \|\mathcal{V}_2\|_{H^1(\omega)}^2 + \|\mathcal{V}_3\|_{H^2(\omega)}^2 \leq C'\|\mathcal{V}_3\|_{L^2(\omega)}^2 + \|\mathcal{V}_3\|_{H^2(\omega)}^2 \leq C\|\mathcal{V}\|_{\mathbb{D}_I}^2.$$

For the other direction we obtain

$$\begin{aligned}
\|\mathcal{V}\|_{\mathbb{D}_I}^2 &= \|\mathcal{V}_3\|_{H^2(\omega)}^2 = \langle \mathcal{V}_3, \mathcal{V}_3 \rangle_{L^2(\omega)} + \langle \nabla \mathcal{V}_3, \nabla \mathcal{V}_3 \rangle_{L^2(\omega)} + \langle D^2 \mathcal{V}_3, D^2 \mathcal{V}_3 \rangle_{L^2(\omega)} \\
&= \int_{\omega} \left[ \frac{1}{2} \left( \frac{\partial \mathcal{V}_1}{\partial s_1} + \frac{1}{a} \mathcal{V}_3 \right)^2 + \left( \frac{\partial \mathcal{V}_2}{\partial s_2} \right)^2 + \frac{1}{2} \left( \frac{\partial \mathcal{V}_1}{\partial s_2} + \frac{\partial \mathcal{V}_2}{\partial s_1} \right)^2 + \mathcal{V}_3^2 \right] ds' \\
&\quad + \langle \nabla \mathcal{V}_3, \nabla \mathcal{V}_3 \rangle_{L^2(\omega)} + \langle D^2 \mathcal{V}_3, D^2 \mathcal{V}_3 \rangle_{L^2(\omega)} \\
&\leq C \left( \|\mathcal{V}_1\|_{H^1(\omega)}^2 + \|\mathcal{V}_2\|_{H^1(\omega)}^2 + \|\mathcal{V}_3\|_{H^2(\omega)}^2 \right) \\
&= C \|\mathcal{V}\|_{[H^1(\omega)]^2 \times H^2(\omega)}^2.
\end{aligned}$$

Step 2. We prove the inequalities (2.5.2). With expression (2.5.1)<sub>3</sub> we obtain

$$\begin{aligned}
\|\mathcal{V}\|_{D_I}^2 &= \|\mathcal{V}_3\|_{L^2(\omega)}^2 = \int_{\omega} \mathcal{V}_3^2 ds_1 ds_2 \\
&= \int_{\omega} a^2 (s_2^c V_2''(s_1) - V_1'(s_1))^2 ds_1 ds_2 \\
&= a^2 \int_0^{a\pi} \int_0^l [(s_2^c V_2''(s_1))^2 - 2s_2^c V_2''(s_1) V_1'(s_1) + (V_1'(s_1))^2] ds_2 ds_1 \\
&= a^2 \int_0^{a\pi} \left[ \frac{l^3}{12} (V_2''(s_1))^2 + l (V_1'(s_1))^2 \right] ds_1 \\
&\leq C (\|V_2''\|_{L^2(0, a\pi)}^2 + \|V_1'\|_{L^2(0, a\pi)}^2) \\
&\leq C (\|V_2\|_{H^2(0, a\pi)}^2 + \|V_1\|_{H^1(0, a\pi)}^2).
\end{aligned}$$

First, note that  $V_2(s_1) = V_2'(s_1) = 0$  for  $s_1 \in \{0, a\pi\}$ , which follows by the expressions in (2.5.1) and since  $\mathcal{V}_1(0, s_2) = \mathcal{V}_1(a\pi, s_2) = \mathcal{V}_2(0, s_2) = \mathcal{V}_2(a\pi, s_2) = 0$  for a.e.  $s_2 \in (0, l)$ . Moreover, the Poincaré inequality in  $H_0^1(0, a\pi)$  and  $H_0^2(0, a\pi)$  yields

$$\begin{aligned}
\|V_2\|_{H^2(0, a\pi)}^2 + \|V_1\|_{H^1(0, a\pi)}^2 &\leq C (\|V_2''\|_{L^2(0, a\pi)}^2 + \|V_1'\|_{L^2(0, a\pi)}^2) \\
&\leq C \left( \frac{12}{l^3} \int_0^{a\pi} \frac{l^3}{12} (V_2'')^2 ds_1 + \frac{1}{l} \int_0^{a\pi} l (V_1')^2 ds_1 \right) \\
&\leq C \left( \int_0^{a\pi} \int_0^l (s_2^c V_2'')^2 ds_2 ds_1 + \int_0^{a\pi} \int_0^l (V_1')^2 ds_2 ds_1 \right) \\
&\leq C \int_{\omega} ((s_2^c V_2'')^2 - 2s_2^c V_2'' V_1' + (V_1')^2) ds' \\
&\leq C \int_{\omega} a^2 (s_2^c V_2'' - V_1')^2 ds' \\
&= C \|\mathcal{V}_3\|_{L^2(\omega)}^2 = C \|\mathcal{V}\|_{D_I}^2.
\end{aligned}$$

For the inequality (2.5.2)<sub>2</sub> we achieve again with the expressions for  $\mathcal{V}_3$  in (2.5.1)<sub>3</sub> that

$$\begin{aligned}
\|\mathcal{V}\|_{\mathbb{D}_I}^2 &= \|\mathcal{V}_3\|_{H^2(\omega)}^2 = \int_{\omega} \mathcal{V}_3^2 ds_1 ds_2 + \int_{\omega} \left[ \left( \frac{\partial \mathcal{V}_3}{\partial s_1} \right)^2 + \left( \frac{\partial \mathcal{V}_3}{\partial s_2} \right)^2 \right] ds_1 ds_2 \\
&\quad + \int_{\omega} \left[ \left( \frac{\partial^2 \mathcal{V}_3}{\partial s_1^2} \right)^2 + 2 \left( \frac{\partial^2 \mathcal{V}_3}{\partial s_1 \partial s_2} \right)^2 + \left( \frac{\partial^2 \mathcal{V}_3}{\partial s_2^2} \right)^2 \right] ds_1 ds_2 \\
&= \int_{\omega} [a^2 (s_2^c V_2''(s_1) - V_1'(s_1))^2 + a^2 (s_2^c V_2'''(s_1) - V_1''(s_1))^2 + (a V_2''(s_1))^2 \\
&\quad + a^2 (s_2^c V_2''''(s_1) - V_1'''(s_1))^2 + 2(a V_2''')^2] ds_1 ds_2 \\
&\leq C \int_0^{a\pi} [(V_2'')^2 + (V_1')^2 + (V_2''')^2 + (V_1'')^2 + (V_2'')^2 + (V_2''')^2 + (V_1''')^2 + (V_2''')^2] ds_1 \\
&\leq C (\|V_2\|_{H^4(0, a\pi)}^2 + \|V_1\|_{H^3(0, a\pi)}^2).
\end{aligned}$$

For the other direction we note that we can use the Poincaré inequality as described above such that we obtain

$$\|V_2\|_{H^4(0,a\pi)}^2 + \|V_1\|_{H^3(0,a\pi)}^2 \leq C \left( \|V_2''\|_{H^2(0,a\pi)}^2 + \|V_1'\|_{H^2(0,a\pi)}^2 \right)$$

Hence, we get

$$\begin{aligned} \|V_2''\|_{H^2(0,a\pi)}^2 + \|V_1'\|_{H^2(0,a\pi)}^2 &\leq \int_0^{a\pi} [(V_2''(s_1))^2 + (V_2'''(s_1))^2 + (V_2''''(s_1))^2 \\ &\quad + (V_1'(s_1))^2 + (V_1''(s_1))^2 + (V_1'''(s_1))^2] ds_1 \\ &\leq C \int_{\omega} [a^2(s_2^c V_2''(s_1) - V_1'(s_1))^2 + a^2(s_2^c V_2'''(s_1) - V_1''(s_1))^2 \\ &\quad + (a V_2''(s_1))^2 + a^2(s_2^c V_2''''(s_1) - V_1'''(s_1))^2 + 2(a V_2''')^2] ds_1 ds_2 \\ &= C \|\mathcal{V}_3\|_{H^2(\omega)}^2 = C \|\mathcal{V}\|_{\mathbb{D}_I}^2, \end{aligned}$$

which concludes the proof.  $\square$

### 2.5.2 Extensional displacements

Denote with  $D_E$  the orthogonal complement of  $D_I$  in  $\mathbb{H}$  w.r.t. the scalar product of  $\mathbb{H}$ . For every  $\phi$  in  $L^2(\omega)$ , set

$$\begin{aligned} \mathcal{M}_2(\phi)(s_1) &= \frac{1}{l} \int_0^l \phi(s_1, s_2) ds_2, \quad \text{for a.e. } s_1 \in (0, a\pi), \\ \mathcal{M}_2^c(\phi)(s_1) &= \frac{1}{l} \int_0^l \phi(s_1, s_2) s_2^c ds_2, \quad \text{for a.e. } s_1 \in (0, a\pi). \end{aligned}$$

Note that for every  $\mathcal{U} \in D_E$ , one has  $\mathcal{M}_2(\mathcal{U}_\alpha), \mathcal{M}_2^c(\mathcal{U}_\alpha) \in H_0^1(0, a\pi)$  while  $\mathcal{M}_2(\mathcal{U}_3), \mathcal{M}_2^c(\mathcal{U}_3) \in L^2(0, a\pi)$  ( $\alpha \in \{1, 2\}$ ).

Let  $\mathcal{U}$  be in  $D_E$ , then it satisfies

$$\langle \mathcal{U}, \mathcal{V} \rangle = \int_{\omega} \mathcal{U}_3 \mathcal{V}_3 ds_1 ds_2, \quad \forall \mathcal{V} \in D_I.$$

Thus, we have to fulfill

$$\int_{\omega} \mathcal{U}_3(s_1, s_2) (s_2^c V_2''(s_1) - V_1'(s_1)) ds_1 ds_2 = 0, \quad \forall V_1 \in H_0^1(0, a\pi), \quad \forall V_2 \in H_0^2(0, a\pi),$$

where we used the expression for  $\mathcal{V}_3$  from (2.5.1)<sub>3</sub>. This yields the two conditions that

$$\begin{aligned} \int_0^{a\pi} \mathcal{M}_2^c(\mathcal{U}_3)(s_1) V_2'' ds_1 &= 0, \quad \forall V_2 \in H_0^2(0, a\pi), \\ \int_0^{a\pi} \mathcal{M}_2(\mathcal{U}_3)(s_1) V_1' ds_1 &= 0, \quad \forall V_1 \in H_0^1(0, a\pi). \end{aligned}$$

By partial integration and the properties of  $V_1$  and  $V_2$  we obtain

$$\begin{aligned} \int_0^{a\pi} \frac{d^2 \mathcal{M}_2^c(\mathcal{U}_3)(s_1)}{ds_1^2} V_2 ds_1 &= 0, \quad \forall V_2 \in H_0^2(0, a\pi), \\ \int_0^{a\pi} \frac{d \mathcal{M}_2(\mathcal{U}_3)(s_1)}{ds_1} V_1 ds_1 &= 0, \quad \forall V_1 \in H_0^1(0, a\pi). \end{aligned}$$

Therefore,

$$\begin{aligned} \mathcal{M}_2(\mathcal{U}_3)(s_1) &= C_1, & \mathcal{M}_2^c(\mathcal{U}_3)(s_1) &= C_2 s_1^c + C_3, \\ (C_1, C_2, C_3) &\in \mathbb{R}^3, & \text{for a.e. } s_1 &\in (0, a\pi). \end{aligned} \quad (2.5.3)$$

Hence,

$$D_E = \left\{ \mathcal{U} \in \mathbb{H} \mid \frac{d\mathcal{M}_2(\mathcal{U}_3)}{ds_1} = \frac{d^2 \mathcal{M}_2^c(\mathcal{U}_3)}{ds_1^2} = 0 \quad \text{in } (0, a\pi) \right\}.$$

We equip  $D_E$  with the norm

$$\|\Phi\|_E = \sqrt{\int_{\omega} \left[ \frac{1}{2} \left| \frac{\partial \Phi_1}{\partial s_1} + \frac{1}{a} \Phi_3 \right|^2 + \left| \frac{\partial \Phi_2}{\partial s_2} \right|^2 + \frac{1}{2} \left| \frac{\partial \Phi_1}{\partial s_2} + \frac{\partial \Phi_2}{\partial s_1} \right|^2 \right] ds_1 ds_2}.$$

Note, that  $D_E$  is not a Hilbert space with this norm.  $\mathbb{D}_E$  denotes the completion of  $D_E$  w.r.t. this norm.

**Lemma 2.5.2** *For every  $\mathcal{U}$  in  $\mathbb{D}_E$ , one has*

$$\|\mathcal{U}_2\|_{H^1(0,l;L^2(0,a\pi))} + \|\mathcal{U}_1\|_{H^1(0,l;(H^1(0,a\pi))')} + \|\mathcal{U}_3\|_{L^2(0,l;(H^2(0,a\pi))')} \leq C \|\mathcal{U}\|_E. \quad (2.5.4)$$

*Proof.* Since  $\mathbb{D}_E$  is the completion of  $D_E$  for the norm  $\|\cdot\|_E$ , we can prove the estimates of the Lemma for  $\mathcal{U} \in D_E$ , then by density they will be satisfied for every element in  $\mathbb{D}_E$ .

Let  $\mathcal{U}$  be in  $D_E$ , recall that

$$\begin{aligned} \left\| \frac{\partial \mathcal{U}_1}{\partial s_1} + \frac{1}{a} \mathcal{U}_3 \right\|_{L^2(\omega)} &\leq \|\mathcal{U}\|_E, & \left\| \frac{\partial \mathcal{U}_2}{\partial s_2} \right\|_{L^2(\omega)} &\leq \|\mathcal{U}\|_E, \\ \left\| \frac{\partial \mathcal{U}_1}{\partial s_2} + \frac{\partial \mathcal{U}_2}{\partial s_1} \right\|_{L^2(\omega)} &\leq \|\mathcal{U}\|_E. \end{aligned} \quad (2.5.5)$$

Moreover, we also have that  $\mathcal{U}_3$  fulfills the properties from (2.5.3).

Step 1. In this step we prove

$$\begin{aligned} \|\mathcal{M}_2(\mathcal{U}_1)\|_{H^1(0,a\pi)} + \|\mathcal{M}_2^c(\mathcal{U}_1)\|_{H^1(0,a\pi)} + \|\mathcal{M}_2(\mathcal{U}_2)\|_{L^2(0,a\pi)} \\ + \|\mathcal{M}_2(\mathcal{U}_3)\|_{L^2(0,a\pi)} + \|\mathcal{M}_2^c(\mathcal{U}_3)\|_{L^2(0,a\pi)} \leq C \|\mathcal{U}\|_E. \end{aligned} \quad (2.5.6)$$

Set

$$\begin{aligned} \widetilde{\mathcal{M}}_2^c(\mathcal{U}_3)(s_1) &= C_2 \frac{s_1(s_1 - a\pi)}{2}, \\ \mathcal{M}_{22}(\mathcal{U}_2)(s_1) &= \frac{1}{l} \int_0^l \mathcal{U}_2(s_1, s_2) \frac{s_2(s_2 - l)}{2} ds_2, \end{aligned} \quad \text{for a.e. } s_1 \in (0, a\pi). \quad (2.5.7)$$

Hence, one has  $\widetilde{\mathcal{M}}_2^c(\mathcal{U}_3), \mathcal{M}_{22}(\mathcal{U}_2) \in H_0^1(0, a\pi)$ .

We first show that

$$\left\| \frac{d\mathcal{M}_2(\mathcal{U}_1)}{ds_1} + \frac{1}{a} \mathcal{M}_2(\mathcal{U}_3) \right\|_{L^2(0,a\pi)} \leq \frac{1}{\sqrt{l}} \|\mathcal{U}\|_E.$$

By plugging in the definition for  $\mathcal{M}_2(\mathcal{U}_i)$  we get

$$\left\| \frac{1}{l} \frac{d}{ds_1} \int_0^l \mathcal{U}_1(s_1, s_2) ds_2 + \frac{1}{al} \int_0^l \mathcal{U}_3(s_1, s_2) ds_2 \right\|_{L^2(0,a\pi)}.$$



We interchange differentiation and integration, such that with Jensen and (2.5.5)<sub>1</sub> we obtain

$$\left\| \frac{1}{l} \int_0^l \left( \frac{\partial \mathcal{U}_1}{\partial s_1} + \frac{1}{a} \mathcal{U}_3 \right) ds_2 \right\|_{L^2(0, a\pi)} \leq \frac{1}{\sqrt{l}} \left\| \frac{\partial \mathcal{U}_1}{\partial s_1} + \frac{1}{a} \mathcal{U}_3 \right\|_{L^2(\omega)} \leq \frac{1}{\sqrt{l}} \|\mathcal{U}\|_E.$$

Moreover, we have

$$\begin{aligned} \left\| \frac{d\mathcal{M}_2(\mathcal{U}_1)}{ds_1} \right\|_{L^2(0, a\pi)}^2 + \left\| \frac{1}{a} \mathcal{M}_2(\mathcal{U}_3) \right\|_{L^2(0, a\pi)}^2 &= \int_0^{a\pi} \left[ \left( \frac{d\mathcal{M}_2(\mathcal{U}_1)}{ds_1} \right)^2 + \left( \frac{1}{a} \mathcal{M}_2(\mathcal{U}_3) \right)^2 \right] ds_1 \\ &= \int_0^{a\pi} \left( \frac{d\mathcal{M}_2(\mathcal{U}_1)}{ds_1} + \frac{1}{a} \mathcal{M}_2(\mathcal{U}_3) \right)^2 ds_1 \\ &= \left\| \frac{d\mathcal{M}_2(\mathcal{U}_1)}{ds_1} + \frac{1}{a} \mathcal{M}_2(\mathcal{U}_3) \right\|_{L^2(0, a\pi)}^2, \end{aligned}$$

where we use for the second inequality the partial integration

$$\begin{aligned} &\int_0^{a\pi} \frac{d\mathcal{M}_2(\mathcal{U}_1)}{ds_1} \mathcal{M}_2(\mathcal{U}_3) ds_1 \\ &= \underbrace{\left[ \mathcal{M}_2(\mathcal{U}_1) \mathcal{M}_2(\mathcal{U}_3) \right]_0^{a\pi}}_{=0, \text{ because } \mathcal{M}_2(\mathcal{U}_1) \in H_0^1(0, a\pi)} - \int_0^{a\pi} \mathcal{M}_2(\mathcal{U}_1) \underbrace{\frac{d\mathcal{M}_2(\mathcal{U}_3)}{ds_1}}_{=0} ds_1 = 0. \end{aligned}$$

Therefore, we obtain

$$\left\| \frac{d\mathcal{M}_2(\mathcal{U}_1)}{ds_1} \right\|_{L^2(0, a\pi)}^2 + \left\| \frac{1}{a} \mathcal{M}_2(\mathcal{U}_3) \right\|_{L^2(0, a\pi)}^2 \leq C \|\mathcal{U}\|_E^2.$$

The Poincaré inequality in  $H_0^1(0, a\pi)$  and the previous results lead to

$$\|\mathcal{M}_2(\mathcal{U}_1)\|_{H^1(0, a\pi)} \leq C \left\| \frac{d\mathcal{M}_2(\mathcal{U}_1)}{ds_1} \right\|_{L^2(0, a\pi)} \leq C \|\mathcal{U}\|_E,$$

and since  $\mathcal{M}_2(\mathcal{U}_3)$  is independent of  $s_1$  we get

$$|\mathcal{M}_2(\mathcal{U}_3)| \leq C \|\mathcal{U}\|_E.$$

Below we show the inequality

$$\left\| \frac{d\mathcal{M}_2^c(\mathcal{U}_1)}{ds_1} + \frac{1}{a} \frac{d\widetilde{\mathcal{M}}_2^c(\mathcal{U}_3)}{ds_1} + \frac{C_3}{a} \right\|_{L^2(0, a\pi)} \leq C \|\mathcal{U}\|_E. \quad (2.5.8)$$

Plugging in the definition for  $\mathcal{M}_2^c$  and  $\widetilde{\mathcal{M}}_2^c$  we get with Jensen and for  $s_2^c \in (-l/2, l/2)$

$$\begin{aligned} &\left\| \frac{d\mathcal{M}_2^c(\mathcal{U}_1)}{ds_1} + \frac{1}{a} \frac{d\widetilde{\mathcal{M}}_2^c(\mathcal{U}_3)}{ds_1} + \frac{C_3}{a} \right\|_{L^2(0, a\pi)} \\ &= \left\| \frac{d}{ds_1} \frac{1}{l} \int_0^l \mathcal{U}_1 s_2^c ds_2 + \frac{1}{a} \frac{d}{ds_1} \left( C_2 \frac{s_1(s_1 - a\pi)}{2} \right) + \frac{C_3}{a} \right\|_{L^2(0, a\pi)} \\ &= \left\| \frac{1}{l} \int_0^l \frac{\partial \mathcal{U}_1}{\partial s_1} s_2^c ds_2 + \frac{1}{a} \underbrace{\left( C_2 \left( s_1 - \frac{a\pi}{2} \right) + C_3 \right)}_{\mathcal{M}_2^c(\mathcal{U}_3)} \right\|_{L^2(0, a\pi)} \\ &= \left\| \frac{1}{l} \int_0^l \left( \frac{\partial \mathcal{U}_1}{\partial s_1} + \frac{1}{a} \mathcal{U}_3 \right) s_2^c ds_2 \right\|_{L^2(0, a\pi)} \leq \left\| \frac{1}{\sqrt{l}} \left( \frac{\partial \mathcal{U}_1}{\partial s_1} + \frac{1}{a} \mathcal{U}_3 \right) s_2^c \right\|_{L^2(\omega)} \leq C \|\mathcal{U}\|_E. \end{aligned}$$

Now, we prove the inequality

$$\left\| \mathcal{M}_2^c(\mathcal{U}_1) + \frac{1}{a} \widetilde{\mathcal{M}}_2^c(\mathcal{U}_3) \right\|_{L^2(0, a\pi)}^2 + |C_3|^2 \leq C \|\mathcal{U}\|_E^2. \quad (2.5.9)$$

With the Poincaré inequality,  $C_3 \in \mathbb{R}$  and since  $\mathcal{M}_2^c(\mathcal{U}_1), \widetilde{\mathcal{M}}_2^c(\mathcal{U}_3) \in H_0^1(0, a\pi)$  we obtain

$$\begin{aligned} & \left\| \mathcal{M}_2^c(\mathcal{U}_1) + \frac{1}{a} \widetilde{\mathcal{M}}_2^c(\mathcal{U}_3) \right\|_{L^2(0, a\pi)}^2 + |C_3|^2 \\ & \leq C \left( \left\| \frac{d}{ds_1} \mathcal{M}_2^c(\mathcal{U}_1) + \frac{1}{a} \frac{d}{ds_1} \widetilde{\mathcal{M}}_2^c(\mathcal{U}_3) \right\|_{L^2(0, a\pi)}^2 + \left\| \frac{C_3}{a} \right\|_{L^2(0, a\pi)}^2 \right) \\ & = C \left\| \frac{d}{ds_1} \mathcal{M}_2^c(\mathcal{U}_1) + \frac{1}{a} \frac{d}{ds_1} \widetilde{\mathcal{M}}_2^c(\mathcal{U}_3) + \frac{C_3}{a} \right\|_{L^2(0, a\pi)}^2 \\ & \leq C \|\mathcal{U}\|_E, \end{aligned}$$

using

$$\int_0^{a\pi} \left( \frac{d}{ds_1} \mathcal{M}_2^c(\mathcal{U}_1) + \frac{1}{a} \frac{d}{ds_1} \widetilde{\mathcal{M}}_2^c(\mathcal{U}_3) \right) \frac{C_3}{a} ds_1 = 0.$$

In the following we prove the inequality

$$\left\| \frac{d\mathcal{M}_{22}(\mathcal{U}_2)}{ds_1} + \frac{1}{a} \widetilde{\mathcal{M}}_2^c(\mathcal{U}_3) \right\|_{L^2(0, a\pi)} \leq C \|\mathcal{U}\|_E. \quad (2.5.10)$$

With the previous result, partial integration and (2.5.5) we get

$$\begin{aligned} & \left\| \frac{d\mathcal{M}_{22}(\mathcal{U}_2)}{ds_1} + \frac{1}{a} \widetilde{\mathcal{M}}_2^c(\mathcal{U}_3) \right\|_{L^2(0, a\pi)} \\ & = \left\| \frac{d\mathcal{M}_{22}(\mathcal{U}_2)}{ds_1} - \mathcal{M}_2^c(\mathcal{U}_1) + \mathcal{M}_2^c(\mathcal{U}_1) + \frac{1}{a} \widetilde{\mathcal{M}}_2^c(\mathcal{U}_3) \right\|_{L^2(0, a\pi)} \\ & \leq \left\| \frac{d\mathcal{M}_{22}(\mathcal{U}_2)}{ds_1} - \mathcal{M}_2^c(\mathcal{U}_1) \right\| + \left\| \mathcal{M}_2^c(\mathcal{U}_1) + \frac{1}{a} \widetilde{\mathcal{M}}_2^c(\mathcal{U}_3) \right\|_{L^2(0, a\pi)}, \end{aligned}$$

where we estimate the first term by plugging in the definition and swapping integration with differentiation together with Jensen

$$\begin{aligned} & \left\| \frac{1}{l} \int_0^l \frac{\partial \mathcal{U}_2}{\partial s_1} \frac{s_2(s_2 - l)}{2} ds_2 - \frac{1}{l} \int_0^l \mathcal{U}_1(\cdot, s_2) (s_2 - \frac{l}{2}) ds_2 \right\|_{L^2(0, a\pi)} \\ & = \left\| \frac{1}{l} \int_0^l \frac{\partial \mathcal{U}_2}{\partial s_1} \frac{s_2(s_2 - l)}{2} ds_2 - \frac{1}{l} \left( \left[ \mathcal{U}_1 \frac{s_2(s_2 - l)}{2} \right]_0^l - \int_0^l \frac{\partial \mathcal{U}_1}{\partial s_2} \frac{s_2(s_2 - l)}{2} ds_2 \right) \right\|_{L^2(0, a\pi)} \\ & = \left\| \frac{1}{l} \int_0^l \left( \frac{\partial \mathcal{U}_2}{\partial s_1} + \frac{\partial \mathcal{U}_1}{\partial s_2} \right) \frac{s_2(s_2 - l)}{2} ds_2 \right\|_{L^2(0, a\pi)} \\ & \leq C \left\| \frac{\partial \mathcal{U}_2}{\partial s_1} + \frac{\partial \mathcal{U}_1}{\partial s_2} \right\|_{L^2(\omega)} \leq C \|\mathcal{U}\|_E. \end{aligned}$$

Integrating  $\frac{d\mathcal{M}_{22}(\mathcal{U}_2)}{ds_1} + \frac{1}{a} \widetilde{\mathcal{M}}_2^c(\mathcal{U}_3)$  over  $(0, a\pi)$  and due to the above estimate (2.5.10), one obtains

$$|C_2| \leq C \|\mathcal{U}\|_E$$

and then with again with (2.5.10) and (2.5.8)-(2.5.9)

$$\begin{aligned} & \|\widetilde{\mathcal{M}}_2^c(\mathcal{U}_3)\|_{L^2(0,a\pi)} + \|\mathcal{M}_2^c(\mathcal{U}_3)\|_{L^2(0,a\pi)} + \|\mathcal{M}_2^c(\mathcal{U}_1)\|_{H^1(0,a\pi)} \leq C\|\mathcal{U}\|_E, \\ & \left\| \frac{d\mathcal{M}_{22}(\mathcal{U}_2)}{ds_1} \right\|_{L^2(0,a\pi)} \leq C\|\mathcal{U}\|_E. \end{aligned}$$

Since  $\mathcal{M}_{22}(\mathcal{U}_2) \in H_0^1(0, a\pi)$  we get

$$\|\mathcal{M}_{22}(\mathcal{U}_2)\|_{L^2(0,a\pi)} \leq C \left\| \frac{d\mathcal{M}_{22}(\mathcal{U}_2)}{ds_1} \right\|_{L^2(0,a\pi)} \leq C\|\mathcal{U}\|_E.$$

The Poincaré-Wirtinger inequality gives together with (2.5.5)<sub>2</sub>

$$\|\mathcal{U}_2 - \mathcal{M}_2(\mathcal{U}_2)\|_{L^2(\omega)} \leq C\|\mathcal{U}\|_E. \quad (2.5.11)$$

Multiplying  $\mathcal{U}_2 - \mathcal{M}_2(\mathcal{U}_2)$  with  $\frac{s_2(s_2 - l)}{2}$  and then integrate with respect to  $s_2$  yields

$$\left\| \mathcal{M}_{22}(\mathcal{U}_2) + \frac{l^2}{12} \mathcal{M}_2(\mathcal{U}_2) \right\|_{L^2(0,a\pi)} \leq C\|\mathcal{U}\|_E.$$

Therefore,

$$\|\mathcal{M}_2(\mathcal{U}_2)\|_{L^2(0,a\pi)} \leq C\|\mathcal{U}\|_E. \quad (2.5.12)$$

Step 2. We show the 3 inequalities in equation (2.5.4) by using the Poincaré-Wirtinger inequality. We start with

$$\|\mathcal{U}_2\|_{L^2(\omega)} \leq C\|\mathcal{U}\|_E.$$

With the inequalities in (2.5.11)-(2.5.12) we get

$$\|\mathcal{U}_2\|_{L^2(\omega)} \leq \|\mathcal{U}_2 - \mathcal{M}_2(\mathcal{U}_2)\|_{L^2(\omega)} + \|\mathcal{M}_2(\mathcal{U}_2)\|_{L^2(\omega)} \leq C\|\mathcal{U}\|_E. \quad (2.5.13)$$

Recall that if  $X$  is a separable Hilbert space, then the Poincaré-Wirtinger inequality is valid in  $W^{1,p}(0, l; X)$  ( $p \in [1, +\infty]$ ). From (2.5.13) and (2.5.5)<sub>3</sub> we obtain

$$\left\| \frac{\partial \mathcal{U}_2}{\partial s_1} \right\|_{L^2(0,l;(H^1(0,a\pi))')} + \left\| \frac{\partial \mathcal{U}_1}{\partial s_2} \right\|_{L^2(0,l;(H^1(0,a\pi))')} \leq C\|\mathcal{U}\|_E.$$

Then the Poincaré-Wirtinger inequality and estimate (2.5.6)<sub>1</sub> in  $H^1(0, l; (H^1(0, a\pi))')$  gives

$$\begin{aligned} \|\mathcal{U}_1\|_{L^2(0,l;(H^1(0,a\pi))')} & \leq \|\mathcal{U}_1 - \mathcal{M}_2(\mathcal{U}_1)\|_{L^2(0,l;(H^1(0,a\pi))')} + \|\mathcal{M}_2(\mathcal{U}_1)\|_{L^2(0,l;(H^1(0,a\pi))')} \\ & \leq C\|\mathcal{U}\|_E. \end{aligned}$$

The above inequality leads to

$$\left\| \frac{\partial \mathcal{U}_1}{\partial s_1} \right\|_{L^2(0,l;(H^2(0,a\pi))')} \leq C\|\mathcal{U}\|_E,$$

which together with (2.5.5)<sub>1</sub> yields

$$\|\mathcal{U}_3\|_{L^2(0,l;(H^2(0,a\pi))')} \leq C\|\mathcal{U}\|_E.$$

This ends the proof of the Lemma.  $\square$

Now, consider the field  $\mathcal{U}_\varepsilon$ , the mid-surface displacement associated to  $u_\varepsilon$ , which belongs to  $\mathbb{H}$ . We decompose it as the sum of an inextensional displacement  $\mathcal{U}_{I,\varepsilon}$  and an extensional one  $\mathcal{U}_{E,\varepsilon}$ . By the definition of  $\|\cdot\|_E$  and Lemma 2.1.1 we obtain

$$\|\mathcal{U}_{E,\varepsilon}\|_E \leq \sum_{\alpha,\beta=1}^2 \left\| \frac{\partial \mathcal{U}_\varepsilon}{\partial s_\alpha} \cdot \mathbf{t}_\beta + \frac{\partial \mathcal{U}_\varepsilon}{\partial s_\beta} \cdot \mathbf{t}_\alpha \right\|_{L^2(\omega)} \leq C\varepsilon.$$

**Lemma 2.5.3** *There exists a subsequence of  $\{\varepsilon\}$  (still denoted  $\{\varepsilon\}$ ) and  $\mathcal{U}_E \in \mathbb{D}_E$  such that*

$$\begin{aligned} \frac{1}{\varepsilon} \mathcal{U}_{E,\varepsilon,1} &\rightharpoonup \mathcal{U}_{E,1} && \text{weakly in } H^1(0,l; (H^1(0,a\pi))') \\ \frac{1}{\varepsilon} \mathcal{U}_{E,\varepsilon,2} &\rightharpoonup \mathcal{U}_{E,2} && \text{weakly in } H^1(0,l; L^2(0,a\pi)) \\ \frac{1}{\varepsilon} \mathcal{U}_{E,\varepsilon,3} &\rightharpoonup \mathcal{U}_{E,3} && \text{weakly in } L^2(0,l; (H^2(0,a\pi))'). \end{aligned}$$

*Proof.* From Lemma 2.5.2, one has

$$\|\mathcal{U}_{E,\varepsilon,1}\|_{H^1(0,l;(H^1(0,a\pi))')} + \|\mathcal{U}_{E,\varepsilon,2}\|_{H^1(0,l;L^2(0,a\pi))} + \|\mathcal{U}_{E,\varepsilon,3}\|_{L^2(0,l;(H^2(0,a\pi))')} \leq C\varepsilon,$$

which yields the claim.  $\square$

Going back to the expressions for  $\mathcal{Z}_{\alpha\beta}$  introduced in Lemma 2.3.1 and Proposition 2.4.1 we get with Lemma 2.5.3 that

$$\mathcal{Z}_{\alpha\beta} = \frac{1}{2} \left[ \frac{\partial \mathcal{U}_E}{\partial s_\alpha} \mathbf{t}_\beta + \frac{\partial \mathcal{U}_E}{\partial s_\beta} \mathbf{t}_\alpha \right].$$

## 2.6 The linear elasticity problem

Let  $a_{ijkl} \in L^\infty(Y)$ ,  $i, j, k, l \in \{1, 2, 3\}$  and it should satisfy both the symmetry condition

$$a_{ijkl}(y) = a_{jikl}(y) = a_{klij}(y), \quad \text{for a.e. } y \in Y \quad (2.6.1)$$

and the coercivity condition ( $c_0 > 0$ )

$$a_{ijkl}(y) \tau_{ij} \tau_{kl} \geq c_0 \tau_{ij} \tau_{ij}, \quad \text{for a.e. } y \in Y, \quad (2.6.2)$$

where  $\tau$  is any  $3 \times 3$  symmetric real matrix. The coefficients  $a_{ijkl}^\varepsilon$  of the Hooke's tensor for the shell with  $x = \Phi(s)$  are given by

$$a_{ijkl}^\varepsilon(x) = a_{ijkl} \left( \left\{ \frac{s'_i}{\varepsilon} \right\}, \frac{s_3}{\varepsilon} \right), \quad \text{for a.e. } x \in \Omega_\varepsilon. \quad (2.6.3)$$

The stress tensor is defined as

$$\sigma_{ij}^\varepsilon(v) = a_{ijkl}^\varepsilon e_{kl}(v), \quad \forall v \in V_\varepsilon. \quad (2.6.4)$$

For a given applied force  $f_\varepsilon$  the displacement  $u_\varepsilon$  of a shell is the solution to the linear elasticity problem

$$\begin{aligned} -\nabla_x \cdot (\sigma_x^\varepsilon(u_\varepsilon)) &= f_\varepsilon \text{ in } \mathcal{Q}_\varepsilon^* \\ u_\varepsilon &= 0 \text{ on } \Gamma_{0,\varepsilon}, \end{aligned} \quad (2.6.5)$$

in the strong form. The corresponding weak formulation is given by

$$\int_{Q_\varepsilon^*} \sigma_x^\varepsilon(u_\varepsilon) : e_x(v) dx = \int_{Q_\varepsilon^*} f_\varepsilon(x) v(x) dx, \quad (2.6.6)$$

where we can transform it to the reference domain obtaining

$$\begin{aligned} & \int_{\Omega_\varepsilon^*} \sigma^\varepsilon(u_\varepsilon) : e(v) \det(\mathbf{t}_1 + \frac{s_3}{a} \mathbf{t}_1 | \mathbf{t}_2 | \mathbf{n}) ds \\ &= \int_{\Omega_\varepsilon^*} f_\varepsilon(s) v(s) \det(\mathbf{t}_1 + \frac{s_3}{a} \mathbf{t}_1 | \mathbf{t}_2 | \mathbf{n}) ds. \end{aligned} \quad (2.6.7)$$

The  $\cdot$ -operator denotes the Frobenius scalar product.

### 2.6.1 Assumptions on the forces

We assume that the force is given by

$$f_\varepsilon(s_1, s_2, s_3) = \varepsilon^2 f(s_1, s_2) + \varepsilon F(s_1, s_2) + s_3 g(s_1, s_2), \quad \text{for a.e. } (s_1, s_2) \in \omega,$$

where  $f = f_1 \mathbf{t}_1 + f_2 \mathbf{t}_2 + f_3 \mathbf{n}$ ,  $(f_1, f_2, f_3) \in L^2(\omega)^3$  and  $g = g_1 \mathbf{t}_1 + g_2 \mathbf{t}_2$ ,  $(g_1, g_2) \in L^2(\omega)^2$ . The force  $F$  is chosen such that it only interacts with extensional displacements. First, in view of Lemma 2.5.2, we take

$$F_1 \in L^2(0, l; H^1(0, a\pi)), \quad F_2 \in L^2(\omega), \quad F_3 \in L^2(0, l; H^2(0, a\pi)).$$

Then let  $V_E \in \mathbb{D}_E$  and consider

$$\begin{aligned} \langle F, V_E \rangle &= \int_0^l \langle F_1, V_{E,1} \rangle_{H^1(0, a\pi), (H^1(0, a\pi))'} ds_2 + \int_\omega F_2 V_{E,2} ds_1 ds_2 \\ &\quad + \int_0^l \langle F_3, V_{E,3} \rangle_{H^2(0, a\pi), (H^2(0, a\pi))'} ds_2. \end{aligned}$$

Due to Lemma 2.5.2, one has for all  $V_E \in \mathbb{D}_E$  the inequality

$$|\langle F, V_E \rangle| \leq (\|F_1\|_{L^2(0, l; H^1(0, a\pi))} + \|F_2\|_{L^2(\omega)} + \|F_3\|_{L^2(0, l; H^2(0, a\pi))}) \|V_E\|_E. \quad (2.6.8)$$

Now recall that this field has to satisfy for all  $\mathcal{V} \in D_I$  that

$$\int_\omega F(s_1, s_2) \cdot \mathcal{V}(s_1, s_2) ds = 0.$$

Hence, for all  $(V_1, V_2) \in H_0^1(0, a\pi) \times H_0^2(0, a\pi)$

$$\int_\omega \begin{pmatrix} F_1(s_1, s_2) \\ F_2(s_1, s_2) \\ F_3(s_1, s_2) \end{pmatrix} \cdot \begin{pmatrix} -s_2^\varepsilon V_2'(s_1) + V_1(s_1) \\ V_2(s_1) \\ a(s_2^\varepsilon V_2''(s_1) - V_1'(s_1)) \end{pmatrix} ds = 0.$$

With partial integration and the boundary conditions for  $V_1$  and  $V_2$  we get

$$\int_\omega \left[ \left( \frac{\partial F_1}{\partial s_1} s_2^\varepsilon + F_2 + a \frac{\partial^2 F_3}{\partial s_1^2} s_2^\varepsilon \right) V_2 + \left( F_1 + a \frac{\partial F_3}{\partial s_1} \right) V_1 \right] ds_1 ds_2 = 0,$$

holds for all  $V_1 \in H_0^1(0, a\pi)$  and  $V_2 \in H_0^2(0, a\pi)$ . Therefore, the field  $F \in L^2(\omega)^3$  has to satisfy

$$\begin{aligned} & \mathcal{M}_2(F_1) + a \frac{d\mathcal{M}_2(F_3)}{ds_1} = 0 \\ \text{and} \quad & \frac{d\mathcal{M}_2^c(F_1)}{ds_1} + \mathcal{M}_2(F_2) + a \frac{d^2 \mathcal{M}_2^c(F_3)}{ds_1^2} = 0. \end{aligned} \quad (2.6.9)$$

**Remark 2.6.1** For instance take  $(\mathcal{F}_2, \mathcal{F}_3) \in L^2(0, a\pi) \times H^2(0, a\pi)$  and set

$$F(s_1, s_2) = s_2^c \left( -a \frac{d\mathcal{F}_3}{ds_1}(s_1) \mathbf{t}_1 + \mathcal{F}_2(s_1) \mathbf{t}_2 + \mathcal{F}_3(s_1) \mathbf{n} \right), \quad \text{for a.e. } (s_1, s_2) \in \omega.$$

In Lemma 2.9.2 we show that there exists a field  $\mathbf{F} \in L^2(\omega)^3$ , with  $\mathbf{F} = (\mathbf{F}_{11}, \mathbf{F}_{12}, \mathbf{F}_{22})$  such that

$$\langle F, V \rangle = \int_{\omega} (\mathbf{F}_{11} e_{11}(V) + \mathbf{F}_{12} e_{12}(V) + \mathbf{F}_{22} e_{22}(V)) ds_1 ds_2.$$

Taking the holes into account, we need an additional assumption on the forces  $F$ . We will check this in the proof of the Lemma below.

From now on, we assume that  $F$  satisfies (2.6.9) and moreover  $F \in H^1(\omega)^3$ .

**Lemma 2.6.1** One has

$$\begin{aligned} & \left| \frac{1}{2\kappa} \int_{Q_\varepsilon^*} f_\varepsilon \cdot u \, dx - \varepsilon^3 \left( \int_{\omega_\varepsilon^*} f \cdot \mathcal{U} \, ds_1 ds_2 + \frac{1}{\varepsilon} \int_{\omega_\varepsilon^*} F \cdot \mathcal{U}_E \, ds_1 ds_2 \right. \right. \\ & \quad \left. \left. + \frac{\kappa^2}{3a} \int_{\omega_\varepsilon^*} g_\alpha \mathcal{U}_\alpha \, ds_1 ds_2 + \frac{\kappa^2}{3} \int_{\omega_\varepsilon^*} g_\alpha \mathcal{R}_\alpha \, ds_1 ds_2 \right) \right| \\ & \leq C \varepsilon^{5/2} (\|f\|_{L^2(\omega)} + \|g\|_{L^2(\omega)} + \|F\|_{L^2(\omega)}) \|e(u)\|_{L^2(\Omega_\varepsilon^*)}. \end{aligned} \quad (2.6.10)$$

Furthermore

$$\left| \int_{Q_\varepsilon^*} f_\varepsilon \cdot u \, dx \right| \leq C \varepsilon^{3/2} (\|f\|_{L^2(\omega)} + \|g\|_{L^2(\omega)} + \|F_3\|_{L^2(0, L; H^2(0, a\pi))} + \|F\|_{H^1(\omega)}) \|e(u)\|_{L^2(\Omega_\varepsilon^*)}. \quad (2.6.11)$$

The constants do not depend on  $\varepsilon$ .

*Proof.* Using the decomposition of  $u$  we can write (see Remark 2.1.2)

$$\begin{aligned} \int_{Q_\varepsilon^*} f_\varepsilon \cdot u \, dx &= \int_{\Omega_\varepsilon^*} f_\varepsilon \cdot u \det(\mathbf{t}_1 + \frac{s_3}{a} \mathbf{t}_1 |\mathbf{t}_2| \mathbf{n}) \, ds \\ &= \varepsilon^3 2\kappa \int_{\omega_\varepsilon^*} f \cdot \mathcal{U} \, ds_1 ds_2 + 2\kappa \varepsilon^2 \int_{\omega_\varepsilon^*} F \cdot \mathcal{U}_E \, ds_1 ds_2 + \frac{2\varepsilon^3 \kappa^3}{3a} \int_{\omega_\varepsilon^*} g_\alpha \mathcal{U}_\alpha \, ds_1 ds_2 \\ & \quad + \frac{2\varepsilon^3 \kappa^3}{3} \int_{\omega_\varepsilon^*} g_\alpha \mathcal{R}_\alpha \, ds_1 ds_2 + \frac{2\varepsilon^4 \kappa^3}{3a} \int_{\omega_\varepsilon^*} F \cdot \mathcal{R} \, ds_1 ds_2 + \frac{2\varepsilon^5 \kappa^3}{3a} \int_{\omega_\varepsilon^*} f_\alpha \mathcal{R}_\alpha \, ds_1 ds_2 \\ & \quad + \int_{\Omega_\varepsilon^*} \frac{s_3^2}{a} g \cdot \bar{u} \, ds + \int_{\Omega_\varepsilon^*} \frac{\varepsilon}{a} s_3 F \cdot \bar{u} \, ds + \int_{\Omega_\varepsilon^*} \frac{s_3}{a} \varepsilon^2 f_3 \bar{u} \cdot \mathbf{n} \, ds. \end{aligned} \quad (2.6.12)$$

First, using the estimates (2.1.21)<sub>2</sub> and (2.1.24)<sub>2</sub> one gets

$$\begin{aligned} \left| \int_{\Omega_\varepsilon^*} \varepsilon s_3^2 g \cdot \bar{u} \, ds \right| &\leq C \varepsilon^{9/2} \|g\|_{L^2(\omega)} \|e(u)\|_{L^2(Q_\varepsilon^*)}, \\ \left| \int_{\Omega_\varepsilon^*} \varepsilon s_3 F \cdot \bar{u} \, ds \right| &\leq C \varepsilon^{7/2} \|F\|_{L^2(\omega)} \|e(u)\|_{L^2(Q_\varepsilon^*)}, \\ \left| \int_{\Omega_\varepsilon^*} \varepsilon^2 s_3 f_3 \bar{u} \cdot \mathbf{n} \, ds \right| &\leq C \varepsilon^{9/2} \|f\|_{L^2(\omega)} \|e(u)\|_{L^2(Q_\varepsilon^*)}, \\ \left| \int_{\omega_\varepsilon^*} \varepsilon^4 F \cdot \mathcal{R} \, ds_1 ds_2 \right| &\leq C \varepsilon^{5/2} \|F\|_{L^2(\omega)} \|e(u)\|_{L^2(Q_\varepsilon^*)}, \\ \left| \int_{\omega_\varepsilon^*} \varepsilon^5 f_\alpha \mathcal{R}_\alpha \, ds_1 ds_2 \right| &\leq C \varepsilon^{7/2} \|F\|_{L^2(\omega)} \|e(u)\|_{L^2(Q_\varepsilon^*)}. \end{aligned}$$

Hence, (2.6.10) is proved. For (2.6.11) note that (2.1.24)<sub>2</sub> also leads to

$$\begin{aligned} \left| \varepsilon^3 2\kappa \int_{\omega_\varepsilon^*} f \cdot \mathcal{U} \, ds_1 ds_2 + \frac{2\varepsilon^3 \kappa^3}{3a} \int_{\omega_\varepsilon^*} g_\alpha \mathcal{U}_\alpha \, ds_1 ds_2 + \frac{2\varepsilon^3 \kappa^3}{3} \int_{\omega_\varepsilon^*} g_\alpha \mathcal{R}_\alpha \, ds_1 ds_2 \right| \\ \leq C\varepsilon^{3/2} (\|f\|_{L^2(\omega)} + \|g\|_{L^2(\omega)}) \|e(u)\|_{L^2(\mathcal{Q}_\varepsilon^*)}. \end{aligned}$$

Now, it remains to estimate  $\int_{\omega_\varepsilon^*} F \cdot \mathcal{U}_E \, ds_1 ds_2$ . For every function  $\phi$  in  $L^1(\omega)$ , we denote

$$\mathcal{M}_\varepsilon(\phi)(s') = \frac{1}{\varepsilon^2 |Y'|} \int_{Y'} \phi \left( \varepsilon \left[ \frac{s'}{\varepsilon} \right]_{Y'} + \varepsilon z \right) dz_1 dz_2, \quad \text{for a.e. } s' \in \widehat{\omega}_\varepsilon.$$

The function  $\mathcal{M}_\varepsilon(\phi)$  belongs to  $L^1(\widehat{\omega}_\varepsilon)$  (see [15, 16] for the properties of the operator  $\mathcal{M}_\varepsilon$ ).

Recall that by (2.1.25), (2.1.24)<sub>2</sub>, Lemma 2.5.1 and the estimate (2.5.4) one has

$$\|\mathcal{U}\|_E \leq \frac{C}{\varepsilon^{1/2}} \|e(u)\|_{L^2(\Omega_\varepsilon^*)}, \quad \|\mathcal{U}_E\|_{H^1(\omega)} \leq \frac{C}{\varepsilon^{3/2}} \|e(u)\|_{L^2(\Omega_\varepsilon^*)}.$$

Moreover, we get with [16, Proposition 1.38 ]

$$\begin{aligned} \left| \int_{\widehat{\omega}_\varepsilon^*} F \cdot \mathcal{U}_E \, ds_1 ds_2 - \int_{\widehat{\omega}_\varepsilon^*} F \cdot \mathcal{M}_\varepsilon(\mathcal{U}_E) \, ds_1 ds_2 \right| &\leq C\varepsilon \|\nabla \mathcal{U}_E\|_{L^2(\omega)} \|F\|_{L^2(\omega)}, \\ \left| \int_{\widehat{\omega}_\varepsilon^*} F \cdot \mathcal{M}_\varepsilon(\mathcal{U}_E) \, ds_1 ds_2 - \int_{\widehat{\omega}_\varepsilon^*} \mathcal{M}_\varepsilon(F) \cdot \mathcal{M}_\varepsilon(\mathcal{U}_E) \, ds_1 ds_2 \right| &\leq C\varepsilon \|\mathcal{U}_E\|_{L^2(\omega)} \|\nabla F\|_{L^2(\omega)}. \end{aligned}$$

Hence,

$$\begin{aligned} \left| \int_{\widehat{\omega}_\varepsilon^*} F \cdot \mathcal{U}_E \, ds_1 ds_2 - \int_{\widehat{\omega}_\varepsilon^*} \mathcal{M}_\varepsilon(F) \cdot \mathcal{M}_\varepsilon(\mathcal{U}_E) \, ds_1 ds_2 \right| &\leq C\varepsilon \|\mathcal{U}_E\|_{H^1(\omega)} \|F\|_{H^1(\Omega)} \\ &\leq \frac{C}{\varepsilon^{1/2}} \|F\|_{H^1(\omega)} \|e(u)\|_{L^2(\mathcal{Q}_\varepsilon^*)}. \end{aligned}$$

Since  $\mathcal{M}_\varepsilon(F) \cdot \mathcal{M}_\varepsilon(\mathcal{U}_E)$  is constant on every  $\varepsilon$ -cell, we have

$$\int_{\widehat{\omega}_\varepsilon^*} \mathcal{M}_\varepsilon(F) \cdot \mathcal{M}_\varepsilon(\mathcal{U}_E) \, ds_1 ds_2 = \frac{|Y'^*|}{|Y'|} \int_{\widehat{\omega}_\varepsilon} \mathcal{M}_\varepsilon(F) \cdot \mathcal{M}_\varepsilon(\mathcal{U}_E) \, ds_1 ds_2.$$

Proceeding as above, one shows that

$$\left| \int_{\widehat{\omega}_\varepsilon} F \cdot \mathcal{U}_E \, ds_1 ds_2 - \int_{\widehat{\omega}_\varepsilon} \mathcal{M}_\varepsilon(F) \cdot \mathcal{M}_\varepsilon(\mathcal{U}_E) \, ds_1 ds_2 \right| \leq \frac{C}{\varepsilon^{1/2}} \|F\|_{H^1(\omega)} \|e(u)\|_{L^2(\mathcal{Q}_\varepsilon^*)}.$$

Summarizing the above estimates and using (2.6.8) gives (recall that there are no holes in  $\Lambda_\varepsilon$ )

$$\begin{aligned} \left| \int_{\omega_\varepsilon^*} F \cdot \mathcal{U}_E \, ds_1 ds_2 - \frac{|Y'^*|}{|Y'|} \int_{\omega} F \cdot \mathcal{U}_E \, ds_1 ds_2 \right| &\leq \frac{C}{\varepsilon^{1/2}} \|F\|_{H^1(\omega)} \|e(u)\|_{L^2(\Omega_\varepsilon^*)}, \\ \left| \int_{\omega} F \cdot \mathcal{U}_E \, ds_1 ds_2 \right| &\leq \frac{C}{\varepsilon^{1/2}} (\|F_3\|_{L^2(0,L;H^2(0,a\pi))} + \|F\|_{H^1(\omega)}) \|e(u)\|_{L^2(\Omega_\varepsilon^*)}, \end{aligned}$$

which leads to (2.6.11). □

Eventually, using  $u = u_\varepsilon$  as test function in 2.6.6 we obtain

$$\|e(u_\varepsilon)\|_{L^2(\Omega_\varepsilon)} \leq C\varepsilon^{3/2} (\|f\|_{L^2(\omega)} + \|g\|_{L^2(\omega)}).$$

## 2.7 Unfolded limit problems

For every  $(\mathcal{V}_E, \mathcal{V})$  in  $\mathbb{D}_E \times \mathbb{D}_I$  we define the symmetric tensor  $\mathcal{E}(\mathcal{V}_E, \mathcal{V})$  by

$$\mathcal{E}(\mathcal{V}_E, \mathcal{V}) = \begin{pmatrix} \mathcal{Z}_{11}(\mathcal{V}_E) - y_3 \Lambda_{11}(\mathcal{V}) & \mathcal{Z}_{12}(\mathcal{V}_E) - y_3 \Lambda_{12}(\mathcal{V}) & 0 \\ \mathcal{Z}_{12}(\mathcal{V}_E) - y_3 \Lambda_{12}(\mathcal{V}) & \mathcal{Z}_{22}(\mathcal{V}_E) - y_3 \Lambda_{22}(\mathcal{V}) & 0 \\ 0 & 0 & 0 \end{pmatrix}$$

with

$$\mathcal{Z}_{\alpha\beta}(\mathcal{V}_E) = \frac{1}{2} \left[ \frac{\partial \mathcal{V}_E}{\partial s_\alpha} \mathbf{t}_\beta + \frac{\partial \mathcal{V}_E}{\partial s_\beta} \mathbf{t}_\alpha \right]$$

and

$$\begin{aligned} \Lambda_{11}(\mathcal{V}) &= \frac{\partial^2 \mathcal{V}_3}{\partial s_1^2} - \frac{1}{a} \frac{\partial \mathcal{V}_1}{\partial s_1} = \frac{\partial}{\partial s_1} \left( \frac{\partial \mathcal{V}}{\partial s_1} \mathbf{n} \right), & \Lambda_{22}(\mathcal{V}) &= \frac{\partial^2 \mathcal{V}_3}{\partial s_2^2} = \frac{\partial}{\partial s_2} \left( \frac{\partial \mathcal{V}}{\partial s_2} \mathbf{n} \right), \\ \Lambda_{12}(\mathcal{V}) &= \frac{\partial^2 \mathcal{V}_3}{\partial s_1 \partial s_2} - \frac{1}{a} \frac{\partial \mathcal{V}_1}{\partial s_2} = \frac{\partial}{\partial s_2} \left( \frac{\partial \mathcal{V}}{\partial s_1} \mathbf{n} \right). \end{aligned}$$

Denote  $H_{per}^1(Y^*)$  the subspace of  $H^1(Y^*)$  containing the functions, which are  $\mathbf{G}$  periodic and

$$\mathbb{D} \doteq \mathbb{D}_I \times \mathbb{D}_E \times L^2(\Omega; H_{per}^1(Y^*))^3.$$

For every  $v = (\mathcal{V}_E, \mathcal{V}, \hat{v}) \in \mathbb{D}$  we consider the symmetric tensor

$$\mathcal{E}(\mathcal{V}_E, \mathcal{V}) + \mathcal{E}_y(\hat{v})$$

and the semi-norm

$$\|v\|_{\mathbb{D}} = \|\mathcal{E}(\mathcal{V}_E, \mathcal{V}) + \mathcal{E}_y(\hat{v})\|_{L^2(\omega \times Y^*)}.$$

**Lemma 2.7.1** *Given the expressions (2.3.8) for  $\mathcal{V} \in \mathbb{D}_I$ , there exist  $c, C \in \mathbb{R}_+$  such that*

$$c \|\mathcal{V}\|_{\mathbb{D}_I}^2 \leq \sum_{\alpha, \beta=1}^2 \|\Lambda_{\alpha\beta}(\mathcal{V})\|_{L^2(\omega)}^2 \leq C \|\mathcal{V}\|_{\mathbb{D}_I}^2.$$

*Proof.* First, one has

$$\sum_{\alpha, \beta=1}^2 \|\Lambda_{\alpha\beta}(\mathcal{V})\|_{L^2(\omega)}^2 \leq C (\|D_2 \mathcal{V}_3\|_{L^2(\omega)} + \|\nabla \mathcal{V}_1\|_{L^2(\omega)}).$$

This inequality and Lemma 2.5.1 give the inequality on the right-hand side.

We prove the left-hand side of the inequality by contradiction. We assume that there exists a sequence  $(\mathcal{V}_n)_{n \in \mathbb{N}}$  in  $\mathbb{D}_I$ , such that

$$\|\mathcal{V}_n\|_{\mathbb{D}_I} = 1, \quad \sum_{\alpha, \beta=1}^2 \|\Lambda_{\alpha\beta}(\mathcal{V}_n)\|_{L^2(\omega)}^2 \longrightarrow 0 \text{ as } n \rightarrow \infty.$$

By Lemma 2.5.1 and the expressions introduced in (2.5.1), we can also consider a sequence  $(V_{1,n}, V_{2,n})_{n \in \mathbb{N}}$  in  $H_0^3(0, a\pi) \times H_0^4(0, a\pi)$  with

$$\|V_{1,n}\|_{H_0^3(0, a\pi)}^2 + \|V_{2,n}\|_{H_0^4(0, a\pi)}^2 = 1$$



and the components  $\Lambda_{\alpha\beta}$  can be expressed as

$$\begin{aligned}\Lambda_{11}(\mathcal{V}_n) &= \frac{1}{a}(s_2^c V_{2,n}''(s_1) - V_{1,n}'(s_1)) + a(s_2^c V_{2,n}''''(s_1) - V_{1,n}'''), \\ \Lambda_{12}(\mathcal{V}_n) &= \frac{1}{a}V_{2,n}'(s_1) + aV_{2,n}''', \\ \Lambda_{22}(\mathcal{V}_n) &= 0.\end{aligned}\tag{2.7.1}$$

Furthermore, there exists  $(V_1, V_2) \in H_0^3(0, a\pi) \times H_0^4(0, a\pi)$  such that

$$(V_{1,n}, V_{2,n}) \rightharpoonup (V_1, V_2) \quad \text{weakly in } H_0^3(0, a\pi) \times H_0^4(0, a\pi).$$

By Sobolev embedding we get

$$(V_{1,n}, V_{2,n}) \longrightarrow (V_1, V_2) \quad \text{strongly in } H_0^2(0, a\pi) \times H_0^3(0, a\pi).$$

Moreover, since  $\|\Lambda_{\alpha\beta}(\mathcal{V}_n)\| \longrightarrow 0$  for  $(\alpha, \beta) \in \{(1, 1), (1, 2), (2, 2)\}$ , we have that

$$\begin{aligned}\frac{1}{a}(s_2^c V_2''(s_1) - V_1'(s_1)) + a(s_2^c V_2''''(s_1) - V_1''') &= 0, \\ \frac{1}{a}V_2'(s_1) + aV_2'''(s_1) &= 0.\end{aligned}\tag{2.7.2}$$

Solving the differential equations with the respective boundary conditions we obtain for (2.7.2)<sub>2</sub> that

$$V_2 = c_3 + c_2 \sin\left(\frac{s_1}{a}\right) + c_1 \cos\left(\frac{s_1}{a}\right).$$

Together with  $V_2(0) = V_2'(0) = V_2''(0) = 0$  we conclude that  $V_2 = 0$ . Plugging that result into (2.7.2)<sub>1</sub>, gives

$$\frac{1}{a}V_1'(s_1) + aV_1'''(s_1) = 0.$$

With the corresponding boundary condition this yields  $V_1 = 0$  and therefore that  $(V_{1,n}, V_{2,n})$  converges strongly to  $(0, 0)$  in  $H_0^2(0, a\pi) \times H_0^3(0, a\pi)$ .

Considering again equation (2.7.1) with our assumption that  $\|\Lambda_{11}(\mathcal{V}_n)\|_{L^2(\omega)} \longrightarrow 0$ , we also get  $(V_{1,n}, V_{2,n}) \longrightarrow (0, 0)$  strongly in  $L^2(0, a\pi) \times L^2(0, a\pi)$ .

Then the convergence  $(V_{1,n}, V_{2,n}) \longrightarrow (0, 0)$  strongly in  $H_0^3(0, a\pi) \times H_0^4(0, a\pi)$ , which contradicts the fact that  $\|V_1\|_{H_0^3(0, a\pi)}^2 + \|V_2\|_{H_0^4(0, a\pi)}^2 = 1$ , coming from the assumption  $\|V_{1,n}\|_{H_0^3(0, a\pi)}^2 + \|V_{2,n}\|_{H_0^4(0, a\pi)}^2 = 1$  for all  $n \in \mathbb{N}$ .  $\square$

We define

$$H_{per,0}^1(Y^*)^3 = \{\psi \in H_{per}^1(Y^*)^3 \mid \psi = 0 \text{ on } \partial Y^*\}.$$

**Lemma 2.7.2** *Consider the space  $\mathbb{S} \doteq \mathbb{R}^3 \times \mathbb{R}^3 \times H_{per,0}^1(Y^*)^3$ . Then*

$$\begin{aligned}\|(\tau_A, \tau_B, \hat{w})\|_{\mathbb{S}}^2 &= \sum_{\substack{\alpha, \beta=1 \\ \alpha \leq \beta}}^2 \|\tau_A^{\alpha\beta} + y_3 \tau_B^{\alpha\beta} + e_{\alpha\beta, y}(\hat{w})\|_{L^2(Y^*)}^2 \\ &\quad + \|e_{13, y}(\hat{w})\|_{L^2(Y^*)}^2 + \|e_{23, y}(\hat{w})\|_{L^2(Y^*)}^2 + \|e_{33, y}(\hat{w})\|_{L^2(Y^*)}^2.\end{aligned}$$

*defines a norm on  $\mathbb{S}$  equivalent to the product-norm.*

*Proof.* We introduce the field  $\Phi \in H^1(\mathbb{R}^3)^3$  given by

$$\begin{aligned}\Phi_1(y) &= y_1 \left( \tau_A^{11} + y_3 \tau_B^{11} \right) + y_2 \left( \tau_A^{12} + y_3 \tau_B^{12} \right) \\ \Phi_2(y) &= y_2 \left( \tau_A^{22} + y_3 \tau_B^{22} \right) + y_1 \left( \tau_A^{12} + y_3 \tau_B^{12} \right) \\ \Phi_3(y) &= - \left[ \frac{(y_1)^2}{2} \tau_B^{11} + \frac{(y_2)^2}{2} \tau_B^{22} + y_2 y_1 \tau_B^{12} \right].\end{aligned}$$

Hence, we have

$$\|(\tau_A, \tau_B, \hat{w})\|_{\mathbb{S}} = \|\mathcal{E}_y(\Phi + \hat{w})\|_{L^2(Y^*)^{3 \times 3}}.$$

We will show now that  $\|\mathcal{E}_y(\Phi + \hat{w})\|_{L^2(Y^*)^{3 \times 3}} = 0$  implies that  $\Phi = 0$  and  $\hat{w} = 0$ .

Consider the case  $\mathcal{E}_y(\Phi + \hat{w}) = 0$ , which yields that  $\Phi + \hat{w}$  is a rigid displacement. Hence, there exist  $a, b \in \mathbb{R}^3$  such that

$$\Phi + \hat{w} = r, \quad \text{with } r(y) = \begin{pmatrix} a_1 + b_2 y_3 - b_3 y_2 \\ a_2 + b_3 y_1 - b_1 y_3 \\ a_3 + b_1 y_2 - b_2 y_1 \end{pmatrix}.$$

Since,  $\hat{w}$  is a periodic function with periods  $\mathbf{p}_1, \mathbf{p}_2$ , one has  $(\Phi - r)(y + \mathbf{p}_i) = (\Phi - r)(y)$  for a.e.  $y \in (\mathbb{R}^2 \setminus \bigcup_{\xi \in \mathbf{G}} (\xi + \bar{S})) \times (-\kappa, \kappa)$ . The two first components yield the equations

$$\begin{aligned}\tau_A^{11} + y_3 \tau_B^{11} &= 0, & \tau_A^{12} + y_3 \tau_B^{12} &= -b_3, \\ \tau_A^{22} + y_3 \tau_B^{22} &= 0, & \tau_A^{12} + y_3 \tau_B^{12} &= b_3,\end{aligned} \quad \text{for a.e. } y_3 \in (-\kappa, \kappa).$$

Therefore, we obtain  $\tau_A^{11} = \tau_B^{11} = \tau_A^{22} = \tau_B^{22} = \tau_A^{12} = \tau_B^{12} = 0$  and  $b_3 = 0$ . Now, the equality of the third component gives  $b_1 = b_2 = 0$ . Hence, we conclude that  $\Phi = 0$  and that  $r$  is a constant displacement. Moreover, since  $\hat{w} \in H_{per,0}^1(Y^*)^3$  the displacement  $r = 0$  and therefore  $\hat{w} = 0$ , which proves that  $\|\cdot\|_{\mathbb{S}}$  is a norm.

The proof that there exists a constant  $C > 0$  such that

$$C(|\tau_A| + |\tau_B| + \|\hat{w}\|_{H^1(Y^*)}) \leq \|(\tau_A, \tau_B, \hat{w})\|_{\mathbb{S}}, \quad \forall (\tau_A, \tau_B, \hat{w}) \in \mathbb{S},$$

is easily done by contradiction. □

**Lemma 2.7.3** *The semi-norm  $\|\cdot\|_{\mathbb{D}}$  is a norm equivalent to the product-norm of  $\mathbb{D}_I \times \mathbb{D}_E \times L^2(\Omega; H_{per}^1(Y^*))^3$ .*

*Proof.* By the definition of  $\|\cdot\|_{\mathbb{D}_I}$ , we get that

$$\begin{aligned}\|v\|_{\mathbb{D}}^2 &= \sum_{\alpha, \beta=1}^2 \|\mathcal{Z}_{\alpha\beta}(\mathcal{V}_E) - y_3 \Lambda_{\alpha\beta}(\mathcal{V}) + e_{\alpha\beta, y}(\hat{v})\|_{L^2(\omega \times Y^*)}^2 \\ &\quad + 2\|e_{13, y}(\hat{v})\|_{L^2(\omega \times Y^*)}^2 + 2\|e_{23, y}(\hat{v})\|_{L^2(\omega \times Y^*)}^2 + 2\|e_{33, y}(\hat{v})\|_{L^2(\omega \times Y^*)}^2.\end{aligned}$$

Furthermore, note that we have

$$\begin{aligned}\|\mathcal{E}(\mathcal{V}_E, \mathcal{V})\|_{L^2(\Omega)}^2 &= \sum_{\alpha, \beta=1}^2 \int_{\Omega} (Z_{\alpha\beta}(\mathcal{V}_E) + y_3 \Lambda_{\alpha\beta}(\mathcal{V}))^2 ds \\ &= \sum_{\alpha, \beta=1}^2 \int_{\Omega} Z_{\alpha\beta}(\mathcal{V}_E)^2 + (y_3 \Lambda_{\alpha\beta}(\mathcal{V}))^2 ds \\ &= 2\kappa \sum_{\alpha, \beta=1}^2 \|\mathcal{Z}_{\alpha\beta}(\mathcal{V}_E)\|_{L^2(\omega)}^2 + \frac{2\kappa^3}{3} \sum_{\alpha, \beta=1}^2 \|\Lambda_{\alpha\beta}(\mathcal{V})\|_{L^2(\omega)}^2.\end{aligned}$$

With Lemma 2.7.2 and the equivalence of norms we obtain that

$$\begin{aligned} c \left( \sum_{\alpha, \beta=1}^2 \|\mathcal{Z}_{\alpha\beta}(\mathcal{V}_E)\|_{L^2(\omega)} + \sum_{\alpha, \beta=1}^2 \|\Lambda_{\alpha\beta}(\mathcal{V})\|_{L^2(\omega)} + \|\widehat{v}\|_{L^2(\omega \times Y^*)} \right) &\leq \|\mathcal{V}\|_{\mathbb{D}_I} \\ &\leq C \left( \sum_{\alpha, \beta=1}^2 \|\mathcal{Z}_{\alpha\beta}(\mathcal{V}_E)\|_{L^2(\omega)} + \sum_{\alpha, \beta=1}^2 \|\Lambda_{\alpha\beta}(\mathcal{V})\|_{L^2(\omega)} + \|\widehat{v}\|_{L^2(\omega \times Y^*)} \right). \end{aligned}$$

Moreover, we get that  $\sum_{\alpha, \beta=1}^2 \|\mathcal{Z}_{\alpha\beta}(\mathcal{V}_E)\|_{L^2(\omega)}^2 = \|\mathcal{V}_E\|_E^2$ .

Besides, Lemma 2.7.1 yields

$$c\|\mathcal{V}\|_{\mathbb{D}_I}^2 \leq \sum_{\alpha, \beta=1}^2 \|\Lambda_{\alpha\beta}(\mathcal{V})\|_{L^2(\omega)}^2 \leq C\|\mathcal{V}\|_{\mathbb{D}_I}^2.$$

Finally, we conclude

$$c \left( \|\mathcal{V}_E\|_E + \|\mathcal{V}\|_{\mathbb{D}_I} + \|\widehat{v}\|_{L^2(\omega \times Y^*)} \right) \leq \|v\|_{\mathbb{D}} \leq C \left( \|\mathcal{V}_E\|_E + \|\mathcal{V}\|_{\mathbb{D}_I} + \|\widehat{v}\|_{L^2(\omega \times Y^*)} \right).$$

□

**Theorem 2.7.1** *Let  $u_\varepsilon$  be the solution of the elasticity problem (2.6.6). Then the following convergence holds:*

$$\frac{1}{\varepsilon} \Pi_\varepsilon(e(u_\varepsilon)) \rightarrow \mathcal{E}(\mathcal{U}_E, \mathcal{U}) + \mathcal{E}_y(\widehat{u}) \quad \text{strongly in } L^2(\omega \times Y^*)^9, \quad (2.7.3)$$

where  $(\mathcal{U}_E, \mathcal{U}, \widehat{u}) \in \mathbb{D}$  is the unique solution of the rescaled and unfolded problem

$$\begin{aligned} \frac{1}{2\kappa} \int_{\omega \times Y^*} a_{ijkl} \left( \mathcal{E}_{ij}(\mathcal{U}_E, \mathcal{U}) + \mathcal{E}_{y,ij}(\widehat{u}) \right) \left( \mathcal{E}_{kl}(\mathcal{V}_E, \mathcal{V}) + \mathcal{E}_{y,kl}(\widehat{v}) \right) ds' dy \\ = |Y'^*| \int_{\omega} \left( f \cdot \mathcal{V} + \frac{\kappa^2}{3a} g_\alpha \mathcal{V}_\alpha - \frac{\kappa^2}{3} g_\alpha \frac{\partial \mathcal{V}}{\partial s_\alpha} \mathbf{n} \right) ds', \quad \forall (\mathcal{V}_E, \mathcal{V}, \widehat{v}) \in \mathbb{D}. \end{aligned} \quad (2.7.4)$$

*Proof.* Take  $v = (\mathcal{V}_E, \mathcal{V}, \widehat{v})$  such that

$$\mathcal{V}_E \in \mathcal{C}^1(\overline{\omega})^3 \cap \mathbb{D}_E, \quad \mathcal{V} \in \mathcal{C}^2(\overline{\omega})^3 \cap \mathbb{D}_I,$$

and consider the test function  $v_\varepsilon = v_\varepsilon^1 + v_\varepsilon^2$ , where

$$\begin{aligned} v_\varepsilon^1(s) &= \mathcal{V}(s') + \varepsilon \mathcal{V}_E(s') - s_3 \left[ \frac{\partial(\mathcal{V} + \varepsilon \mathcal{V}_E)}{\partial s_\alpha}(s') \cdot \mathbf{n}(s') \right] \mathbf{t}_\alpha(s'), \\ v_\varepsilon^2(s) &= \varepsilon^2 \widehat{v} \left( s', \left\{ \frac{s}{\varepsilon} \right\} \right), \end{aligned} \quad \text{for a.e. } s \in \Omega_\varepsilon,$$

with  $\widehat{v} \in \mathcal{C}^1(\overline{\omega}; H_{per}^1(Y^*)^3)$  satisfying  $\widehat{v}(0, s_2, y) = \widehat{v}(a\pi, s_2, y)$  for a.e.  $(s_2, y) \in (0, L) \times Y^*$ . We only calculate the elements  $e_{12}(v_\varepsilon^1)$  and  $e_{13}(v_\varepsilon^1)$ , since the rest follows in a similar way. We obtain

$$\begin{aligned} e_{12}(v_\varepsilon^1) &= \frac{1}{2} \left[ \frac{a}{a + s_3} \frac{\partial v_\varepsilon^1}{\partial s_1} \mathbf{t}_2 + \frac{\partial v_\varepsilon^1}{\partial s_2} \mathbf{t}_1 \right] = \frac{1}{2} \frac{a}{a + s_3} \left[ \frac{\partial v_\varepsilon^1}{\partial s_1} \mathbf{t}_2 + \left( 1 + \frac{s_3}{a} \right) \frac{\partial v_\varepsilon^1}{\partial s_2} \mathbf{t}_1 \right] \\ &= \frac{1}{2} \frac{a}{a + s_3} \left[ \frac{\partial \mathcal{V}_2}{\partial s_1} + \varepsilon \frac{\partial \mathcal{V}_{E,2}}{\partial s_1} - s_3 \left( \frac{\partial^2 \mathcal{V}_3}{\partial s_1 \partial s_2} + \varepsilon \frac{\partial^2 \mathcal{V}_{E,3}}{\partial s_1 \partial s_2} \right) + \left( 1 + \frac{s_3}{a} \right) \left( \frac{\partial \mathcal{V}_1}{\partial s_2} + \varepsilon \frac{\partial \mathcal{V}_{E,1}}{\partial s_2} \right) \right. \\ &\quad \left. - \left( s_3 + \frac{s_3^2}{a} \right) \left( \frac{\partial^2 \mathcal{V}_3}{\partial s_1 \partial s_2} - \frac{1}{a} \frac{\partial \mathcal{V}_1}{\partial s_2} + \varepsilon \left( \frac{\partial^2 \mathcal{V}_{E,3}}{\partial s_1 \partial s_2} - \frac{1}{a} \frac{\partial \mathcal{V}_{E,1}}{\partial s_2} \right) \right) \right]. \end{aligned}$$

Applying the rescaling-unfolding operator  $\Pi_\varepsilon$  and dividing by  $\varepsilon$  yields together with the properties for  $\mathbb{D}_I$  that

$$\begin{aligned} \frac{1}{\varepsilon} \Pi_\varepsilon(e_{12}(v_\varepsilon^1)) &= \frac{1}{2} \frac{a}{a + \varepsilon y_3} \left[ \left( \frac{\partial \mathcal{V}_{E,2}}{\partial s_1} + \frac{\partial \mathcal{V}_{E,1}}{\partial s_2} \right) - 2y_3 \frac{\partial^2 \mathcal{V}_3}{\partial s_1 \partial s_2} + 2 \frac{y_3}{a} \frac{\partial \mathcal{V}_1}{\partial s_2} + \frac{\varepsilon y_3}{a} \frac{\partial \mathcal{V}_{E,1}}{\partial s_2} \right. \\ &\quad \left. - \frac{\varepsilon y_3}{a} \frac{\partial^2 \mathcal{V}_3}{\partial s_1 \partial s_2} + \frac{\varepsilon y_3}{a} \frac{\partial \mathcal{V}_1}{\partial s_2} - \varepsilon y_3 \frac{\partial^2 \mathcal{V}_{E,3}}{\partial s_1 \partial s_2} - \left( \varepsilon + \frac{\varepsilon^2}{a} \right) \left( \frac{\partial^2 \mathcal{V}_{E,3}}{\partial s_1 \partial s_2} - \frac{1}{a} \frac{\partial \mathcal{V}_{E,1}}{\partial s_2} \right) \right] \\ &\longrightarrow \frac{1}{2} \mathcal{Z}_{12}(\mathcal{V}_E) - y_3 \left( \frac{\partial^2 \mathcal{V}_3}{\partial s_1 \partial s_2} - \frac{\partial \mathcal{V}_1}{\partial s_2} \right) \quad \text{strongly in } L^2(\omega \times Y^*). \end{aligned}$$

For  $e_{13}(v_\varepsilon^1)$  we then obtain

$$\begin{aligned} e_{13}(v_\varepsilon^1) &= \frac{1}{2} \left[ \frac{a}{a + s_3} \frac{\partial v_\varepsilon^1}{\partial s_1} \mathbf{n} + \frac{\partial v_\varepsilon^1}{\partial s_3} \mathbf{t}_1 \right] = \frac{1}{2} \frac{a}{a + s_3} \left[ \frac{\partial v_\varepsilon^1}{\partial s_1} \mathbf{n} + \left( 1 + \frac{s_3}{a} \right) \frac{\partial v_\varepsilon^1}{\partial s_3} \mathbf{t}_1 \right] \\ &= \frac{1}{2} \frac{a}{a + s_3} \left[ \left( \frac{\partial \mathcal{V}_3}{\partial s_1} - \frac{1}{a} \mathcal{V}_1 \right) + \varepsilon \left( \frac{\partial \mathcal{V}_{E,3}}{\partial s_1} - \frac{1}{a} \mathcal{V}_1 \right) + \frac{s_3}{a} \left( \frac{\partial \mathcal{V}_3}{\partial s_1} - \frac{1}{a} \mathcal{V}_1 \right) \right. \\ &\quad \left. + \frac{s_3 \varepsilon}{a} \left( \frac{\partial \mathcal{V}_{E,3}}{\partial s_1} - \frac{1}{a} \mathcal{V}_1 \right) + \left( 1 + \frac{s_3}{a} \right) \left( - \left( \frac{\partial \mathcal{V}_3}{\partial s_1} - \frac{1}{a} \mathcal{V}_1 \right) - \varepsilon \left( \frac{\partial \mathcal{V}_{E,3}}{\partial s_1} - \frac{1}{a} \mathcal{V}_1 \right) \right) \right] = 0, \end{aligned}$$

by summing up all the terms in the square bracket. In conclusion we get that

$$\frac{1}{\varepsilon} \Pi_\varepsilon(e(v_\varepsilon^1)) \longrightarrow \mathcal{E}(\mathcal{V}_E, \mathcal{V}) \quad \text{strongly in } L^2(\omega \times Y^*)^9.$$

In the next step we consider  $e_{ij}(v_\varepsilon^2)$ , where we again just examine  $e_{12}$  and  $e_{13}$ . One has

$$\begin{aligned} e_{12}(v_\varepsilon^2)(s) &= \frac{\varepsilon^2}{2} \left( \frac{a}{a + s_3} \frac{\partial \hat{v}}{\partial s_1} \mathbf{t}_2 + \frac{\partial \hat{v}}{\partial s_2} \mathbf{t}_1 \right) \left( s', \left\{ \frac{s}{\varepsilon} \right\} \right) \\ &\quad + \frac{\varepsilon}{2} \left( \frac{a}{a + s_3} \frac{\partial \hat{v}}{\partial y_1} \mathbf{t}_2 + \frac{\partial \hat{v}}{\partial y_2} \mathbf{t}_1 \right) \left( s', \left\{ \frac{s}{\varepsilon} \right\} \right) \end{aligned}$$

and

$$\begin{aligned} e_{13}(v_\varepsilon^2)(s) &= \frac{\varepsilon^2}{2} \left( \frac{a}{a + s_3} \frac{\partial \hat{v}}{\partial s_1} \mathbf{n} + \frac{\partial \hat{v}}{\partial s_3} \mathbf{t}_1 \right) \left( s', \left\{ \frac{s}{\varepsilon} \right\} \right) \\ &\quad + \frac{\varepsilon}{2} \left( \frac{a}{a + s_3} \frac{\partial \hat{v}}{\partial y_1} \mathbf{n} + \frac{\partial \hat{v}}{\partial y_3} \mathbf{t}_1 \right) \left( s', \left\{ \frac{s}{\varepsilon} \right\} \right). \end{aligned}$$

Considering now  $\frac{1}{\varepsilon} \Pi_\varepsilon(e_{12}(v_\varepsilon^2))$  and  $\frac{1}{\varepsilon} \Pi_\varepsilon(e_{13}(v_\varepsilon^2))$ , we obtain

$$\begin{aligned} \frac{1}{\varepsilon} \Pi_\varepsilon(e_{12}(v_\varepsilon^2)) &\longrightarrow e_{y,12}(\hat{v}) \quad \text{strongly in } L^2(\omega \times Y^*), \\ \frac{1}{\varepsilon} \Pi_\varepsilon(e_{13}(v_\varepsilon^2)) &\longrightarrow e_{y,13}(\hat{v}) \quad \text{strongly in } L^2(\omega \times Y^*), \end{aligned}$$

which then yields

$$\frac{1}{\varepsilon} \Pi_\varepsilon(e(v_\varepsilon^2)) \longrightarrow \mathcal{E}_y(\hat{v}) \quad \text{strongly in } L^2(\omega \times Y^*)^9.$$

Therefore,

$$\frac{1}{\varepsilon} \Pi_\varepsilon(e(v_\varepsilon)) \longrightarrow \mathcal{E}(\mathcal{V}_E, \mathcal{V}) + \mathcal{E}_y(\hat{v}) \quad \text{strongly in } L^2(\omega \times Y^*)^9.$$

We plug in our test function  $v_\varepsilon$  into the weak formulation (2.6.6), apply the rescaling-unfolding operator on both sides, divide by  $2\kappa\varepsilon^3$  and pass to the limit. We then obtain the formulation (2.7.4) with respect to the chosen test function (regarding the right-hand side, we use the results from Lemma 2.6.1 and [16, Proposition 4.8] to represent it as an integral over the whole domain  $\omega$  in the limit). Then, by density of  $\mathcal{C}^1(\bar{\omega})^3 \cap \mathbb{D}_E$  in  $\mathbb{D}_E$ ,  $\mathcal{C}^2(\bar{\omega})^3 \cap \mathbb{D}_I$  in  $\mathbb{D}_I$  and  $\mathcal{C}^1(\bar{\omega}; H_{per}^1(Y^*)^3)$  in  $L^2(\omega; H_{per}^1(Y^*)^3)$ , this yields (2.7.4) for every  $(\mathcal{V}_E, \mathcal{V}, \hat{v}) \in \mathbb{D}$ .

The existence and uniqueness is a consequence of the coercivity of  $a_{ijkl}$ , Lemma 2.7.3 and the Lax-Milgram Lemma.  $\square$

## 2.8 Homogenization of the shell

In this section we want to express the warping-microscopic displacement  $\hat{u}$  with respect to the macroscopic  $\mathcal{U}_E$  and  $\mathcal{U}$ . Therefore, we choose  $\mathcal{V} = 0$  in equation (2.7.4), which leads to

$$\int_{Y^*} a_{ijkl} \left( \mathcal{E}_{ij}(\mathcal{U}_E, \mathcal{U}) + \mathcal{E}_{y,ij}(\hat{u}) \right) \mathcal{E}_{y,kl}(\hat{v}) dy = 0, \quad \forall \hat{v} \in H_{per}^1(Y^*)^3.$$

Hence, we rewrite  $\hat{u}$  in terms of  $(\mathcal{U}_E, \mathcal{U})$ . Thus, we define the 3 matrices

$$\mathbf{M}^{11} = \begin{pmatrix} 1 & 0 & 0 \\ 0 & 0 & 0 \\ 0 & 0 & 0 \end{pmatrix}, \quad \mathbf{M}^{12} = \mathbf{M}^{21} = \begin{pmatrix} 0 & 1 & 0 \\ 1 & 0 & 0 \\ 0 & 0 & 0 \end{pmatrix}, \quad \mathbf{M}^{22} = \begin{pmatrix} 0 & 0 & 0 \\ 0 & 1 & 0 \\ 0 & 0 & 0 \end{pmatrix},$$

and introduce the 6 distinct correctors  $((\alpha, \beta) \in \{1, 2\}^2)$

$$\widetilde{\chi_E^{\alpha\beta}} \in H_{per}^1(Y^*)^3, \quad \widetilde{\chi_I^{\alpha\beta}} \in H_{per}^1(Y^*)^3, \quad \text{where} \quad \widetilde{\chi_E^{12}} = \widetilde{\chi_E^{21}}, \quad \widetilde{\chi_I^{12}} = \widetilde{\chi_I^{21}},$$

which are defined by

$$\begin{aligned} \int_{Y^*} a_{ijkl} \left( \mathbf{M}_{ij}^{\alpha\beta} + \mathcal{E}_{y,ij}(\widetilde{\chi_E^{\alpha\beta}}) \right) \mathcal{E}_{y,kl}(\tilde{\psi}) dy &= 0, \\ \int_{Y^*} a_{ijkl} \left( y_3 \mathbf{M}_{ij}^{\alpha\beta} + \mathcal{E}_{y,ij}(\widetilde{\chi_I^{\alpha\beta}}) \right) \mathcal{E}_{y,kl}(\tilde{\psi}) dy &= 0, \end{aligned} \quad \forall \tilde{\psi} \in H_{per}^1(Y^*)^3. \quad (2.8.1)$$

Hence, we are able to express  $\hat{u}$  as

$$\hat{u}(s', y) = e_{\alpha\beta}(\mathcal{U}_E)(s') \widetilde{\chi_E^{\alpha\beta}}(y) + \Lambda_{\alpha\beta}(\mathcal{U})(s') \widetilde{\chi_I^{\alpha\beta}}(y), \quad \text{for a.e. } (s', y) \in \omega \times Y^*.$$

**Remark 2.8.1** The cell problems defined in (2.8.1) are uniquely solvable up to an additive constant and unique in  $H_{per,[0]}^1(Y^*)$ , see e.g. [48, chapter 6]. Here,

$$H_{per,[0]}^1(Y^*) = \left\{ \psi \in H_{per}^1(Y^*) \mid \int_{Y^*} \psi dy = 0 \right\}.$$

### 2.8.1 The limit problems in the shell's mid surface

**Theorem 2.8.1** *The limit displacement  $(\mathcal{U}_E, \mathcal{U}) \in \mathbb{D}_E \times \mathbb{D}_I$  solves the homogenized problem*

$$\begin{aligned} & \int_{\omega} \left[ a_{\alpha\beta\alpha'\beta'}^{hom} e_{\alpha\beta}(\mathcal{U}_E) e_{\alpha'\beta'}(\mathcal{V}_E) + b_{\alpha\beta\alpha'\beta'}^{hom} \left( e_{\alpha\beta}(\mathcal{U}_E) \Lambda_{\alpha'\beta'}(\mathcal{V}) \right. \right. \\ & \quad \left. \left. + \Lambda_{\alpha\beta}(\mathcal{U}) e_{\alpha'\beta'}(\mathcal{V}_E) \right) + c_{\alpha\beta\alpha'\beta'}^{hom} \Lambda_{\alpha\beta}(\mathcal{U}) \Lambda_{\alpha'\beta'}(\mathcal{V}) \right] ds' \\ & = \frac{|Y'^*|}{|Y'|} \left( \int_{\omega} \left( f \cdot \mathcal{V} + \frac{\kappa^2}{3a} g_{\alpha} \mathcal{V}_{\alpha} - \frac{\kappa^2}{3} g_{\alpha} \frac{\partial \mathcal{V}}{\partial s_{\alpha}} \mathbf{n} \right) ds' + \langle F, \mathcal{V}_E \rangle \right), \\ & \quad \forall (\mathcal{V}_E, \mathcal{V}) \in \mathbb{D}_E \times \mathbb{D}_I, \end{aligned} \quad (2.8.2)$$

where

$$\begin{aligned} a_{\alpha\beta\alpha'\beta'}^{hom} &= \frac{1}{|Y^*|} \int_{Y^*} a_{ijkl}(y) \left[ \mathbf{M}_{ij}^{\alpha\beta} + \mathcal{E}_{y,ij}(\widetilde{\chi_E^{\alpha\beta}}) \right] \mathbf{M}_{kl}^{\alpha'\beta'} dy, \\ b_{\alpha\beta\alpha'\beta'}^{hom} &= \frac{1}{|Y^*|} \int_{Y^*} a_{ijkl}(y) \left[ y_3 \mathbf{M}_{ij}^{\alpha\beta} + \mathcal{E}_{y,ij}(\widetilde{\chi_I^{\alpha\beta}}) \right] \mathbf{M}_{kl}^{\alpha'\beta'} dy, \\ c_{\alpha\beta\alpha'\beta'}^{hom} &= \frac{1}{|Y^*|} \int_{Y^*} a_{ijkl}(y) \left[ y_3 \mathbf{M}_{ij}^{\alpha\beta} + \mathcal{E}_{y,ij}(\widetilde{\chi_I^{\alpha\beta}}) \right] y_3 \mathbf{M}_{kl}^{\alpha'\beta'} dy. \end{aligned}$$

*Proof.* Consider equation (2.7.4) and choose the test function such that  $(\mathcal{V}_E, \mathcal{V}) \in \mathbb{D}_E \times \mathbb{D}_I$  and  $\hat{v} = 0$ . Moreover, with the expression for  $\hat{u}$  we obtain for the left-hand side in (2.7.4)

$$\frac{1}{2\kappa} \int_{\omega \times Y} a_{ijkl}(y) \left( \mathcal{E}_{ij}(\mathcal{U}_E, \mathcal{U}) + \mathcal{E}_{y,ij}(\hat{u}) \right) \mathcal{E}_{kl}(\mathcal{V}_E, \mathcal{V}) ds' dy.$$

Hence,

$$\begin{aligned} & \int_{\omega \times Y^*} a_{ijkl}(y) \left[ e_{\alpha\beta}(\mathcal{U}_E)(s') (\mathbf{M}_{ij}^{\alpha\beta} + \mathcal{E}_{y,ij}(\widetilde{\chi_E^{\alpha\beta}})(y)) + \Lambda_{\alpha\beta}(\mathcal{U})(s') (y_3 \mathbf{M}_{ij}^{\alpha\beta} + \mathcal{E}_{y,ij}(\widetilde{\chi_I^{\alpha\beta}})(y)) \right] \\ & \quad \times \mathbf{M}_{kl}^{\alpha'\beta'} \left[ e_{\alpha'\beta'}(\mathcal{V}_E)(s') + y_3 \Lambda_{\alpha'\beta'}(\mathcal{V})(s') \right] ds' dy \\ & = |Y^*| \left( \int_{\omega} \left( f \cdot \mathcal{V} + \frac{\kappa^2}{3a} g_{\alpha} \mathcal{V}_{\alpha} - \frac{\kappa^2}{3} g_{\alpha} \frac{\partial \mathcal{V}}{\partial s_{\alpha}} \mathbf{n} \right) ds' + \langle F, \mathcal{V}_E \rangle \right). \end{aligned}$$

Computing the expressions yields,

$$\begin{aligned} & \frac{1}{|Y^*|} \int_{\omega \times Y^*} a_{ijkl}(y) e_{\alpha\beta}(\mathcal{U}_E) \left( \mathbf{M}_{ij}^{\alpha\beta} + \mathcal{E}_{y,ij}(\widetilde{\chi_E^{\alpha\beta}}) \right) \mathbf{M}_{kl}^{\alpha'\beta'} e_{\alpha'\beta'}(\mathcal{V}_E) \\ & \quad + a_{ijkl}(y) \Lambda_{\alpha\beta}(\mathcal{U}) \left( y_3 \mathbf{M}_{ij}^{\alpha\beta} + \mathcal{E}_{y,ij}(\widetilde{\chi_I^{\alpha\beta}}) \right) \mathbf{M}_{kl}^{\alpha'\beta'} e_{\alpha'\beta'}(\mathcal{V}_E) \\ & \quad + a_{ijkl}(y) e_{\alpha\beta}(\mathcal{U}_E) \left( \mathbf{M}_{ij}^{\alpha\beta} + \mathcal{E}_{y,ij}(\widetilde{\chi_E^{\alpha\beta}}) \right) y_3 \mathbf{M}_{kl}^{\alpha'\beta'} \Lambda_{\alpha'\beta'}(\mathcal{V}) \\ & \quad + a_{ijkl}(y) \Lambda_{\alpha\beta}(\mathcal{U}) \left( y_3 \mathbf{M}_{ij}^{\alpha\beta} + \mathcal{E}_{y,ij}(\widetilde{\chi_I^{\alpha\beta}}) \right) y_3 \mathbf{M}_{kl}^{\alpha'\beta'} \Lambda_{\alpha'\beta'}(\mathcal{V}) dy ds' \\ & = \frac{|Y'^*|}{|Y'|} \left( \int_{\omega} \left( f \cdot \mathcal{V} + \frac{\kappa^2}{3a} g_{\alpha} \mathcal{V}_{\alpha} - \frac{\kappa^2}{3} g_{\alpha} \frac{\partial \mathcal{V}}{\partial s_{\alpha}} \mathbf{n} \right) ds' + \langle F, \mathcal{V}_E \rangle \right). \end{aligned}$$

With the expression for the homogenized coefficients we end up with equation (2.8.2).  $\square$

**Remark 2.8.2** *Given the Hooke's tensor as  $a_{ijkl}(y) = a_{ijkl}(y_1, y_2)$ , i.e., being independent of  $y_3$ , we can conclude that  $b_{\alpha\beta\alpha'\beta'} = 0$ , for all  $\alpha, \beta, \alpha', \beta' \in \{1, 2\}$ . In those cases the model only consists of membrane and bending effects.*

**Lemma 2.8.1** *Let  $\mathbb{S}_2$  be the set of  $2 \times 2$  symmetric matrices. There exists a constant  $C > 0$  such that the homogenized coefficients satisfy for all  $(\tau_E, \tau_I) \in \mathbb{S}_2 \times \mathbb{S}_2$*

$$a_{\alpha\beta\alpha'\beta'}^{hom} \tau_E^{\alpha\beta} \tau_E^{\alpha'\beta'} + b_{\alpha\beta\alpha'\beta'}^{hom} (\tau_E^{\alpha\beta} \tau_I^{\alpha'\beta'} + \tau_I^{\alpha\beta} \tau_E^{\alpha'\beta'}) + c_{\alpha\beta\alpha'\beta'}^{hom} \tau_I^{\alpha\beta} \tau_I^{\alpha'\beta'} \geq C (\tau_E^{\alpha\beta} \tau_E^{\alpha\beta} + \tau_I^{\alpha\beta} \tau_I^{\alpha\beta}).$$

*Proof.* First, we note that with the variational formulation (2.8.1) the homogenized coefficients read as

$$\begin{aligned} a_{\alpha\beta\alpha'\beta'}^{hom} &= \frac{1}{|Y^*|} \int_{Y^*} a_{ijkl}(y) \left[ \mathbf{M}_{ij}^{\alpha\beta} + \mathcal{E}_{y,ij}(\widetilde{\chi_E^{\alpha\beta}}) \right] \left[ \mathbf{M}_{kl}^{\alpha'\beta'} + \mathcal{E}_{y,kl}(\widetilde{\chi_E^{\alpha'\beta'}}) \right] dy, \\ b_{\alpha\beta\alpha'\beta'}^{hom} &= \frac{1}{|Y^*|} \int_{Y^*} a_{ijkl}(y) \left[ y_3 \mathbf{M}_{ij}^{\alpha\beta} + \mathcal{E}_{y,ij}(\widetilde{\chi_I^{\alpha\beta}}) \right] \left[ \mathbf{M}_{kl}^{\alpha'\beta'} + \mathcal{E}_{y,kl}(\widetilde{\chi_E^{\alpha'\beta'}}) \right] dy \\ &= \frac{1}{|Y^*|} \int_{Y^*} a_{ijkl}(y) \left[ \mathbf{M}_{ij}^{\alpha\beta} + \mathcal{E}_{y,ij}(\widetilde{\chi_E^{\alpha\beta}}) \right] \left[ y_3 \mathbf{M}_{kl}^{\alpha'\beta'} + \mathcal{E}_{y,kl}(\widetilde{\chi_I^{\alpha'\beta'}}) \right] dy, \\ c_{\alpha\beta\alpha'\beta'}^{hom} &= \frac{1}{|Y^*|} \int_{Y^*} a_{ijkl}(y) \left[ y_3 \mathbf{M}_{ij}^{\alpha\beta} + \mathcal{E}_{y,ij}(\widetilde{\chi_I^{\alpha\beta}}) \right] \left[ y_3 \mathbf{M}_{kl}^{\alpha'\beta'} + \mathcal{E}_{y,kl}(\widetilde{\chi_I^{\alpha'\beta'}}) \right] dy. \end{aligned}$$

For every  $(\tau_E, \tau_I) \in \mathbb{S}_2 \times \mathbb{S}_2$ , one has

$$\begin{aligned} a_{\alpha\beta\alpha'\beta'}^{hom} \tau_E^{\alpha\beta} \tau_E^{\alpha'\beta'} + b_{\alpha\beta\alpha'\beta'}^{hom} (\tau_E^{\alpha\beta} \tau_I^{\alpha'\beta'} + \tau_I^{\alpha\beta} \tau_E^{\alpha'\beta'}) + c_{\alpha\beta\alpha'\beta'}^{hom} \tau_I^{\alpha\beta} \tau_I^{\alpha'\beta'} \\ = \frac{1}{|Y^*|} \int_{Y^*} a_{ijkl} \left[ M_{ij} + \mathcal{E}_{y,ij}(\Psi) \right] \left[ M_{kl} + \mathcal{E}_{y,kl}(\Psi) \right] dy, \end{aligned}$$

with

$$M = (\tau_E^{\alpha\beta} + y_3 \tau_I^{\alpha\beta}) \mathbf{M}^{\alpha\beta} \quad \text{and} \quad \Psi = \tau_E^{\alpha\beta} \widetilde{\chi_E^{\alpha\beta}} + \tau_I^{\alpha\beta} \widetilde{\chi_I^{\alpha\beta}}.$$

By the coercivity of  $a_{ijkl}$ , see (2.6.2), we obtain

$$\begin{aligned} \int_{Y^*} a_{ijkl}(y) \left[ M_{ij} + \mathcal{E}_{y,ij}(\Psi) \right] \left[ M_{kl} + \mathcal{E}_{y,kl}(\Psi) \right] dy \\ \geq c_0 \int_{Y^*} \left[ M_{ij} + \mathcal{E}_{y,ij}(\Psi) \right] \left[ M_{ij} + \mathcal{E}_{y,ij}(\Psi) \right] dy. \end{aligned}$$

Then Lemma 2.7.2 yields together with the equivalence of the norms that for all  $(\tau_E, \tau_I) \in \mathbb{S}_2 \times \mathbb{S}_2$

$$\begin{aligned} \int_{Y^*} \left[ M_{ij} + \mathcal{E}_{ij,y}(\Psi) \right] \left[ M_{ij} + \mathcal{E}_{ij,y}(\Psi) \right] dy &\geq C (|\tau_E|^2 + |\tau_I|^2 + \|\Psi\|_{L^2(Y^*)}^2) \\ &\geq C (\tau_E^{\alpha\beta} \tau_E^{\alpha\beta} + \tau_I^{\alpha\beta} \tau_I^{\alpha\beta}). \end{aligned}$$

□

With that Lemma we conclude that the left-hand side of (2.8.2) is a coercive and bounded bilinear form. Hence, we obtain with the Lax-Milgram Lemma that it is uniquely solvable.

## 2.9 Different boundary conditions

In this section we want to emphasize on a change of the boundary conditions, such that the previously free part is clamped, i.e.,  $\Gamma_0 = \phi([0, a\pi] \times \{0\} \cup [0, a\pi] \times \{l\})$ . We may note, that all presented estimates and resulting limits are not affected by the change of

boundary conditions until we consider the split of  $\mathcal{U} = \mathcal{U}_I + \mathcal{U}_E$ . As in (2.5.1), we first obtain that  $\mathcal{U}_I$  can be presented as

$$\begin{aligned}\mathcal{U}_1(s_1, s_2) &= -s_2^c U_2'(s_1) + U_1(s_1), \\ \mathcal{U}_2(s_1, s_2) &= U_2(s_1), \\ \mathcal{U}_3(s_1, s_2) &= a(s_2^c U_2''(s_1) - U_1'(s_1)),\end{aligned}\quad U_1 \in H_0^1(0, a\pi), \quad U_2 \in H_0^2(0, a\pi).$$

With respect to our new boundary conditions we need that

$$\mathcal{U}_2(s_1, 0) = \mathcal{U}_2(s_1, l) = 0, \quad \text{for a.e. } s_1.$$

Hence, we obtain

$$U_2(s_1) = 0, \quad \text{for a.e. } s_1.$$

With the same reasoning we conclude that

$$U_1(s_1) = 0, \quad \text{for a.e. } s_1,$$

and therefore we see that  $D_I = \mathbb{D}_I = \{0\}$ .

**Remark 2.9.1** *In the applied forces we consider  $F$  such that*

$$\begin{aligned}F_1 &\in L^2(0, l; H^1(0, a\pi)), \\ F_2 &\in L^2(\omega), \\ F_3 &\in L^2(0, l; H^2(0, a\pi)).\end{aligned}\tag{2.9.1}$$

*In the case of a fully clamped shell along  $\partial\omega$  the assumptions on the forces do not change and we obtain  $D_I = \mathbb{D}_I = 0$ . Hence, we immediately get equation (2.9.2).*

**Lemma 2.9.1** *For every  $\mathcal{U}$  in  $\mathbb{D}_E$ , where  $\Gamma_0 = \partial\omega$ , one has*

$$\|\mathcal{U}_2\|_{H^1(0, l; L^2(0, a\pi))} + \|\mathcal{U}_1\|_{H^1(0, l; (H^1(0, a\pi))')} + \|\mathcal{U}_3\|_{L^2(0, l; (H^2(0, a\pi))')} \leq C\|\mathcal{U}\|_E.$$

*Proof.* This estimate is an immediate consequence of Lemma 2.5.2 and the fact that  $D_E = H_0^1(\omega) \times H_0^1(\omega) \times L^2(\omega)$ .  $\square$

If we consider the linear elasticity problem presented in section 2.6 and passing to the limit, as presented earlier, we obtain that the limit homogenized equation is given by

$$\int_{\omega} a_{\alpha\beta\alpha'\beta'}^{hom} e_{\alpha\beta}(\mathcal{U}_E) e_{\alpha'\beta'}(\mathcal{V}_E) ds' = \langle F, \mathcal{V}_E \rangle, \quad \forall \mathcal{V}_E \in \mathbb{D}_E. \tag{2.9.2}$$

Now, we show that  $\langle F, \mathcal{V}_E \rangle$  can be expressed in terms of  $e_{\alpha'\beta'}(\mathcal{V}_E)$  for every  $V \in \mathbb{D}_E$ . Denote with  $\mathcal{F}$  and  $\tilde{\mathcal{F}}$  the fields, which are defined by

$$\begin{aligned}\mathcal{F}(\cdot, 0) &= 0, & \frac{\partial \mathcal{F}}{\partial s_2} &= F, \\ \tilde{\mathcal{F}}(\cdot, 0) &= 0, & \frac{\partial \tilde{\mathcal{F}}}{\partial s_2} &= \mathcal{F}.\end{aligned}$$

Recall that the components of  $F$  are given by (2.9.1).



**Lemma 2.9.2** *For every  $V \in \mathbb{D}_E$  one has*

$$\langle F, \mathcal{V}_E \rangle = \int_{\omega} (\mathbf{F}_{11} e_{11}(V) + \mathbf{F}_{12} e_{12}(V) + \mathbf{F}_{22} e_{22}(V)) ds_1 ds_2,$$

where

$$\mathbf{F}_{11} = aF_3, \quad \mathbf{F}_{12} = -2(\mathcal{F}_1 + a\partial_1 \mathcal{F}_3), \quad \mathbf{F}_{22} = -\mathcal{F}_2 + \partial_1 \tilde{\mathcal{F}}_1 + a\partial_{11} \tilde{\mathcal{F}}_3.$$

*Proof.* Consider  $V \in D_E$ . We get that

$$\begin{aligned} \int_{\omega} F_3 V_3 ds_1 ds_2 &= a \int_{\omega} F_3 e_{11}(V) ds_1 ds_2 - a \int_{\omega} F_3 \partial_1 V_1 ds_1 ds_2, \\ &= a \int_{\omega} F_3 e_{11}(V) ds_1 ds_2 + a \int_{\omega} \partial_1 F_3 V_1 ds_1 ds_2. \end{aligned}$$

Then

$$\begin{aligned} \int_{\omega} (F_1 + a\partial_1 F_3) V_1 ds_1 ds_2 &= - \int_{\omega} (\mathcal{F}_1 + a\partial_1 \mathcal{F}_3) \partial_2 V_1 ds_1 ds_2 \\ &= -2 \int_{\omega} (\mathcal{F}_1 + a\partial_1 \mathcal{F}_3) e_{12}(V) ds_1 ds_2 \\ &\quad + \int_{\omega} (\mathcal{F}_1 + a\partial_1 \mathcal{F}_3) \partial_1 V_2 ds_1 ds_2 \\ &= -2 \int_{\omega} (\mathcal{F}_1 + a\partial_1 \mathcal{F}_3) e_{12}(V) ds_1 ds_2 \\ &\quad - \int_{\omega} (\partial_1 \mathcal{F}_1 + a\partial_{11} \mathcal{F}_3) V_2 ds_1 ds_2 \end{aligned}$$

and finally

$$\int_{\omega} (F_2 - \partial_1 \mathcal{F}_1 - a\partial_{11} \mathcal{F}_3) V_2 ds_1 ds_2 = - \int_{\omega} (\mathcal{F}_2 - \partial_1 \tilde{\mathcal{F}}_1 - a\partial_{11} \tilde{\mathcal{F}}_3) \partial_2 V_2 ds_1 ds_2$$

With those calculations we obtain for every  $V$  in  $D_E$

$$\begin{aligned} &\int_{\omega} F \cdot V ds_1 ds_2 \\ &= \int_{\omega} (F_1 V_1 + F_2 V_2 + F_3 V_3) ds_1 ds_2 \\ &= \int_{\omega} ((F_1 + a\partial_1 F_3) V_1 + F_2 V_2 + aF_3 e_{11}(V)) ds_1 ds_2 \\ &= \int_{\omega} (-2(\mathcal{F}_1 + a\partial_1 \mathcal{F}_3) e_{12}(V) + (F_2 - \partial_1 \mathcal{F}_1 - a\partial_{11} \mathcal{F}_3) V_2 + aF_3 e_{11}(V)) ds_1 ds_2 \\ &= \int_{\omega} (-2(\mathcal{F}_1 + a\partial_1 \mathcal{F}_3) e_{12}(V) + (-\mathcal{F}_2 + \partial_1 \tilde{\mathcal{F}}_1 + a\partial_{11} \tilde{\mathcal{F}}_3) e_{22}(V) + aF_3 e_{11}(V)) ds_1 ds_2. \end{aligned}$$

We conclude the proof by the density of  $D_E$  in  $\mathbb{D}_E$ .  $\square$

### 3 Analytic Solution to Pinching a Homogeneous Shell

In the previous chapter we have started with the full 3D linear elasticity problem for a heterogeneous shell and reduced it to an equivalent homogeneous 2D formulation, where the effective properties are obtained by six auxiliary cell experiments. Our goal in this chapter is to derive an analytic solution to the homogenized problem for a point load, which we call in the following a pinching load, acting on the shell. Usually, this kind of load is Dirac type and does not fit to the derivation in chapter 2. We overcome this problem by substituting the pinching with an approximated load on a small rectangular strip later defined in the chapter. Then we transform the weak formulation back into its strong form. This yields a system of three differential equations, which have to be solved simultaneously. Next step is to use Airy's stress function ansatz, see for example [37] and [43], such that we get a single 8th order PDE, which describes the effects of bending w.r.t. the described pinching load. After that we closely follow the procedure presented in [62], where the author considers an isotropic shell, and most importantly [33], where a full cylindrical orthotropic shell with opposite pinching loads is considered. We will see that one can easily implement the presented Fourier transform and series ansatz to get the solution for our half-cylindrical shell, where we clamp the lateral boundary. After that we investigate the general structure of the analytic solution by considering different parameters and locations of the load. In the end we solve the weak formulation numerically via the finite element solver FEniCS, [2], and compare both solutions with each other. Moreover, we verify with ANSYS the derivation from section 2.9. The analytic solution is used in chapter 5 as the objective functional, which should be minimized with respect to the underlying design space.

#### 3.1 Deriving the strong formulation

We proceed with the homogenized equation for shells having  $b_{\alpha\beta\alpha'\beta'}^{hom} = 0$ , i.e., where the Hooke's tensor is constant in the  $y_3$  direction as mentioned in remark 2.8.2. This yields the weak formulation of the form

$$\begin{aligned} & \int_{\omega} \left[ a_{\alpha\beta\alpha'\beta'}^{hom} e_{\alpha\beta}(\mathcal{U}_E) e_{\alpha'\beta'}(\mathcal{V}_E) + c_{\alpha\beta\alpha'\beta'}^{hom} \Lambda_{\alpha\beta}(\mathcal{U}) \Lambda_{\alpha'\beta'}(\mathcal{V}) \right] ds' \\ &= \int_{\omega} \left( f \cdot \mathcal{V} + \frac{\kappa^2}{3a} g_{\alpha} \mathcal{V}_{\alpha} - \frac{\kappa^2}{3} g_{\alpha} \frac{\partial \mathcal{V}}{\partial s_{\alpha}} \mathbf{n} \right) ds' + \langle F, \mathcal{V}_E \rangle, \\ & \forall (\mathcal{V}_E, \mathcal{V}) \in \mathbb{D}_E \times \mathbb{D}_I. \end{aligned} \tag{3.1.1}$$

The effective properties are obtained as presented in the previous chapter. Moreover, we have seen that it is necessary in our analysis to decompose the displacements into an inextensional and an extensional one. For simplicity, we introduce the complete displacement  $\mathcal{U} = \mathcal{U}_E + \mathcal{U}_I$ . Since we want to study the effects of a pinching load, which only acts in the shell's normal direction, we set the surface force  $g = 0$ . The volumetric

forces  $f$  and  $F$  are put together to a single load still denoted as  $f$ . Hence, given some  $q \in L^2(\omega)$  we take  $f = q \cdot \mathbf{n}$ . Therefore, (3.1.1) reduces to

$$\int_{\omega} \left[ a_{\alpha\beta\alpha'\beta'}^{hom} e_{\alpha\beta}(\mathcal{U}) e_{\alpha'\beta'}(\mathcal{V}) + c_{\alpha\beta\alpha'\beta'}^{hom} \Lambda_{\alpha\beta}(\mathcal{U}) \Lambda_{\alpha'\beta'}(\mathcal{V}) \right] ds' = \int_{\omega} q \cdot \mathcal{V}_3 ds', \quad (3.1.2)$$

$$\forall \mathcal{V} \in [H_{\Gamma_0}^1(\omega)]^2 \times H_{\Gamma_0}^2(\omega).$$

**Remark 3.1.1** *In the following we compare the obtained limit model with the Koiter shell equation. Hence, throughout this chapter we assume that the shell's thickness is denoted by  $h > 0$  and fixed.*

**Remark 3.1.2** *In the derivation of the homogenized 2D limit problem (2.8.2), we initially scaled the forces such that we have no dependencies on  $\varepsilon$  in the limit. If we consider the forces without the scaling assumptions, therefore being of order  $\mathcal{O}(1)$ , we obtain an  $\varepsilon$  dependency in our left-hand side. Consequently, due to the estimates (2.1.24) and for the extensional displacements (2.5.4) we get after applying the rescaling-unfolding operator  $\Pi_{\varepsilon}$ , that the membrane part is scaled with  $\varepsilon$ , while the bending part is of order  $\varepsilon^3$ . Thus, the so received weak formulation coincides in the isotropic case with the Koiter shell equation as shown in [14, chapter 7] applied to the geometry of a cylindrical half shell. There the effective properties are calculated with respect to the Lamé constants  $\lambda$  and  $\mu$  by*

$$a_{\alpha\beta\sigma\tau} = 2 \frac{\lambda\mu}{\lambda + 2\mu} \mathbf{a}^{\alpha\beta} \mathbf{a}^{\sigma\tau} + \mu (\mathbf{a}^{\alpha\sigma} \mathbf{a}^{\beta\tau} + \mathbf{a}^{\alpha\tau} \mathbf{a}^{\beta\sigma})$$

and the full equation is given by

$$\mathcal{U} \in V = \{\eta \in H^1(\omega) \times H^1(\omega) \times H^2(\omega) | \eta = 0 \text{ on } \gamma_0\}$$

$$\int_{\omega} \left( h a_{\alpha\beta\sigma\tau} \gamma_{\sigma\tau}(\mathcal{U}) \gamma_{\alpha\beta}(\mathcal{V}) + \frac{h^3}{12} a_{\alpha\beta\sigma\tau} \rho_{\sigma\tau}(\mathcal{U}) \rho_{\alpha\beta}(\mathcal{V}) \right) ds' = \int_{\omega} f \mathcal{V} ds', \quad \forall \mathcal{V} \in V.$$

The appearing operators are derived for general shells as

$$\gamma_{\alpha\beta}(\mathcal{U}) = \frac{1}{2} \left( \frac{\partial \mathcal{U}_{\alpha}}{\partial s_{\beta}} + \frac{\partial \mathcal{U}_{\beta}}{\partial s_{\alpha}} \right) - \Gamma_{\alpha\beta}^{\sigma} \mathcal{U}_{\sigma} - b_{\alpha\beta} \mathcal{U}_3,$$

$$\rho_{\alpha\beta}(\mathcal{U}) = \frac{\partial^2 \mathcal{U}_3}{\partial s_{\alpha} \partial s_{\beta}} - \Gamma_{\alpha\beta}^{\sigma} \frac{\partial \mathcal{U}_3}{\partial s_{\sigma}} - b_{\alpha}^{\sigma} b_{\sigma\beta} \mathcal{U}_3 + b_{\alpha}^{\sigma} \left( \frac{\partial \mathcal{U}_{\sigma}}{\partial s_{\beta}} - \Gamma_{\beta\sigma}^{\tau} \mathcal{U}_{\tau} \right) + b_{\beta}^{\tau} \left( \frac{\partial \mathcal{U}_{\tau}}{\partial s_{\alpha}} - \Gamma_{\alpha\tau}^{\sigma} \mathcal{U}_{\sigma} \right)$$

$$+ \left( \frac{\partial b_{\beta}^{\tau}}{\partial s_{\alpha}} + \Gamma_{\alpha\sigma}^{\tau} b_{\beta}^{\sigma} - \Gamma_{\alpha\beta}^{\sigma} b_{\sigma}^{\tau} \right) \mathcal{U}_{\tau},$$

where  $\Gamma_{\alpha\beta}^{\sigma}$  are the Christoffel symbols,  $\mathbf{a}^{\alpha\beta}$  the contravariant components of the metric tensor,  $b_{\alpha\beta}$  the covariant components of the curvature tensor and  $b_{\alpha}^{\beta}$  the mixed components of the curvature tensor. Considering now the cylindrical shell geometry we obtain that

$$\Gamma_{\alpha\beta}^{\sigma} = 0, \quad b_{\alpha\beta} = 0, \quad \mathbf{a}^{\alpha\beta} = \delta_{\alpha\beta} \quad \text{for all } \alpha, \beta, \sigma \in \{1, 2\},$$

$$b_1^1 = -\frac{1}{a}, \quad b_1^2 = b_2^1 = b_2^2 = 0.$$

Here  $\delta_{\alpha\beta}$  denotes the Kronecker delta. Due to the equivalence of the derived model in chapter 2 to the Koiter shell we can continue to transform the weak formulation (3.1.2) back into its corresponding strong form. Moreover, we want to mention that a general derivation together with error estimates is presented in [34]. It is worth noting that the bending part coincides with the energy formulation in [37, chapter 9] for pure bending.

**Lemma 3.1.1** *Given the weak formulation (3.1.2) for an orthotropic homogeneous half-cylindrical shell we obtain the strong formulation as a system of the three PDEs*

$$\begin{aligned} \frac{E_2}{1 - \nu_{12}\nu_{21}} \frac{\partial^2 \mathcal{U}_2}{\partial s_2^2} + G \frac{\partial^2 \mathcal{U}_2}{\partial s_1^2} + \left( \frac{E_1 \nu_{21}}{1 - \nu_{12}\nu_{21}} + G \right) \frac{\partial^2 \mathcal{U}_1}{\partial s_1 \partial s_2} + \frac{E_1 \nu_{21}}{1 - \nu_{12}\nu_{21}} \frac{1}{a} \frac{\partial \mathcal{U}_3}{\partial s_2} = 0, \\ \frac{E_1}{1 - \nu_{12}\nu_{21}} \left( \frac{\partial^2 \mathcal{U}_1}{\partial s_1^2} + \frac{1}{a} \frac{\partial \mathcal{U}_3}{\partial s_1} \right) + \frac{E_1 \nu_{21}}{1 - \nu_{12}\nu_{21}} \frac{\partial^2 \mathcal{U}_2}{\partial s_1 \partial s_2} + G \left( \frac{\partial^2 \mathcal{U}_1}{\partial s_2^2} + \frac{\partial^2 \mathcal{U}_2}{\partial s_1 \partial s_2} \right) \\ + \frac{E_1 h^2}{12(1 - \nu_{12}\nu_{21})} \left( -\frac{1}{a} \frac{\partial^3 \mathcal{U}_3}{\partial s_1^3} + \frac{1}{a^2} \frac{\partial^2 \mathcal{U}_1}{\partial s_1^2} \right) - \frac{E_1 h^2 \nu_{21}}{12(1 - \nu^2)} \frac{1}{a} \frac{\partial^3 \mathcal{U}_3}{\partial s_1 \partial s_2^2} \\ + \frac{4Gh^2}{12} \left( -\frac{1}{a} \frac{\partial^3 \mathcal{U}_3}{\partial s_1 \partial s_2^2} + \frac{1}{a^2} \frac{\partial^2 \mathcal{U}_1}{\partial s_2^2} \right) = 0, \quad (3.1.3) \end{aligned}$$

$$\begin{aligned} \frac{E_1}{1 - \nu_{12}\nu_{21}} \left( \frac{1}{a} \frac{\partial \mathcal{U}_1}{\partial s_1} + \frac{1}{a^2} \mathcal{U}_3 \right) + \frac{E_1 \nu_{21}}{1 - \nu_{12}\nu_{21}} \frac{1}{a} \frac{\partial \mathcal{U}_2}{\partial s_2} + \frac{E_1 h^2}{12} \left( \frac{\partial^4 \mathcal{U}_3}{\partial s_1^4} - \frac{1}{a} \frac{\partial^3 \mathcal{U}_1}{\partial s_1^3} \right) \\ + \frac{E_1 \nu_{21} h^2}{12} \left( \frac{\partial^4 \mathcal{U}_3}{\partial s_1^2 \partial s_2^2} - \frac{1}{a} \frac{\partial^3 \mathcal{U}_1}{\partial s_1 \partial s_2^2} \right) + \frac{E_1 \nu_{21} h^2}{12} \frac{\partial^4 \mathcal{U}_3}{\partial s_1^2 \partial s_2^2} \\ + \frac{E_2 h^2}{12} \frac{\partial^4 \mathcal{U}_3}{\partial s_2^4} + \frac{4Gh^2}{12} \left( \frac{\partial^4 \mathcal{U}_3}{\partial s_1^2 \partial s_2^2} - \frac{1}{a} \frac{\partial^3 \mathcal{U}_1}{\partial s_1 \partial s_2^2} \right) = \frac{q}{h}, \end{aligned}$$

where  $E_1, E_2$  are the orthotropic Young's moduli, corresponding to the directions  $s_1$  and  $s_2$ ,  $\nu_{12}, \nu_{21}$  the Poisson's ratio and  $G$  is the shear modulus.

*Proof.* Since we have for orthotropic materials that  $a_{1211}^{hom} = a_{1222}^{hom} = c_{1211}^{hom} = c_{1222}^{hom} = 0$  we consider the expressions  $\Lambda_{\alpha\beta}(\mathcal{U})\Lambda_{\alpha'\beta'}(\mathcal{V})$  and  $\mathcal{Z}_{\alpha\beta}(\mathcal{U})\mathcal{Z}_{\alpha'\beta'}(\mathcal{V})$  with non-zero coefficients and perform partial integrations, such that we get rid of the derivatives for  $\mathcal{V} \in C_0^8(\mathbb{R})^3$ . Due to the properties of  $\mathcal{V}$  we obtain

$$\begin{aligned} \int_{\omega} \mathcal{Z}_{11}(\mathcal{U})\mathcal{Z}_{11}(\mathcal{V})ds' &= \int_{\omega} -\frac{\partial^2 \mathcal{U}_1}{\partial s_1^2} \mathcal{V}_1 - \frac{1}{a} \frac{\partial \mathcal{U}_3}{\partial s_1} \mathcal{V}_1 + \frac{1}{a} \frac{\partial \mathcal{U}_1}{\partial s_1} \mathcal{V}_3 + \frac{1}{a^2} \mathcal{U}_3 \mathcal{V}_3 ds', \\ \int_{\omega} \mathcal{Z}_{11}(\mathcal{U})\mathcal{Z}_{22}(\mathcal{V})ds' &= \int_{\omega} -\frac{\partial^2 \mathcal{U}_1}{\partial s_1 \partial s_2} \mathcal{V}_2 - \frac{1}{a} \frac{\partial \mathcal{U}_3}{\partial s_2} \mathcal{V}_2 ds', \\ \int_{\omega} \mathcal{Z}_{22}(\mathcal{U})\mathcal{Z}_{11}(\mathcal{V})ds' &= \int_{\omega} -\frac{\partial^2 \mathcal{U}_2}{\partial s_1 \partial s_2} \mathcal{V}_1 + \frac{1}{a} \frac{\partial \mathcal{U}_2}{\partial s_2} \mathcal{V}_3 ds', \\ \int_{\omega} \mathcal{Z}_{22}(\mathcal{U})\mathcal{Z}_{22}(\mathcal{V})ds' &= \int_{\omega} -\frac{\partial^2 \mathcal{U}_2}{\partial s_2^2} \mathcal{V}_2 ds', \\ \int_{\omega} \mathcal{Z}_{12}(\mathcal{U})\mathcal{Z}_{12}(\mathcal{V})ds' &= \frac{1}{4} \int_{\omega} -\frac{\partial^2 \mathcal{U}_1}{\partial s_2^2} \mathcal{V}_1 - \frac{\partial^2 \mathcal{U}_2}{\partial s_1 \partial s_2} \mathcal{V}_1 - \frac{\partial^2 \mathcal{U}_1}{\partial s_1 \partial s_2} \mathcal{V}_2 - \frac{\partial^2 \mathcal{U}_2}{\partial s_1^2} \mathcal{V}_2 ds', \\ \int_{\omega} \Lambda_{11}(\mathcal{U})\Lambda_{11}(\mathcal{V})ds' &= \int_{\omega} \frac{\partial^4 \mathcal{U}_3}{\partial s_1^4} \mathcal{V}_3 - \frac{1}{a} \frac{\partial^3 \mathcal{U}_1}{\partial s_1^3} \mathcal{V}_3 + \frac{1}{a} \frac{\partial^3 \mathcal{U}_3}{\partial s_1^3} \mathcal{V}_1 - \frac{1}{a^2} \frac{\partial^2 \mathcal{U}_1}{\partial s_1^2} \mathcal{V}_1 ds', \\ \int_{\omega} \Lambda_{11}(\mathcal{U})\Lambda_{22}(\mathcal{V})ds' &= \int_{\omega} \frac{\partial^4 \mathcal{U}_3}{\partial s_1^2 \partial s_2^2} \mathcal{V}_3 - \frac{1}{a} \frac{\partial^3 \mathcal{U}_1}{\partial s_1 \partial s_2^2} \mathcal{V}_3 ds', \\ \int_{\omega} \Lambda_{22}(\mathcal{U})\Lambda_{11}(\mathcal{V})ds' &= \int_{\omega} \frac{\partial^4 \mathcal{U}_3}{\partial s_1^2 \partial s_2^2} \mathcal{V}_3 + \frac{1}{a} \frac{\partial^3 \mathcal{U}_3}{\partial s_1 \partial s_2^2} \mathcal{V}_1 ds', \\ \int_{\omega} \Lambda_{22}(\mathcal{U})\Lambda_{22}(\mathcal{V})ds' &= \int_{\omega} \frac{\partial^4 \mathcal{U}_3}{\partial s_2^4} \mathcal{V}_3 ds', \\ \int_{\omega} \Lambda_{12}(\mathcal{U})\Lambda_{12}(\mathcal{V})ds' &= \int_{\omega} \frac{\partial^4 \mathcal{U}_3}{\partial s_1^2 \partial s_2^2} \mathcal{V}_3 - \frac{1}{a} \frac{\partial^3 \mathcal{U}_1}{\partial s_1 \partial s_2^2} \mathcal{V}_3 + \frac{1}{a} \frac{\partial^3 \mathcal{U}_3}{\partial s_1 \partial s_2^2} \mathcal{V}_1 - \frac{1}{a^2} \frac{\partial^2 \mathcal{U}_1}{\partial s_2^2} \mathcal{V}_1 ds'. \end{aligned} \quad (3.1.4)$$

Due to the symmetry condition we have  $a_{1212}^{hom} = a_{2112}^{hom} = a_{1221}^{hom} = a_{2121}^{hom}$  and  $c_{1212}^{hom} = c_{2112}^{hom} = c_{1221}^{hom}$ . In the next step we collect the terms appearing with each  $\mathcal{V}_i$ , which then yields the system of three equations. We start with terms involving  $\mathcal{V}_2$ , where we only have membrane effects and obtain the equation

$$a_{1122}^{hom} \left( -\frac{\partial^2 \mathcal{U}_1}{\partial s_1 \partial s_2} - \frac{1}{a} \frac{\partial \mathcal{U}_3}{\partial s_2} \right) + a_{2222}^{hom} - \frac{\partial^2 \mathcal{U}_2}{\partial s_2^2} + a_{1212}^{hom} \left( -\frac{\partial^2 \mathcal{U}_1}{\partial s_1 \partial s_2} - \frac{\partial^2 \mathcal{U}_2}{\partial s_1^2} \right) = 0.$$

We can express the coefficients  $a_{\alpha\beta\alpha'\beta'}^{hom}$  in terms of the orthotropic Young's moduli  $E_1$ ,  $E_2$  and Poisson's ratio  $\nu_{12}$ ,  $\nu_{21}$  together with the shear modulus  $G$ . Thus, having from [50, section 3.3] that

$$\begin{aligned} a_{1122}^{hom} &= \frac{\nu_{21} E_1 h}{(1 - \nu_{12} \nu_{21})}, \\ a_{2222}^{hom} &= \frac{E_2 h}{(1 - \nu_{12} \nu_{21})}, \\ a_{1212}^{hom} &= Gh, \end{aligned}$$

the equation can be written as

$$\frac{\nu_{21} E_1 h}{1 - \nu_{12} \nu_{21}} \left( \frac{\partial^2 \mathcal{U}_1}{\partial s_1 \partial s_2} + \frac{1}{a} \frac{\partial \mathcal{U}_3}{\partial s_2} \right) + \frac{E_2 h}{1 - \nu_{12} \nu_{21}} \frac{\partial^2 \mathcal{U}_2}{\partial s_2^2} + Gh \left( \frac{\partial^2 \mathcal{U}_1}{\partial s_1 \partial s_2} + \frac{\partial^2 \mathcal{U}_2}{\partial s_1^2} \right) = 0,$$

which yields by some simplifications

$$\frac{E_2}{1 - \nu_{12} \nu_{21}} \frac{\partial^2 \mathcal{U}_2}{\partial s_2^2} + G \frac{\partial^2 \mathcal{U}_2}{\partial s_1^2} + \left( \frac{E_1 \nu_{21}}{1 - \nu_{12} \nu_{21}} + G \right) \frac{\partial^2 \mathcal{U}_1}{\partial s_1 \partial s_2} + \frac{E_1 \nu_{21}}{1 - \nu_{12} \nu_{21}} \frac{1}{a} \frac{\partial \mathcal{U}_3}{\partial s_2} = 0. \quad (3.1.5)$$

This concludes the first equation in (3.1.3). We continue with the terms involving  $\mathcal{V}_1$ , where we do not only have membrane effects, but also bending terms. Going through all expressions in (3.1.4) we obtain

$$\begin{aligned} &a_{1111}^{hom} \left( -\frac{\partial^2 \mathcal{U}_1}{\partial s_1^2} - \frac{1}{a} \frac{\partial \mathcal{U}_3}{\partial s_1} \right) - a_{2211}^{hom} \frac{\partial^2 \mathcal{U}_2}{\partial s_1 \partial s_2} + a_{1212}^{hom} \left( -\frac{\partial^2 \mathcal{U}_1}{\partial s_2^2} - \frac{\partial^2 \mathcal{U}_2}{\partial s_1 \partial s_2} \right) \\ &+ c_{1111}^{hom} \left( \frac{1}{a} \frac{\partial^3 \mathcal{U}_3}{\partial s_1^3} - \frac{1}{a^2} \frac{\partial^2 \mathcal{U}_1}{\partial s_1^2} \right) + c_{2211}^{hom} \frac{1}{a} \frac{\partial^3 \mathcal{U}_3}{\partial s_1 \partial s_2^2} + 4c_{1212}^{hom} \left( \frac{1}{a} \frac{\partial^3 \mathcal{U}_3}{\partial s_1 \partial s_2^2} - \frac{1}{a^2} \frac{\partial^2 \mathcal{U}_1}{\partial s_2^2} \right) = 0. \end{aligned}$$

Again from [50] we have that

$$\begin{aligned} a_{1111}^{hom} &= \frac{E_1 h}{12(1 - \nu_{12} \nu_{21})}, & a_{2211}^{hom} &= \frac{\nu_{21} E_1 h}{12(1 - \nu_{12} \nu_{21})}, \\ c_{1111}^{hom} &= \frac{E_1 h^3}{12(1 - \nu_{12} \nu_{21})}, & c_{2211}^{hom} &= \frac{E_1 \nu_{21} h^3}{12(1 - \nu_{12} \nu_{21})}, & c_{1212}^{hom} &= \frac{Gh^3}{12}, \end{aligned}$$

and plugging these results into the previous equation while dividing it by  $h$  yields

$$\begin{aligned} &\frac{E_1}{1 - \nu_{12} \nu_{21}} \left( \frac{\partial^2 \mathcal{U}_1}{\partial s_1^2} + \frac{1}{a} \frac{\partial \mathcal{U}_3}{\partial s_1} \right) + \frac{\nu_{21} E_1}{1 - \nu_{12} \nu_{21}} \frac{\partial^2 \mathcal{U}_2}{\partial s_1 \partial s_2} + G \left( \frac{\partial^2 \mathcal{U}_1}{\partial s_2^2} + \frac{\partial^2 \mathcal{U}_2}{\partial s_1 \partial s_2} \right) \\ &+ \frac{E_1 h^2}{12(1 - \nu_{12} \nu_{21})} \left( -\frac{1}{a} \frac{\partial^3 \mathcal{U}_3}{\partial s_1^3} + \frac{1}{a^2} \frac{\partial^2 \mathcal{U}_1}{\partial s_1^2} \right) - \frac{\nu_{21} E_1 h^2}{12(1 - \nu_{12} \nu_{21})} \frac{1}{a} \frac{\partial^3 \mathcal{U}_3}{\partial s_1 \partial s_2^2} \\ &+ \frac{4Gh^2}{12} \left( -\frac{1}{a} \frac{\partial^3 \mathcal{U}_3}{\partial s_1 \partial s_2^2} + \frac{1}{a^2} \frac{\partial^2 \mathcal{U}_1}{\partial s_2^2} \right) = 0. \end{aligned} \quad (3.1.6)$$

For the last part we collect the remaining terms with  $\mathcal{V}_3$  and together with the non-zero right-hand side we obtain

$$\begin{aligned} a_{1111}^{hom} \left( \frac{1}{a} \frac{\partial \mathcal{U}_1}{\partial s_1} + \frac{1}{a^2} \mathcal{U}_3 \right) + a_{2211}^{hom} \frac{1}{a} \frac{\partial \mathcal{U}_2}{\partial s_2} + c_{1111}^{hom} \left( \frac{\partial^4 \mathcal{U}_3}{\partial s_1^4} - \frac{1}{a} \frac{\partial^3 \mathcal{U}_1}{\partial s_1^3} \right) + c_{1122}^{hom} \left( \frac{\partial^4 \mathcal{U}_3}{\partial s_1^2 \partial s_2^2} - \frac{1}{a} \frac{\partial^3 \mathcal{U}_1}{\partial s_1 \partial s_2^2} \right) \\ + c_{2211}^{hom} \frac{\partial^4 \mathcal{U}_3}{\partial s_1^2 \partial s_2^2} + c_{2222}^{hom} \frac{\partial^4 \mathcal{U}_3}{\partial s_2^4} + 4c_{1212}^{hom} \left( \frac{\partial^4 \mathcal{U}_3}{\partial s_1^2 \partial s_2^2} - \frac{1}{a} \frac{\partial^3 \mathcal{U}_3}{\partial s_1 \partial s_2^2} \right) = q. \end{aligned}$$

We insert the expressions for the effective properties and divide both sides by  $h$ , such that we get

$$\begin{aligned} \frac{E_1}{1 - \nu_{12}\nu_{21}} \left( \frac{1}{a} \frac{\partial \mathcal{U}_1}{\partial s_1} + \frac{1}{a^2} \mathcal{U}_3 \right) + \frac{\nu_{21}E_1}{1 - \nu_{12}\nu_{21}} \frac{1}{a} \frac{\partial \mathcal{U}_2}{\partial s_2} + \frac{E_1 h^2}{12} \left( \frac{\partial^4 \mathcal{U}_3}{\partial s_1^4} - \frac{1}{a} \frac{\partial^3 \mathcal{U}_1}{\partial s_1^3} \right) \\ + \frac{\nu_{21}E_1 h^2}{12} \left( \frac{\partial^4 \mathcal{U}_3}{\partial s_1^2 \partial s_2^2} - \frac{1}{a} \frac{\partial^3 \mathcal{U}_1}{\partial s_1 \partial s_2^2} \right) + \frac{\nu_{21}E_1 h^2}{12} \frac{\partial^4 \mathcal{U}_3}{\partial s_1^2 \partial s_2^2} \\ + \frac{E_2 h^2}{12} \frac{\partial^4 \mathcal{U}_3}{\partial s_2^4} + \frac{4Gh^2}{12} \left( \frac{\partial^4 \mathcal{U}_3}{\partial s_1^2 \partial s_2^2} - \frac{1}{a} \frac{\partial^3 \mathcal{U}_3}{\partial s_1 \partial s_2^2} \right) = \frac{q}{h}, \end{aligned} \quad (3.1.7)$$

which concludes our claim.  $\square$

**Remark 3.1.3** *At this point we have a model similar to the one presented in [56]. Anyhow, we want to further simplify it as in [59, Art. 121] and [62] for a better symbolic treatment in chapter 5.*

By the remarks given in [62] and [59, p. 513] we have that  $\mathcal{U}_1$  and  $\mathcal{U}_2$  are of the order  $\sqrt{\frac{h\mathcal{U}_3}{a}}$ . Therefore, we can neglect the last three terms in the second equation of (3.1.3), which arose from the bending effects, and the third order terms in the third equation of (3.1.3). Hence, we can simplify the system to

$$\begin{aligned} \frac{E_2}{1 - \nu_{12}\nu_{21}} \frac{\partial^2 \mathcal{U}_2}{\partial s_2^2} + G \frac{\partial^2 \mathcal{U}_2}{\partial s_1^2} + \left( \frac{\nu_{21}E_1}{1 - \nu_{12}\nu_{21}} + G \right) \frac{\partial^2 \mathcal{U}_1}{\partial s_1 \partial s_2} + \frac{\nu_{21}E_1}{1 - \nu_{12}\nu_{21}} \frac{1}{a} \frac{\partial \mathcal{U}_3}{\partial s_2} = 0 \\ \frac{E_1}{1 - \nu_{12}\nu_{21}} \left( \frac{\partial^2 \mathcal{U}_1}{\partial s_1^2} + \frac{1}{a} \frac{\partial \mathcal{U}_3}{\partial s_1} \right) + \frac{\nu_{21}E_1}{1 - \nu_{12}\nu_{21}} \frac{\partial^2 \mathcal{U}_2}{\partial s_1 \partial s_2} + G \left( \frac{\partial^2 \mathcal{U}_1}{\partial s_2^2} + \frac{\partial^2 \mathcal{U}_2}{\partial s_1 \partial s_2} \right) = 0 \\ \frac{E_1}{1 - \nu_{12}\nu_{21}} \left( \frac{1}{a} \frac{\partial \mathcal{U}_1}{\partial s_1} + \frac{1}{a^2} \mathcal{U}_3 \right) + \frac{\nu_{21}E_1}{1 - \nu_{12}\nu_{21}} \frac{1}{a} \frac{\partial \mathcal{U}_2}{\partial s_2} + \frac{E_1 h^2}{12(1 - \nu_{12}\nu_{21})} \frac{\partial^4 \mathcal{U}_3}{\partial s_1^4} \\ + \frac{2\nu_{21}E_1 h^2}{12(1 - \nu_{12}\nu_{21})} \frac{\partial^4 \mathcal{U}_3}{\partial s_1^2 \partial s_2^2} + \frac{E_2 h^2}{12(1 - \nu_{12}\nu_{21})} \frac{\partial^4 \mathcal{U}_3}{\partial s_2^4} + \frac{4Gh^2}{12} \frac{\partial^4 \mathcal{U}_3}{\partial s_1^2 \partial s_2^2} = \frac{q}{h}. \end{aligned} \quad (3.1.8)$$

Note that by using the approximation for the shear modulus

$$G \approx \frac{\sqrt{E_1 E_2}}{2(1 + \sqrt{\nu_{12}\nu_{21}})}$$

and introducing the parameters  $H = E_1/E_2$ ,  $\bar{\nu} = \sqrt{\nu_{12}\nu_{21}}$  and  $c_{2222}^{hom}$ , the flexural rigidity in the  $s_2$  direction, we obtain the Donnell type formulation, see [20]. We can now follow the Airy stress function ansatz, as presented in [43, chapter 5]. This procedure can be seen as finding a potential for the stress distribution in the material. It is for example widely used in the investigation of stresses around holes as in [55]. Via this method it

is then possible to express  $\mathcal{U}_1$  and  $\mathcal{U}_2$  in terms of  $\mathcal{U}_3$  as presented in [56] and [59]. We then obtain the 8th order PDE

$$\left( \frac{\partial^2}{\partial s_2^2} + H^2 \frac{\partial^2}{\partial s_1^2} \right)^4 \mathcal{U}_3 + \frac{12(1-\bar{\nu})}{a^2 h^2} H^4 \frac{\partial^4 \mathcal{U}_3}{\partial s_2^4} - \frac{1}{c_{2222}^{hom}} \left( \frac{\partial^2}{\partial s_2^2} + H^2 \frac{\partial^2}{\partial s_1^2} \right)^2 q = 0, \quad (3.1.9)$$

describing the bending effect  $\mathcal{U}_3$ .

**Remark 3.1.4** *We want to mention here that in the isotropic case, i.e.,  $E_1 = E_2 = E$ ,  $\nu_{21} = \nu_{12} = \nu$  and  $G = \frac{E}{2(1+\nu)}$ , equation (3.1.8) corresponds to [59, equation (304)].*

**Remark 3.1.5** *It is mentioned in [10] that the pinched cylindrical shell is analog to a plate/beam on elastic foundation. This problem has been considered for example in [31].*

## 3.2 Analytic solution to the pinched cylinder problem

In this section we want to derive the solution of (3.1.9) in terms of a Fourier series in the circumferential direction and Fourier transform in the longitudinal one. Therefore, we assume that the half-cylinder is infinitely long. This assumption is an adequate simplification, due to the free boundary conditions as described in chapter 2. As a preliminary step we want to recall the definitions of Fourier series and transform as well as a corollary to the residual theorem, which allows us to calculate integrals over the real axis.

**Lemma 3.2.1** *Let  $Z$  and  $Q$  be two polynomials, such that  $\deg Z + 1 \leq \deg Q$ . Assume that  $Q$  has no real roots and define*

$$\mathbb{L} = \{z \in \mathbb{C} | \operatorname{Im}(z) > 0, Q(z) = 0\}.$$

*Then we have that*

$$\int_{-\infty}^{\infty} \frac{Z(\xi)}{Q(\xi)} \exp(ix\xi) d\xi = 2\pi i \sum_{\vartheta \in \mathbb{L}} \operatorname{Res}_{\vartheta} \frac{Z(\xi)}{Q(\xi)} \exp(ix\xi),$$

*where  $\operatorname{Res}_{\vartheta} f$  denotes the residual of  $f$  in  $\vartheta$ .*

*Proof.* We refer for a proof of this classical result to [8, Theorem 7.11]. □

**Definition 3.2.1** *The Fourier transform  $\tilde{w}$  of a function  $w \in L^1(\mathbb{R}^n)$  is defined as*

$$\mathcal{F}[w](\xi) = \int_{\mathbb{R}^n} w(x) e^{-i\xi \cdot x} dx, \quad (3.2.1)$$

*where  $x = (x_1, x_2, \dots, x_n)^T$ ,  $\xi = (\xi_1, \xi_2, \dots, \xi_n)^T$  and  $\xi \cdot x$  is the dot product. The inverse Fourier transform is then defined as*

$$\mathcal{F}^{-1}[\tilde{w}](x) = \frac{1}{(2\pi)^n} \int_{\mathbb{R}^n} \tilde{w}(\xi) e^{i\xi \cdot x} d\xi. \quad (3.2.2)$$

**Definition 3.2.2** A function  $f \in L^2((0, a\pi); \mathbb{R})$  can be expressed by its Fourier series given as

$$f(s) = \frac{a_0}{2} + \sum_{n=1}^{\infty} \left( a_n \cos\left(\frac{ns}{a}\right) + b_n \sin\left(\frac{ns}{a}\right) \right),$$

where

$$a_n = \frac{2}{a\pi} \int_0^{a\pi} f(s) \cdot \cos\left(\frac{ns}{a}\right) ds \text{ for } n \geq 0, \quad b_n = \frac{2}{a\pi} \int_0^{a\pi} f(s) \cdot \sin\left(\frac{ns}{a}\right) ds \text{ for } n \geq 1.$$

In our subsequent analysis we do not need to go any deeper into the theory. For some more references on this topic we refer to [3, Lemma 7.11, Lemma 7.12] for a functional analytic point of view and [21, chapter 4] for the applications in partial differential equations.

Now we use the classical ansatz of separation of variables and consider the function  $\mathcal{U}_3(s_1, s_2) = w_1(s_1)w_2(s_2)$ . Moreover, we want to follow the ideas presented in [33]. Note that in our case we consider a half shell with clamping conditions along the lateral boundaries. In [33] a full shell with symmetric loading is considered. The importance in our analysis is to capture the effects of different pinching locations. We assume that a pinching load is applied at  $(a\varphi_0, 0)$ ,  $\varphi_0 \in (0, \frac{\pi}{2}]$ . The choice  $s_2 = 0$  is w.l.o.g. possible, since we can always shift the cylinder along the  $s_2$ -axis. In order to solve for  $\mathcal{U}_3$  we calculate the Fourier transformation of  $w_2$  in the longitudinal direction while we take the Fourier series of  $w_1$  in the circumferential direction  $s_1$ . We can non-dimensionalize the equation by substituting  $s_2$  with  $\frac{s_2}{a}$ . This yields the representation of the deflection as

$$\mathcal{U}_3(s_1, s_2) = \left( \frac{1}{2\pi} \int_{-\infty}^{\infty} \tilde{w}_2(\xi) e^{-i\frac{s_2\xi}{a}} d\xi \right) \left( \frac{a_0}{2} + \sum_{n=1}^{\infty} a_n \cos\left(\frac{ns_1}{a}\right) + b_n \sin\left(\frac{ns_1}{a}\right) \right). \quad (3.2.3)$$

The crucial part is to ensure that  $\mathcal{U}_3$  satisfies the conditions  $\mathcal{U}_3(0, s_2) = \mathcal{U}_3(a\pi, s_2) = 0$ . Besides, we assume that  $\mathcal{U}_3$  also satisfies the six additional boundary conditions given as  $\mathcal{U}_3''(0, s_2) = \mathcal{U}_3''(a\pi, s_2) = \mathcal{U}_3^{IV}(0, s_2) = \mathcal{U}_3^{IV}(a\pi, s_2) = \mathcal{U}_3^{VI}(0, s_2) = \mathcal{U}_3^{VI}(a\pi, s_2) = 0$ . Thus, we can take  $a_n = 0$  for all  $n \in \mathbb{N}$  and have that the series only consists of  $\sum_{n=1}^{\infty} b_n \sin\left(\frac{ns}{a}\right)$ . A similar strategy was used in [37, section 72]. Furthermore, we can simplify the Fourier transform along the longitudinal direction by using the symmetry condition  $\mathcal{U}_3(s_1, s_2) = \mathcal{U}_3(s_1, -s_2)$ . Since the integral over uneven functions is zero we obtain the representation

$$\mathcal{U}_3(s_1, s_2) = \sum_{n=1}^{\infty} b_n \sin\left(\frac{ns_1}{a}\right) \int_0^{\infty} \frac{1}{\pi} \tilde{w}_2(\xi) \cos\left(\frac{\xi s_2}{a}\right) d\xi. \quad (3.2.4)$$

It is easy to see that  $\mathcal{U}_3$  satisfies our initial boundary conditions, since

$$\begin{aligned} \mathcal{U}_3(0, s_2) &= \frac{1}{\pi} \sum_{n=1}^{\infty} b_n \sin(0) \int_0^{\infty} \tilde{w}_2(\xi) \cos\left(\frac{\xi s_2}{a}\right) d\xi = 0, \\ \mathcal{U}_3(a\pi, s_2) &= \frac{1}{\pi} \sum_{n=1}^{\infty} b_n \sin(n\pi) \int_0^{\infty} \tilde{w}_2(\xi) \cos\left(\frac{\xi s_2}{a}\right) d\xi = 0. \end{aligned}$$

For the further analysis we introduce the coefficients  $\tilde{w}_n = \tilde{w}_2 \cdot b_n$ . Hence, we get

$$\mathcal{U}_3(s_1, s_2) = \frac{1}{\pi} \sum_{n=1}^{\infty} \sin\left(\frac{ns_1}{a}\right) \int_0^{\infty} \tilde{w}_n(\xi) \cos\left(\frac{\xi s_2}{a}\right) d\xi. \quad (3.2.5)$$



Moreover, we need that the load  $q$  has to be expressed in the same way as

$$q(s_1, s_2) = \sum_{n=1}^{\infty} q_n \sin\left(\frac{ns_1}{a}\right) \int_0^{\infty} \frac{1}{\pi} \tilde{q}(\xi) \cos\left(\frac{\xi s_2}{a}\right) d\xi. \quad (3.2.6)$$

**Remark 3.2.1** *Given a pinching load, represented by expression (3.2.6), applied to a full shell, we obtain a setup with two opposing pinches at  $(0, a\varphi_0)$  and  $(0, -a\varphi_0)$  as shown in figure 3.1. The consequence of that choice is that the resulting displacements cancel each other out at  $(0, s_2)$  and  $(a\pi, s_2)$ .*

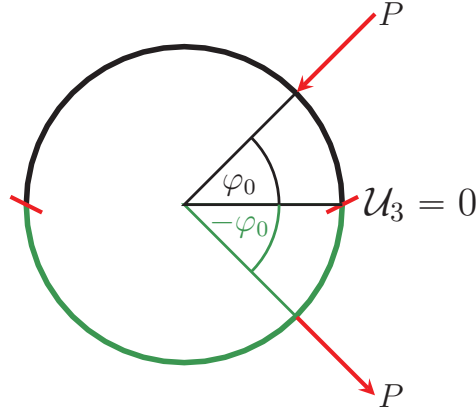


Figure 3.1: Full cylindrical shell with opposing force on each half circle.

Inserting the expressions (3.2.3) and (3.2.6) into (3.1.9) yields the equation

$$\begin{aligned} \sum_{n=1}^{\infty} \int_0^{\infty} \left[ \left( \left( \frac{\xi}{a} \right)^2 + H^2 \left( \frac{n}{a} \right)^2 \right)^4 + \frac{12(1-\bar{\nu})}{a^2 h^2} H^4 \left( \frac{\xi}{a} \right)^4 \right] \tilde{w}_n(\xi) \sin\left(\frac{ns_1}{a}\right) \cos\left(\frac{\xi s_2}{a}\right) d\xi = \\ \sum_{n=1}^{\infty} \int_0^{\infty} \left[ \frac{1}{c_{2222}^{hom}} \left( \left( \frac{\xi}{a} \right)^2 + H^2 \left( \frac{n}{a} \right)^2 \right)^2 \right] \tilde{q}(\xi) q_n \sin\left(\frac{ns_1}{a}\right) \cos\left(\frac{\xi s_2}{a}\right) d\xi. \end{aligned}$$

By comparison of the coefficients we have to ensure that

$$\begin{aligned} \left[ \left( \left( \frac{\xi}{a} \right)^2 + H^2 \left( \frac{n}{a} \right)^2 \right)^4 + \frac{12(1-\bar{\nu})}{a^2 h^2} H^4 \left( \frac{\xi}{a} \right)^4 \right] \tilde{w}_n(\xi) = \\ \left[ \frac{1}{c_{2222}^{hom}} \left( \left( \frac{\xi}{a} \right)^2 + H^2 \left( \frac{n}{a} \right)^2 \right)^2 \right] \tilde{q}(\xi) q_n, \end{aligned}$$

is fulfilled for all  $n \in \mathbb{N}$ . This equation implies that the Fourier transform  $\tilde{w}_n$  has to be chosen such that

$$\tilde{w}_n(\xi) = \frac{\left[ \frac{1}{c_{2222}^{hom}} \left( \left( \frac{\xi}{a} \right)^2 + H^2 \left( \frac{n}{a} \right)^2 \right)^2 \right] \tilde{q}(\xi) q_n}{\left[ \left( \left( \frac{\xi}{a} \right)^2 + H^2 \left( \frac{n}{a} \right)^2 \right)^4 + \frac{12(1-\bar{\nu})}{a^2 h^2} H^4 \left( \frac{\xi}{a} \right)^4 \right]}, \quad (3.2.7)$$

where  $\tilde{q}$  is the Fourier transform of  $q$  along the  $s_2$ -axis and the  $q_n$  are the coefficients of the Fourier series along the circumferential direction  $s_1$ . In our analysis we actually want to study the effects of a point load  $q^{\text{pinch}}(s_1, s_2)$  at  $(a\varphi_0, 0)$ . In general this leads to problems in the calculation of  $\tilde{q}$  and  $q_n$ , hence we consider an approximation given as  $q(s_1, s_2)$ .

**Definition 3.2.3** Take  $c, \theta, P \in \mathbb{R}$ , such that both  $0 < c \ll 1$  and  $0 < \theta \ll 1$ . We consider a pinching load

$$q^{pinch}(s_1, s_2) = P \delta^D(s_1 - a\varphi_0) \delta^D(s_2),$$

where  $\delta^D(\cdot)$  denotes the Dirac distribution.

The approximate pinching load is defined as

$$q(s_1, s_2) = \begin{cases} \tilde{P}, & \text{if } a\varphi_0 - c \leq s_1 \leq a\varphi_0 + c, \quad -\theta \leq s_2 \leq \theta \\ 0, & \text{else} \end{cases}. \quad (3.2.8)$$

We can split  $q(s_1, s_2) = \hat{q}(s_1) \cdot q^*(s_2)$ , where

$$\hat{q}(s_1) = \begin{cases} \tilde{P}, & \text{if } a\varphi_0 - c \leq s_1 \leq a\varphi_0 + c, \\ 0, & \text{else} \end{cases} \quad q^*(s_2) = \begin{cases} 1, & \text{if } -\theta \leq s_2 \leq \theta, \\ 0, & \text{else} \end{cases}$$

and  $\tilde{P}$  can be chosen as  $\frac{P}{4c\theta}$ .

**Remark 3.2.2** In general one has  $q^{pinch} \in H^{-2}(\omega)$ , while for the approximation we obtain  $q \in L^2(\omega)$ . The results on  $q^{pinch}$  are presented in [31].

In figure 3.2 we illustrate the mentioned approximated load to  $q^{pinch}$ .

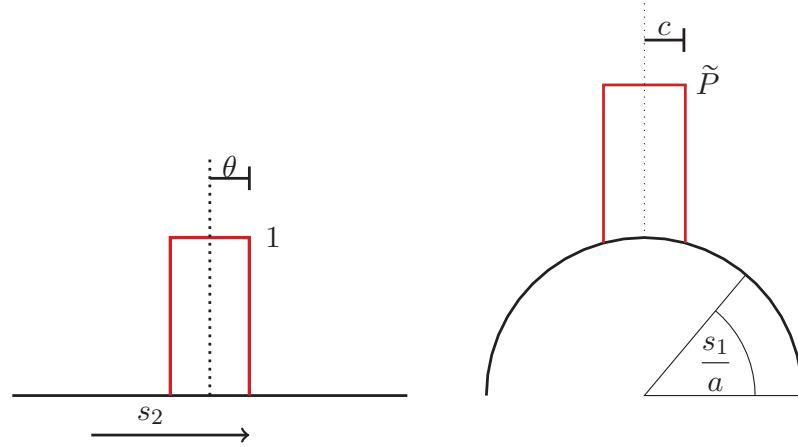


Figure 3.2: Approximate pinching load on the shell.

The Fourier transformation and the Fourier series coefficients are straight forward to calculate and summarized in the following Lemma.

**Lemma 3.2.2** Given the load  $q$  as defined above we can express it as in (3.2.6), where

$$\begin{aligned} \tilde{q}(\xi) &= \frac{2}{\xi} \sin\left(\xi \frac{\theta}{a}\right), \\ q_n &= -\frac{4\tilde{P}}{n\pi} \sin\left(\frac{nc}{a}\right) \sin(n\varphi_0). \end{aligned}$$

*Proof.* We start with the Fourier transform of  $q$  in the longitudinal direction. For this step we may identify  $q$  only with  $q^*$ . Thus, we obtain

$$\begin{aligned}\tilde{q}(\xi) &= \int_{-\infty}^{\infty} q^*(s_2) \cos\left(\frac{\xi s_2}{a}\right) d\left(\frac{s_2}{a}\right) = \int_{-\theta}^{\theta} \cos\left(\frac{\xi s_2}{a}\right) d\left(\frac{s_2}{a}\right) \\ &= \frac{2}{\xi} \sin\left(\xi \frac{\theta}{a}\right).\end{aligned}\quad (3.2.9)$$

For the Fourier series coefficients we take  $\hat{q}$  and consider the integrals of the form

$$q_n = \frac{2}{a\pi} \int_0^{a\pi} \hat{q}(s_1) \sin\left(\frac{ns_1}{a}\right) ds_1. \quad (3.2.10)$$

This has to be calculated for all  $n \in \mathbb{N}$ . By the properties of  $\hat{q}$  we get

$$\frac{2}{a\pi} \int_0^{a\pi} \hat{q}(s_1) \sin\left(\frac{ns_1}{a}\right) ds_1 = \frac{2\tilde{P}}{a\pi} \int_{a\varphi_0-c}^{a\varphi_0+c} \sin\left(\frac{ns_1}{a}\right) ds_1.$$

With the linear transformation  $z = s_1 - a\varphi_0$  and employing the well-known addition theorem for cosine we obtain

$$\begin{aligned}\int_{a\varphi_0-c}^{a\varphi_0+c} \sin\left(\frac{ns}{a}\right) ds &= \int_{-c}^c \sin\left(\frac{n}{a}(z + a\varphi_0)\right) dz = \int_{-c}^c \sin\left(\frac{nz}{a} + n\varphi_0\right) dz \\ &= -\frac{a}{n} \left[ \cos\left(\frac{nc}{a} + n\varphi_0\right) - \cos\left(\frac{nc}{a} - n\varphi_0\right) \right] \\ &= -\frac{a}{n} \left[ \cos\left(\frac{nc}{a}\right) \cos(n\varphi_0) - \sin\left(\frac{nc}{a}\right) \sin(n\varphi_0) \right. \\ &\quad \left. - \cos\left(\frac{nc}{a}\right) \cos(n\varphi_0) - \sin\left(\frac{nc}{a}\right) \sin(n\varphi_0) \right] \\ &= -\frac{2a}{n} \sin\left(\frac{nc}{a}\right) \sin(n\varphi_0).\end{aligned}$$

Plugging this back into expression (3.2.10) yields

$$q_n = -\frac{4\tilde{P}}{n\pi} \sin\left(\frac{nc}{a}\right) \sin(n\varphi_0). \quad (3.2.11)$$

□

**Remark 3.2.3** It holds that  $\theta \ll 1$  and  $c \ll 1$ . Hence, we can use the approximations

$$\begin{aligned}\frac{2}{\xi} \sin\left(\xi \frac{\theta}{a}\right) &\approx \frac{2\theta}{a}, \\ -\frac{4\tilde{P}}{n\pi} \sin\left(\frac{nc}{a}\right) \sin(n\varphi_0) &\approx -\frac{4\tilde{P}c}{a\pi} \sin(n\varphi_0).\end{aligned}\quad (3.2.12)$$

Inserting now the approximate formulas (3.2.12) back into equation (3.2.7) yields the relation

$$\tilde{w}_n(\xi) = -\frac{8\tilde{P}\theta c}{\pi a^2} \sin(n\varphi_0) \frac{\left[ \frac{1}{c_{2222}^{hom}} \left( \left( \frac{\xi}{a} \right)^2 + H^2 \left( \frac{n}{a} \right)^2 \right)^2 \right]}{\left[ \left( \left( \frac{\xi}{a} \right)^2 + H^2 \left( \frac{n}{a} \right)^2 \right)^4 + \frac{12(1-\bar{\nu})}{a^2 h^2} H^4 \left( \frac{\xi}{a} \right)^4 \right]}.$$

Using now that  $P = 4\tilde{P}\theta c$  and with  $k = (3(1 - \bar{\nu}^2)(a/h)^2)^{\frac{1}{4}}$  we can express the deflection  $\mathcal{U}_3$  as

$$\mathcal{U}_3(s_1, s_2) = -\frac{2Pa^2}{\pi^2 c_{2222}^{hom}} \sum_{n=1}^{\infty} \sin\left(\frac{ns_1}{a}\right) \sin(n\varphi_0) \int_0^{\infty} \frac{(\xi^2 + H^2 n^2)^2}{(\xi^2 + H^2 n^2)^4 + 4k^4 H^4 \xi^4} \cos\left(\frac{\xi s_1}{a}\right) d\xi, \quad (3.2.13)$$

where we are left with the calculation of the integral. By applying the corollary to the residue theorem shown in Lemma 3.2.1 we are able to derive each integral with respect to  $n \in \mathbb{N}$ . This was actually already shown in [33] for the case of an orthotropic full cylindrical shell with a symmetrical pinching load, where the identical integral expressions are obtained. The isotropic case was shown in full detail in [62]. Since the derivation in [33] is rather condensed we want to present some details in the following Lemma.

**Lemma 3.2.3** *Given the expression (3.2.13) for  $\mathcal{U}_3$ , we obtain with Lemma 3.2.1 that*

$$\begin{aligned} \mathcal{U}_3(s_1, s_2) = & \frac{2Pk^4}{\pi E_2 h H^3} \sum_{n=1,2,3,4,\dots}^{\infty} \frac{\sin(n\varphi_0)}{R_2 n^2} \sin\left(\frac{ns_1}{a}\right) \\ & \times \left\{ \left[ \left( \zeta C + \eta G \right) \cos\left(\frac{HA|s_2|}{a}\right) + \left( \zeta G - \eta C \right) \sin\left(\frac{HA|s_2|}{a}\right) \right] \exp\left(-\frac{HB|s_2|}{a}\right) \right. \\ & \left. + \left[ \left( \zeta A - \eta B \right) \cos\left(\frac{HC|s_2|}{a}\right) + \left( \eta A + \zeta B \right) \sin\left(\frac{HC|s_2|}{a}\right) \right] \exp\left(-\frac{HG|s_2|}{a}\right) \right\}, \end{aligned} \quad (3.2.14)$$

where the parameters appearing in the formula are given as

$$\begin{aligned} k &= (3(1 - \nu_{12}\nu_{21})(a/h)^2)^{\frac{1}{4}}, & H &= \frac{c_{1111}^{hom}}{c_{2222}^{hom}}, \\ J &= 2k^2, & R_2 &= n^2 J \sqrt{1 + (J/4n^2)^2}, \\ \zeta &= \sqrt{\frac{1}{2}(R_2 + \frac{1}{4}J^2)}, & \eta &= \sqrt{\frac{1}{2}(R_2 - \frac{1}{4}J^2)}, \\ A &= \frac{1}{\sqrt{2}} \left[ \sqrt{(-n^2 + \eta)^2 + \left(-\frac{J}{2} + \zeta\right)^2} - (n^2 - \eta) \right] \frac{1}{2}, \\ B &= \frac{1}{\sqrt{2}} \left[ \sqrt{(-n^2 + \eta)^2 + \left(-\frac{J}{2} + \zeta\right)^2} + (n^2 - \eta) \right] \frac{1}{2}, \\ C &= \frac{1}{\sqrt{2}} \left[ \sqrt{(n^2 + \eta)^2 + \left(\frac{J}{2} + \zeta\right)^2} - (n^2 + \eta) \right] \frac{1}{2}, \\ G &= \frac{1}{\sqrt{2}} \left[ \sqrt{(n^2 + \eta)^2 + \left(\frac{J}{2} + \zeta\right)^2} + (n^2 + \eta) \right] \frac{1}{2}. \end{aligned}$$

*Proof.* We are mainly interested in the evaluation of

$$\int_0^\infty \frac{\left(\xi^2 + H^2 n^2\right)^2}{\underbrace{\left(\xi^2 + H^2 n^2\right)^4 + 4k^4 H^4 \xi^4}_{=f(\xi)}} \cos\left(\frac{\xi s_1}{a}\right) d\xi. \quad (3.2.15)$$

We first note that  $f(\xi)$  can be represented by  $f(\xi) = \frac{Z(\xi)}{Q(\xi)}$ , where  $Z, Q$  are polynomials given as

$$Z(\xi) = \left(\xi^2 + H^2 n^2\right)^2, \quad Q(\xi) = \left(\xi^2 + H^2 n^2\right)^4 + 4k^4 H^4 \xi^4.$$

We can easily see that  $\deg(Z) + 1 = 5 \leq 8 = \deg(Q)$ . Moreover, we conclude that  $Q(\xi)$  does not have real roots, since  $Q(\xi) \geq H^8 n^8$ , for all  $n \in \mathbb{N}$ . Hence, the requirements of Lemma 3.2.1 are fulfilled and it is applicable. In the next step we explicitly calculate the roots of  $Q$  by solving

$$\left(\xi^2 + H^2 n^2\right)^4 + 4k^4 H^4 \xi^4 = 0.$$

Introducing  $\tilde{\lambda} = \frac{\xi}{H}$ , we get the equation

$$\left(\tilde{\lambda}^2 + n^2\right)^4 + J^2 \tilde{\lambda}^4 = 0$$

or equivalently written as

$$\left(\underbrace{\left(\tilde{\lambda}^2 + n^2\right)^2 + iJ\tilde{\lambda}^2}_I\right) \cdot \left(\underbrace{\left(\tilde{\lambda}^2 + n^2\right)^2 - iJ\tilde{\lambda}^2}_{II}\right) = 0.$$

By introducing  $x = \tilde{\lambda}^2$  we obtain for  $I$

$$(x + n^2)^2 + iJx = x^2 + (2n^2 + iJ)x + n^4 = 0.$$

Solving for  $x$  yields

$$\begin{aligned} x_{1,2} &= -\frac{(2n^2 + iJ)}{2} \pm \sqrt{\left(\frac{2n^2 + iJ}{2}\right)^2 - n^4} \\ &= -n^2 - i\frac{J}{2} \pm \underbrace{\sqrt{-\frac{J^2}{4} + iJn^2}}_{(*)}. \end{aligned}$$

It can be easily shown that for  $z \in \mathbb{C}$ , with  $z = c + di$ , we have that

$$\sqrt{z} = \frac{1}{\sqrt{2}} \sqrt{\sqrt{c^2 + d^2} + c} + \frac{i \operatorname{sgn}(d)}{\sqrt{2}} \frac{1}{\sqrt{2}} \sqrt{\sqrt{c^2 + d^2} - c}$$

is a root of  $z$ . With that result we can simplify  $(*)$  to

$$\begin{aligned} &\frac{1}{\sqrt{2}} \sqrt{\sqrt{\frac{J^4}{16} + J^2 n^4} - \frac{J^2}{4}} + \frac{i}{\sqrt{2}} \sqrt{\sqrt{\frac{J^4}{16} + J^2 n^4} + \frac{J^2}{4}} \\ &= \frac{1}{\sqrt{2}} \sqrt{R_2 - \frac{J^2}{4}} + \frac{i}{\sqrt{2}} \sqrt{R_2 + \frac{J^2}{4}} = \eta + i\zeta. \end{aligned}$$

Going back to the equation  $x = \tilde{\lambda}^2$  we need that

$$\tilde{\lambda}^2 = -(n^2 \mp \eta) + i(-\frac{J}{2} \pm \zeta).$$

Thus, we obtain

$$\begin{aligned} \tilde{\lambda}_{1,2} &= \pm \sqrt{-(n^2 - \eta) + i(-\frac{J}{2} + \zeta)} \\ &= \pm \frac{1}{\sqrt{2}} \sqrt{\sqrt{(n^2 - \eta)^2 + (-\frac{J}{2} + \zeta)^2} - (n^2 - \eta)} \\ &\quad \pm \frac{i}{\sqrt{2}} \sqrt{\sqrt{(n^2 - \eta)^2 + (-\frac{J}{2} + \zeta)^2} + (n^2 - \eta)} \\ &= \pm A \pm Bi. \end{aligned}$$

Moreover, we have that  $\tilde{\lambda}_{3,4} = \bar{\tilde{\lambda}}_{1,2}$ , where the bar denotes the complex conjugation. These are the 4 roots given by  $I$ . In the same way we get the other 4 roots from  $II$  expressed as

$$\tilde{\lambda}_{5,6} = \bar{\tilde{\lambda}}_{7,8} = \pm C \mp iG.$$

Therefore, we get the 8 roots  $\xi_i$ ,  $i = 1, \dots, 8$ , of  $Q(\xi)$  with  $\xi_{1,2} = \bar{\xi}_{3,4} = \pm H(A \pm Bi)$  and  $\xi_{5,6} = \bar{\xi}_{7,8} = \pm H(C \mp Gi)$ . In the next step we want to apply Lemma 3.2.1 to evaluate the integral. We note that the function  $f(\xi)$  is even and therefore satisfies that

$$\int_{-\infty}^{\infty} f(\xi) \sin\left(\frac{\xi s_1}{a}\right) d\xi = 0.$$

Hence, we can calculate the integral (3.2.15) as

$$\int_0^{\infty} f(\xi) \cos\left(\frac{\xi s_1}{a}\right) d\xi = \frac{1}{2} \int_{-\infty}^{\infty} f(\xi) \exp\left(\frac{i\xi s_1}{a}\right) d\xi = \pi i \sum_{\vartheta \in \mathbb{L}} \text{Res}_{\vartheta} f(\xi) \exp\left(\frac{i\xi s_1}{a}\right),$$

where we have by [8, remark 6.4 (2)] that

$$\text{Res}_{\vartheta} f(\xi) \exp\left(\frac{i\xi s_1}{a}\right) = \frac{\left(\vartheta^2 + H^2 n^2\right)^2 \exp\left(\frac{i\vartheta s_1}{a}\right)}{8\vartheta(\vartheta^2 + H^2 n^2)^3 + 16k^4 H^4 \vartheta^3}.$$

We observe that  $|\mathbb{L}| = 4$  and calculate  $\text{Res}_{\vartheta} f(\xi) \exp\left(\frac{i\xi s_1}{a}\right)$  for  $\vartheta_1 = H(A + Bi) = H\hat{\vartheta}_1$ . The other cases follow in the same way. Moreover, we focus on the calculation of the expression

$$\frac{\left(\vartheta_1^2 + H^2 n^2\right)^2}{8\vartheta_1(\vartheta_1^2 + H^2 n^2)^3 + 16k^4 H^4 \vartheta_1^3}. \quad (3.2.16)$$

For the evaluation we need the identities

$$\begin{aligned} (A + Bi)^2 &= -n^2 + \eta + \left(\frac{J}{2} + \zeta\right)i, \\ \hat{\vartheta}_1 \hat{\vartheta}_5 &= -n^2, \end{aligned} \quad (3.2.17)$$

which are easily verified. Moreover, we conclude that  $\hat{\vartheta}$  satisfies the equation

$$(\hat{\vartheta}_1^2 + n^2)^2 + iJ\hat{\vartheta}_1^2 = 0. \quad (3.2.18)$$

Then we simplify expression (3.2.16) to

$$\frac{1}{8H^3} \frac{(\hat{\vartheta}_1^2 + n^2)^2}{\hat{\vartheta}_1(\hat{\vartheta}_1^2 + n^2)^3 + \frac{J^2}{2}\hat{\vartheta}_1^3}.$$

With the property (3.2.18) this reduces to

$$\frac{1}{8H^3} \frac{-iJ\hat{\vartheta}_1^2}{\hat{\vartheta}_1^3 \left( -iJ(\hat{\vartheta}_1^2 + n^2) + \frac{J^2}{2} \right)}.$$

Together with (3.2.17)<sub>1</sub> and then using (3.2.17)<sub>2</sub> we obtain

$$\begin{aligned} \frac{1}{8H^3} \frac{1}{\hat{\vartheta}_1(\eta + \zeta i)} &= \frac{1}{8H^3} \frac{\hat{\vartheta}_5(\eta - \zeta i)}{\hat{\vartheta}_5 \hat{\vartheta}_1 \underbrace{(\eta^2 + \zeta^2)}_{=R_2}} \\ &= -\frac{1}{8H^3 R_2 n^2} (C - Gi)(\eta + \zeta i). \end{aligned}$$

Altogether, this yields

$$\begin{aligned} \int_0^\infty f(\xi) \cos\left(\frac{\xi s_1}{a}\right) d\xi = & -\frac{\pi i}{8H^3 R_2 n^2} \left[ (C - Gi)(\eta - \zeta i) \exp\left(\frac{i(A + Bi)s_1}{a}\right) \right. \\ & + (-C - Gi)(\eta - i\zeta) \exp\left(\frac{i(-A + Bi)s_1}{a}\right) \\ & - (A + Bi)(\eta - i\zeta) \exp\left(\frac{i(C - Gi)s_1}{a}\right) \\ & \left. - (-A + Bi)(\eta - i\zeta) \exp\left(\frac{i(-C - Gi)s_1}{a}\right) \right], \end{aligned}$$

which can then, by a small computation, be further simplified to our equation (3.2.14).  $\square$

It is crucial to note, that the applicability of this model highly depends on the ratio  $a/h$  and the magnitude of the corresponding Young's moduli. Such an investigation is provided in [62].

### 3.2.1 Examples

In the following part we want to investigate the function, which we have derived in the previous calculation by visualizing different parameter settings. Since we cannot calculate the complete Fourier series we restrict ourselves to the first 30 series elements and check their impact on the complete solution, by plotting the respective percentage for the maximal deflection and checking the convergence of the partial sums

$$S_n = \sum_{i=1}^n \tilde{w}_n.$$

From that we can deduce up to which element  $\tilde{w}_n$  one should derive the series before the values get negligible. These observations are crucial for chapter 5, because in the symbolic calculation we do not want to add unnecessary elements. Moreover, we fix throughout our examples the applied force, such that  $P = -0.8$  N as well as the thickness  $h = 0.1$  cm and radius  $a = 2$  cm. The shell's length is equal to 20 cm. In the following we start with an isotropic shell and apply the load at  $\varphi_0 \in \left\{\frac{\pi}{2}, \frac{\pi}{4}, \frac{\pi}{6}, \frac{\pi}{8}\right\}$ . After that we consider an orthotropic one with the same configurations. In the end we conclude the section by comparing our model with the numerical solution to the full weak formulation (3.1.2).

### Isotropic Shell

In the first example we deal with an isotropic homogeneous shell, where we assume that the Young's modulus is given by  $E_1 = E_2 = 200$  MPa and the Poisson's ratio is  $\nu = 0.27$ . In figure 3.3 we have plotted the deflected shell given the described load at  $\varphi = \frac{\pi}{2}$ . The underlying colormap represents the absolute values of  $\mathcal{U}_3$ . We can see that the maximal deflection is indeed attained at  $\frac{\pi}{2}$  and the effects of the prescribed boundary conditions are clearly visible. While at the lateral boundary the deflection is  $\mathcal{U}_3 = 0$ , we have some small displacements at the free boundaries  $s_2 = \pm 10$ . Moreover, we compare in figure 3.4 the original configuration with the deflected shell at  $s_2 = 0$ . There we can see that even for small loads the shell deforms in a way, such that the deflected shell is always smaller than the original one.

In the next step we want to investigate the elements  $\tilde{w}_n$  of the Fourier series. We

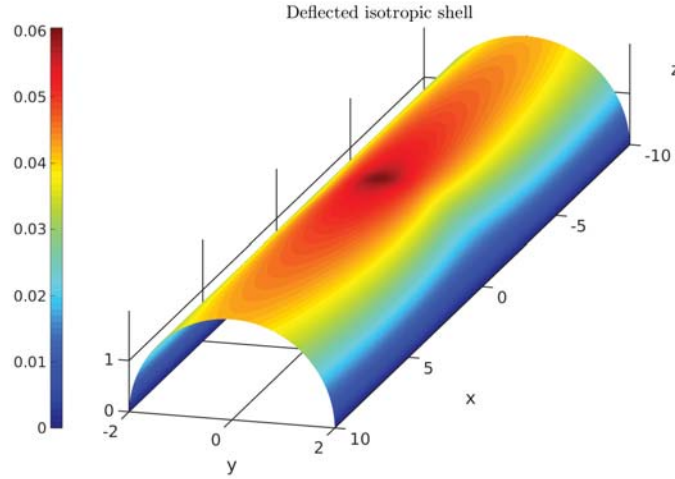


Figure 3.3: Isotropic shell with load at  $\varphi_0 = \frac{\pi}{2}$ .

have summarized the values for the first 12 elements in table 3.1 calculated at  $(a\frac{\pi}{2}, 0)$ . Note that we obviously have  $\tilde{w}_n = 0$  for  $n$  even, since our formula depends on the coefficient  $\sin(n\varphi_0) = \sin(n\frac{\pi}{2})$ . We can see that the values get smaller rather quickly. For example is  $\tilde{w}_{11}$  almost 200 times smaller than the first one. In figure 3.5 we have plotted the impact of each element by calculating what percentage they contribute to the maximal deflection at  $\varphi_0 = \frac{\pi}{2}$ . We see that the first four non-zero elements have the biggest effects. This observation is verified by looking at figure 3.6. The partial sums are already for  $n = 11$  at  $-0.06$ , where the value for  $S_{30}$  is  $-0.061$ . This means, that



### Comparison of deformed and undeformed shell

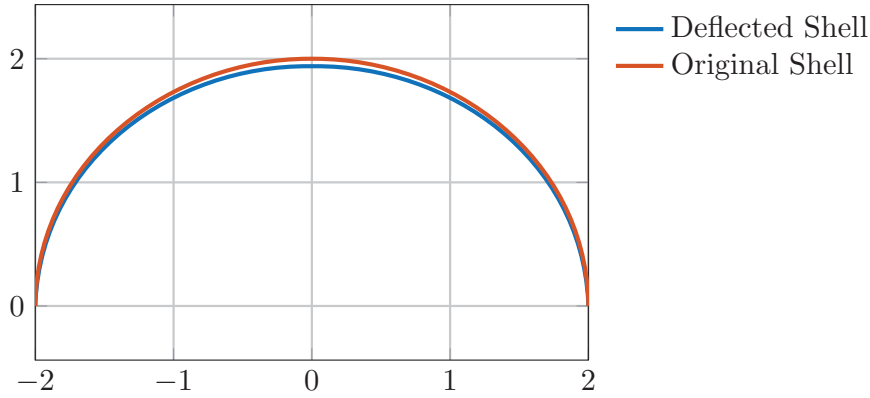


Figure 3.4: Deflected shell at  $s_2 = 0$ .

for the isotropic case with the loading at  $\frac{a\pi}{2}$  we can terminate the Fourier series earlier at around  $n = 11$ .

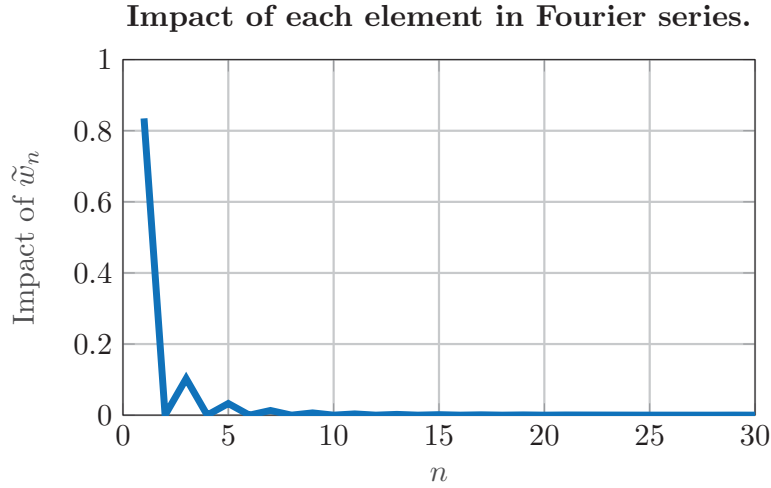
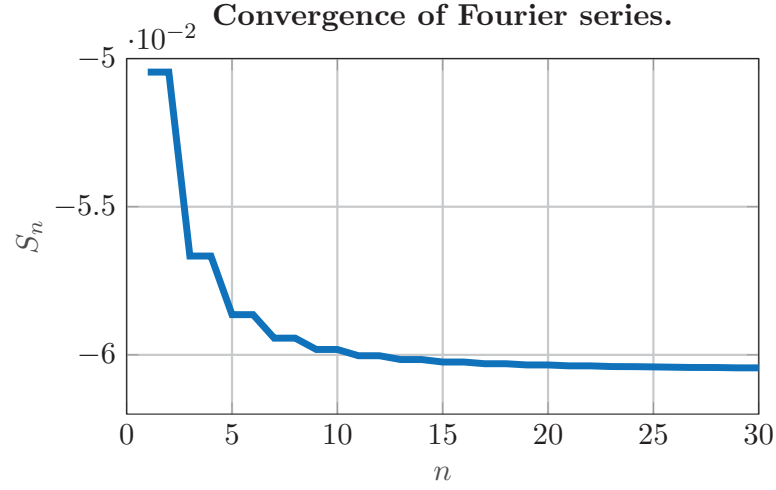
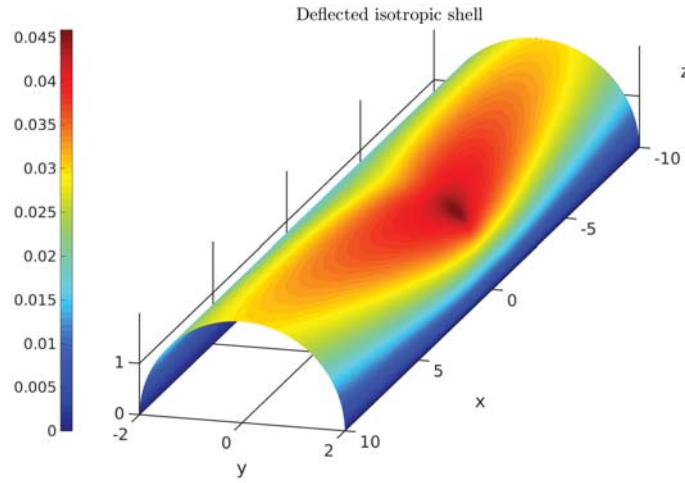


Figure 3.5: Respective impact of each element

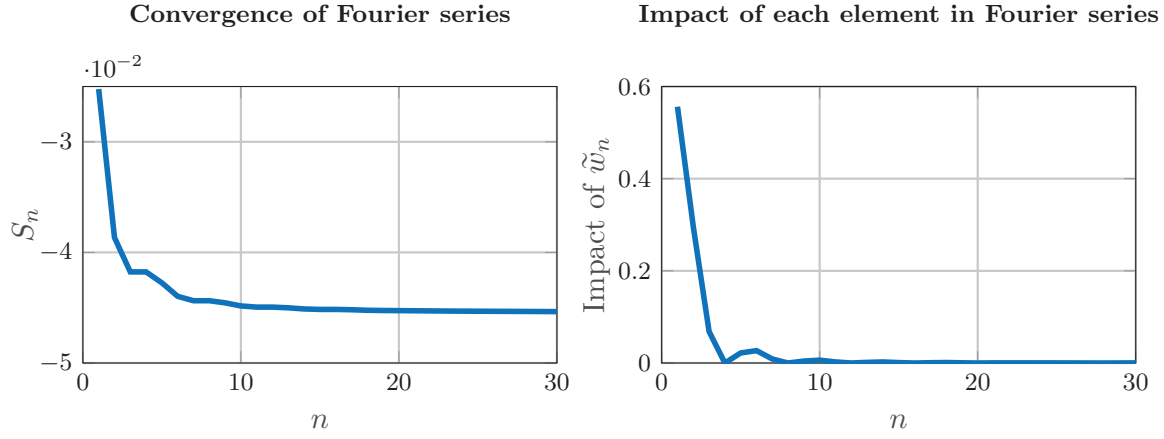
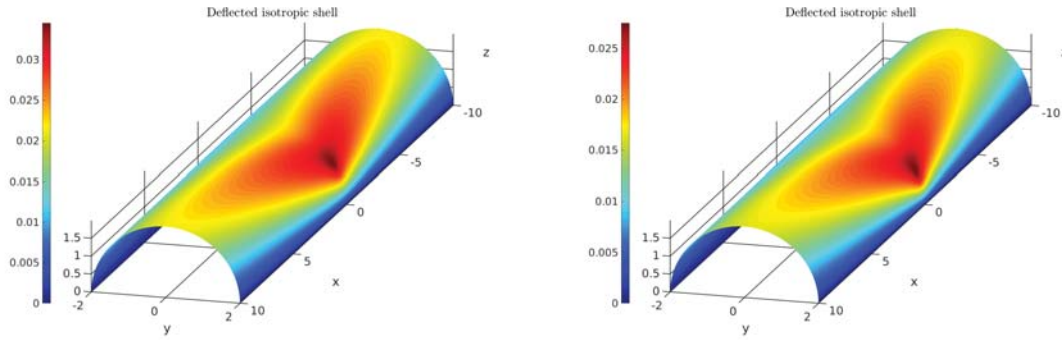
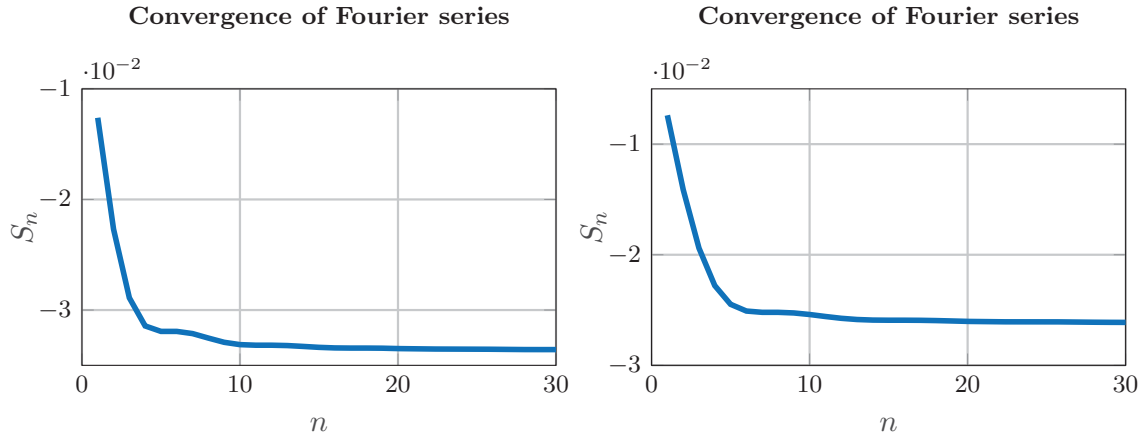
n	1	3	5	7	9	11
$\tilde{w}_n$	-0.050455	-0.0062096	-0.0019784	-0.0007928	-0.0003826	-0.0002114

Table 3.1: Fourier series elements for isotropic shell.

We keep the current shell configuration, but change the location of the applied load to  $\varphi_0 = \frac{\pi}{4}$ . We should then be able to observe the boundary effects more clearly. For this setup we plot again the full deflected shell in figure 3.7 and analyze the role of each Fourier series element. The first important difference we want to mention, caused by changing the applied load's location, is that the maximal deflection gets smaller compared to the previous case. In the current setup the maximal deflection is approximately  $-0.045$ . Moreover, we have that the areas of larger deflections occur on the line from  $(\frac{a\pi}{4}, 0)$  to  $(\frac{a\pi}{2}, \pm 10)$ . We see later on that moving the load even closer to the boundary reduces the maximal deflection further. Next up we want to investigate the Fourier series elements. In figure 3.8 we show both the convergence of the partial

Figure 3.6: Convergence of the partial sums  $S_n$ .Figure 3.7: Isotropic shell with load at  $\varphi_0 = \frac{\pi}{4}$ .

sums and the effective impact of each element. We can see that due to the factor  $\sin(n\frac{\pi}{4})$  we get that  $\tilde{w}_n = 0$ , if  $n \equiv 0 \pmod{4}$ . Hence, we have less non-zero elements than in the previous case. Anyhow, we note that the first four non-zero elements still have the biggest impact on the Fourier series. For  $n > 10$  we are already in the range of the maximal deflection. Therefore, we can conclude that for this example it is reasonable to break the series before  $n = 30$ , too. In figure 3.9 we give examples for a better understanding of the effects when we change the location of the load. In the figure we show the loads at  $\varphi_0 \in \{\frac{\pi}{6}, \frac{\pi}{8}\}$ . As we have mentioned before, the maximal deflection gets smaller, if we move to the boundary. Moreover, we can also see that the deflection at the free boundaries is reduced. As far as we consider figure 3.10 for the convergence of the partial sums we do not get any additional information. Even though, we have in both cases more non-zero elements than previously, we observe that we do not have any significant effects for  $n > 10$ . We close here the discussion on isotropic shells and move forward to an orthotropic material. For such kind of structures we have initially derived the function in Lemma 3.2.3. For now we can constitute that regarding an isotropic shell the calculation up to  $S_{30}$  is too extensive. Moreover, we saw that a load near the boundary causes a smaller deflection than applied in the shell's middle. Those observations are essential for an efficient optimization as we see in chapter 5.

Figure 3.8: Convergence of Fourier series for load at  $\frac{\pi}{4}$ Figure 3.9: Isotropic shell with load at  $\frac{\pi}{6}$  and  $\frac{\pi}{8}$ .Figure 3.10: Convergence of partial sums with load at  $\frac{\pi}{6}$  and  $\frac{\pi}{8}$ .

### Orthotropic Shell

In the following section we keep the shell's geometry, i.e., having  $a = 2$  cm and  $l = 20$  cm, as well as the applied loads, starting with  $P = -0.8$  N at  $(a\frac{\pi}{2}, 0)$ , such that we are able to compare the effects of changing the effective properties. Therefore, we consider two different materials given by

1.  $E_1 = 250$  MPa,  $E_2 = 200$  MPa,  $\nu_{21} = 0.27$ ,  $\nu_{12} = 0.3375$ ,
2.  $E_1 = 200$  MPa,  $E_2 = 250$  MPa,  $\nu_{21} = 0.27$ ,  $\nu_{12} = 0.216$ .

It is easy to check that we fulfill in both cases

$$\frac{E_2}{E_1} = \frac{\nu_{21}}{\nu_{12}},$$

which is the condition for orthotropic materials. We start with the first configuration. With these values we have increased the stiffness in the circumferential direction. We have plotted the result in figure 3.11. An immediate difference to the isotropic shell is the smaller deflection for  $\mathcal{U}_3(a\frac{\pi}{2}, 0) = -0.0305$  and the general smaller deflections near the free boundaries. The solution's behavior approaching the boundary is still the same. We may also have a look at the series elements in particular. In table 3.2 we have

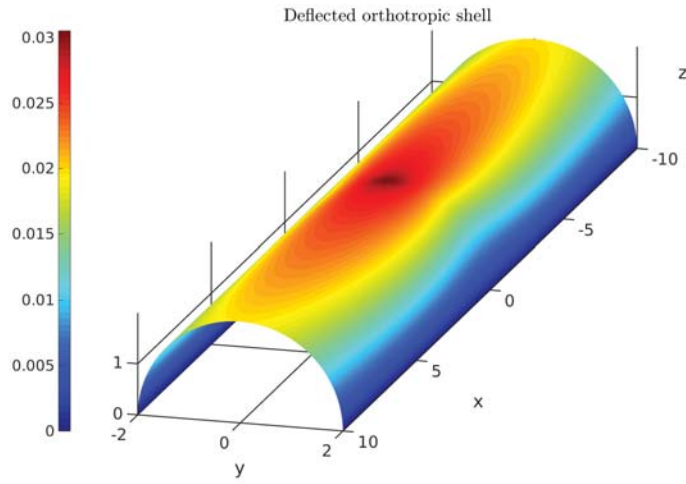


Figure 3.11: Orthotropic shell with load at  $\varphi_0 = \frac{\pi}{2}$ .

summarized the first 6 non-zero elements as well as the diagrams in figure 3.12 showing the convergence of the partial sums and the impact of each element. From the table we can clearly see that  $\tilde{w}_{11}$  is again about 200 times smaller than the first element. In accordance with the left picture in figure 3.12 we can conclude that the elements for  $n > 10$  are getting rather marginal. Looking at the convergence we are already with  $S_9 = -0.0302$  close to the limit. After that we just obtain small improvements. We can deduce that breaking the series earlier would be sufficient. The conclusion we can draw from those results are the same as in the isotropic case.

n	1	3	5	7	9	11
$\tilde{w}_n$	-0.0254578	-0.0031327	-0.0009952	-0.0003983	-0.0001921	-0.0001061

Table 3.2: Fourier series elements for orthotropic shell.

In the next step we focus on the second configuration, where the Young's modulus  $E_2$  is given bigger than  $E_1$ . In figure 3.13 we can have a look on the solution. Surprisingly, we observe that the maximal deflection increases in this case. More precisely, we obtain that  $\mathcal{U}_3(a\frac{\pi}{2}, 0) = -0.0955$ . Actually, one would assume that the deflection decreases if any of the Young's moduli increase. To explain that result we should note here, that we have neglected some terms from the original system of PDEs in Lemma 3.2.3 to

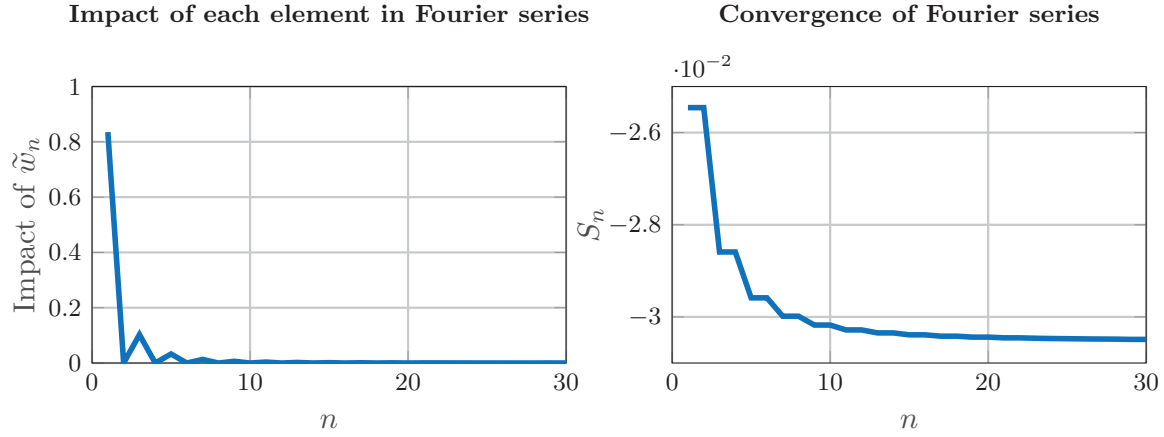
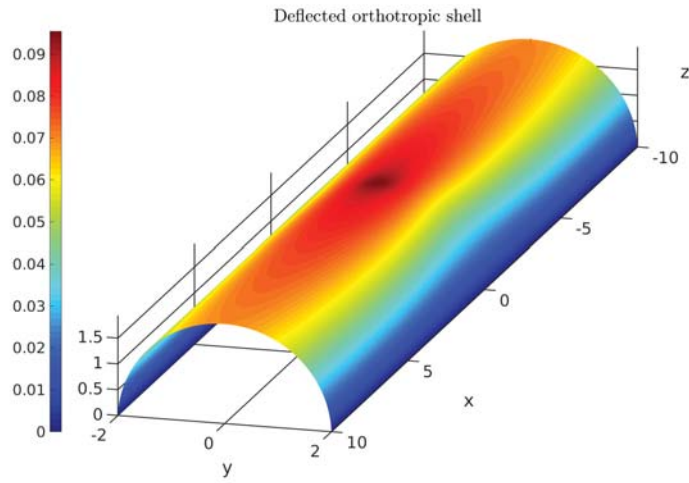


Figure 3.12: Convergence of Fourier elements for orthotropic shell.

Figure 3.13: Isotropic shell with load at  $\varphi_0 = \frac{\pi}{2}$ .

get our analytical solution. Those parts are probably missing in this case. Evaluating the function at  $(a\frac{\pi}{2}, 0)$  yields that the deflection is of the same order as  $E_2^2/E_1^3$ , where we assume that the shell's geometry stays unchanged. This means that in general it is favorable to have a structure, which is stiffer in the circumferential direction than in the longitudinal one. Next up, we want to investigate the convergence of the Fourier series and check if we run in any trouble there. In table 3.3 we have summarized again the first six non-zero elements in the series. These values confirm the conclusions we have drawn from the previous simulations. We can also take a look at the convergence results in figure 3.14. Both plots give the same qualitative results as before. Only the values  $\tilde{w}_n$  for  $n < 10$  have a high impact on the total solution.

n	1	3	5	7	9	11
$\tilde{w}_n$	-0.0797477	-0.0098157	-0.0031343	-0.0012575	-0.0006071	-0.0003354

Table 3.3: Fourier series elements for orthotropic shell.

To close this section we shortly have a look on the solution when the load is moved to the boundary. We restrict ourselves on the cases where the load is applied at  $\frac{\pi}{4}$  and  $\frac{\pi}{8}$ . The results are presented in figure 3.15. As in the isotropic case we can see that a

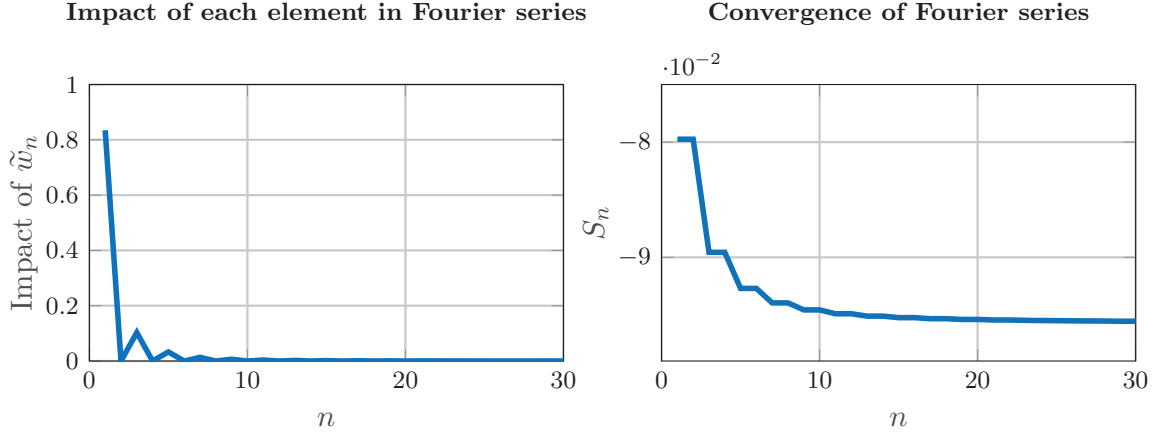
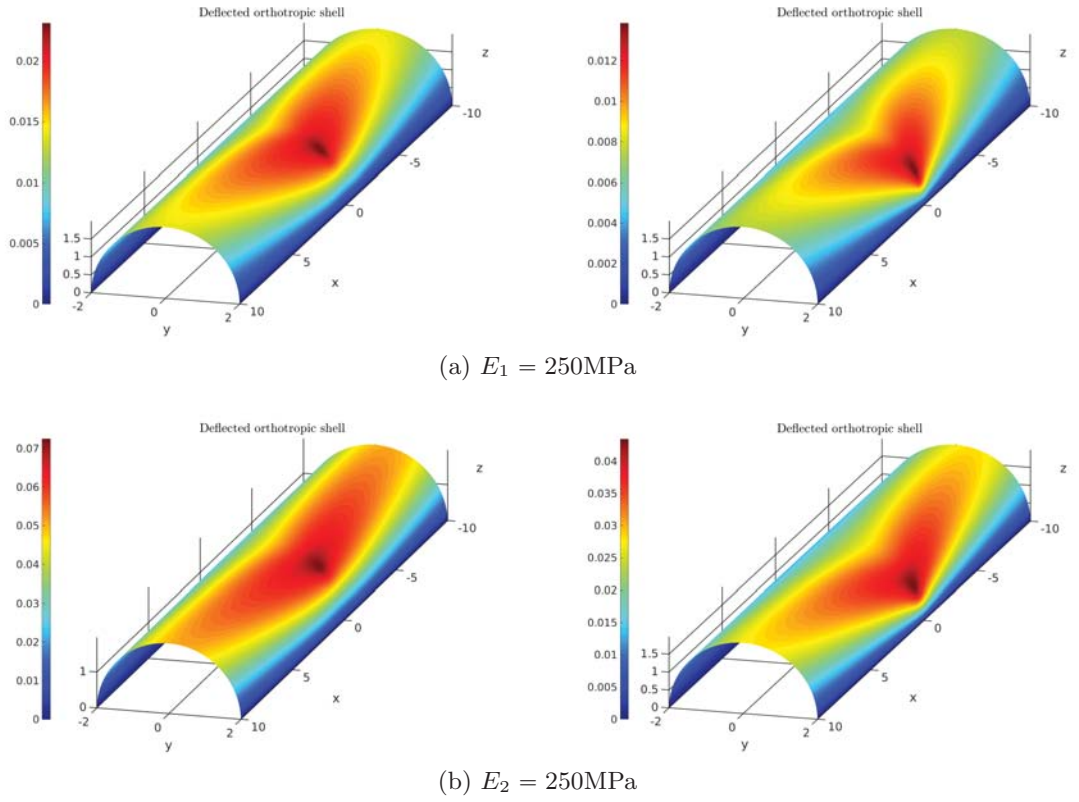


Figure 3.14: Convergence of Fourier elements for orthotropic shell.

Figure 3.15: Orthotropic Shells with load applied at  $\frac{\pi}{4}$  and  $\frac{\pi}{8}$ .

load near the boundary has a lower effect on the deflection than applied in the middle of the shell. Moreover, we can see that a shell, which is stiffer in the circumferential is preferable to a shell with higher values for  $E_2$ . We can establish for chapter 5 that it is sufficient to consider only the first four series elements and minimize the function  $S_4$ . On the other hand, we have seen that our reduced model does not capture all important effects. Anyhow, it is necessary to take this model for the sake of having symbolic expressions, which we introduce in the next chapter 4. For now we continue with investigating the full weak formulation in equation (3.1.2). For that reason we solve the problem numerically via a finite element ansatz and compare it to our analytic solution for small loads. After that we verify the result from 2.9 by considering different BCs in ANSYS.

### 3.3 Numerical models for pinching a cylinder

#### 3.3.1 Solving Koiter equation with FEniCS

To derive our analytical solution we had to simplify the strong formulation of the Koiter equation by neglecting some terms due to asymptotic arguments. The following part is dedicated to achieve a numerical solution for the weak formulation (3.1.2). There are various different techniques for this goal, but we focus on a finite element ansatz with FEniCS, see [2]. In order to obtain a solution with this program we need to consider the following steps:

- Construct triangulation of the domain  $\omega$ .
- Define a suitable function space for the test functions, Galerkin method.
- Implement the weak formulation with boundary conditions.

For the triangulation we use the mesh generator Gmsh [24]. Since  $\omega$  is a rectangular domain the mesh is easy to implement and we obtain 102940 cells with 51869 vertices. As our test function space we use polynomials of degree 2, since the operators  $\Lambda_{\alpha\beta}$  defined in section 2.7 are of the same order. For further information we refer to [32]. For our left-hand side we identify the membrane effects given by

$$a_1(\mathcal{U}, \mathcal{V}) = \int_{\omega} a_{\alpha\beta\alpha'\beta'}^{hom} e_{\alpha\beta}(\mathcal{U}) e_{\alpha'\beta'}(\mathcal{V}) ds'$$

and the bending effects with

$$a_2(\mathcal{U}, \mathcal{V}) = \int_{\omega} c_{\alpha\beta\alpha'\beta'}^{hom} \Lambda_{\alpha\beta}(\mathcal{U}) \Lambda_{\alpha'\beta'}(\mathcal{V}) ds'.$$

We want to mention here, that the presented approach is very basic and we do not address the problem of shear locking in shells. For a more in-depth numerical analysis of shells we refer to [41] and [7]. Our right-hand side will be chosen such that it fits to the pinching load  $q^{\text{pinch}}$  of -1 N. For a better implementation we consider the approximated load  $q$  on a disk with radius 0.001 cm. The right-hand side is described together with  $f = q \cdot n$  by the functional

$$l(\mathcal{V}) = \int_{\omega} f \cdot \mathcal{V} ds'.$$

We consider a shell with radius  $a = 5$  cm and plot it along the middle line for  $s_2 = 0$ . With that approach we immediately see the difference between our analytic solution and the full model. The corresponding results together with the initial undeflected shell are presented in figure 3.16. We first note that the deflections at the point where the pinching load is applied are roughly the same. We obtain here a relative error of

$$\frac{|\mathcal{U}_{3,max}^{\text{num}} - \mathcal{U}_{3,max}^{\text{ana}}|}{|\mathcal{U}_{3,max}^{\text{ana}}|} = 0.0271.$$

The values for the maximal deflections are  $\mathcal{U}_{3,max}^{\text{num}} = -0.2038$  and  $\mathcal{U}_{3,max}^{\text{ana}} = -0.1984$ . We can investigate some different effects, if we move closer to the boundaries. Due to the neglected third order terms, the analytic solution is always beneath the original shell and does not preserve the arc length. However, the numerical solution bulges at around  $s_1 = \frac{a\pi}{4}$  and  $s_1 = \frac{3a\pi}{4}$ . Hence, the full model preserves the shell's arc length. For the optimization it is important to note, that the maximal deflections are of the same order.



### Comparison of deformed and undeformed shell

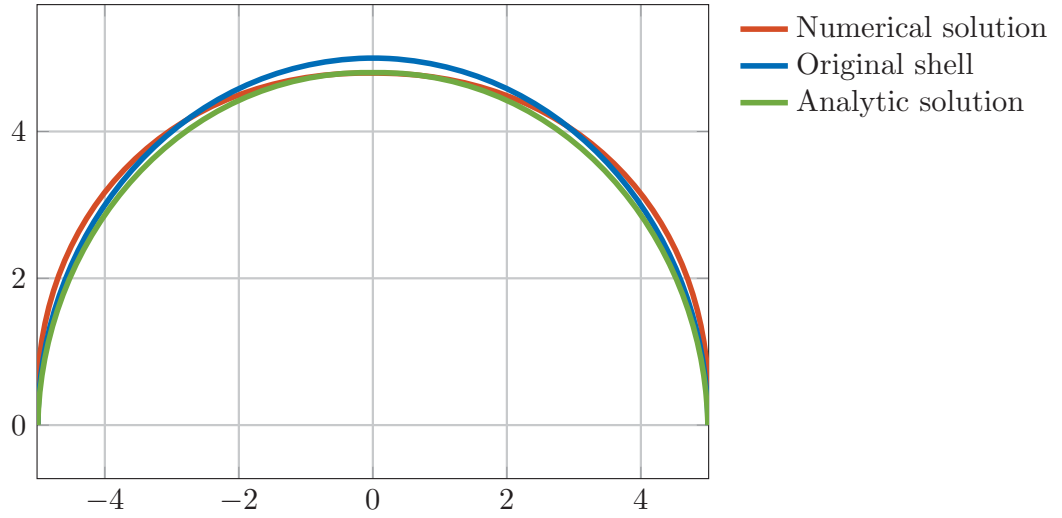


Figure 3.16: Comparison of analytic and numerical solution.

### 3.3.2 Numerical study of different boundary conditions

In this chapter's last section we want to investigate the numerical behavior, if we change the boundary conditions according to section 2.9. Therefore, we consider an orthotropic shell with radius  $a = 3$  mm, length  $l = 40$  mm and thickness  $h = 0.06$  mm. We assume that the shell has Young's moduli  $E_1 = 17.518$  GPa,  $E_2 = 17.536$  GPa and Poisson's ratio  $\nu_{12} = 0.00636$ . Since we obtain the ratio  $E_1/E_2 = 0.999$ , it is reasonable to take  $\nu_{21} = \nu_{12}$ . All the simulations have been computed with ANSYS, where we consider shell finite elements with eight nodes and six degrees of freedom each. The total number of elements is 11040 with 33579 nodes. Next, we define the boundary conditions. We distinguish them into four different groups. The first group consists of the weakest kind of support as shown in figure 3.17. In this case we clamp the shell's four corner points and restrict gradually spatial displacements along the longitudinal boundary. Note, that the first group corresponds to the initial boundary conditions presented in

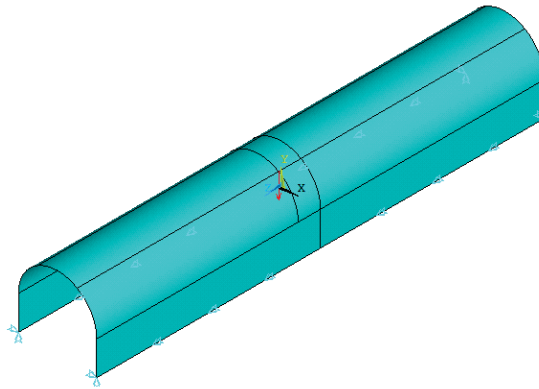


Figure 3.17: Shell with boundary conditions BC0 from group one.

our analysis. The other three groups all have a fixed circumferential boundary. In the second group we summarize all experiments, where we consider the boundary condition described in section 2.9. See for example figure 3.18. In this particular case we limit the



displacements at the circumferential boundary, i.e.,  $\mathcal{U}(\cdot, \pm l/2) = 0$ . This condition varies with the examples. We consider shells, where we only fix the displacements  $\mathcal{U}_1$  and  $\mathcal{U}_3$  at the curved boundary to check the impact of additionally fixing  $\mathcal{U}_2$ . Other cases within this group also restrict some rotational degrees of freedom along the circumferential boundary. The last two groups only consist of one case each. In group three we examine

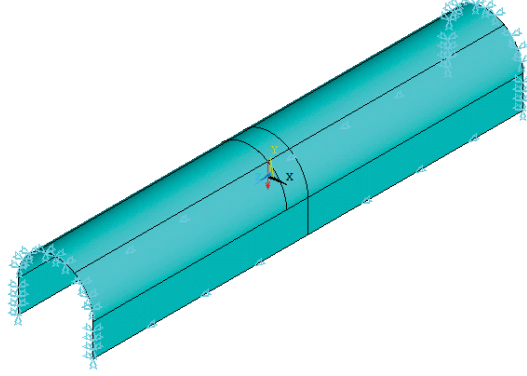


Figure 3.18: Shell with boundary conditions BC3 from group two.

the boundary conditions presented in figure 3.19. Here, we consider a fully clamped shell along its curved boundary, i.e., we also restrict the rotational degrees of freedom. In

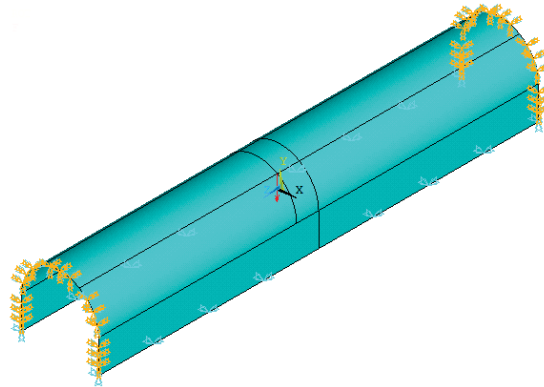


Figure 3.19: Shell with boundary conditions BC7 from group three.

the last case we have a fully clamped shell, where we limit all degrees of freedom along the complete boundary  $\partial\omega$ . This setup is shown in figure 3.20. On all of these shells

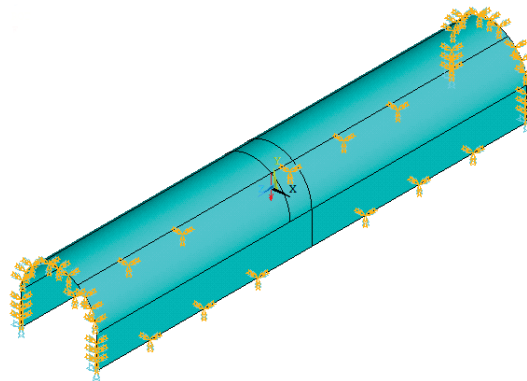


Figure 3.20: Shell with boundary conditions BC8 from group four.

we now apply a successively increasing pinching load of at most  $P = 10$  N. We consider

the normalized deflections  $\mathcal{U}_3/h$ , which are summarized in figure 3.21. We can see that

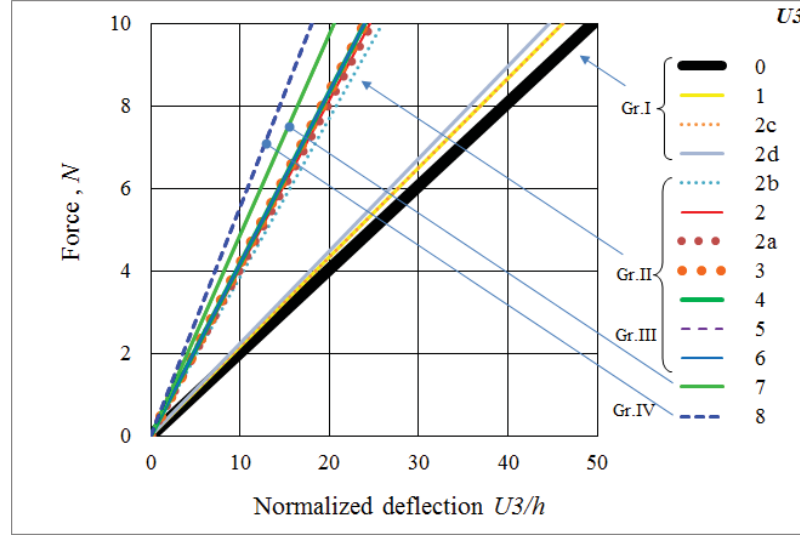


Figure 3.21: Normalized deflections w.r.t. pinching load.

the shells with boundary conditions from group one have the biggest deflections w.r.t. the pinching load. On the contrary, all other shells, where the circumferential boundary conditions are somehow fixated, have smaller displacements. This is in correspondence to our theoretical result. We proved in section 2.9 that in those cases the weak formulation reduces to a membrane model and the bending effects are neglected. If we closer examine the examples from group two, we conclude that if the displacements  $\mathcal{U}_1$  and  $\mathcal{U}_3$  are fixed along the curved boundaries then it does not change the result if we additionally set  $\mathcal{U}_2$  to zero. Moreover, we observe that the groups two to four are quite similar. This means that clamping the whole boundary  $\partial\omega$  is equivalent to a fixation of the curved boundary  $\Gamma_0 = \phi([0, a\pi] \times \{0\} \cup [0, a\pi] \times \{l\})$  as mentioned in remark 2.9.1.



## 4 Calculating Effective Properties with Symbolic Parameters

In this chapter we want to explain how the homogenization of shells can be practically implemented. Our focus lies on methods that utilize the network structure of the periodicity cells. Therefore, we present a reduction of the variational problems (2.8.1) to 1D beam FE. In general the presented algorithm is performed numerically, but our goal in this thesis is to obtain qualitative results, which give a direct insight on how a change of the design variables affects the homogenized model. Hence, we want to modify the algorithm such it can be executed symbolically. We start with a summary of the results presented in [49], where the homogenization and optimization of textile-like structures with respect to their in-plane properties were analyzed, and [50]. In our case we adapt it to the calculation of the effective bending properties as shown in [31]. We will see that the homogenization process can be split into three parts

- Assembling of the global stiffness matrix (GSM) w.r.t. beam finite elements.
- Solving the linear equation.
- Calculation of the effective properties from the obtained displacement field.

For our analysis we implement everything with MATLAB. We will see that solving the symbolic linear equation is in general a non trivial task and should be handled carefully. There are different possibilities to deal with this problem and we consider some preprocessing techniques to reduce the complexity as well as outsourcing the linear equation to Singular, see [19].

### 4.1 Algorithm for calculation of effective properties

In regard of the theoretical derivation in chapter 2 we now want to establish in this section an algorithm for the calculation of the effective properties presented in equation (2.8.2). We mainly focus on the implementation of the effective bending properties, since the in-plane coefficients  $a_{ijkl}^{hom}$  are discussed in great detail in [49, 58] and applied for optimization. In general, we follow the Homogenization approach that was shown in [50], where the cell-problems are reduced to a 1D beam model on the lattice structure. The presented procedure yields the effective plate coefficients, which we have seen in remark 2.4.2 are equivalent to our effective shell coefficients.

**Remark 4.1.1** *We want to mention here that in [50] the derivation of the cell problems is done by an asymptotic expansion method on the plate domain, where we consider the displacement as*

$$u^\varepsilon(s) = u(s, \frac{s}{\varepsilon}) = u^0(s) + \varepsilon \chi_{pq}(y) \frac{\partial u_q^0(s)}{\partial s_p} \Big|_{y=\frac{s}{\varepsilon}} + \mathcal{O}(\varepsilon^2), \quad s \in \Omega, \quad (4.1.1)$$

where  $\chi_{pq} \in H_{per}^1(Y)^3$ , with  $p, q \in \{1, 2, 3\}$  and  $Y$  is the periodicity cell.

The homogenized bending coefficients  $c_{\alpha\beta\alpha'\beta'}^{hom}$ , according to [50, p. 154-157], are equivalently calculated as

$$c_{\alpha\beta\alpha'\beta'}^{hom} = -\frac{1}{|Y|} \int_Y a_{ijkl}(y) \left[ \mathcal{E}_{ij,y}(\widetilde{\chi_I^{\alpha\beta}}) - y_3 \mathbf{M}_{ij}^{\alpha\beta} \right] y_3 \mathbf{M}_{kl}^{\alpha'\beta'} dy \quad (4.1.2)$$

and the  $\widetilde{\chi_I^{\alpha\beta}}$ ,  $\alpha, \beta \in \{1, 2\}$  are the  $Y$ -periodic solutions to the cell problems

$$\int_{Y^*} a_{ijkl} \left( \mathcal{E}_{ij,y}(\widetilde{\chi_I^{\alpha\beta}}) - y_3 \mathbf{M}_{ij}^{\alpha\beta} \right) \mathcal{E}_{kl,y}(\widetilde{\psi}) dy = 0. \quad (4.1.3)$$

**Remark 4.1.2** *It is shown in [50], that the limiting equation of bending an equivalent homogeneous orthotropic plate can be determined as,*

$$c_{1111}^{hom} \frac{\partial^4 w_3^0}{\partial s_1^4} + 2c_{1122}^{hom} \frac{\partial^4 w_3^0}{\partial s_1^2 \partial s_2^2} + c_{2222}^{hom} \frac{\partial^4 w_3^0}{\partial s_2^4} = f_3(s_1, s_2), \quad (s_1, s_2) \in \omega. \quad (4.1.4)$$

The aim is now to derive the solutions to formula (4.1.3). We achieve this by using beam finite elements, related to [39, chapter 6], having six degrees of freedom, three spatial and three rotational, at each end. We also have to implement the periodic boundary conditions, respectively.

### 4.1.1 Reduction to 1D beam problems and stress interpolation

We want to exploit the fact, that the solid pieces of the plate structure are beam-like. Therefore, we introduce a reduction of our periodic cell-problem to an Euler-Bernoulli beam model and compute the effective properties. The derivation of those has been presented earlier and we follow the techniques in [50], which have been applied in [49]. The following lines are a quick summary from mentioned works, where we especially focus on the derivation of the bending coefficients. We assume that the periodicity cell can be represented by a graph network  $\Gamma_Y$  of nodes and edges.  $\mathbf{E}$  denotes the set of all edges in  $\Gamma_Y$ . We consider such an one-dimensional geometry of some cell  $\Gamma_Y$  and take a node  $n$  of  $\Gamma_Y$ . For one of its adjacent edges  $e \in \mathbf{E}(n)$  define  $\gamma(e, n) \in \mathbb{R}^3$  to be the directional vector of the edge pointing to  $n$ . We introduce with  $l^e = \|\gamma(e, n)\|_2$  the edge's length. For each edge  $e$  let  $z_1$  be its longitudinal component. Furthermore, we denote with  $(g_1, g_2, g_3)$  the global basis for each edge  $e$ , and  $(l_1^e, l_2^e, l_3^e)$  defines the local basis. The matrix  $C^e \in \mathbb{R}^{3 \times 3}$  is the transformation matrix, such that  $(l_1^e, l_2^e, l_3^e) = (g_1, g_2, g_3)C^e$ . According to the derived homogenization technique the effective bending coefficients are obtained from the solutions to the cell problems with periodic boundary conditions on  $\Gamma_Y$ . Given the two indices  $\alpha, \beta \in \{1, 2\}$  we can formulate our problems as follows: find the periodic displacement fields  $u_{\alpha\beta} \in \Gamma_Y \rightarrow \mathbb{R}^{1 \times 6}$ , such that the auxiliary vector field  $m_{\alpha\beta} = u_{\alpha\beta} + \mathbf{M}_*^{\alpha\beta}$ , which was shifted by the unit perturbations of the

periodicity cell, corresponding to the bending experiments, solves the following set of equations.

At each edge  $e$  define  $m_{\alpha\beta}^e \in [0; l^e] \rightarrow \mathbb{R}^{1 \times 4}$ ,  
 $[m_{\alpha\beta}^e]_1 \in H^1([0; l^e])$ ,  $[m_{\alpha\beta}^e]_2 \in H^2([0; l^e])$ ,  $[m_{\alpha\beta}^e]_3 \in H^2([0; l^e])$ ,  $[m_{\alpha\beta}^e]_4 \in H^1([0; l^e])$ ,  
equilibrium conditions on edges hold:

$$E^e A^e \frac{\partial^2}{\partial z_1^2} [m_{\alpha\beta}^e]_1 = 0,$$

$$E^e I_2^e \frac{\partial^4}{\partial z_1^4} [m_{\alpha\beta}^e]_2 = 0,$$

$$E^e I_3^e \frac{\partial^4}{\partial z_1^4} [m_{\alpha\beta}^e]_3 = 0,$$

$$G^e J^e \frac{\partial^2}{\partial z_1^2} [m_{\alpha\beta}^e]_4 = 0,$$

force balance conditions in nodes hold:

$$\sum_{e \in \mathbf{E}(n)} E^e C^e \left( A^e \left( [m_{\alpha\beta}^e]_1 \right)'_{z_1} \quad I_2^e \left( [m_{\alpha\beta}^e]_2 \right)'''_{z_1} \quad I_3^e \left( [m_{\alpha\beta}^e]_3 \right)'''_{z_1} \right)^T = 0,$$

moment balance conditions in nodes hold:

$$\sum_{e \in \mathbf{E}(n)} C^e \left( G^e J^e \left( [m_{\alpha\beta}^e]_4 \right)'_{z_1} \quad -E^e I_2^e \left( [m_{\alpha\beta}^e]_3 \right)''_{z_1} \quad E^e I_3^e \left( [m_{\alpha\beta}^e]_2 \right)''_{z_1} \right)^T = 0,$$

and the periodic boundary conditions hold:

$$[u_{\alpha\beta}]_{1:3} \equiv C^e \left( [m_{\alpha\beta}]_{1:3} - \mathbf{M}_*^{\alpha\beta} \right) \text{ and } [u_{\alpha\beta}]_{4:6} \equiv C^e \left( \left( \begin{array}{c} [m_{\alpha\beta}^e]_4 \\ -\frac{\partial}{\partial z_1} [m_{\alpha\beta}^e]_3 \\ \frac{\partial}{\partial z_1} [m_{\alpha\beta}^e]_2 \end{array} \right) - F(\mathbf{M}_*^{\alpha\beta}) \right)$$

are periodic.

+ Dirichlet condition: at one node all six degrees of freedom are fixed

or at two nodes six in total.

(4.1.5)

The constants appearing in this equation are properties of the underlying beams. We express the area of each cross section with  $A^e$ , the area moments w.r.t. the second and third axis with  $I_2^e$ ,  $I_3^e$  and the polar moment  $J^e$  of the element. For a circular beam with radius  $r$  those are determined as  $A^e = \pi r^2$ ,  $I_2^e = I_3^e = \pi r^4/4$  and  $J^e = \pi r^4/2$ . The last two missing constants are the Young's modulus  $E^e$  and the shear moduli  $G^e$  of the element. By the square bracket notation  $[\cdot]_{i:j}$  we denote the  $i$ -th to  $j$ -th component of the vector. We should also specify how the perturbations  $\mathbf{M}_*^{ij}$  for the cell-experiments look like. They are described by the vectors

$$\mathbf{M}_*^{11} = \begin{pmatrix} -y_1 y_3 \\ 0 \\ 0 \end{pmatrix}, \quad \mathbf{M}_*^{12} = \begin{pmatrix} -y_2 y_3 \\ 0 \\ 0 \end{pmatrix}, \quad \mathbf{M}_*^{21} = \begin{pmatrix} 0 \\ -y_1 y_3 \\ 0 \end{pmatrix}, \quad \mathbf{M}_*^{22} = \begin{pmatrix} 0 \\ -y_2 y_3 \\ 0 \end{pmatrix}.$$

**Remark 4.1.3** We note here, that we introduce four corrector problems instead of the mentioned three. In the presented case  $\mathbf{M}_*^{\alpha\alpha}$  corresponds to  $\mathbf{M}^{\alpha\alpha}$ , while we obtain the third corrector for  $\mathbf{M}^{12}$  by  $\mathbf{M}_*^{12} + \mathbf{M}_*^{21}$ . This is important for the calculation of the effective properties.

This yields the three conditions for the spatial components. With the operator  $F$  we can calculate the remaining three rotational conditions, depending on the given  $\mathbf{M}_*^{\alpha\beta}$ . It is based on the formula found in [27] defined as

$$F(\mathbf{M}_*^{\alpha\beta}) = \begin{pmatrix} \theta_1 \\ \theta_2 \\ \theta_3 \end{pmatrix}, \text{ where} \quad (4.1.6)$$

$$\theta_1 = \frac{4}{\pi r^4} \int_{\omega^e} \left[ (z_3 l_3^e + z_2 l_2^e) \times \mathbf{M}_*^{\alpha\beta}(z) \right] l_2^e dz_3 dz_2,$$

$$\theta_2 = \frac{4}{\pi r^4} \int_{\omega^e} \left[ (z_3 l_3^e + z_2 l_2^e) \times \mathbf{M}_*^{\alpha\beta}(z) \right] l_1^e dz_3 dz_2,$$

$$\theta_3 = \frac{2}{\pi r^4} \int_{\omega^e} \left[ (z_3 l_3^e + z_2 l_2^e) \times \mathbf{M}_*^{\alpha\beta}(z) \right] l_3^e dz_3 dz_2,$$

with  $\omega^e$  being the cross section of the fictional beam connecting to periodical dependent nodes. With  $z = (z_1, z_2, z_3)$  we describe the variables in the local beam coordinate system, s.t.

$$z = (y - y_{ln})C^e,$$

where  $y_{ln}$  denotes the left node of the edge in the global coordinate system. We can then finally employ beam finite elements, as for example presented in [39], and express the system (4.1.5) as a linear equation of the form  $Av_{\alpha\beta} = b_{\alpha\beta}$ . The right-hand side depends on the periodic boundary conditions and the applied perturbations  $\mathbf{M}_*^{\alpha\beta}$ . The assembly of the GSM  $A$  is presented in [58]. Moreover, a complete discussion about the matrix's kernel structure is provided. In the case of symbolic design parameters  $\mathbf{x} \in \mathbb{R}^m$  we obtain then a linear equation  $A[x]v_{\alpha\beta} = b_{\alpha\beta}[x]$ , which we investigate in section 4.2. Given the solution for these cell experiments we are able to calculate the effective properties of the cell on a beam level. The corresponding results on an exemplary cell are presented in figure 4.1.

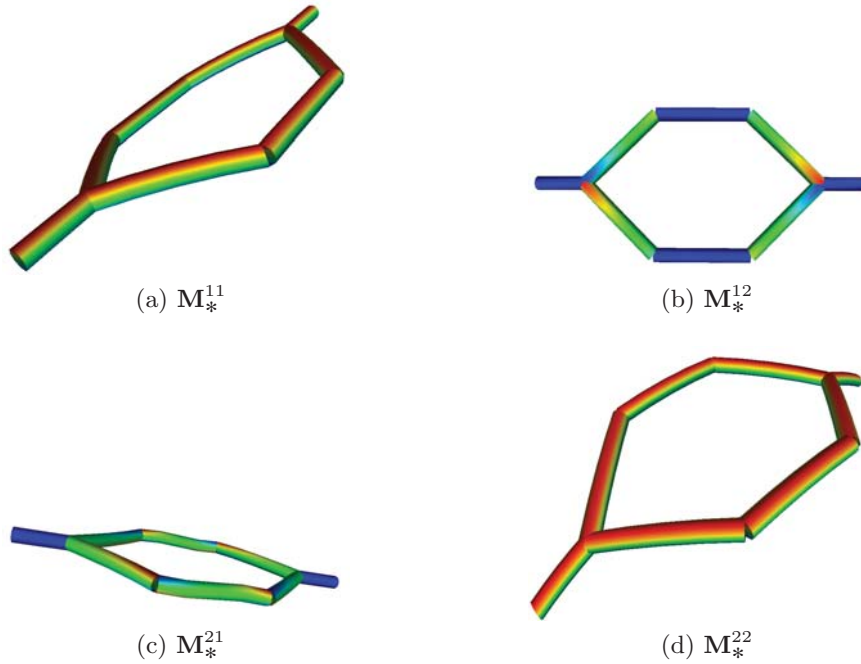


Figure 4.1: Solution to the cell problems

If we follow [50, chapter 5] further, we see that given the stress tensor  $\sigma_{\alpha\beta} \in \mathbb{R}^{3 \times 3}$ , depending on the displacement field obtained by applying  $\mathbf{M}_*^{\alpha\beta}$ , we can calculate the bending coefficients as

$$\begin{aligned} c_{\alpha\alpha\beta'\beta'}^{hom} &= \left( -\frac{1}{|Y|} \int_Y y_3 \sigma_{\alpha\alpha}(y) dy \right)_{\beta'\beta'}, \\ c_{\alpha\beta\alpha'\beta'}^{hom} &= \left( -\frac{1}{|Y|} \int_Y y_3 (\sigma_{\alpha\beta}(y) + \sigma_{\beta\alpha}(y)) dy \right)_{\alpha'\beta'}, \quad \text{for } \alpha \neq \beta. \end{aligned} \quad (4.1.7)$$

Hence, we need to find a way to calculate the stresses from our solution vectors. We introduce a stress interpolation regarding our beam model. Given a single beam from our network, it has in total 12 degrees of freedom. In [39], an approach to achieve from this 12D field a 4D field and finally a 3D field is shown. If we take a beam with nodes  $u$  and  $v$  and components

$$u = (u_1, u_2, u_3, \theta_{u1}, \theta_{u2}, \theta_{u3})^T, \quad (4.1.8)$$

$$v = (v_1, v_2, v_3, \theta_{v1}, \theta_{v2}, \theta_{v3})^T, \quad (4.1.9)$$

then the 4D field is obtained via a polynomial interpolation, as explained in [39, p. 92], where we multiply our component vector with the interpolation matrix  $R \in \mathbb{R}^{4 \times 12}$ , such that

$$R = \begin{pmatrix} P_1 & 0 & 0 & 0 & 0 & 0 & P_2 & 0 & 0 & 0 & 0 & 0 \\ 0 & N_1 & 0 & 0 & 0 & N_2 & 0 & N_3 & 0 & 0 & 0 & N_4 \\ 0 & 0 & N_1 & 0 & -N_2 & 0 & 0 & 0 & N_3 & 0 & -N_4 & 0 \\ 0 & 0 & 0 & P_1 & 0 & 0 & 0 & 0 & 0 & P_2 & 0 & 0 \end{pmatrix}. \quad (4.1.10)$$

For  $P_j, j = 1, 2$  see [39, p. 69] and the  $N_i, i = 1, 2, 3, 4$  are described in [39, p. 92]. We then obtain our 4D field as

$$u^{4D} = R \begin{pmatrix} u \\ v \end{pmatrix}.$$

Given this 4D field, we can follow [60] to reduce it even to a 3D field, where the components are given by

$$\begin{aligned} u_1 &= u_1^{4D} - z_2 \frac{\partial u_2^{4D}}{\partial z_1} - z_3 \frac{\partial u_3^{4D}}{\partial z_1} + w \frac{\partial u_4^{4D}}{\partial z_1}, \\ u_2 &= u_2^{4D} - z_3 u_4^{4D} - \nu z_2 \frac{\partial u_1^{4D}}{\partial z_1}, \\ u_3 &= u_3^{4D} + z_2 u_4^{4D} - \nu z_3 \frac{\partial u_1^{4D}}{\partial z_1}. \end{aligned} \quad (4.1.11)$$

The parameter  $w$  is a warping constant. A higher order approximation may be obtained if desired. This method was also used to obtain the visualizations of the cell-problems. Furthermore, it is shown in [60] that using these interpolations and the initial 4D field we can calculate the stresses in connection to Hooke's law. We introduce the local stress field for a single beam as

$$\sigma^{loc}(z) = \begin{pmatrix} E \left( \frac{\partial u_1^{4D}}{\partial z_1} - z_2 \frac{\partial^2 u_2^{4D}}{\partial z_1^2} - z_3 \frac{\partial^2 u_3^{4D}}{\partial z_1^2} \right) & -\mu z_3 \frac{\partial u_4^{4D}}{\partial z_1} & \mu z_2 \frac{\partial u_4^{4D}}{\partial z_1} \\ -\mu z_3 \frac{\partial u_4^{4D}}{\partial z_1} & 0 & 0 \\ \mu z_2 \frac{\partial u_4^{4D}}{\partial z_1} & 0 & 0 \end{pmatrix}, \quad (4.1.12)$$



with  $\mu$  being the second Lamé constant. Let us denote a beam in its local coordinate systems by  $z \in [-l^e/2, l^e/2] \times \omega_\varepsilon$ . If we pass our beam and local stress field into global coordinates and plug it in formula (4.1.7), this yields

$$c_{\alpha\alpha\beta'\beta'}^{hom} = \left( -\frac{1}{|Y|} \sum_{e \in \mathbf{E}} \int_{[-\frac{l^e}{2}, \frac{l^e}{2}] \times \omega_\varepsilon} (y_{ln,3,e} + C_{13}^e z_1 + C_{23}^e z_2 + C_{33}^e z_3) (C^e \sigma_{\alpha\alpha}^{loc}(z)) (C^e)^T dz \right)_{\beta'\beta'}$$

and

$$c_{\alpha\beta\alpha'\beta'}^{hom} = \left( -\frac{1}{|Y|} \sum_{e \in \mathbf{E}} \int_{[-\frac{l^e}{2}, \frac{l^e}{2}] \times \omega_\varepsilon} (y_{ln,3,e} + C_{13}^e z_1 + C_{23}^e z_2 + C_{33}^e z_3) \times (C^e (\sigma_{\alpha\beta}^{loc}(z) + \sigma_{\beta\alpha}^{loc}(z)) (C^e)^T) dz \right)_{\alpha'\beta'}$$

Here,  $y_{ln,3,e}$  is the third component of the beam's left node. It is then easy to calculate the integrals w.r.t. to the given cross sections. In the case of MATLAB one can use the `int` function to perform the integration symbolically. We want to mention here that for orthotropic materials holds the equality  $c_{1122}^{hom} = c_{2211}^{hom}$ .

**Remark 4.1.4** We note that we can calculate the orthotropic material properties  $E_1$ ,  $E_2$ ,  $\nu_{21}$  and  $\nu_{12}$  according to [50] as

$$\begin{aligned} \nu_{12} &= \frac{c_{1122}^{hom}}{c_{1111}^{hom}}, & \nu_{21} &= \frac{c_{2211}^{hom}}{c_{2222}^{hom}}, \\ E_1 &= \frac{12c_{1111}^{hom}(1 - \nu_{21}\nu_{12})}{h^3}, & E_2 &= \frac{12c_{2222}^{hom}(1 - \nu_{21}\nu_{12})}{h^3}, \end{aligned}$$

with  $h$  the thickness of the shell.

With this procedure we have a fast way to calculate the effective properties for our limit equation. We observe that the whole problem can be split into two crucial steps

- Obtain the displacement field via beam FE,
- Integrate over the interpolated stress fields.

In section 4.2 we perform those tasks completely symbolically and obtain analytic solutions for our effective properties.

## 4.2 Solving symbolic linear equations with Singular

In the previous section we have discussed the homogenization procedure for lattice structures presented in [50]. There we have seen that we can reduce the problem to 1D beam finite elements. In this process we end up with solving a linear equation system denoted by  $Av = b$  with  $A \in \mathbb{R}^{N \times N}$ , being symmetric and positive definite, and  $b \in \mathbb{R}^N$ . Here,  $N$  denotes the total number of free components in system (4.1.5). As we mentioned in the introduction our goal is to obtain expressions for the effective properties with respect to the underlying design parameters. Hence, the matrix and right-hand side not only

consist of numerical values but also of the symbolic design variable  $\mathbf{x} \in G \subset \mathbb{R}^m$ , where  $G$  is compact. Then the linear equation is given as  $A[\mathbf{x}]v = b[\mathbf{x}]$ . This increases the complexity of the problem. In general MATLAB's backslash operator works for symbolic matrices, still we will see that it struggles with more complicated designs. Therefore, we need to process the linear equation in Singular, a computer algebra system, which is more convenient for such problems. In the following we explain how the programs are coupled and what preprocessing steps have to be made. These simplifications are obligatory to obtain solutions in Singular and already help to reduce the computational time in MATLAB.

Given  $C_{ij}, \tilde{C}_i \in \mathbb{R}$  and functions  $f^{ij}(\mathbf{x}), g^{ij}(\mathbf{x}), \tilde{f}^i(\mathbf{x}), \tilde{g}^i(\mathbf{x}) \in C^0(\mathbb{R}^m, \mathbb{R})$ , with  $g^{ij}(\mathbf{x}), \tilde{g}^i(\mathbf{x}) \neq 0, \forall \mathbf{x} \in G$ , we have that

$$A_{ij}[\mathbf{x}] = C_{ij} \frac{f^{ij}(\mathbf{x})}{g^{ij}(\mathbf{x})}, \quad b_i[\mathbf{x}] = \tilde{C}_i \frac{\tilde{f}^i(\mathbf{x})}{\tilde{g}^i(\mathbf{x})}, \quad 1 \leq i, j \leq N.$$

Since the matrix is sparse we get  $C_{ij} = 0$  for a lot of entries. A closer look on the structure of  $f^{ij}$  and  $g^{ij}$  yields that there are polynomial expressions  $h_f^{ij}, k_f^{ij}, h_g^{ij}, k_g^{ij} \in \mathbb{R}[\mathbf{x}]$  as well as rational numbers  $p_f^{ij}, p_g^{ij} \in \mathbb{Q} \setminus \mathbb{Z}$  such that

$$f^{ij} = h_f^{ij}(\mathbf{x}) + k_f^{ij}(\mathbf{x})^{p_f^{ij}}, \quad g^{ij} = h_g^{ij}(\mathbf{x}) + k_g^{ij}(\mathbf{x})^{p_g^{ij}}.$$

The right-hand side  $b[\mathbf{x}]$  is similarly constructed. Our aim is now to replace those expressions, which have a rational exponent, and find the lowest common denominator in the linear equation.

### 4.2.1 Preprocessing

We start with identifying the polynomials  $k_f^{ij}(\mathbf{x})$  and  $k_g^{ij}(\mathbf{x})$ . We have to iterate through all entries  $A_{ij}$ , where  $i \geq j$ , and  $b_i$ , to check them if they contain a rational exponent. Therefore, we have to convert the symbolic expressions to a char. It is crucial to note that all symbolic terms  $k$  with a rational exponent will be displayed as ' $k^{\wedge}(\mathbf{p}/\mathbf{q})$ '. Then it is easy to check if the expression ' $\wedge$ ' appears in the char array. We save the basis and the exponent in two different lists. Repeated occurrences of the same expressions are neglected. This does not include the case of same basis but different exponent. Once we have finished with our iteration we obtain the two lists **basis** and **exponent**. In the next step we identify the unique elements of **basis** together with their corresponding exponents. Thus, we are left with a new list **basis<sub>unique</sub>** and non-empty sets of exponents **exponent<sub>unique</sub><sup>l</sup>** for each element **basis<sub>unique</sub>[l]**. We introduce  $n$  new symbolic variables  $\mathbf{w}_l, l = 1, \dots, n$ , where  $n$  is the length of **basis<sub>unique</sub>**. In the next step we iterate through each list **exponent<sub>unique</sub><sup>l</sup>** and determine the lowest common denominator to the respective entries, which we denote by  $q_l$ . Hence we can substitute all entries in  $A[\mathbf{x}]$  which are given in **basis<sub>unique</sub>[l]** =  $\mathbf{x}_l$  with  $\mathbf{w}_l = \mathbf{x}_l^{1/q_l}$ .

**Remark 4.2.1** *As an example we assume that we find in our matrix  $A$  three polynomial expressions given by  $x^{1/2}, x^{3/2}, y^{5/4}$ . After the first step we obtain the lists **basis** =  $\{x, x, y\}$  and **exponent** =  $\{1/2, 3/2, 5/4\}$ . We see that the expression  $x$  appears twice in **basis**, but with different rational exponents. Hence, we get after eliminating the multiple entries the lists **basis<sub>unique</sub>** =  $\{x, y\}$  and **exponent<sub>unique</sub><sup>x</sup>** =  $\{1/2, 3/2\}$ , **exponent<sub>unique</sub><sup>y</sup>** =  $\{5/4\}$ . We now introduce the symbolic variables  $\mathbf{w}_x, \mathbf{w}_y$  together with the numbers  $q_x = 2, q_y = 4$ .*

The substitution is then practically done by using  $\text{subs}(A, x^{1/q_x}, \mathbf{w}_x)$  and  $\text{subs}(A, y^{1/q_y}, \mathbf{w}_y)$  in *MATLAB*.

With that technique, also applied to our right-hand side, we can replace  $A[\mathbf{x}]$  with

$$A[\mathbf{x}, \mathbf{w}_1, \dots, \mathbf{w}_n] = C_{ij} \frac{f^{ij}(\mathbf{x}, \mathbf{w}_1, \dots, \mathbf{w}_n)}{g^{ij}(\mathbf{x}, \mathbf{w}_1, \dots, \mathbf{w}_n)}, \text{ where } f^{ij}, g^{ij} \in \mathbb{R}[\mathbf{x}, \mathbf{w}_1, \dots, \mathbf{w}_n]$$

are polynomials without any rational exponents. Once we have substituted our initial linear equation

$$A[\mathbf{x}]v = b[\mathbf{x}], \text{ with } A[\mathbf{x}, \mathbf{w}_1, \dots, \mathbf{w}_n]v = b[\mathbf{x}, \mathbf{w}_1, \dots, \mathbf{w}_n],$$

we have to get rid of all appearing denominators.

We go through the entries of  $A$  and  $b$  to find the least common multiplier of all  $g^{ij}$  together with  $\tilde{g}^i$  denoted by

$$g_{lcm}(\mathbf{x}, \mathbf{w}_1, \dots, \mathbf{w}_n).$$

Once we have found this candidate we replace  $A[\mathbf{x}, \mathbf{w}_1, \dots, \mathbf{w}_n]v = b[\mathbf{x}, \mathbf{w}_1, \dots, \mathbf{w}_n]$  with

$$\begin{aligned} \tilde{A}[\mathbf{x}, \mathbf{w}_1, \dots, \mathbf{w}_n]v &= \tilde{b}[\mathbf{x}, \mathbf{w}_1, \dots, \mathbf{w}_n], \quad \text{where} \\ \tilde{A}[\mathbf{x}, \mathbf{w}_1, \dots, \mathbf{w}_n] &= A[\mathbf{x}, \mathbf{w}_1, \dots, \mathbf{w}_n] \cdot g_{lcm}, \quad \tilde{b}[\mathbf{x}, \mathbf{w}_1, \dots, \mathbf{w}_n] = b[\mathbf{x}, \mathbf{w}_1, \dots, \mathbf{w}_n] \cdot g_{lcm}. \end{aligned}$$

We have finally arrived with a linear equation, where all entries are given by

$$\tilde{A}_{ij}, \tilde{b}_i \in \mathbb{R}[\mathbf{x}, \mathbf{w}_1, \dots, \mathbf{w}_n].$$

Next, we have to discuss how to forward the linear equation, which was assembled and preprocessed in *MATLAB*, to *Singular*.

### 4.2.2 Calling Singular

The most essential part is the discussion on how to save the matrix  $\tilde{A}$  and vector  $\tilde{b}$ , such that it can be handled in *Singular*. Moreover, we have to clarify the structure of the underlying ring. Since the matrix  $\tilde{A}$  is sparse we declare it in *Singular* as a module  $\mathbf{M}$  and save only the non-zero entries. Therefore, we implement each row of the matrix in the format

$$\mathbf{M}[\mathbf{i}] = \tilde{A}_{ij} * \text{gen}(\mathbf{j}),$$

where  $\text{gen}(\mathbf{j})$  is the  $\mathbf{j}$ -th generator. Anyhow, the right-hand side  $b$  will be declared as a matrix of size  $N \times 1$ . This means we save the entries as

$$\text{rhs}[\mathbf{i}, 1] = \tilde{b}_i.$$

Since the coefficients still depend on the design parameters  $\mathbf{x}, \mathbf{w}_1, \dots, \mathbf{w}_n$  and we want to find the solution  $v \in \mathbb{R}[\mathbf{x}]^N$  we have to declare the ring  $r$  appropriately. It is defined as

$$\text{ring } r = (0, \mathbf{x}, \mathbf{w}_1, \dots, \mathbf{w}_n, \text{pi}), (\text{v}(1..N)), (\text{c}, \text{dp});$$

The first round bracket indicates the coefficients of the ring. In our example we consider  $\mathbb{Q}$  extended by our design parameters and a placeholder  $\text{pi}$  for  $\pi$ . We want to mention here that  $\pi$  will appear, if we calculate effective properties of structures consisting of one or more elliptical beam elements. The second bracket defines the variables of our

solution vector. And the last part specifies the ordering. For further details we may refer to [26].

After this setup we invoke the `liftstd` function in Singular. This yields the standard basis  $\mathbf{X}$  and transformation matrix  $\mathbf{T}$  to our module  $\mathbf{M}$ . For a deeper understanding we refer to [38] or [51]. From that point on we can replace our linear equation with

$$\mathbf{M}\mathbf{v} = \mathbf{rhs} \Leftrightarrow \mathbf{X}^T \mathbf{v} = \mathbf{T}^T \mathbf{rhs}.$$

The final solution is then obtained by defining the ideal

$$\mathbf{I} = \mathbf{X}^T \mathbf{v} - \mathbf{T}^T \mathbf{rhs}$$

and solve for its linear part. We are now left with a solution vector  $\mathbf{v}$  which will then be transferred back to MATLAB, where we reconstruct the stresses and calculate the effective properties as we have shown in section 4.1.1. We also want to refer to [40], where the author presents other practical examples for using Singular.

At first this whole process looks a bit tedious, but it is inevitable to obtain analytic expressions for arbitrary beam like structures. In the next section we establish some examples with increasing difficulties, where we want to compare the resulting solutions as well as the running time. The linear equations are solved both with Singular and MATLAB's backslash operator. All presented examples are calculated on a **Fujitsu Esprimo P920** desktop PC with 8 **Intel Core i7-4790 CPU @ 3.60GHz** processors.

## 4.3 Examples

With the preprocessing technique, that we have developed in the previous section we want to calculate the effective properties of some real life examples. For each case we consider a different parametrization and obtain the respective solutions in terms of the symbolic variables. Moreover, we have to restrict the choice of each symbolic variable  $\mathbf{x}$  to some given compact interval  $G \subset \mathbb{R}^m$ . This is necessary to guarantee that our linear equation is solvable for each choice of  $\mathbf{x}$ . Since our matrix is derived from beam FE, we do not want to consider values for  $\mathbf{x}$  such that we get singular networks with arbitrary small beams. These precautionary measures yield a GSM, which is symmetric positive definite at any time. We start with a rather simple example, where an analytical solution can be calculated by hand. Next up we focus on the case of hexagonal structures. Given that particular network we consider both a change of geometry and for a fixed hexagon we want to investigate how the choice of different beam structures changes the effective properties. The change of geometry not only means varying the width and length but also shifting some beams vertically to induce more stiffness. After that we also prepare an auxetic structure.

**Remark 4.3.1** *Regarding the indexes we note that we consider everything in the local coordinate system of the periodicity cell given by  $e_i$ . With respect to the global coordinate system, we have that  $e_1$  corresponds to the  $s_1$  direction, i.e.,  $(0, 1, 0)^T$  and  $e_2$  is aligned with  $s_2$ ,  $(1, 0, 0)^T$ .*

### 4.3.1 Open grid structure

In our first example we consider an open grid structure as presented in [61, section 7.2.3]. There we look at the pattern shown in figure 4.2, where the beams have a rectangular

cross section of width  $b_\alpha$ ,  $\alpha \in \{1, 2\}$  and height  $h$ . The distance between two parallel beams is denoted by  $t_\alpha$ .

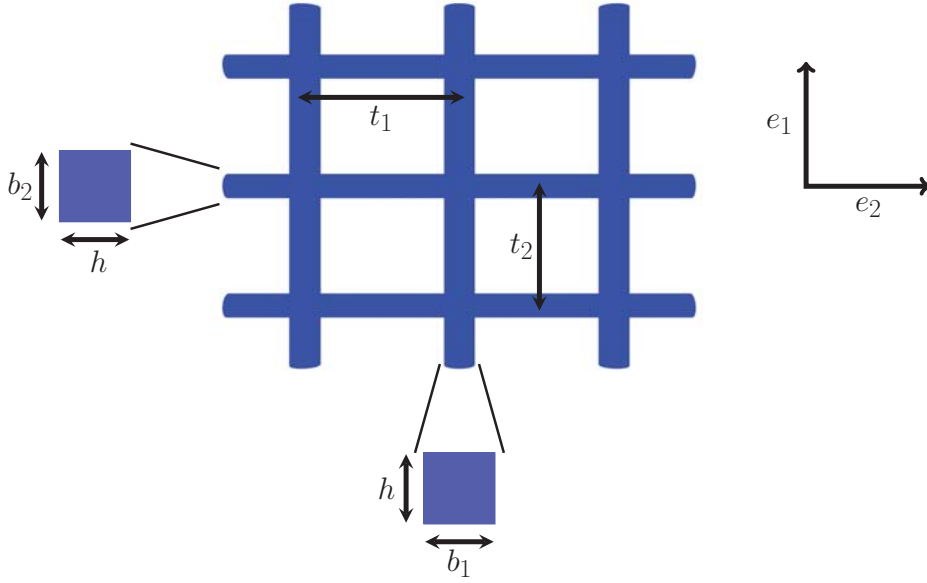


Figure 4.2: Open Grid Structure

This example is good for testing, since the flexural rigidities are analytically given with

$$c_{1111}^{hom} = \frac{Eb_1h^3}{12t_1}, \quad c_{2222}^{hom} = \frac{Eb_2h^3}{12t_2},$$

where  $E$  denotes the Young's modulus of the beam material. We see that increasing the widths  $b_\alpha$  of the beams makes the whole structure stiffer, while widening the distance between two parallel beams decreases the flexural rigidities. In our example we now fix the cross sections and take  $h = b_1 = b_2 = 0.2$  cm. The area moments of inertia are then given by  $I_{z/y} = \frac{0.2^4}{12}$  cm<sup>4</sup>. Moreover, we assume that the beams are made of a material with Young's modulus  $E = 2$  GPa and Poisson's ratio 0.3. Thus, we can only vary the distances between parallel beams. In order to calculate the effective properties with the algorithm presented in section 4.1, we need to identify the periodicity cell  $Y$ . In figure 4.3 we see that taking the red cell as  $Y$  yields by periodical continuation the whole structure. This choice is even the smallest possible periodicity cell that we can take. In the next step we introduce the two symbolic variables  $x$  and  $y$ , and assume that the periodicity cell can be in the  $e_2$  direction at most 4cm long and in the  $e_1$  direction 2 cm long. Furthermore, the cell should be at least bigger than 0.4 cm in both directions. Otherwise the beams would penetrate each other. Concerning those constraints we introduce the parametrization as shown in figure 4.4 with  $x \in [0, 1.8]$  and  $y \in [0, 0.8]$ . The full structure is then obtained by repeating the periodicity cell at the red lines. This yields the relation  $t_1 = 2(2 - x)$  and  $t_2 = 2(1 - y)$ . Plugging in all parameters into the analytic formulas we can conclude that the flexural rigidities are calculated as

$$c_{1111}^{hom} = \frac{320}{24(2 - x)}, \quad c_{2222}^{hom} = \frac{320}{24(1 - y)}. \quad (4.3.1)$$

On the basis of that structure we want to check, if the symbolic solution matches the analytical results. After that we want to investigate, whether solving the linear equation in Singular yields the same results as MATLAB's backslash operator and which

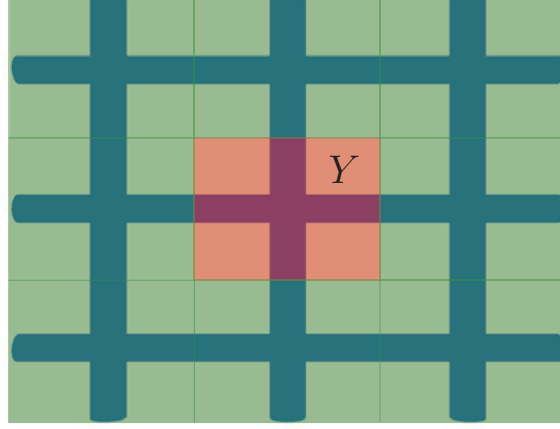


Figure 4.3: Periodicity cell for open grid structure.

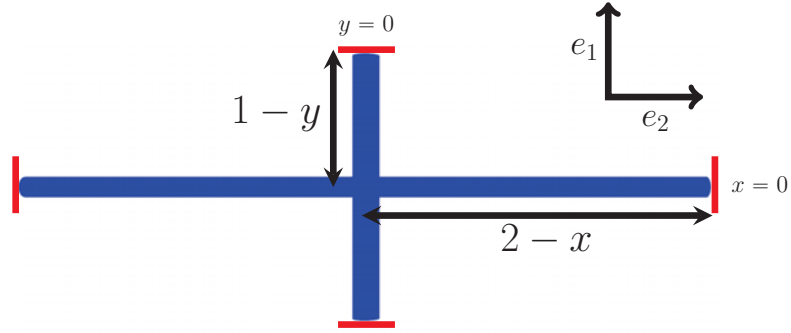


Figure 4.4: Parametrization of periodicity cell for an open grid structure.

method performs better. In figure 4.5 we can see the results that we obtain in the symbolic calculation over the given domain defined by the constraints. For both cell experiments we observe that the symbolic solution corresponds to the results presented in [61]. Therefore, our algorithm performed symbolically yields the exact results. As we have discussed in section 4.2 we can make use of Singular to calculate the solution of the linear equation. In figure 4.6 we can look at the results obtained with both methods. In

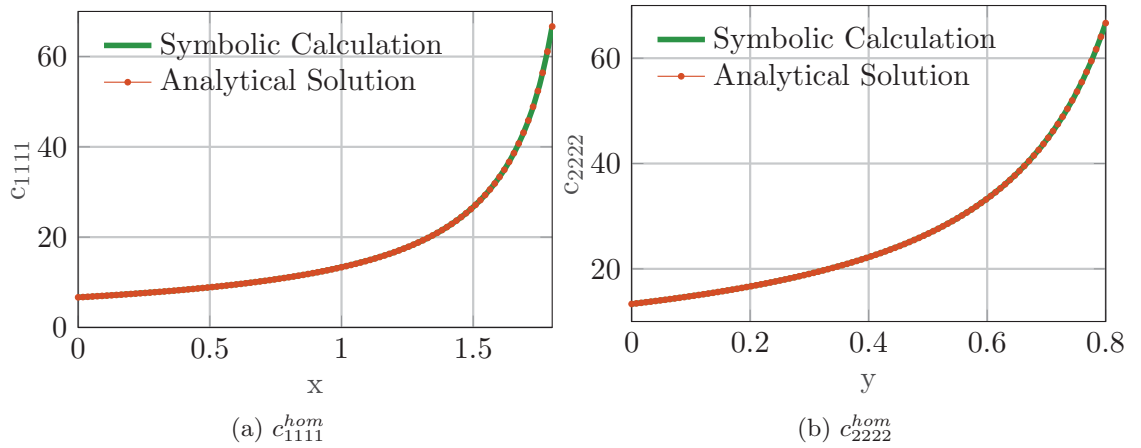


Figure 4.5: Comparison of analytic and symbolic solution.

our case only for the  $c_{2222}^{hom}$  experiment. Since both procedures return the same solution,

we want to compare the time consumptions. We want to remind here that for stopping the time in the Singular part, we not only account for solving the linear equation itself, but also add the time for the I/O process to save the GSM and the right-hand side in their respective format. The cumulated times for all four experiments in the case of the open grid structure are presented in figure 4.7. We immediately see that both methods

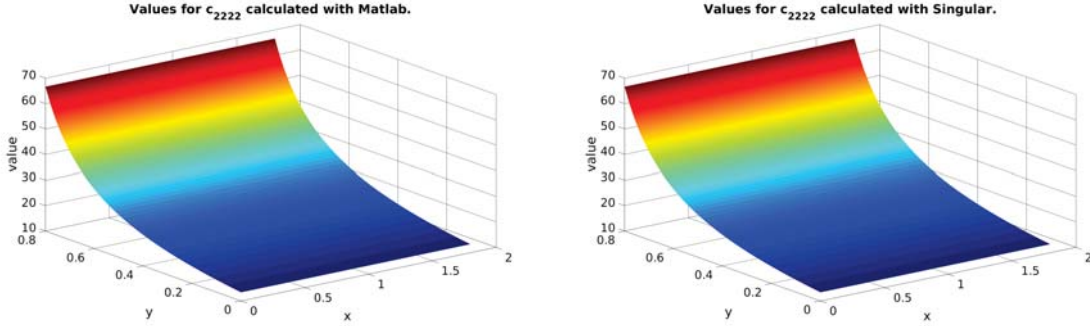


Figure 4.6: Comparison of the solutions.

need less than a second. Note that the  $y$ -axis is in logarithmic scale. However, in all cases MATLAB is faster. We want to mention here, that this is mostly because of the I/O process and since the problem is rather easy. For a complete overview of the other

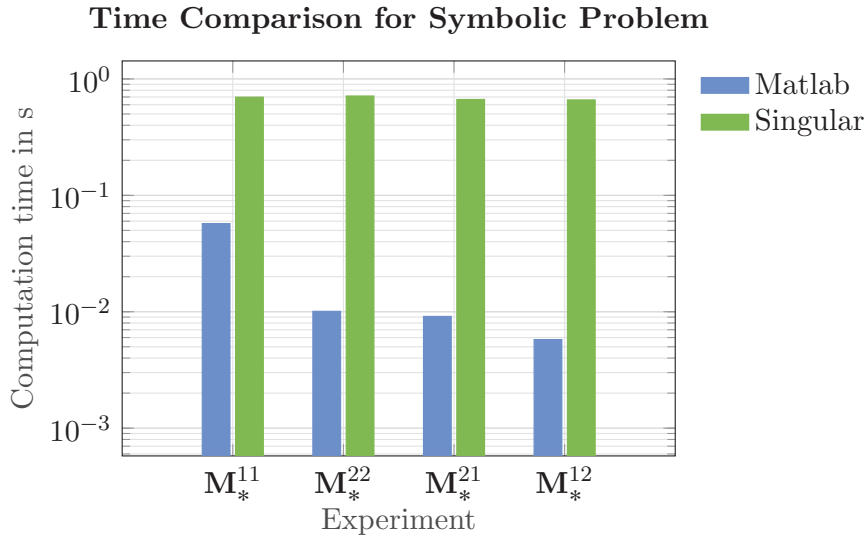


Figure 4.7: Time Comparison for solving the open grid structure.

effective properties we show them in figure 4.8. Here, we can see that  $c_{1122}^{hom} = c_{2211}^{hom} = 0$ . This means that our structure is indeed orthotropic. Moreover, we get that the Poisson's ratio of an equivalent homogeneous shell is zero.

### 4.3.2 Varying hexagon

In this section we want to consider a more elaborate example, where we vary the width and length of a hexagon. Such hexagonal structures appear also in real life applications as for example in filter systems and in foils for cosmetic applications. In the next chapter we can then use the symbolic expressions for the flexural rigidities to find the optimal design. As in the previous case we want to determine the minimal periodicity



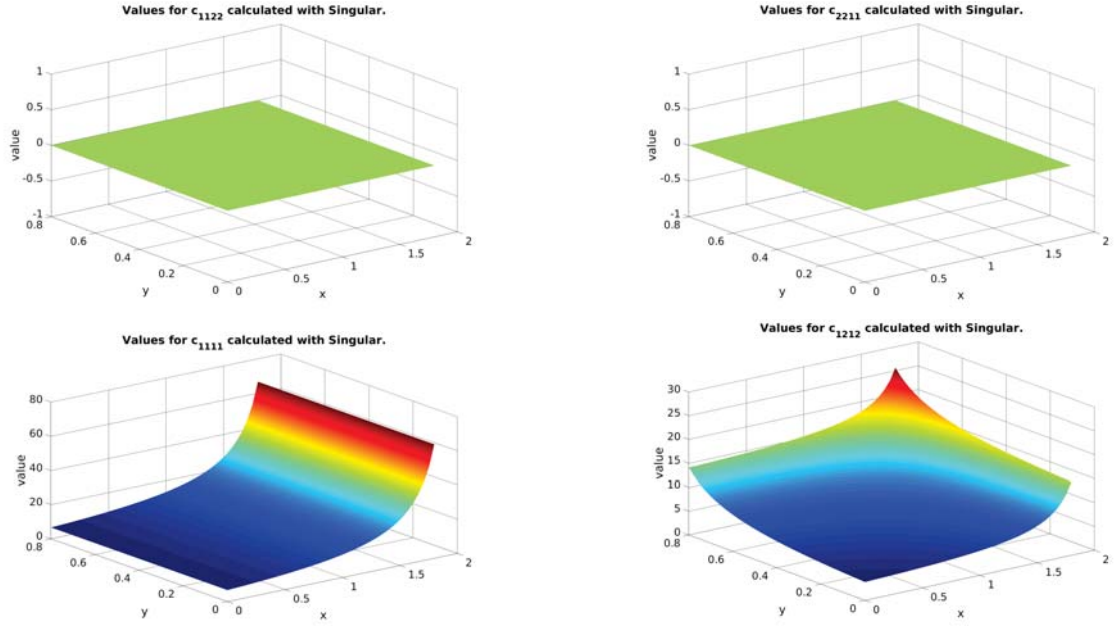


Figure 4.8: Other effective properties for open grid

cell  $Y$ , which we can parametrize. Moreover, we want to specify certain constraints to get realistic solutions. After that we run our symbolic homogenization procedure to express the  $c_{\alpha\beta\alpha'\beta'}^{hom}$  with respect to these variables. In figure 4.9 we have indicated the smallest periodic cell with the red box. The full structure is then received by periodic continuation of the red box in both directions.

The goal now is to parametrize the structure such that we need as few symbolic variables

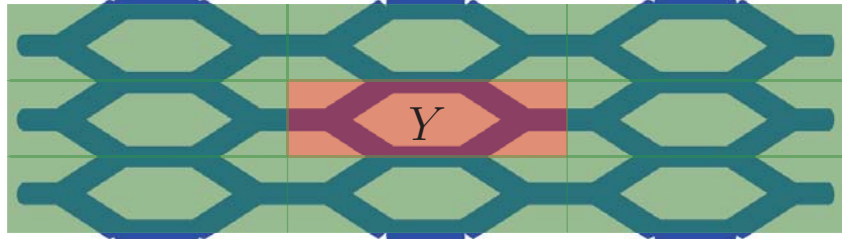


Figure 4.9: Periodicity cell of the hexagon

as possible. In general each newly introduced variable increases the complexity. We look at figure 4.10, where we cut out a quarter of a hexagon, consisting of three beams, as we can see in the left part. We introduce two symbolic variables  $g_x$  and  $g_y$ , which we denote as  $g = (g_x, g_y)$ . This  $g$  is shown as the red dot in the figure and the underlying red box indicates the constraints, which we enforce on the choices for our design parameter. In our structure we fix one point at  $(0, 0.5)$ , the green dot, which is independent of the design parameters and we connect the dots with a beam element. Next we add a beam which is perpendicular to the orange line and connect it with the red dot. Hence, this beam is given by the two nodes  $(g_x, 0)$  and  $(g_x, g_y)$ , where we denote by  $l(g) = g_y$  the beam's length. In the end we have to describe the third beam starting at the green node. This one should be parallel to the  $e_2$  axis and have the length  $l(g)$ , which is necessary to generate a proper periodicity cell. We connect the two points  $(0, 0.5)$  and  $(0, 0.5 + g_y)$ . After that we reflect the beam structure along the orange and green line to obtain a hexagon. In the right part of the picture we can see two examples, where one



is the extreme case of having a rectangle instead of a hexagon. The beams itself have a circular cross section with  $r = 0.03$  mm, Young's modulus  $E = 200$  GPa and Poisson's ratio  $\nu = 0.3$ . We can now set up the mesh to calculate the effective properties with

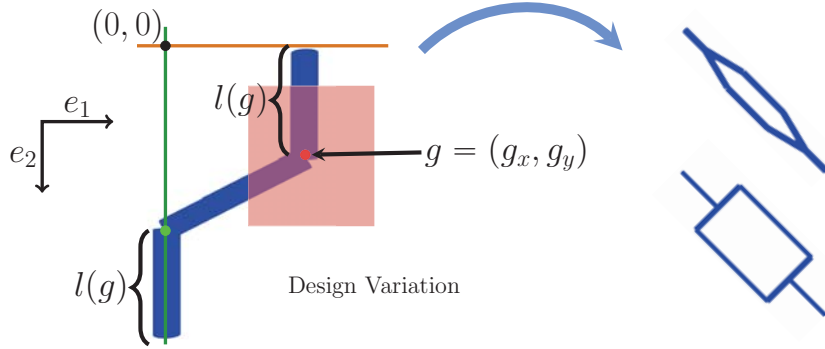


Figure 4.10: Variation of the hexagonal geometry

respect to the given parametrization, where we assume that  $g \in [0.1, 0.4] \times [0.2, 0.5]$ . In figure 4.11 we can see the values for  $c_{1111}^{hom}$  plotted over the constraint domain. Once again we have used both MATLAB's backslash operator and the Singular computation. We notice that both methods yield the same results, where the difference for this example in  $L^2$ -norm is  $2.0543 \cdot 10^{-15}$ . Likewise to the open grid structure we want to compare the

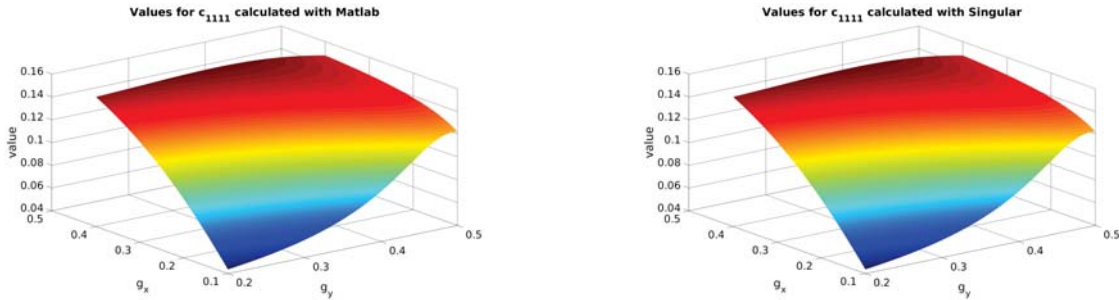


Figure 4.11: Effective  $c_{1111}^{hom}$  for the varying hexagon

time needed with both variants. We immediately see that it takes longer to compute this problem. Especially, the difference between MATLAB and Singular is getting smaller. In all four experiments it takes around 10 s to invoke both the I/O operations and solving the linear system by calling Singular.

In figure 4.13 we can have a look at the other results. Moreover, we have summarized some selected analytic expressions in the appendix C. Another important investigation is that we satisfy the orthotropy condition  $c_{1122}^{hom} = c_{2211}^{hom}$ . This means we can calculate a pinching load on the equivalent homogeneous shell with our function derived in section 3. Hence, we can directly plug in the polynomial expressions and see how the design choice affects the result. We also want to emphasize on the values of  $c_{1122}^{hom}$  for  $g_y = 0.5$ . This is the setup, where we obtain a rectangle instead of a hexagon. We observe that at this point we always obtain the value  $c_{1122}^{hom}(\cdot, 0.5) = 0$ , for all  $g_x \in [0.1, 0.4]$ . This is in correspondence to the open grid examples, where all beams are parallel either to the  $e_1$  or  $e_2$  axis.

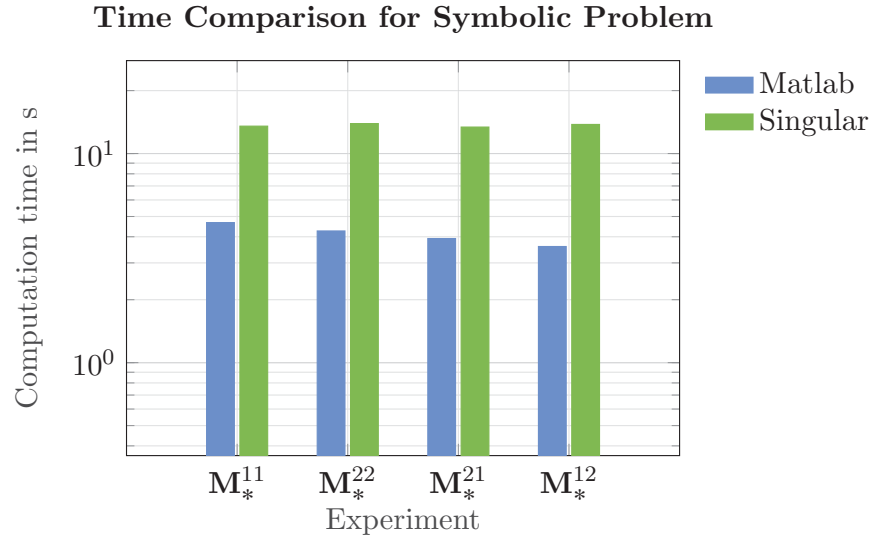


Figure 4.12: Time Comparison Matlab and Singular for varying hexagon

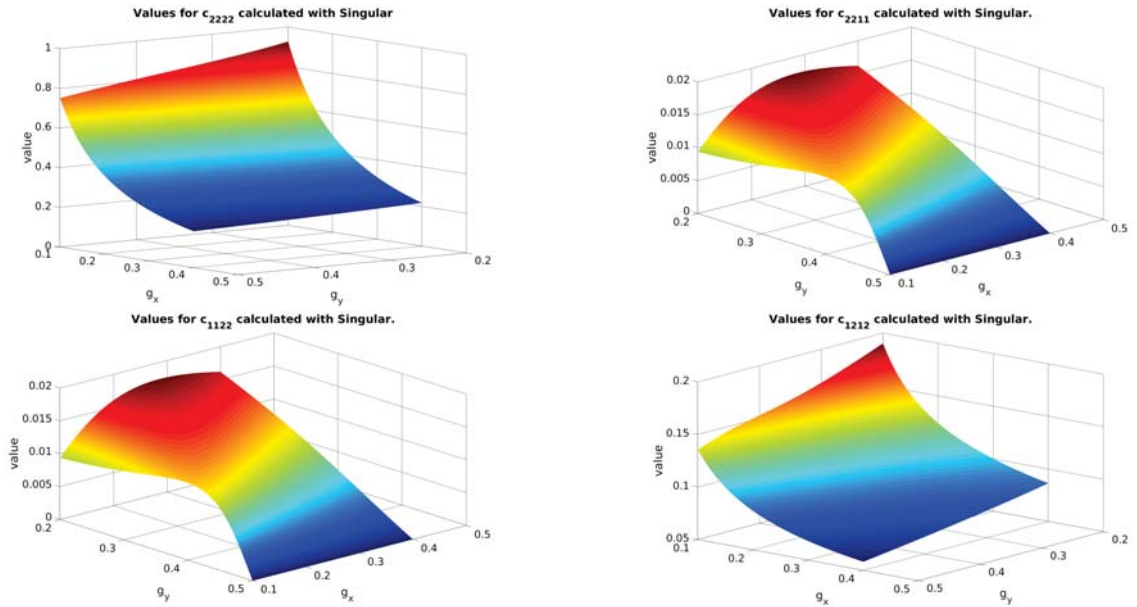


Figure 4.13: Other effective properties for the varying hexagon calculated with Singular.

### 4.3.3 Varying cross sections

In the next example we want to consider the case, where the hexagon's size is fixed, but we are allowed to vary the design of the beams. Thus, we consider a structure as shown in figure 4.14, where the length is 1.8 mm and the width 0.6 mm. There we assume that the hexagon consists of two types of beams, where both are given in the first part with a quadratic cross section and after that with a circular one. We assume that the beams parallel to the  $e_1$  axis have the green cross sections on the right, while the oblique beams have the blue ones. The mechanical properties are the same as in the previous example. We introduce the symbolic variables  $x$  and  $y$  which control the size of the cross sections.

A simple calculation of the area moments of inertia for both cases, the quadratic cross section on top and the circular one on the bottom, yields

$$\begin{aligned} I_{y/z,\blacksquare}^{green} &= \frac{x^4}{12}, & I_{y/z,\blacksquare}^{blue} &= \frac{y^4}{12}, \\ I_{y/z,\bullet}^{green} &= \frac{x^4\pi}{64}, & I_{y/z,\bullet}^{blue} &= \frac{y^4\pi}{64}. \end{aligned}$$

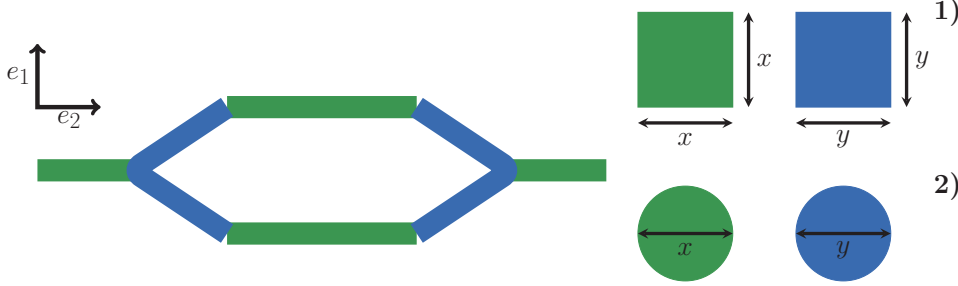


Figure 4.14: Change in cross section

Furthermore, we assume that  $x, y \in [0.03, 0.1]$  for both instances. When we set up the global stiffness matrix we can introduce the area moments of inertia as presented and take them through the whole process. We note that the thickness  $h$  is not constant in this experiment. It is actually given as  $\max(x, y)$ . In figure 4.15 we show the results of the first case for the effective  $c_{2222}^{hom}$  in the top layer and  $c_{1122}^{hom}$  on the bottom. A small calculation of the difference for  $c_{2211}^{hom}$  in  $L^2$ -norm, which is  $4.8986 \cdot 10^{-18}$ , confirms that both methods yield the same result. We note, that in this case the structure is again orthotropic for all combinations of  $(x, y)$ . We provide the exact polynomials in the Appendix C. In the next step we want to check the second case. A closer investigation

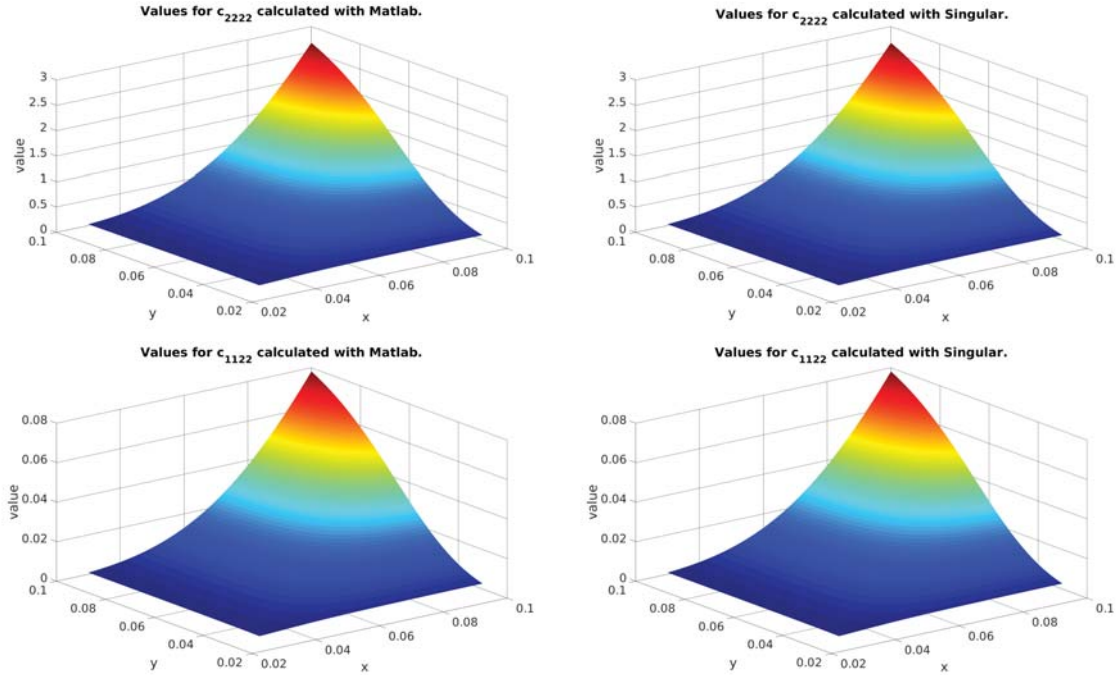


Figure 4.15: Comparison of effective properties for varying quadratic cross sections.

of our parametrization reveals that we are for  $(x, y) = (0.06, 0.06)$  in the configuration

of our example in section 4.3.2. Hence, we should obtain the same value as for choosing  $g = (0.3, 0.4)$  in the previous calculation. In figure 4.16 we present the effective properties for our structures. We focus on the values for  $c_{2222}^{hom}$  and  $c_{1212}^{hom}$ . We first note that the plots look similar to the quadratic cross section, but the current design is less stiff than the other. This corresponds to the classical Euler-Bernoulli beam theory, where a rectangular cross section has a bigger flexural rigidity than a circular one. Moreover, we can calculate the value of  $c_{2222}^{hom}$  at  $(x, y) = (0.06, 0.06)$  and obtain 0.217. The same result is indeed attained for the example in section 4.3.2.

Principally, we can conclude for this example that increasing the width of the beam elements also increases the stiffness. Given this structure we will examine in chapter 5 what the best choice for minimizing the deflection is. Moreover, we also want to investigate how the Poisson's ratio in both cases behave. For now we continue with the

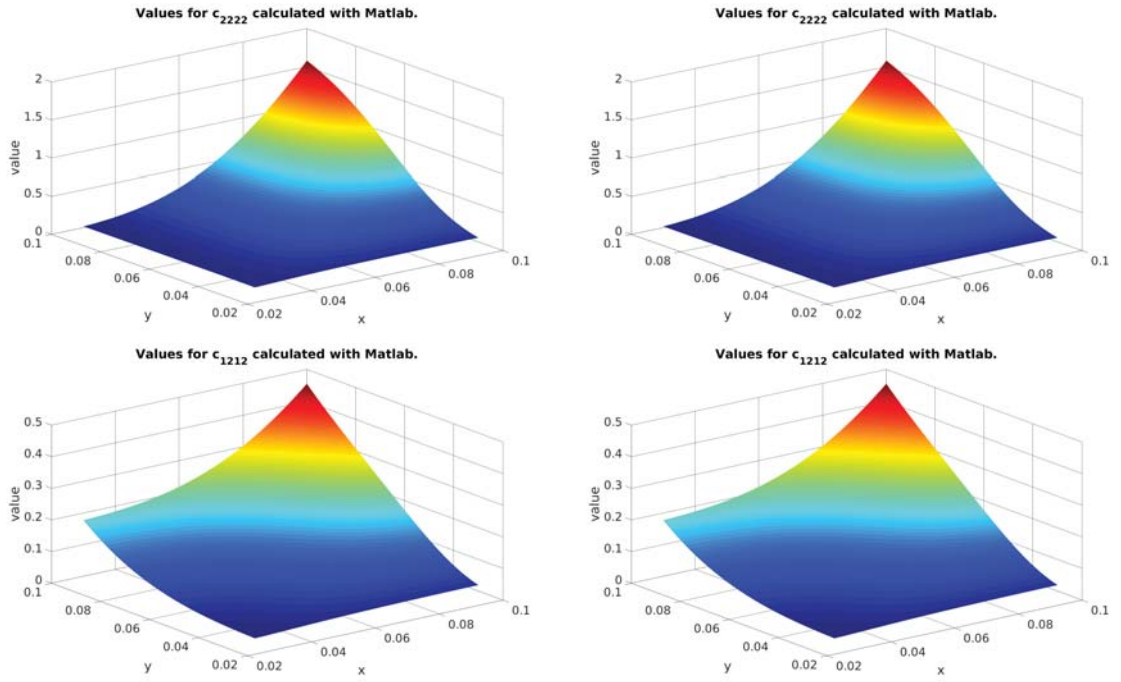


Figure 4.16: Comparison of effective properties for varying circular cross sections.

comparison of the time used for each experiment in MATLAB and Singular. The results are presented in figure 4.17. As we can see in the diagram, the computation time needed for both cross sections, is less than for the varying hexagon. It takes here slightly more than 1 s for each experiment. We still see that it is faster to stay in MATLAB, even though the difference between both methods is rather marginal. Note, that the plot is still in log-scale. We close this example for now and move on to a problem, which uses just one symbolic variable. This example will demonstrate why it is more reasonable to use Singular instead of MATLAB and it shows why one should always be careful, when calculating with symbolic variables.

#### 4.3.4 Shifted beams

In this section we consider a parametrization with just one symbolic variable. This particular example shows that one should be really careful with the parametrizations. Even though it seems easier than the previous ones it is so far the most difficult. We consider a hexagon with fixed width, 0.6 mm, and length, 1.8 mm, but we assume that

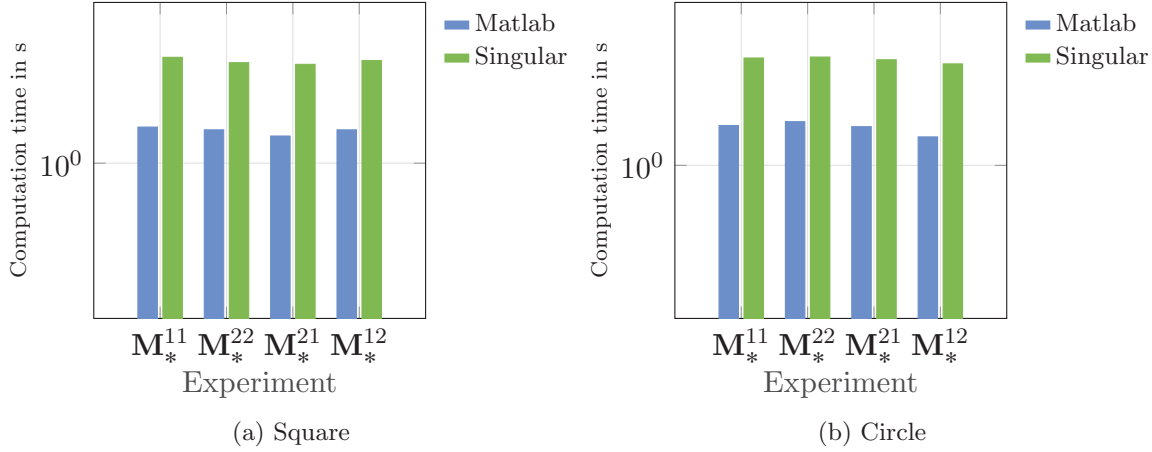
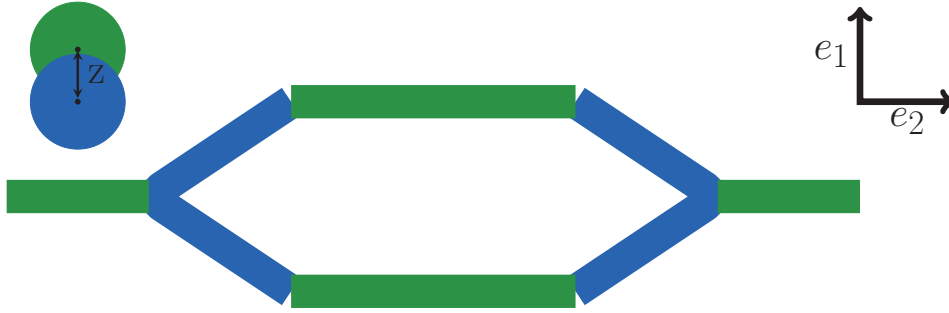
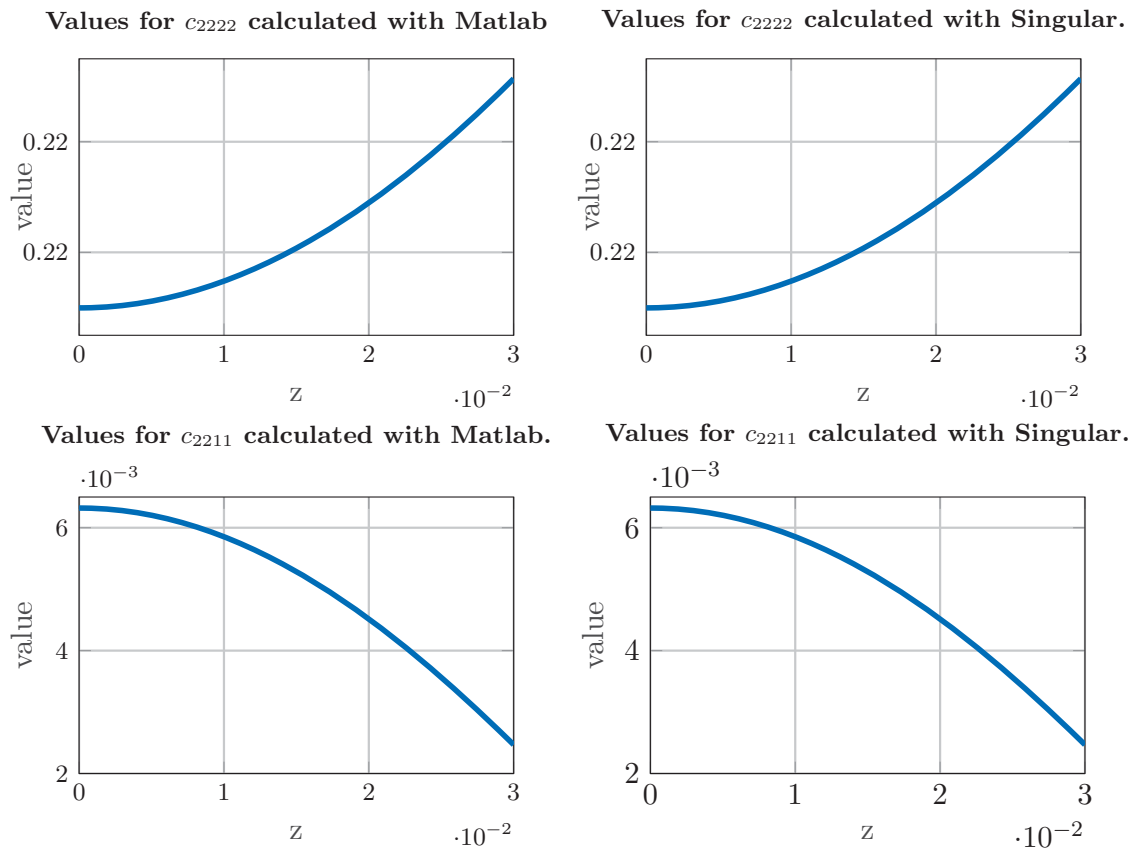
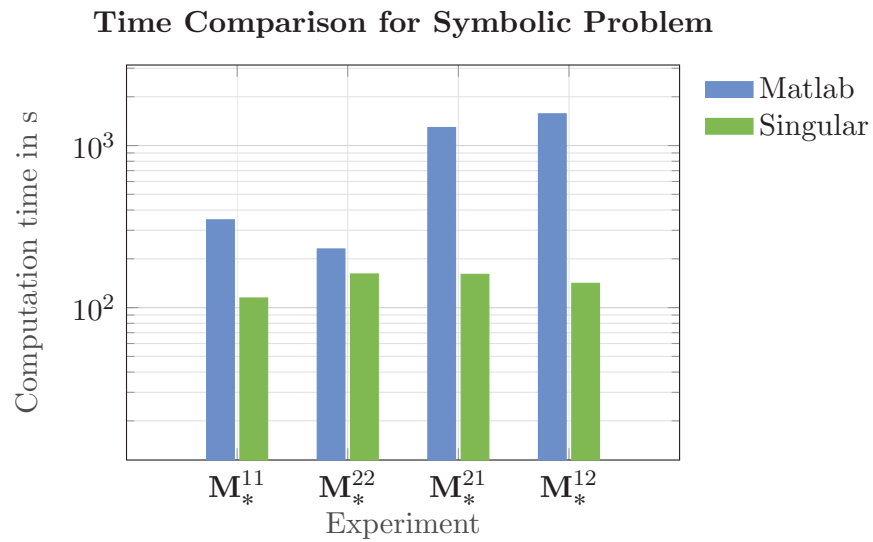


Figure 4.17: Time comparison for varying cross sections.

the green beams can be shifted vertically. Hence, we parametrize the distance between the green and blue beams as shown in figure 4.18 by some variable  $z$ . Moreover, we note that the area moments of inertia of each beam are constant, where we assume that the beams are circular with radius  $r = 0.03$  mm. We consider again the same material properties as before and assume that  $z \in [0, 0.03]$ . After calculating all experiments,

Figure 4.18: Variation in  $z$  direction.

both with Singular and Matlab, the first observation one can make is that the solutions from both methods again coincide. The differences are always of the order  $10^{-16}$ . We want to have a closer look on the flexural rigidities in the  $e_2$ -direction, given as  $c_{2222}^{hom}$ . As we can see in figure 4.19, we have for the case with  $z = 0$  that  $c_{2222}^{hom} = 0.217$ . This result is the same as the corresponding value from the example in section 4.3.2 with  $(g_x, g_y) = (0.3, 0.4)$ . Moreover, we can deduce from the plot that shifting in the  $z$  direction makes the construction stiffer in the  $e_2$  direction. If we compare the maximal with the minimal value, we have an improvement of about 0.04. Therefore, compared to other design approaches the shifts do not induce that much stiffness. It is important to note that this example actually attains configurations, which are not orthotropic. Anyhow, the differences between  $c_{1122}^{hom}$  and  $c_{2211}^{hom}$  are small. Moreover, due to the shifts we have that  $b_{\alpha\beta\alpha'\beta'}^{hom} \neq 0$ . We assume in chapter 5 that this structure is orthotropic and perform the minimization of the maximal deflection. A look at the time comparison in figure 4.20 reveals that in this case Singular outperforms MATLAB. While it takes for the backslash operator between 10-20 minutes, Singular needs together with the I/O operation just about 10 seconds. This result is rather surprising, if we consider that there are actually fewer variables. On the contrary, it shows us that we cannot determine a priori which method should be chosen. We close now this example with the

Figure 4.19: Shift in  $z$  direction with contact condition.Figure 4.20: Time comparison shift in  $z$  direction.

observation that Singular should indeed be chosen in favor of MATLAB. Even though in most examples MATLAB was slightly faster, we can run into a lot of trouble for special parametrizations as seen in this case.



### 4.3.5 Auxetic structure

As a last example for periodic structures we want to discuss a periodicity cell which inherits an auxetic behavior, i.e., having negative Poisson's ratio for all configurations. Such materials are of interest in different engineering applications, as shown in [22] and in the framework of optimization in [57]. For that case we consider the beam structure given in figure 4.21. We first need to identify the minimal periodicity cell  $Y$  of the structure and introduce a suitable parametrization in figure 4.22. We assume that the beam in the middle, which is parallel to the  $e_2$ -axis and starting at the green dot, has a fixed length  $l_{\text{aux}}$ . Moreover, the oblique beams connected with the green dot have the same length and their direction is given by the angle  $\gamma$ . This parameter will be our symbolic design variable in the homogenization process. The distance from the green dot to the origin is  $l_{\text{aux}}$ . The full cell  $Y$  is then obtained by reflecting the described parametrization along the  $e_1$ -axis, which is drawn in orange. In the following example we choose the parameter  $l_{\text{aux}} = 0.6$  mm. This means that the periodicity cell's length is constant with  $4 \cdot l_{\text{aux}}$ , while the width is dependent on the angle  $\gamma$  by  $2l_{\text{aux}} \cdot \sin(\gamma)$ . The beams are assumed to be circular with radius  $r = 0.03$  mm and Young's modulus  $E = 200$  GPa.

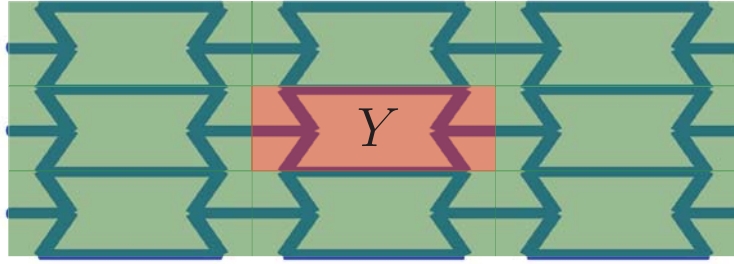


Figure 4.21: Periodic structure of an auxetic material.

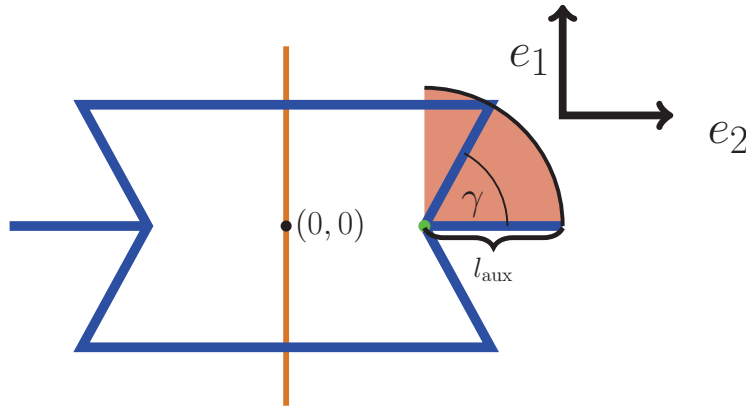


Figure 4.22: The auxetic cell

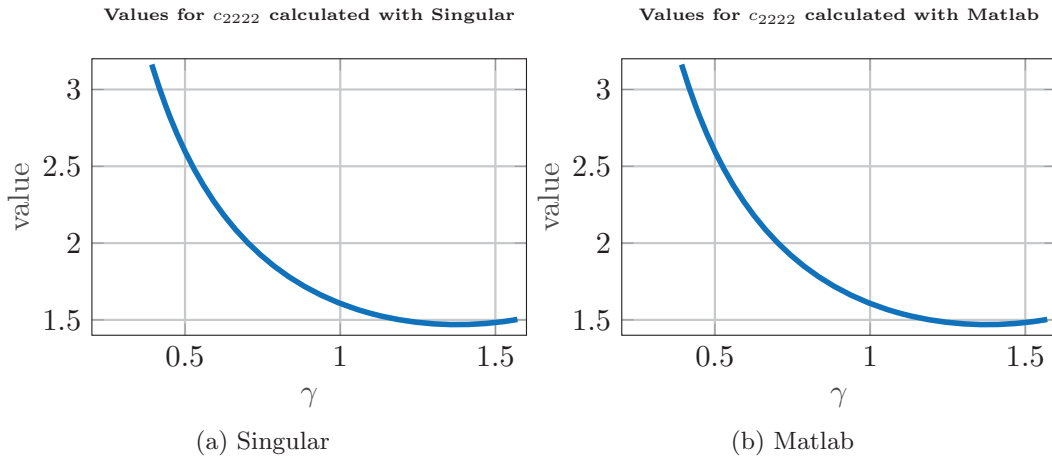
For this special structure we include two pictures demonstrating the  $\mathbf{M}_*^{22}$  experiment in figure 4.23, which yields the values for  $c_{2222}^{\text{hom}}$  and  $c_{2211}^{\text{hom}}$ . Next up we want to verify that our structure is indeed auxetic for all choices of  $\gamma$ . To investigate that we show the obtained effective properties  $c_{2222}^{\text{hom}}$  and  $c_{2211}^{\text{hom}}$  calculated both with MATLAB and Singular. The results are presented in the figures 4.24 and 4.25. We can not only observe that both methods yield again the same result, but also that the values  $c_{2222}^{\text{hom}}$  are always bigger than 0, while the  $c_{2211}^{\text{hom}}$  are always negative for all  $\gamma \in [\frac{\pi}{8}, \frac{\pi}{2}]$ . Hence, calculating the Poisson's

Figure 4.23: Cell Experiment  $\mathbf{M}_*^{22}$  for auxetic material.

ratio  $\nu_{12}$  gives the result on the right side of figure 4.26. For the sake of completion, we also show the values for  $\nu_{21}$ , which is not as interesting as the other case. For  $\nu_{12}$  we can see that increasing the angle  $\gamma$  makes the Poisson's ratio smaller. Moreover, we can conclude that

$$\lim_{\gamma \rightarrow \frac{\pi}{2}} \nu_{21}(\gamma) = 0.$$

This configuration coincides with the geometry of an open grid structure or to the case that  $g_y = 0.5$  in example 4.3.2. The corresponding result are in accordance with the analytic solution for the open grid structure given in [61]. Another interesting task is finding the minimal Poisson's ratio. We will consider this problem in the next chapter, where we implement optimization techniques to find this value. To finish this section we want to check the time needed to solve the linear equation system. The bar diagram in figure 4.27 presents the total processing times. For this example we can only deduce that the I/O procedures are rather time-consuming.

Figure 4.24:  $c_{2222}^{hom}$  for auxetic materials.

### 4.3.6 Summary

In the five presented examples we have shown the advantages of calculating effective properties with symbolic expressions. The greatest improvement we have achieved with this method is obtaining analytic expressions for the flexural rigidities, shear modulus, Poisson's ratio and Young's moduli depending on our parametrization. In the sense of example 4.3.1, the open grid structure, one does not have to calculate the values by hand, instead it reduces to defining a reasonable parametrization and progress the mesh with our algorithm. We are also able to calculate the analytic expressions for more elaborate examples, 4.3.2-4.3.5. Moreover, we have developed a way to solve the problem with



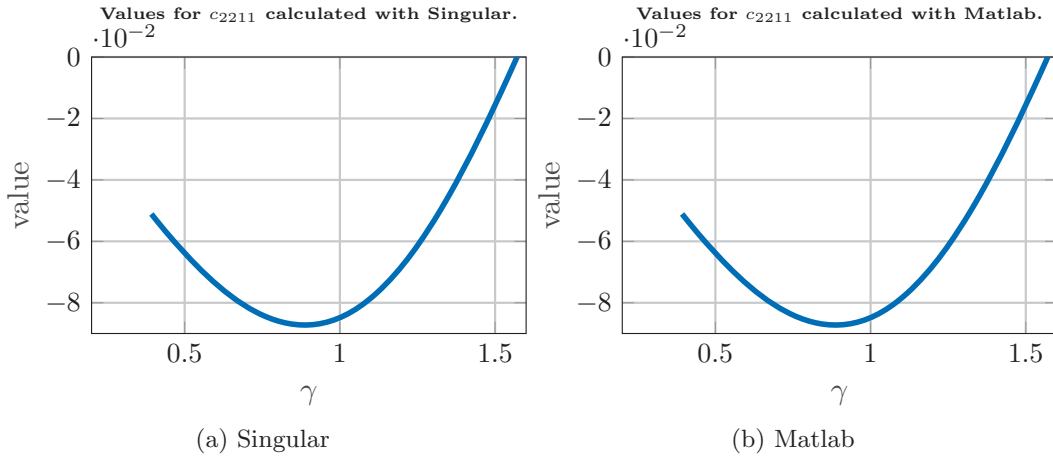
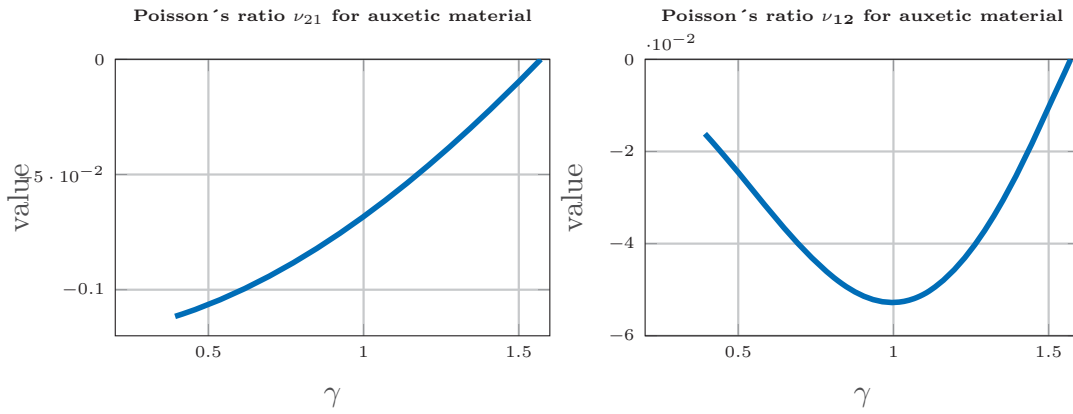
Figure 4.25:  $c_{2211}^{hom}$  for auxetic materials.

Figure 4.26: Poisson's ratio for auxetic materials.

### Time Comparison for Symbolic Problem

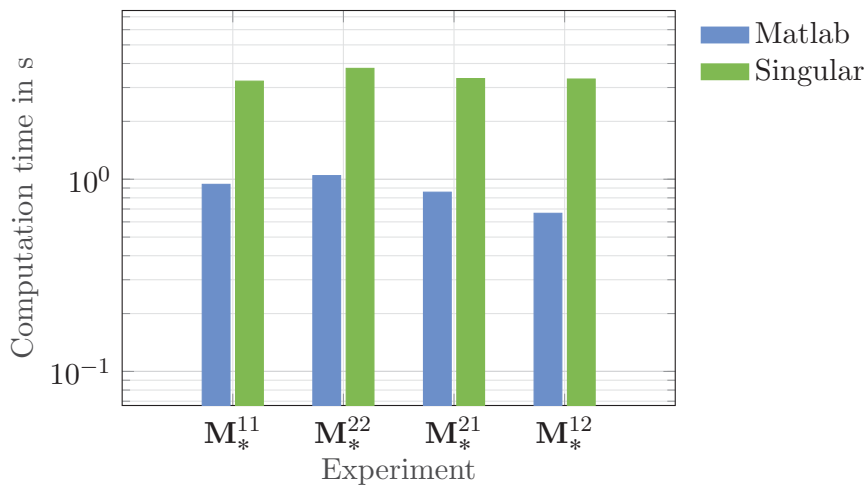


Figure 4.27: Time comparison for the auxetic material.

an efficient computer algebra system. In most cases the I/O procedures are tedious but for meshes, where one considers shifting elements in the outer plane direction, we can

reduce the computation time by using Singular and therefore it is preferable to use this procedure. Regarding the time consumption we should discuss one more question: What are the benefits of the symbolic calculation compared to a numerical parameter study? In the next section we will solve two examples via a parameter study in contrast to our described method.

## 4.4 Comparison symbolical and numerical homogenization

Of course the presented algorithm can be implemented numerically. To obtain the effective properties of one particular setup this variant is incredibly faster. Anyhow, if we want to study the behavior of different variations in the mesh it can also get computationally costly. For those cases it may be of advantage to calculate the symbolic effective properties. Therefore, we want to investigate two questions

- Do both procedures yield the same results?
- When is the symbolic calculation faster than the parameter study?

We restrict ourselves to the examples of the open grid structure and the varying hexagon. Beginning with the open grid parametrization we first compare the results. For that reason we discretize the intervals  $[0, 1.8]$  and  $[0, 0.8]$  both with 10 points and calculate the  $L^2$ -norm of the difference between the symbolical and numerical solution. The values are summarized in table 4.1. Since  $c_{1122}^{hom}$  and  $c_{2211}^{hom}$  should be 0 anyway by the theoretical results in [61], it is not surprising to see that the difference is exactly 0. For the other two bending experiments we see that both values are of the order  $10^{-6}$ . Moreover, we can check in figure 4.28 the convergence of the numerical solution to the symbolical one. We see that for refined meshes the difference gets smaller up to around  $5 \cdot 10^{-7}$ . We should keep in mind that we introduce two numerical errors in the comparison. The first one lies in the numerical solution itself and the second one in the conversion of symbolic parameters to numerical values. We can conclude for this example that the numerical method yields the same values as the symbolic calculation. Introducing more discretizations points will then decrease the difference. We now want to compare the

	$c_{1111}^{hom}$	$c_{1122}^{hom}$	$c_{2211}^{hom}$	$c_{2222}^{hom}$
Difference	$2.662 \cdot 10^{-6}$	0	0	$3.611 \cdot 10^{-6}$

Table 4.1: Difference in  $L^2$  for open grid.

time consumption. In order to make reasonable conclusions we measure the complete processes. This involves the setup of the global stiffness matrix, solving the linear equation and calculating the effective properties.

Since we obtain in our presented variant the symbolic expressions, which can be later converted to functions, we get a discretization independent time. Once we have calculated the effective properties the evaluation of certain points is done instantaneously. For the numerical method we will successively increase the number of discretization points in the intervals and take track of the time for evaluating all points. We start with 100 points and go up to 3600. In figure 4.29 we present the results. Obviously, the time for the numerical method increases linearly. It is interesting to see that solving the symbolic problem is as fast as a parameter study with  $\sim 900$  discretization points. Considering that the analytical expressions are more meaningful, it is important to underline that in this example the presented approach is as efficient as the numerical one.

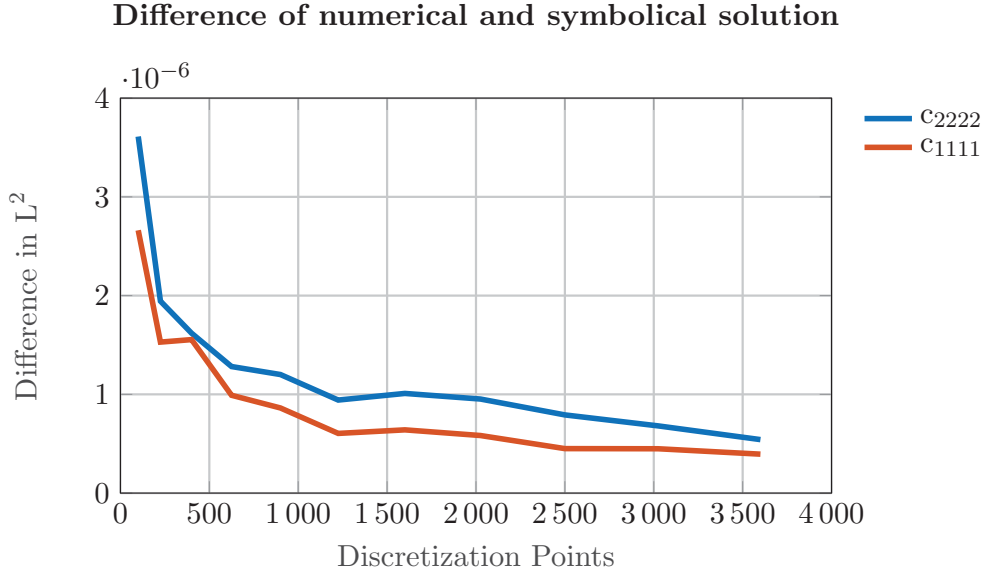


Figure 4.28: Convergence of numerical solution to symbolic.

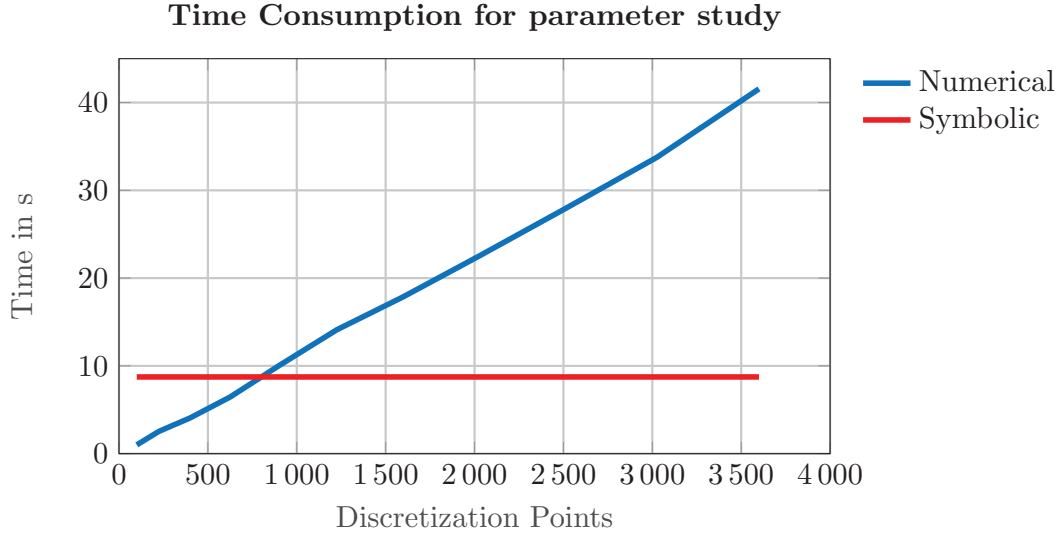


Figure 4.29: Time consumption for numerical and symbolical calculation of open grid.

We continue with the same comparisons for the varying hexagons. Of course this parametrization is a bit more complex. In table 4.2 we show the calculated differences again on a grid with 100 points. The values are sufficiently small. It may surprise that the differences for  $c_{1122}^{hom}$  and  $c_{2211}^{hom}$  are the same. Anyhow, since the hexagon is an orthotropic structure we have to get  $c_{1122}^{hom} = c_{2211}^{hom}$  and therefore we end up with the same numbers. The convergence of the numerical solution to the symbolic one, in the case of a hexagon, is shown in figure 4.30. Also for the second mesh we can conclude that both methods yield the same results.

	$c_{1111}^{hom}$	$c_{1122}^{hom}$	$c_{2211}^{hom}$	$c_{2222}^{hom}$
Difference	$1.585 \cdot 10^{-4}$	$1.252 \cdot 10^{-5}$	$1.252 \cdot 10^{-5}$	$3.484 \cdot 10^{-4}$

Table 4.2: Difference in  $L^2$  for hexagon.

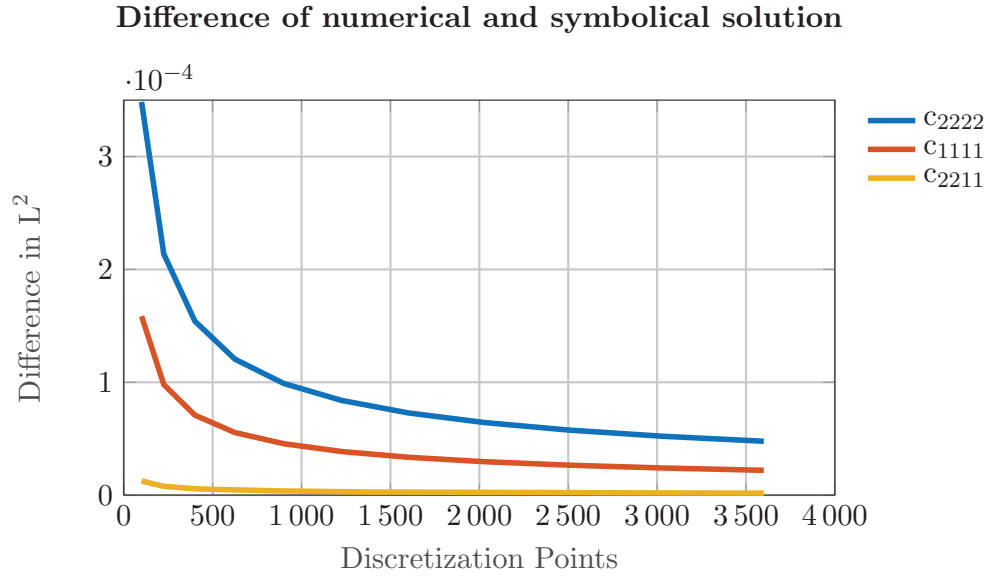


Figure 4.30: Convergence of numerical solution to symbolical.

Next, we take a look on the time consumptions in figure 4.31. We have the identical setup as in the previous case, where we now discretize the interval  $[0.1, 0.4] \times [0.2, 0.5]$  first with 100 points and then up to 3600. We can observe that the symbolical method needs almost a minute. We see that for a study over the complete domain the numerical treatment is still faster. Hence, for more complex geometries the numerical method outperforms the symbolical one.

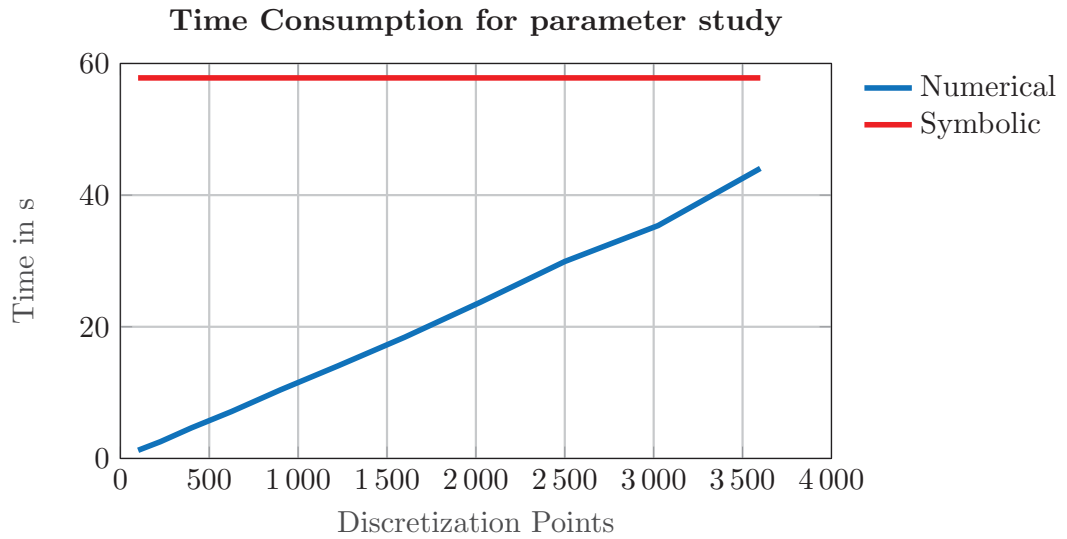


Figure 4.31: Time consumption for numerical and symbolical calculation of hexagon.

In conclusion we should keep in mind that it is in general computationally more expensive to get analytic expressions with the symbolical calculation than performing a numerical parameter study. However, the time factor is mostly relevant for complex structures and the benefit of having analytic expressions is more valuable.



## 5 Optimization

In this chapter we want to combine all the obtained results and use them to optimize structures given certain objective functions. All of this should be done within the structures' mechanical possible range. We consider here both the minimization of displacements due to pinching loads and the Poisson's ratio optimization. In each case we investigate the equivalent homogenized shells, where we use the results derived in chapter 2. Since each periodicity cell can be parametrized via symbolic design variables we perform the calculations symbolically as presented in 4. Especially, for the case of minimizing the maximal deflection we use the analytic formulation of the pinched cylinder problem, discussed in chapter 3. We see that the design choice affects the coefficients in the Fourier series. In the following section we focus on the setup of our optimization algorithm and after that we reconsider the examples from section 4.3 and optimize them w.r.t. the underlying constraints.

**Remark 5.0.1** *We want to recall here that the local  $e_1$  direction of the periodicity cell corresponds to the global  $(0, 1, 0)^T$  direction for the full shell. Hence, it is aligned with the direction of the curvature. Consequently, the local vector  $e_2$  is aligned with  $(1, 0, 0)^T$  the shell's longitudinal direction.*

### 5.1 Objective functionals

In this section we present the derivation of the objective functionals. We start with minimizing the maximal absolute deflection caused by a pinching load. Therefore, we take the analytic function, which we have derived for homogeneous orthotropic shells, given by

$$\begin{aligned} \mathcal{U}_3(s_1, s_2) = & \frac{2Pk^4}{\pi E_2 h H^3} \sum_{n=1,2,3,4,\dots}^{\infty} \frac{\sin(n\varphi_0)}{R_2 n^2} \sin\left(\frac{ns_1}{a}\right) \\ & \times \left\{ \left[ (\zeta C + \eta G) \cos\left(\frac{HA|s_2|}{a}\right) + (\zeta G - \eta C) \sin\left(\frac{HA|s_2|}{a}\right) \right] e^{-\frac{HB|s_2|}{a}} \right. \\ & \left. + \left[ (\zeta A - \eta B) \cos\left(\frac{HC|s_2|}{a}\right) + (\eta A + \zeta B) \sin\left(\frac{HC|s_2|}{a}\right) \right] e^{-\frac{HG|s_2|}{a}} \right\}, \end{aligned}$$

where we refer to Lemma 3.2.3 for details on the parameters and how they are obtained. Since we have considered a pinching load, we know that the maximal absolute deflection will occur at the same point as the load itself. Hence, we need to insert  $(a\varphi_0, 0)$  into our formula to obtain

$$\begin{aligned} \|\mathcal{U}_3(s_1, s_2)\|_{L^\infty(\omega)} &= \left| \frac{2Pk^4}{\pi E_2 h H^3} \sum_{n=1}^{\infty} \frac{1}{R_2 n^2} \sin(n\varphi_0)^2 \cdot [(\zeta C + \eta G) + (\zeta A - \eta B)] \right| \quad (5.1.1) \\ &= \mathcal{U}_{3,\max}. \end{aligned}$$

We note here that all parameters in the formula are bigger than 0, except the applied force  $P$ . Therefore, we can also consider

$$\mathcal{U}_{3,\max} = \frac{2|P|k^4}{\pi E_2 h H^3} \sum_{n=1}^{\infty} \frac{1}{R_2 n^2} \sin(n\varphi_0)^2 \cdot \left[ (\zeta C + \eta G) + (\zeta A - \eta B) \right]. \quad (5.1.2)$$

From that point on we assume that  $P$  is positive. We concluded in section 3.2.1 that we can terminate the series with  $n < 10$ , since the partial sums converge rather fast. In this part we proceed with  $S_8$  to simplify the calculations. Hence, we continue with

$$\mathcal{U}_{3,\max} = \frac{2Pk^4}{\pi E_2 h H^3} \sum_{n=1}^8 \frac{1}{R_2 n^2} \sin(n\varphi_0)^2 \cdot \left[ (\zeta C + \eta G) + (\zeta A - \eta B) \right]. \quad (5.1.3)$$

Furthermore, we saw in that section that the maximal deflection gets smaller the closer the pinching load is applied to the boundary. Thus, we will get the biggest deflection if we apply the load at  $(a\varphi_0, s_2) = (\frac{a\pi}{2}, 0)$ . Due to the expression  $\sin(n\varphi_0)$  we have only 4 non-zero elements in the series and we can simplify it to

$$\mathcal{U}_{3,\max} = \frac{2Pk^4}{\pi E_2 h H^3} \sum_{n=0}^3 \frac{1}{R_2 (2n+1)^2} \cdot \left[ (\zeta C + \eta G) + (\zeta A - \eta B) \right]. \quad (5.1.4)$$

This yields our objective functional, where all the parameters in the sum also depend on  $2n+1$ . We know that they rely on the shell's effective properties, too. We can plug in the symbolic expressions of our effective properties into this function. This means, that given our design variables  $\mathbf{x} \in \mathbb{R}^m$ , the expression  $\mathcal{U}_{3,\max}$  can be identified as a function

$$\begin{aligned} \mathcal{U}_{3,\max} : \mathbb{R}^m &\mapsto \mathbb{R}, \\ \mathcal{U}_{3,\max}(\mathbf{x}) &= \frac{2Pk(\mathbf{x})^4}{\pi E_2(\mathbf{x})h(\mathbf{x})H(\mathbf{x})^3} \sum_{n=0}^3 \frac{1}{R_2(\mathbf{x})(2n+1)^2} \left[ (\zeta(\mathbf{x})C(\mathbf{x}) + \eta(\mathbf{x})G(\mathbf{x})) \right. \\ &\quad \left. + (\zeta(\mathbf{x})A(\mathbf{x}) - \eta(\mathbf{x})B(\mathbf{x})) \right]. \end{aligned} \quad (5.1.5)$$

Moreover, we impose constraints on each design variable  $\mathbf{x}_i$ . There are  $a_i, b_i \in \mathbb{R}$  such that  $\mathbf{x}_i \in [a_i, b_i]$ . With that we can formulate our optimization problem as

$$\begin{aligned} \min_{\mathbf{x}} \quad & \|\mathcal{U}_3(s_1, s_2, \mathbf{x})\|_{L^\infty(\omega)} = \mathcal{U}_{3,\max}(\mathbf{x}) \\ \text{s.t.} \quad & a_i \leq \mathbf{x}_i \leq b_i. \end{aligned} \quad (5.1.6)$$

The optimization problem for the Poisson's ratio is then obtained in a similar way. We know from remark 4.1.4 that we can calculate the expressions from the effective bending properties as

$$\nu_{21} = \frac{c_{1122}^{\text{hom}}}{c_{1111}^{\text{hom}}}, \quad \nu_{12} = \frac{c_{2211}^{\text{hom}}}{c_{2222}^{\text{hom}}}.$$

Since both parameters depend on the design variable  $\mathbf{x}$  we can formulate the Poisson's ratio optimization as

$$\begin{aligned} \max / \min_{\mathbf{x}} \quad & \nu_{21}(\mathbf{x}) = \frac{c_{1122}^{\text{hom}}(\mathbf{x})}{c_{1111}^{\text{hom}}(\mathbf{x})} \\ \text{s.t.} \quad & a_i \leq \mathbf{x}_i \leq b_i, \end{aligned}$$

where the formulation for  $\nu_{12}$  follows respectively.

There are various different methods for solving such a constrained optimization problem. We focus on the projected gradient method as discussed in [5, section 2.3]. There we consider a steepest descent approach, where we choose the length of the step size via the Armijo rule along the projection arc. Moreover, if the current iteration  $\mathbf{x}^i$  violates one or more constraint we project the value back into the admissible set. We define the projection

$$\mathbf{P} : \mathbb{R}^m \mapsto \mathbb{R}^m$$

$$\mathbf{P}(\mathbf{x}) = \left( \max(\min(\mathbf{x}, b_i), a_i) \right)_{i=1, \dots, m}.$$

We have summarized the procedure in algorithm 1.

**Remark 5.1.1** *Since our homogenization process has been done completely symbolically we can calculate the gradients with MATLAB's `diff` operator. This can be used to obtain the search direction in the projected gradient method.*

---

**Algorithm 1** Projected Gradient Method

---

```

1: procedure PROJECTED GRADIENT( $f, \nabla f, \mathbf{P}, x^0$ )  $\triangleright$  Calculate the minimum of  $f$ 
2:    $x^0 = \mathbf{P}(x^0)$ 
3:    $tol = 10^{-12}$ 
4:    $\sigma \in (0, 1), \quad \alpha = 1$ 
5:   while  $k < M$  do  $\triangleright$  M is maximal number of allowed iterations
6:      $d = -\nabla f(x^k)$ 
7:      $x^{k+1} = \mathbf{P}(x^k + \alpha d)$ 
8:     while  $f(x^k) - f(x^{k+1}) < -\sigma d^T(x^k - x^{k+1})$  do
9:        $\alpha = \alpha \cdot \frac{1}{2}$ 
10:     $x^{k+1} = \mathbf{P}(x^k + \alpha d)$ 
11:    end while
12:    if  $\|f(x^{k+1}) - f(x^k)\|_2 < tol$  then
13:      break
14:    end if
15:     $\alpha = 1$ 
16:  end while
17:  return  $x^{k+1}$ 
18: end procedure

```

---

We want to emphasize here again that the effort we put into the setup of our symbolic homogenization procedure benefits the optimization process. It is not only possible to directly analyze the analytic formulation for the partial sum  $S_n$  and see how they depend on the underlying parametrization, but also the gradients are easily obtained.

## 5.2 Examples for minimization

We revisit the examples presented in chapter 4 and plug the effective properties, which have been calculated symbolically, into our function  $\mathcal{U}_{3,max}$  or the Poisson's ratio  $\nu_{12}, \nu_{21}$ . We use then the projected gradient method to obtain the optimal designs with respect to the given constraints. Since the coefficients  $P$  and  $a$  do not affect the choice of  $x_{\min}$



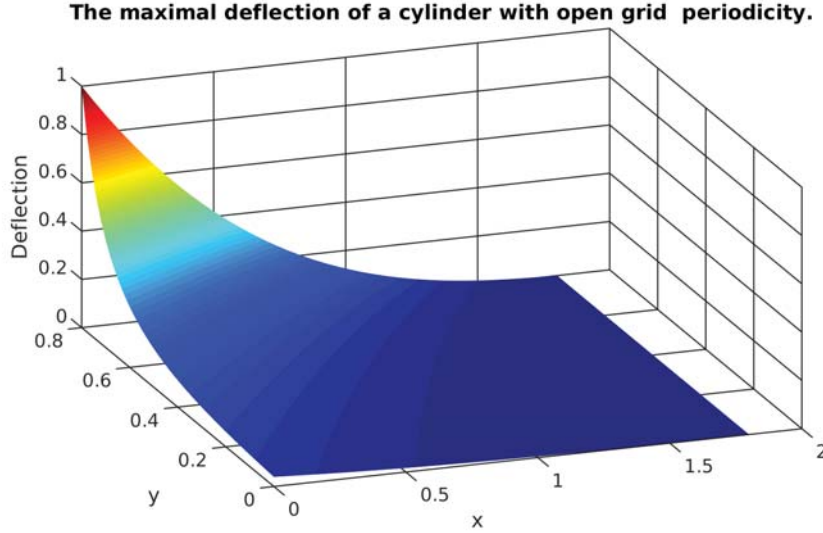


Figure 5.1: Maximal Displacement for open grid structure normalized.

in the minimization of the deflection, we fix those values with  $P = 1$ ,  $a = 2$  and consider the normalized displacements.

### 5.2.1 Optimize: Open grid structure

We consider the parametrization of the open grid structure as presented in section 4.3.1 and assume that a shell with this periodic structure is under the pinching load  $P$ . With the formula (4.3.1) in section 4.3.1 we can easily calculate that

$$E_1 = \frac{20000}{2-x}, \quad E_2 = \frac{20000}{1-y}$$

and consequently our parameter  $H$  in the functional simplifies to

$$H = \frac{1-y}{2-x}.$$

Since we have  $\nu_{12} = \nu_{21} = 0$ , we deduce that in the functional (5.1.5) only  $E_2$  and  $H$  depend on the choice of the design variables. This simplifies the function to

$$\mathcal{U}_{3,max}(x, y) = \sum_{n=0}^3 C_n \frac{(2-x)^3}{(1-y)^2},$$

where  $C_n$  are some coefficients in  $\mathbb{R}$ . The gradient is then given as

$$\nabla \mathcal{U}_{3,max}(x, y) = \sum_{n=0}^3 C_n \begin{pmatrix} -3 \frac{(2-x)^2}{(1-y)^2} \\ 2 \frac{(2-x)^3}{(1-y)^3} \end{pmatrix}.$$

We have plotted the function  $\mathcal{U}_{3,max}$  over the domain in figure 5.1, where the results are normalized with the maximal value being 1. We can see how the figure resembles the theoretically derived function  $\mathcal{U}_{3,max}$ . As we move closer to the singularity  $y = 1$ , our deflection explodes. Furthermore, plugging the function and its gradient into the

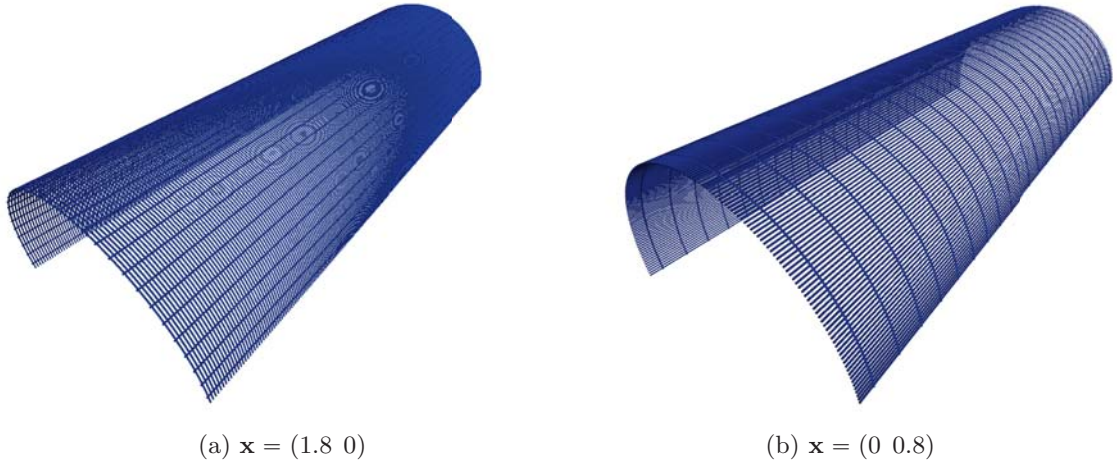


Figure 5.2: The best and worst shape w.r.t. our design space compared.

optimization method yields that the minimal deflection is obtained for  $(x, y) = [1.8 \ 0]$ . In order to qualitatively discuss the result we take a look on the shells with the best and the worst choice of design parameters given in figure 5.2. We can see that in order to minimize the deflection we have to stabilize the shell along the circumferential direction. As we can observe in the left picture of figure 5.2, the shell has a lot of beams in this direction, while the configuration on the right just has a few.

In the next step we will keep the open grid structure, but consider a different parametrization.

### Different design space

Here we investigate the example presented in [31] to demonstrate that the design variables can be chosen freely. We take again an open grid structure, but the choice of the design space is different. Especially, we do not only vary the spatial properties of the length, but we also want to change the thickness of some beam elements. Therefore, we need to specify the area moments of inertia as symbolic variables. We consider the setup in figure 4.2 and make the following assumptions that

$$\begin{aligned} b_1 + b_2 &= 1, \\ t_1 &= 2 \cdot t_2. \end{aligned}$$

We take  $\mathbf{x} = (t_2, b_1)$ , together with the requirement that  $t_2 \in [2, 3]$  and  $b_1 \in [0.5, 0.9]$ . Furthermore, we assume that all beam elements still have the properties  $E = 2 \text{ GPa}$  and Poisson's ratio  $\nu = 0.3$ .

**Remark 5.2.1** *We want to mention here that the example presented in [31] was a heterogeneous plate on an elastic foundation.*

Once we have implemented this mesh structure we can run it through our algorithm, which yields  $(t_2, b_1) = (2.0 \ 0.9)$  as the optimal solution. This means that the distance between two parallel beams should be as small as possible, as we have seen in the previous example. Moreover, the condition  $b_1 = 0.9$  can be understood as making the beams in the circumferential direction as big as possible to increase  $E_1$ , even if this

means to get smaller beams in the longitudinal direction. In figure 5.3 we have plotted the normalized deflection over the given constraints. We can see how marginal the choice of  $t_2$  is compared to  $b_1$ . This is mostly due to the coupling of  $t_1$  and  $t_2$  in this experiment.

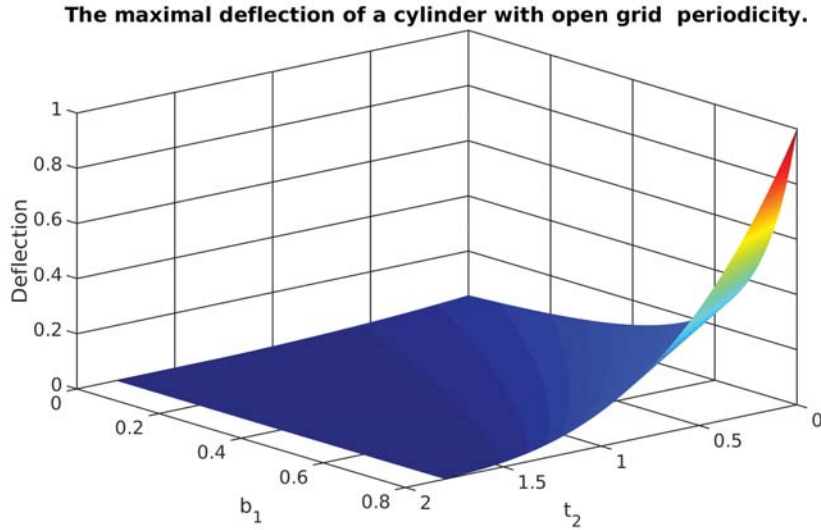


Figure 5.3: Normalized Displacements for the second parametrization of an open grid structure

### 5.2.2 Optimize: Varying hexagon

We now continue with the example of a varying hexagonal structure. We remind that for the following analysis we consider circular beams with radius 0.03 mm, which have a Young's modulus of 200 GPa. We want to vary the length and the width of the periodicity cell according to section 4.3.2. In figure 5.4 we show the normalized deflection for the current example. We can immediately see that the function explodes, if we choose the hexagon as small and narrow as possible. We are able to calculate the optimal solution with  $(g_x, g_y) = (0.4, 0.4209)$ . In figure 5.5 we present the best and worst set of design parameters. Similar to the open grid structure, we need a configuration which increases the Young's modulus  $E_1$  in the circumferential direction. We note here that the best solution on the left side is almost the extreme case of having a rectangle instead of a hexagon. Apparently, it is beneficial to still keep a hexagonal structure. Also the cell should be as big as possible. We can conclude the discussion of the spatial optimization for hexagons. We have seen that the best solution for this case is non-trivial. We later on see that the Poisson's ratio optimization is closely related to the one of the auxetic structure.

### 5.2.3 Optimize: Varying cross sections

We move on with our next example, where we consider the different design approach for a fixed hexagon, where we let our cross section either be circular or quadratical and control the size of the beam elements. We have seen that both cases yield similar results. Therefore, we focus on the quadratical cross section. We consider both the minimization problem and Poisson's ratio optimization. We take  $x$  and  $y$  as the design variables described

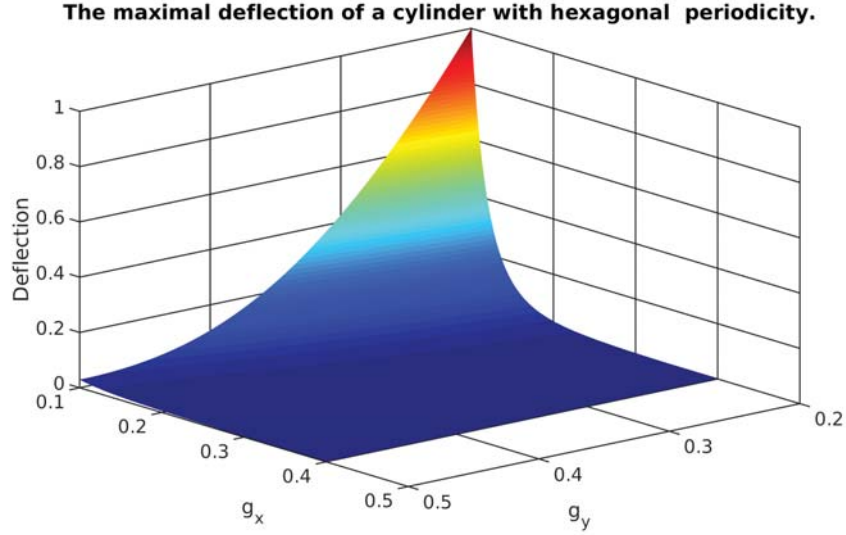


Figure 5.4: Normalized deflection for varying hexagon problem.

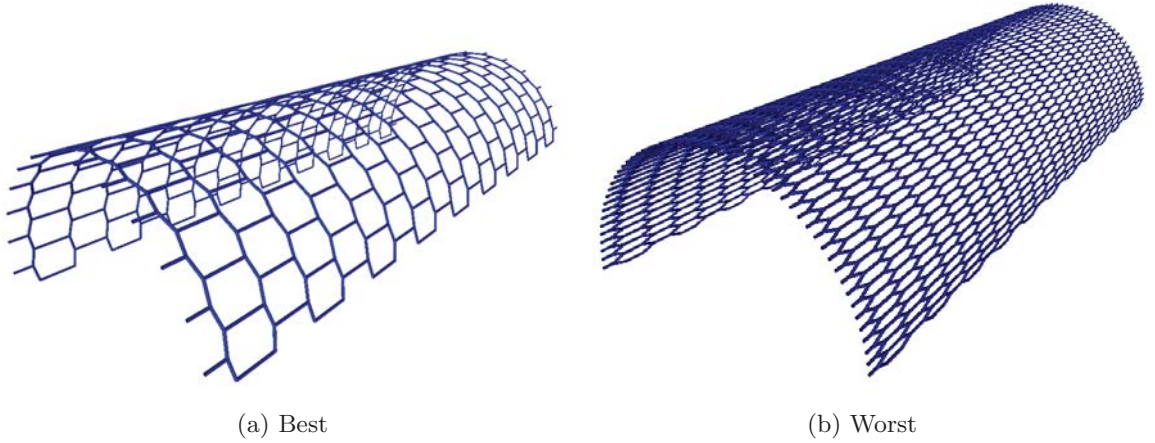


Figure 5.5: Best and worst choice for the varying hexagon problem.

in section 4.3.3, and assume that  $(x, y) \in [0.03, 0.1]^2$ . By plugging the effective properties into 5.1.2 we obtain the result shown in figure 5.6.

It is easy to see from the plot that the beams parallel to the longitudinal direction should be chosen rather thin, while the oblique beams are very wide. A small computation of the optimum confirms our suspicion that the optimal choice is  $(x, y) = (0.03, 0.1)$ . In figure 5.7 we present the optimal solution and relatively show the scales between the green beam and the blue beam. We can see that the choice of  $y$  has a higher impact than  $x$ . This is similar to the previous examples, where we have seen that the effective stiffness in the circumferential direction should be chosen as large as possible. For this example we also want to find the design choice, which maximizes, respectively minimizes, the values of  $\nu_{21}$ . We start with the minimum for  $\nu_{21}$ , which is attained at  $(x, y) = (0.03, 0.1)$ . Our gradient method can also be easily adapted to find the maximum, which we obtain at  $(0.1, 0.03)$ . The corresponding plot of  $\nu_{21}$  is in figure 5.8. This parametrization is a great example to show the impact of our method, since actually any geometrical or mechanical property could be introduced as a variable and optimization can be performed w.r.t. these designs.

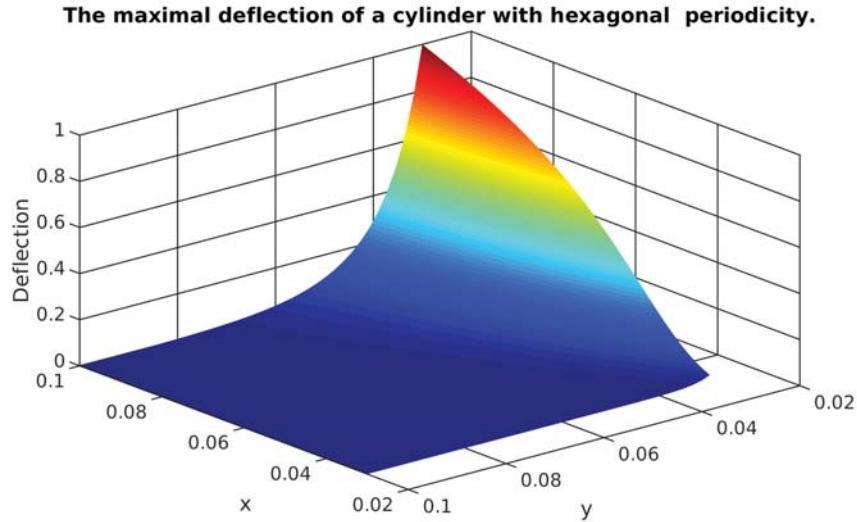


Figure 5.6: Normalized Deflection w.r.t. change of cross section

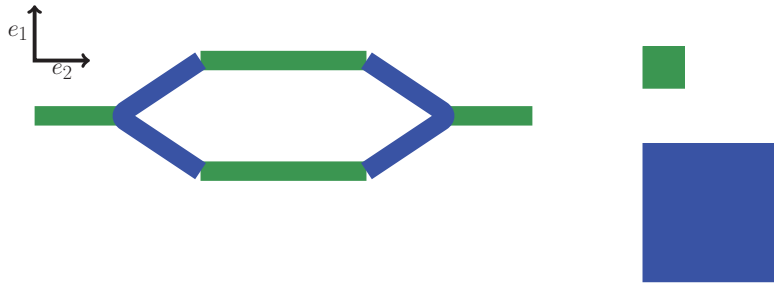


Figure 5.7: Change in cross section

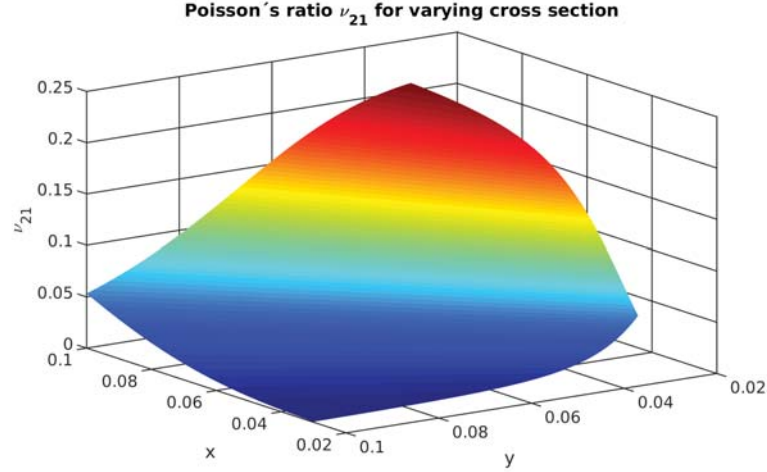
#### 5.2.4 Optimize: Shifted beams

In this section we want to study the 1D optimization problem, where the beams parallel to the longitudinal axis are shifted into the vertical direction. We have seen that especially this problem can be rather time consuming. For the optimization it is interesting to see if such shifts introduce a certain stiffness, which minimizes the deflection caused by pinching loads. Remember, that we have fixed the in-plane geometry of the hexagon and take circular beam elements with radius  $r = 0.03$  mm,  $E = 200$  GPa and  $\nu = 0.3$ . Our shift is bounded by  $r = 0.03$ . In figure 5.9 we have plotted the maximal deflection given this parametrization. As we can see, increasing the shift yields at first a bigger deflection. The maximal deflection is then attained for  $z = 0.0034$ . It is easy to see from the plot that the minimal deflection is reached for the biggest shift  $z = 0.03$ . Moreover, we can also consider for this case the Poisson's ratio maximization of  $\nu_{12}$ . In figure 5.10 we show the corresponding plot. For the presented function we can conclude that the maximal Poisson's ratio is reached at  $z = 0$ , while the minimal one is at  $z = 0.03$ .

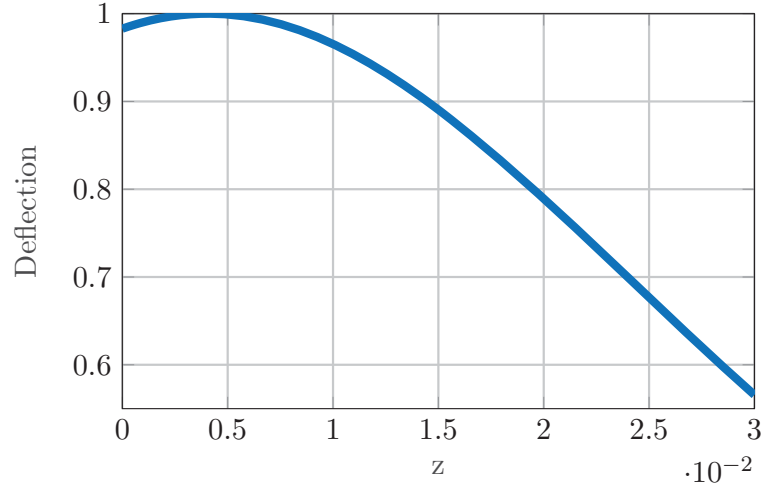
#### 5.2.5 Optimize: Auxetic structure

In our last example we investigate the auxetic periodicity cell. For those structures it is particularly interesting to optimize the Poisson's ratio. As we have described in the



Figure 5.8: Poisson's ratio  $\nu_{21}$ 

**The maximal deflection of a cylinder with hexagonal periodicity.**

Figure 5.9: Deflection w.r.t. to shifting beams along the  $z$  axis.

beginning of the chapter we minimize the value of  $\nu_{12}$ . Besides, one can notice that this parametrization is certainly similar to the one of the hexagon and we want to check if an auxetic setup is better than the hexagon, given the maximal deflection. But we first proceed with the Poisson's ratio optimization. In figure 5.11 we show the values of  $\nu_{12}$ . We can see that increasing the angle  $\gamma$  makes  $\nu_{12}$  smaller until we reach the minimum at  $\gamma = 0.9966$ . This point is then the solution to our optimization problem. We show the pattern for this design choice in figure 5.12. Moreover, we want to emphasize again that for  $\gamma = \frac{\pi}{2}$  we obtain  $\nu_{12} = 0$ , which coincides with the results given for the open grid structure and the hexagon. Moreover, we compare the best solution for the Poisson's ratio optimization with the one for minimizing the deflection. Therefore, we also deal with our objective functional  $\mathcal{U}_{3,max}$ . Here we obtain the deflection given in figure 5.13. Similar to the varying hexagon we need to have beams that are almost parallel to the  $e_1$  axis. We then receive that the best configuration is given for  $\gamma = 1.5063$ . We have plotted the shell with such a structure in figure 5.14. Finally, we want to conclude this chapter with closing the gap between the auxetic material and the hexagon. As we mentioned in the beginning of this subsection we can actually generate auxetic materials via the parametrization of the hexagon. Therefore, we need to change the constraints on

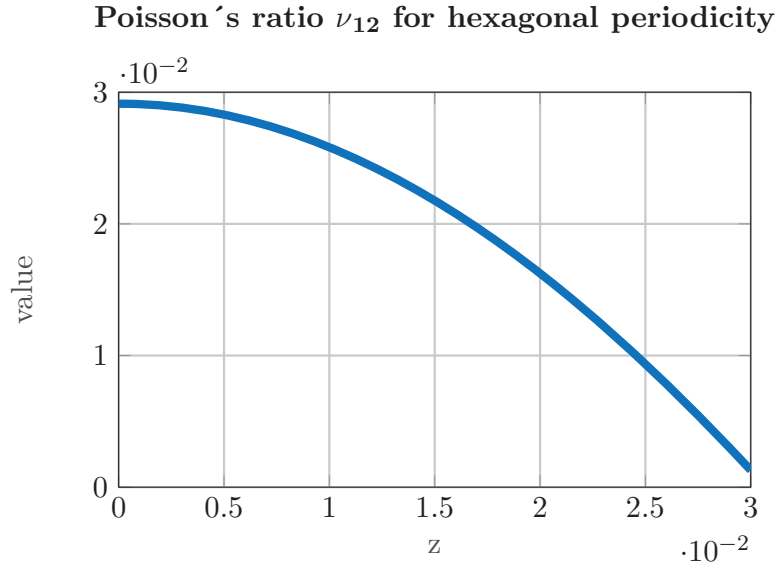


Figure 5.10: Poisson's ratio for vertical shifts.

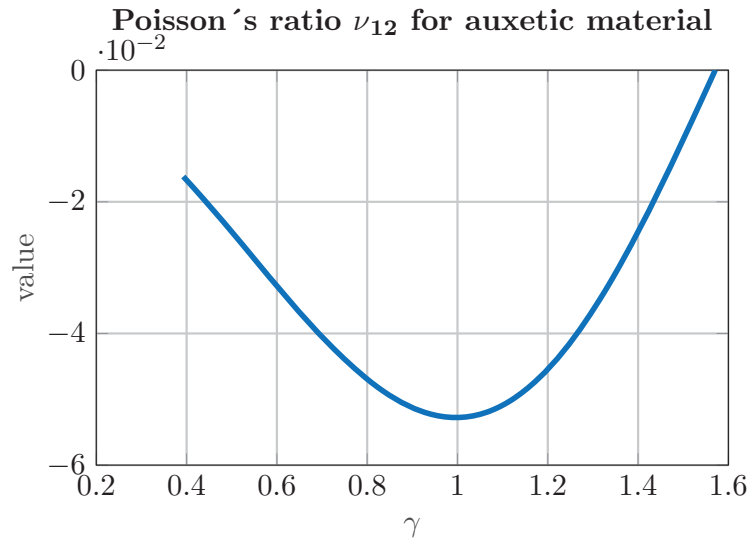
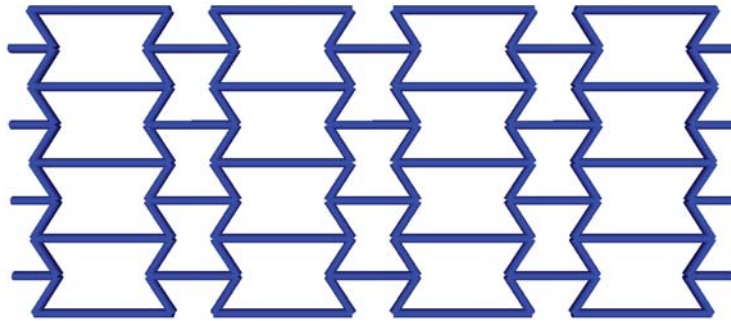
Figure 5.11:  $\nu_{12}$  w.r.t.  $\gamma$ 

Figure 5.12: Auxetic material with optimal Poisson's ratio.

$g_y$ , where we initially only allowed  $0.2 \leq g_y \leq 0.5$ . For the following example we assume that  $g_y \leq 0.8$ . Then we obtain the deflection as shown in figure 5.15. One can clearly see that the configurations with  $g_y$  near 0.5 yield smaller deflections. But an extreme

### The maximal deflection of a cylinder with hexagonal auxetic periodicity

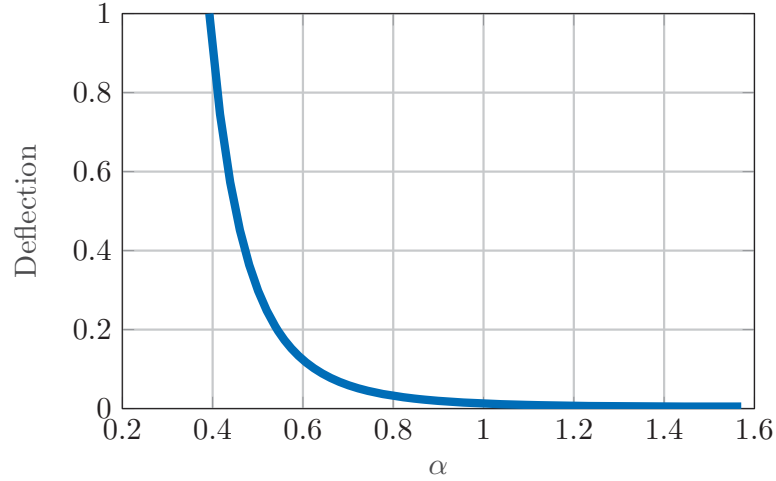


Figure 5.13: Normalized deflection for auxetic material.

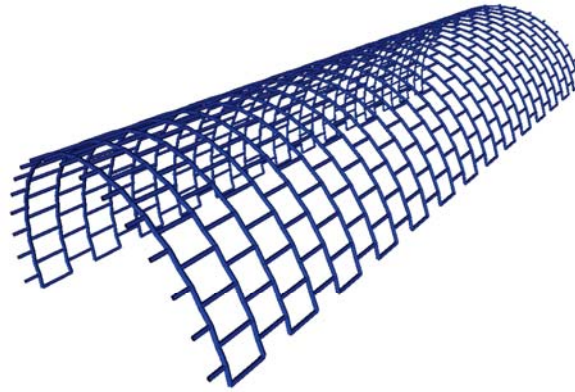


Figure 5.14: Optimal shell with auxetic structure.

auxetic design choice gives a better result than the corresponding worst combination for  $g$  as derived in section 5.2.2. Anyhow, we get with the optimization scheme that the minimal deflection is still obtained for  $(g_x, g_y) = (0.4, 0.4209)$ .

This finally closes the discussion on the optimization. With the given examples we have not only shown that the symbolic homogenization process gives analytic formulations for the effective properties, but also makes the optimization easier. Both objective functionals are easily implemented and we obtain the gradients by using the `diff` operator. With a projected gradient method we are able to get the optimal designs w.r.t. to the underlying parametrization. Since the computation times are reasonable we can solve industrial problems very efficiently.



**The maximal deflection of a cylinder with hexagonal/auxetic periodicity.**

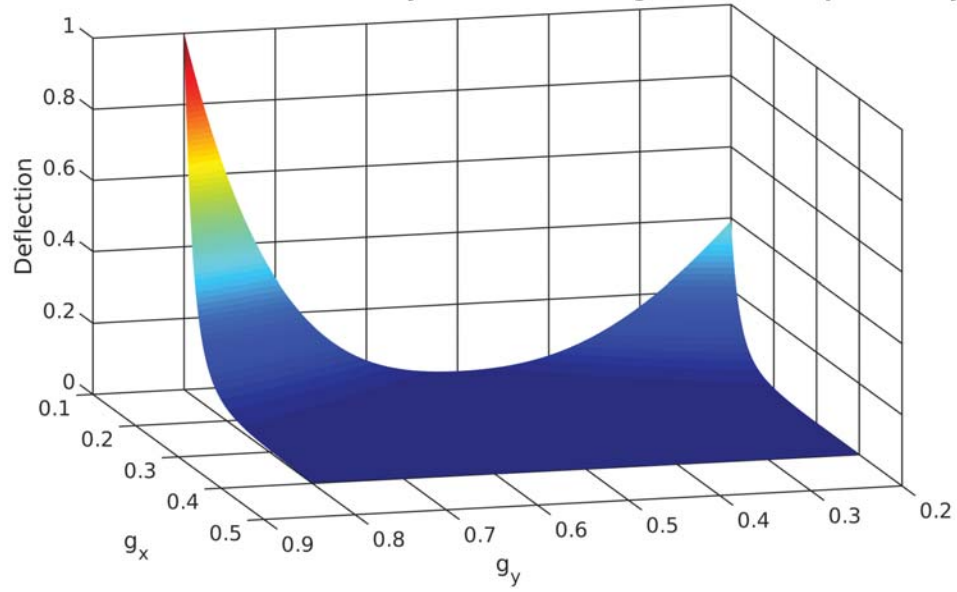


Figure 5.15: Deflection for hexagon to auxetic

## 6 Conclusion

In the presented work we have successfully managed to analyze the pinched cylinder problem, which arises in various different real life applications. We have started with developing the homogenization procedure for cylindrical shells in chapter 2. This development is new in the context of linear elastic shells, where we used classical decomposition techniques for the displacements. After applying the rescaled-unfolding operator  $\Pi_\varepsilon$ , we were able to pass to the limit and arrive with an equivalent homogeneous equation. Moreover, we could study the effects of the boundary conditions on our model. Since the curvature does not affect the calculation of the effective properties we could use an efficient plate homogenization algorithm for lattice structures, which uses a reduction to 1D beam finite elements. The effective bending properties were then obtained by four unit cell experiments.

Considering our weak formulation from chapter 2 we could formulate our problem in the strong formulation given as a system of three PDEs as presented in chapter 3. To simplify this PDE we used classical results to obtain an 8th order single PDE, which describes the bending effects due to a given load. We henceforth assumed our load to be a pinching load. By assuming the shell to be infinitely long we could employ a Fourier transform in the longitudinal direction. In the circumferential direction we introduced the Fourier series, which could then capture the clamping conditions. Using the residue theorem we finally derived an analytic function for the pinching problem.

Since we wanted to investigate the effects of design choices on our periodicity cell we established the homogenization as a symbolic procedure in chapter 4. We focused on solving linear equations of the type  $A[\mathbf{x}]v = b[\mathbf{x}]$ , where both  $A$  and  $b$  depend on symbolic parameters. It was crucial to introduce a certain pre-processing routine to decrease the complexity of the problem. Moreover, we were able to use the computer algebra programming language Singular for our problem and got a robust method for various different cases. After that we investigated a lot of different examples and compared the symbolic calculation to classical numerical methods.

In chapter 5 we inserted the so obtained analytic expressions for the effective properties into the solution of chapter 3. Due to the symbolic treatment it was easy to implement the projected gradient method for the minimization of maximal deflections caused by the point load. The optimal solutions for the presented examples were calculated and discussed.

All in all we not only performed the asymptotic analysis for the periodic perforated shells but also found qualitative answers to industrial problems.



# Appendices



## A Important Results

### Korn's inequality

*The first Korn inequality:*

**Theorem A.0.1** *Let  $\Omega \subset \mathbb{R}^m$  be bounded. Then every function  $u \in H_0^1(\Omega)$  satisfies the inequality*

$$\|\nabla u\|_{L^2(\Omega)}^2 \leq 2\|e(u)\|_{L^2(\Omega)}^2.$$

*The second Korn inequality:*

**Theorem A.0.2** *Let  $\Omega \subset \mathbb{R}^m$  be bounded and a Lipschitz domain. Then every function  $u \in H^1(\Omega)$  satisfies the inequality*

$$\|u\|_{H^1(\Omega)} \leq C \left( \|u\|_{L^2(\Omega)} + \|e(u)\|_{L^2(\Omega)} \right).$$

*Proof.* The proofs for these classical results are summarized in [48, chapter 2].  $\square$

### Young's inequality

**Theorem A.0.3** *Given  $a, b \in \mathbb{R}_+$  and  $p, q \geq 1$ , such that  $1/p + 1/q = 1$  the following inequality holds:*

$$ab \leq \frac{1}{p}a^p + \frac{1}{q}b^q.$$

*Proof.* A proof for this inequality can be found in [3, Lemma 1.18].  $\square$

### Jensen inequality

This inequality was initially derived for integrals w.r.t. to probability measures.

**Theorem A.0.4** *Let  $(S, \mathcal{B}, \mu)$ , with  $S \subset \mathbb{R}^m$ , be a probability space and  $\varphi : \mathbb{R}^m \mapsto \mathbb{R}$  convex function. Let  $f \in L^1(\mu; \mathbb{R}^m)$  then*

$$\varphi \left( \int_S f d\mu \right) \leq \int_S \varphi \circ f d\mu.$$

*Proof.* This theorem was proved in [3, p. 139].  $\square$

**Corollary A.0.1** *If we take  $f : [a, b] \mapsto \mathbb{R}$  Lebesgue-integrable we obtain*

$$\varphi \left( \frac{1}{b-a} \int_a^b f(x) dx \right) \leq \frac{1}{b-a} \int_a^b (\varphi \circ f)(x) dx.$$

*Proof.* Due to the normalization  $\frac{1}{b-a}$  we can use the previous classical version.  $\square$

### Poincaré inequality

**Theorem A.0.5** *Let  $\Omega \subset \mathbb{R}^m$  be a bounded Lipschitz domain. Then all  $u \in H^1(\Omega)$  satisfy*

$$\|u - u_\Omega\|_{L^2(\Omega)} \leq C \|\nabla u\|_{L^2(\Omega)},$$

where  $u_\Omega = \frac{1}{|\Omega|} \int_\Omega u(x) dx$ .

If we consider  $u \in H_0^1(\Omega)$  we get

$$\|u\|_{L^2(\Omega)} \leq \|\nabla u\|_{L^2(\Omega)}.$$

In the latter case  $\Omega$  does not have to be Lipschitz.

*Proof.* For a proof we refer to [17, section 4.2]. □

### Lax-Milgram

**Theorem A.0.6** *Let  $X$  be a Hilbert space and consider a continuous bilinear form  $a : X \times X \mapsto \mathbb{R}$  and take a linear functional  $l \in X'$ , where  $X'$  denotes the dual space. If there are constants  $c, C$  such that  $a$  fulfills*

1.  $a(x, y) \leq C \|x\|_X \|y\|_X$ , for all  $x, y \in X$  (boundedness),
2.  $a(x, x) \geq c \|x\|_X^2$ , for all  $x \in X$  (coercivity),

then there exists a unique  $x^* \in X$  such that

$$a(x^*, y) = l(y), \quad \text{for all } y \in X.$$

*Proof.* We refer to [17, Theorem 4.6] for a proof. □

### Sobolev embedding

**Theorem A.0.7** *Let  $m, n \geq 0$  and  $p, q \geq 1$  and  $\Omega \subset \mathbb{R}^n$  be a bounded Lipschitz domain.*

If  $m - \frac{n}{p} \geq j - \frac{n}{q}$ , then the embedding  $W^{m,p}(\Omega) \hookrightarrow W^{j,q}(\Omega)$  is continuous.

If  $m - \frac{n}{p} > j - \frac{n}{q}$ , then the embedding  $W^{m,p}(\Omega) \hookrightarrow W^{j,q}(\Omega)$  is compact.

If  $m - \frac{n}{p} > j$ , then the embedding  $W^{m,p} \hookrightarrow C^j(\overline{\Omega})$  is compact.

*Proof.* This well-known theorem is proved in [3, section 8.9] □

### Transformation theorem for integrals

**Theorem A.0.8** *Let  $O, U \subset \mathbb{R}^m$  be open and consider a diffeomorphism  $\Phi : O \mapsto U$ . Then for every  $f : U \mapsto \mathbb{R}$  continuous and with compact support holds*

$$\int_U f(y) dy = \int_O f(\Phi(x)) |\det D\Phi(x)| dx.$$

## B Homogenization of Shell

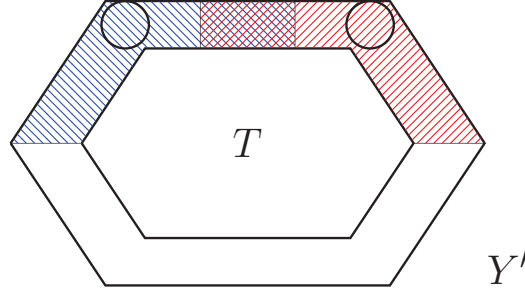


Figure B.1: Cell  $Y'$  and the perforated domain  $Y'^*$

### B.1 Proof of Proposition 2.1.1

There exists  $\kappa_0 > 0$  such that

$$\mathcal{O}'_{\kappa_0} = \{s \in \mathbb{R}^2 \setminus \overline{T} \mid \text{dist}(s, T) < \kappa_0\} \subset Y'^*.$$

Since the boundary of  $T$  is Lipschitz, there exist  $R', R'_1 > 0$  and  $N \geq 2$  open sets  $\mathcal{O}'_1, \dots, \mathcal{O}'_N$  such that

- $\mathcal{O}'_i$  is included in a ball of radius  $R'$  and is star-shaped with respect to a ball of radius  $R'_1$ ,  $i \in \{1, \dots, N\}$ ,
- $\mathcal{O}'_i \cap \mathcal{O}'_{i+1} \neq \emptyset$ ,  $i \in \{1, \dots, N-1\}$ , and  $\mathcal{O}'_N \cap \mathcal{O}'_1 \neq \emptyset$ ,
- $\mathcal{O}'_{\kappa_0} \subset \bigcup_{i=1}^N \mathcal{O}'_i \subset Y'^*$ .

Set  $\mathcal{O}_{\kappa_0} = \mathcal{O}'_{\kappa_0} \times (-\kappa, \kappa)$ ,  $\mathcal{O}_i = \mathcal{O}'_i \times (-\kappa, \kappa)$ ,  $i \in \{1, \dots, N\}$ . One has

- **P<sub>1</sub>**:  $\mathcal{O}_i$  is included in a ball of radius  $R = R' + \kappa$  and is star-shaped with respect to a ball of radius  $R_1 = \inf\{R'_1, \kappa\}$ ,  $i \in \{1, \dots, N\}$ ,
- **P<sub>2</sub>**:  $\mathcal{O}_i \cap \mathcal{O}_{i+1} \neq \emptyset$ ,  $i \in \{1, \dots, N-1\}$ , and  $\mathcal{O}_N \cap \mathcal{O}_1 \neq \emptyset$ ,
- **P<sub>3</sub>**:  $\mathcal{O}_{\kappa_0} \subset \bigcup_{i=1}^N \mathcal{O}_i \subset Y^*$ .

Set  $\mathcal{O}_{\kappa_0}^\diamond = \mathcal{O}_{\kappa_0} \cup (\overline{T} \times (-\kappa, \kappa))$ . Below, we will use the classical extension result

**Lemma B.1.1** *There exists an extension operator  $\mathcal{P}$  from  $H^1(\mathcal{O}_{\kappa_0})$  into  $H^1(\mathcal{O}_{\kappa_0}^\diamond)$  satisfying for all  $\phi \in H^1(\mathcal{O}_{\kappa_0})$*

$$\mathcal{P}(\phi)|_{\mathcal{O}_{\kappa_0}} = \phi, \quad \|\nabla(\mathcal{P}(\phi))\|_{L^2(\mathcal{O}_{\kappa_0}^\diamond)} \leq C \|\nabla \phi\|_{L^2(\mathcal{O}_{\kappa_0})}$$

*The constant only depends on  $\partial T^1$ .*

---

<sup>1</sup>Note that if we transform the domain  $\mathcal{O}_{\kappa_0}$  by a dilation, the constant does not change.



*Proof of Proposition 2.1.1.* For every  $\xi \in \Xi_\varepsilon$  and  $\mathcal{O}_i$ ,  $i \in \{1, \dots, N\}$ , if  $\varepsilon$  is small enough, the domain  $\Phi(\varepsilon\xi + \varepsilon\mathcal{O}_i)$  is included in a ball of radius  $2R\varepsilon$  and is star-shaped with respect to a ball of radius  $R_1\varepsilon/4$  (due to property **P**<sub>1</sub> and Lemma A2 in [27]).

Now, let  $u$  be a displacement belonging to  $H^1(\mathcal{Q}_\varepsilon)^3$ . For every  $(\xi, i) \in \Xi_\varepsilon \times \{1, \dots, N\}$  there exists a rigid displacement  $r_{\xi,i}$  such that

$$\|\nabla_x(u - r_{\xi,i})\|_{L^2(\Phi(\varepsilon\xi + \varepsilon\mathcal{O}_i))} \leq C\|e(u)\|_{L^2(\Phi(\varepsilon\xi + \varepsilon\mathcal{O}_i))}. \quad (\text{B.1.1})$$

The constant does not depend on  $\varepsilon$ ,  $\xi$  and  $\mathcal{O}_i$ , it only depends on the ratio  $R/R_1$  (see Theorem 2.3 in [27]). Then, step by step we compare the rigid displacements  $r_{\xi,1}$ ,  $r_{\xi,2}$ ,  $\dots$ ,  $r_{\xi,N}$  thanks to the properties **P**<sub>2</sub> and **P**<sub>3</sub>. To do that, observe that there exist two constants independent of  $\varepsilon$  and  $\xi$  such that

$$\begin{aligned} c\varepsilon^3|\mathcal{O}_i \cap \mathcal{O}_{i+1}| &\leq |\Phi(\varepsilon\xi + \varepsilon\mathcal{O}_i \cap \mathcal{O}_{i+1})| \leq C\varepsilon^3|\mathcal{O}_i \cap \mathcal{O}_{i+1}|, \quad i \in \{1, \dots, N-1\}, \\ c\varepsilon^3|\mathcal{O}_N \cap \mathcal{O}_1| &\leq |\Phi(\varepsilon\xi + \varepsilon\mathcal{O}_N \cap \mathcal{O}_1)| \leq C\varepsilon^3|\mathcal{O}_N \cap \mathcal{O}_1|. \end{aligned}$$

As a consequence, there exists a rigid displacement  $r_\xi$  such that

$$\|\nabla_x(u - r_\xi)\|_{L^2(\Phi(\varepsilon\xi + \varepsilon Y^*))} \leq C\|e(u)\|_{L^2(\Phi(\varepsilon\xi + \varepsilon Y^*))}. \quad (\text{B.1.2})$$

The constant does not depend on  $\varepsilon$  and  $\xi$ .

At this point, transform the domain  $\Phi(\varepsilon\xi + \varepsilon Y^*)$  by the inverse map  $z \in Y^* \mapsto \Phi(\varepsilon\xi + \varepsilon z)$ , then apply Lemma B.1.1 in order to extend the function in the hole  $T$  and finally transform by the map  $z \in Y \mapsto \Phi(\varepsilon\xi + \varepsilon z)$  and to the result add the displacement  $r_\xi$ . The  $L^2$  norm of the strain tensor of the extended displacement (now defined in  $\Phi(\varepsilon\xi + \varepsilon Y)$ ) is bounded by a constant (independent of  $\varepsilon$  and  $\xi$ ) multiply by  $\|e(u)\|_{L^2(\Phi(\varepsilon\xi + \varepsilon Y^*))}$ .

We apply this process to every domain of  $\varepsilon\xi + \varepsilon Y^*$ ,  $\xi \in \Xi_\varepsilon$ . Finally, we obtain an extension of the displacement  $u$  satisfying (2.1.6).  $\square$

## B.2 Two lemmas

For the definitions and properties of the unfolding operators  $\mathcal{T}_\varepsilon$ ,  $\mathcal{M}_\varepsilon$  we refer to [15, 16] Lemma B.2.1 is proved in [16]. Let  $\Omega$  be a bounded domain in  $\mathcal{R}^N$  with Lipschitz boundary and  $Y = \Pi_{i=1}^N(0, l_i)$ ,  $l_i > 0$ ,  $i = 1, \dots, N$ .

**Lemma B.2.1** *Suppose  $p \in (1, +\infty)$ . Let  $\{(u_{\varepsilon,\delta}, v_{\varepsilon,\delta})\}_{\varepsilon,\delta}$  be a sequence in  $W^{1,p}(\Omega)^N \times W^{1,p}(\Omega)^{N \times N}$  (with  $v_{\varepsilon,\delta}$  a symmetric matrix) converging weakly to  $(u, v)$  in  $W^{1,p}(\Omega)^N \times W^{1,p}(\Omega)^{N \times N}$ .*

*Assume furthermore that there exist  $\mathcal{X}$  in  $L^p(\Omega)^{N \times N}$  and  $\hat{v}$  in  $L^p(\Omega; W_{per,0}^{1,p}(Y))^{N \times N}$  such that as  $(\varepsilon, \delta) \rightarrow (0, 0)$*

$$\begin{aligned} \frac{1}{\delta}(e(u_{\varepsilon,\delta}) + v_{\varepsilon,\delta}) &\rightharpoonup \mathcal{X} \quad \text{weakly in } L^p(\Omega)^{N \times N}, \\ \mathcal{T}_{\varepsilon,\delta}(\nabla v_{\varepsilon,\delta}) &\rightharpoonup \nabla v + \nabla_y \hat{v} \quad \text{weakly in } L^p(\Omega \times Y)^{N \times N \times N}. \end{aligned} \quad (\text{B.2.1})$$

*Then  $u$  belongs to  $W^{2,p}(\Omega)^N$  and there exists  $u \in L^p(\Omega; W_{per,0}^{1,p}(Y))^N$  such that, up to a subsequence,*

$$\begin{aligned} \text{if } \frac{\varepsilon}{\delta} \rightarrow \theta \in [0, +\infty), \quad & \frac{1}{\delta}\mathcal{T}_{\varepsilon,\delta}(e(u_{\varepsilon,\delta}) + v_{\varepsilon,\delta}) \rightharpoonup \mathcal{X} + e_y(u) + \theta \hat{v} \quad \text{weakly in } L^p(\Omega \times Y)^{N \times N}, \\ \text{if } \frac{\varepsilon}{\delta} \rightarrow +\infty, \quad & \hat{v} = e_y(u). \end{aligned} \quad (\text{B.2.2})$$

*Proof.* First, from (B.2.1) one obtains that  $e(\mathbf{u}) + \mathbf{v} = 0$ , then since  $\Omega$  is a bounded domain with Lipschitz boundary  $\mathbf{u}$  belongs to  $W^{2,p}(\Omega)^N$ . We also deduce from this convergence and the Korn inequality that  $\mathbf{u}_{\varepsilon,\delta}$  strongly converges to  $\mathbf{u}$  in  $W^{1,p}(\Omega)^N$ . Then, up to a subsequence, there exists  $\hat{\mathcal{X}} \in L^p(\Omega \times Y)^N$  such that

$$\frac{1}{\delta} \mathcal{T}_{\varepsilon,\delta}(e(\mathbf{u}_{\varepsilon,\delta}) + \mathbf{v}_{\varepsilon,\delta}) \rightharpoonup \hat{\mathcal{X}} \quad \text{weakly in } L^p(\Omega \times Y)^{N \times N}.$$

*Step 1.* In this first step we assume that  $\frac{\varepsilon}{\delta} \rightarrow \theta \in [0, +\infty)$ .

Introduce the function  $\mathbf{Z}_{\varepsilon,\delta}$  belonging to  $L^p(\Omega; W^{1,p}(Y))^N$ , defined as

$$\mathbf{Z}_{\varepsilon,\delta} = \frac{1}{\varepsilon} \mathcal{T}_{\varepsilon}(\mathbf{u}_{\varepsilon,\delta} - \mathcal{M}_{\varepsilon}(\mathbf{u}_{\varepsilon,\delta})) - \mathcal{M}_{\varepsilon}(\nabla \mathbf{u}_{\varepsilon,\delta}) \cdot y^c. \quad (\text{B.2.3})$$

Its gradient and symmetric gradient with respect to  $y$  are

$$\begin{aligned} \nabla_y \mathbf{Z}_{\varepsilon,\delta} &= \mathcal{T}_{\varepsilon}(\nabla \mathbf{u}_{\varepsilon,\delta}) - \mathcal{M}_{\varepsilon}(\nabla \mathbf{u}_{\varepsilon,\delta}) \\ e_y(\mathbf{Z}_{\varepsilon,\delta}) &= \mathcal{T}_{\varepsilon}(e(\mathbf{u}_{\varepsilon,\delta})) - \mathcal{M}_{\varepsilon}(e(\mathbf{u}_{\varepsilon,\delta})) \\ &= \mathcal{T}_{\varepsilon}(e(\mathbf{u}_{\varepsilon,\delta}) + \mathbf{v}_{\varepsilon,\delta}) - (\mathcal{T}_{\varepsilon}(\mathbf{v}_{\varepsilon,\delta}) - \mathcal{M}_{\varepsilon}(\mathbf{v}_{\varepsilon,\delta})) - \mathcal{M}_{\varepsilon}(e(\mathbf{u}_{\varepsilon,\delta}) + \mathbf{v}_{\varepsilon,\delta}). \end{aligned} \quad (\text{B.2.4})$$

Convergence (B.2.1)<sub>1</sub> on one side together with the fact that  $\|\nabla \mathbf{v}_{\varepsilon,\delta}\|_{L^p(\Omega)}$  and  $\frac{\varepsilon}{\delta}$  are bounded, give

$$\|e_y(\mathbf{Z}_{\varepsilon,\delta})\|_{L^p(\Omega \times Y)^N} \leq C(\delta + \varepsilon) \leq C\delta.$$

The Korn inequality implies

$$\|\mathbf{Z}_{\varepsilon,\delta}\|_{L^p(\Omega; W^{1,p}(Y))} \leq C\delta.$$

Consequently, up to a subsequence, there exists  $\hat{\mathbf{Z}}$  in  $L^p(\Omega; W^{1,p}(Y))^N$  such that,

$$\frac{1}{\delta} \mathbf{Z}_{\varepsilon,\delta} \rightharpoonup \hat{\mathbf{Z}} \quad \text{weakly in } L^p(\Omega; W^{1,p}(Y))^N. \quad (\text{B.2.5})$$

By (B.2.4) one has

$$\frac{1}{\delta} \mathcal{T}_{\varepsilon}(e(\mathbf{u}_{\varepsilon,\delta}) + \mathbf{v}_{\varepsilon,\delta}) = \frac{1}{\delta} e_y(\mathbf{Z}_{\varepsilon,\delta}) + \frac{\varepsilon}{\delta} \frac{\mathcal{T}_{\varepsilon}(\mathbf{v}_{\varepsilon,\delta}) - \mathcal{M}_{\varepsilon}(\mathbf{v}_{\varepsilon,\delta})}{\varepsilon} + \frac{1}{\delta} \mathcal{M}_{\varepsilon}(e(\mathbf{u}_{\varepsilon,\delta}) + \mathbf{v}_{\varepsilon,\delta}).$$

Then going to the limit using (B.2.5) and [16, Proposition 1.25 and Theorem 1.41]

$$\frac{1}{\delta} \mathcal{T}_{\varepsilon}(\nabla \mathbf{u}_{\varepsilon,\delta} + \mathbf{v}_{\varepsilon,\delta}) \rightharpoonup \hat{\mathcal{X}} = e_y(\hat{\mathbf{Z}}) + \theta(\nabla \mathbf{v} y^c + \hat{\mathbf{v}}) + \mathcal{X} \quad \text{weakly in } L^p(\Omega \times Y)^{N \times N}. \quad (\text{B.2.6})$$

Now, we prove that

$$\mathbf{u} = \hat{\mathbf{Z}} - \frac{\theta}{2} \sum_{j,k=1}^N \frac{\partial^2 \mathbf{u}}{\partial x_j \partial x_k} (y_j^c y_k^c - \mathcal{M}_Y(y_j^c y_k^c))$$

is periodic (note that this function belongs to  $L^p(\Omega; W^{1,p}(Y))^N$ ).

We proceed as in the proof of [16, Theorem 1.36], one first evaluates the difference of the traces of  $\mathbf{Z}_{\varepsilon,\delta}$  on the faces  $Y_1 = \{0\} \times (0, 1)^{N-1}$  and  $Y_1 + \mathbf{e}_1$ . For a.e.  $(x, y') \in \Omega \times Y_1$ , one has

$$\begin{aligned} &\mathbf{Z}_{\varepsilon,\delta}(x, y' + \mathbf{e}_1) - \mathbf{Z}_{\varepsilon,\delta}(x, y') \\ &= \frac{1}{\varepsilon} (\mathcal{T}_{\varepsilon}(\mathbf{u}_{\varepsilon,\delta})(x, y' + \mathbf{e}_1) - \mathcal{T}_{\varepsilon}(\mathbf{u}_{\varepsilon,\delta})(x, y')) - \mathcal{M}_{\varepsilon}\left(\frac{\partial \mathbf{u}_{\varepsilon,\delta}}{\partial x_1}\right)(x) \\ &= \frac{1}{\varepsilon} (\mathcal{T}_{\varepsilon}(\mathbf{u}_{\varepsilon,\delta})(x + \varepsilon \mathbf{e}_1, y') - \mathcal{T}_{\varepsilon}(\mathbf{u}_{\varepsilon,\delta})(x, y')) - \mathcal{M}_{\varepsilon}\left(\frac{\partial \mathbf{u}_{\varepsilon,\delta}}{\partial x_1}\right)(x). \end{aligned}$$

Let  $\Phi$  be in  $\mathcal{D}(\Omega \times Y_1)^N$ , one has successively

$$\begin{aligned}
& \int_{\Omega \times Y_1} (\mathbf{Z}_{\varepsilon, \delta}(x, y' + \mathbf{e}_i) - \mathbf{Z}_{\varepsilon, \delta}(x, y')) \cdot \Phi(x, y') dx dy' \\
&= \int_{\Omega \times Y_1} \left[ \frac{1}{\varepsilon} \left( \mathcal{T}_{\varepsilon}(\mathbf{u}_{\varepsilon, \delta})(x + \varepsilon \mathbf{e}_1, y') - \mathcal{T}_{\varepsilon}(\mathbf{u}_{\varepsilon, \delta})(x, y') \right) - \mathcal{M}_{\varepsilon} \left( \frac{\partial \mathbf{u}_{\varepsilon, \delta}}{\partial x_1} \right)(x) \right] \cdot \Phi(x, y') dx dy' \\
&= \int_{\Omega \times Y_1} \mathcal{T}_{\varepsilon}(\mathbf{u}_{\varepsilon, \delta})(x, y') \cdot \frac{\Phi(x - \varepsilon \mathbf{e}_1, y') - \Phi(x, y')}{\varepsilon} dx dy' \\
&\quad - \int_{\Omega \times Y_1} \mathcal{M}_{\varepsilon} \left( \frac{\partial \mathbf{u}_{\varepsilon, \delta}}{\partial x_1} \right)(x) \cdot \Phi(x, y') dx dy' \\
&= \int_{\Omega \times Y_1} (\mathbf{u}_{\varepsilon, \delta}(x) - \mathcal{T}_{\varepsilon}(\mathbf{u}_{\varepsilon, \delta})(x, y')) \cdot \frac{\partial \Phi}{\partial x_1}(x, y') dx dy' \\
&\quad + \int_{\Omega \times Y_1} \left( \frac{\partial \mathbf{u}_{\varepsilon, \delta}}{\partial x_1} - \mathcal{M}_{\varepsilon} \left( \frac{\partial \mathbf{u}_{\varepsilon, \delta}}{\partial x_1} \right) \right) \cdot \Phi(x, y') dx dy' \\
&\quad + \int_{\Omega \times Y_1} \mathcal{T}_{\varepsilon}(\mathbf{u}_{\varepsilon, \delta})(x, y') \cdot \frac{\Phi(x - \varepsilon \mathbf{e}_1, y') - \Phi(x, y') + \varepsilon \mathbf{e}_1 \cdot \nabla_x \Phi(x, y')}{\varepsilon} dx dy'
\end{aligned}$$

then

$$\begin{aligned}
&= \int_{\Omega \times Y_1} (\mathcal{M}_{\varepsilon}(\mathbf{u}_{\varepsilon, \delta})(x) - \mathcal{T}_{\varepsilon}(\mathbf{u}_{\varepsilon, \delta})(x, y')) \cdot \frac{\partial \Phi}{\partial x_1}(x, y') dx dy' \\
&\quad + \int_{\Omega \times Y_1} (\mathbf{u}_{\varepsilon, \delta}(x) - \mathcal{M}_{\varepsilon}(\mathbf{u}_{\varepsilon, \delta})(x)) \cdot \frac{\partial \Phi}{\partial x_1}(x, y') dx dy' \\
&\quad + \int_{\Omega \times Y_1} \left( \frac{\partial \mathbf{u}_{\varepsilon, \delta}}{\partial x_1} - \mathcal{M}_{\varepsilon} \left( \frac{\partial \mathbf{u}_{\varepsilon, \delta}}{\partial x_1} \right) \right) \cdot \Phi(x, y') dx dy' \\
&\quad + \int_{\Omega \times Y_1} \mathcal{T}_{\varepsilon}(\mathbf{u}_{\varepsilon, \delta})(x, y') \cdot \frac{\Phi(x - \varepsilon \mathbf{e}_1, y') - \Phi(x, y') + \varepsilon \mathbf{e}_1 \cdot \nabla_x \Phi(x, y')}{\varepsilon} dx dy'.
\end{aligned}$$

The last right-hand side is equal to (see [16, Proposition 1.24])

$$\begin{aligned}
& \int_{\Omega \times Y_1} (\mathcal{M}_{\varepsilon}(\mathbf{u}_{\varepsilon, \delta})(x) - \mathcal{T}_{\varepsilon}(\mathbf{u}_{\varepsilon, \delta})(x, y')) \cdot \frac{\partial \Phi}{\partial x_1}(x, y') dx dy' \\
&+ \int_{\Omega} \mathbf{u}_{\varepsilon, \delta}(x) \cdot \left( \int_Y \frac{\partial \Phi}{\partial x_1}(x, y') dy' - \mathcal{M}_{\varepsilon} \left( \int_Y \frac{\partial \Phi}{\partial x_1}(x, y') dy' \right) \right) dx \\
&+ \int_{\Omega} \frac{\partial \mathbf{u}_{\varepsilon, \delta}}{\partial x_1}(x) \cdot \left( \int_Y \Phi(x, y') dy' - \mathcal{M}_{\varepsilon} \left( \int_Y \Phi(x, y') dy' \right) \right) dx \\
&+ \int_{\Omega \times Y_1} \mathcal{T}_{\varepsilon}(\mathbf{u}_{\varepsilon, \delta})(x, y') \cdot \frac{\Phi(x - \varepsilon \mathbf{e}_1, y') - \Phi(x, y') + \varepsilon \mathbf{e}_1 \cdot \nabla_x \Phi(x, y')}{\varepsilon} dx dy'.
\end{aligned}$$

Divide by  $\delta$  and then pass to the limit using [16, Propositions 1.38 and 1.39]. It yields

$$\begin{aligned}
& \int_{\Omega \times Y_1} \frac{\mathbf{Z}_{\varepsilon, \delta}(x, y' + \mathbf{e}_i) - \mathbf{Z}_{\varepsilon, \delta}(x, y')}{\delta} \cdot \Phi(x, y) dx dy' \\
&\longrightarrow \int_{\Omega \times Y_1} -\theta(\nabla \mathbf{u}(x) y^c) \cdot \frac{\partial \Phi}{\partial x_1}(x, y') dx dy' + \frac{\theta}{2} \int_{\Omega \times Y_1} \mathbf{u}(x) \cdot \frac{\partial^2 \Phi}{\partial x_1^2}(x, y') dx dy' \\
&= \int_{\Omega \times Y_1} \theta \sum_{k=2}^N \frac{\partial^2 \mathbf{u}}{\partial x_1 \partial x_k}(x) y_k^c \cdot \Phi(x, y') dx dy'.
\end{aligned}$$

Hence, for a.e.  $(x, y') \in \Omega \times Y_1$ ,  $\hat{\mathbf{Z}}(x, y' + \mathbf{e}_i) - \hat{\mathbf{Z}}(x, y') = \theta \sum_{k=2}^N \frac{\partial^2 \mathbf{u}}{\partial x_1 \partial x_k}(x) y_k'^c$ . We obtain similar equalities for the difference of the traces of  $\hat{\mathbf{Z}}$  over the other faces of  $Y$ . That proves the claim. Then, a straightforward calculation gives (using  $\nabla e(\mathbf{u}) + \nabla \mathbf{v} = 0$ )

$$e_y(\mathbf{u}) = e_y(\hat{\mathbf{Z}}) - \theta \sum_{k=1}^N \frac{\partial e(\mathbf{u})}{\partial x_k} y_k^c = e_y(\hat{\mathbf{Z}}) + \theta \sum_{k=1}^N \frac{\partial \mathbf{v}}{\partial x_k} y_k^c.$$

With (B.2.6), that gives the convergence (B.2.2)<sub>1</sub>.

*Step 2.* In this step we assume that  $\frac{\varepsilon}{\delta} \rightarrow +\infty$ .

Again we consider the function  $\mathbf{Z}_{\varepsilon, \delta}$  introduced in (B.2.3). Now, it satisfies

$$\|\mathbf{Z}_{\varepsilon, \delta}\|_{L^p(\Omega; W^{1,p}(Y))} \leq C\varepsilon.$$

Hence, up to a subsequence, there exists  $\hat{\mathbf{Z}}$  in  $L^p(\Omega; W^{1,p}(Y))^N$  such that,

$$\frac{1}{\varepsilon} \mathbf{Z}_{\varepsilon, \delta} \rightharpoonup \hat{\mathbf{Z}} \quad \text{weakly in } L^p(\Omega; W^{1,p}(Y))^N. \quad (\text{B.2.7})$$

Observe that

$$\begin{aligned} \frac{1}{\varepsilon} \mathcal{T}_\varepsilon(e(\mathbf{u}_{\varepsilon, \delta}) + \mathbf{v}_{\varepsilon, \delta}) &= \frac{\delta}{\varepsilon} \frac{1}{\delta} \mathcal{T}_\varepsilon(e(\mathbf{u}_{\varepsilon, \delta}) + \mathbf{v}_{\varepsilon, \delta}) \longrightarrow 0 \quad \text{strongly in } L^p(\Omega \times Y)^{N \times N}, \\ \frac{1}{\varepsilon} \mathcal{M}_\varepsilon(e(\mathbf{u}_{\varepsilon, \delta}) + \mathbf{v}_{\varepsilon, \delta}) &= \frac{\delta}{\varepsilon} \frac{1}{\delta} \mathcal{M}_\varepsilon(e(\mathbf{u}_{\varepsilon, \delta}) + \mathbf{v}_{\varepsilon, \delta}) \longrightarrow 0 \quad \text{strongly in } L^p(\Omega)^{N \times N}. \end{aligned}$$

One has

$$\frac{1}{\varepsilon} \mathcal{T}_\varepsilon(e(\mathbf{u}_{\varepsilon, \delta}) + \mathbf{v}_{\varepsilon, \delta}) = \frac{1}{\varepsilon} e_y(\mathbf{Z}_{\varepsilon, \delta}) + \frac{\mathcal{T}_\varepsilon(\mathbf{v}_{\varepsilon, \delta}) - \mathcal{M}_\varepsilon(\mathbf{v}_{\varepsilon, \delta})}{\varepsilon} + \frac{1}{\varepsilon} \mathcal{M}_\varepsilon(e(\mathbf{u}_{\varepsilon, \delta}) + \mathbf{v}_{\varepsilon, \delta}).$$

Passing to the limit in the above equality gives

$$e_y(\hat{\mathbf{Z}}) + \nabla \mathbf{v} y^c + \hat{\mathbf{v}} = 0.$$

Then, as in the previous step we prove that

$$\mathbf{v} = \hat{\mathbf{Z}} - \frac{1}{2} \sum_{j,k=1}^N \frac{\partial^2 \mathbf{u}}{\partial x_j \partial x_k} (y_j^c y_k^c - \mathcal{M}_Y(y_j^c y_k^c))$$

is periodic. Thus (B.2.2)<sub>2</sub> is proved with  $\mathbf{u} = -\mathbf{v}$ . □

As a consequence of Lemma B.2.1 one has (see also [16, Lemma 11.11])

**Lemma B.2.2** *Suppose  $p \in (1, +\infty)$ . Let  $\{(u_{\varepsilon, \delta}, v_{\varepsilon, \delta})\}_{\varepsilon, \delta}$  be a sequence in  $W^{1,p}(\Omega) \times W^{1,p}(\Omega)^N$  converging weakly to  $(u, v)$  in  $W^{1,p}(\Omega) \times W^{1,p}(\Omega)^N$ . Assume furthermore that there exist  $\mathcal{X}$  in  $L^p(\Omega)^N$  and  $\hat{v}$  in  $L^p(\Omega; W_{per,0}^{1,p}(Y))^N$  such that as  $(\varepsilon, \delta) \rightarrow (0, 0)$*

$$\begin{aligned} \frac{1}{\delta} (\nabla u_{\varepsilon, \delta} + v_{\varepsilon, \delta}) &\rightharpoonup \mathcal{X} \quad \text{weakly in } L^p(\Omega)^N, \\ \mathcal{T}_{\varepsilon, \delta}(\nabla v_{\varepsilon, \delta}) &\rightharpoonup \nabla v + \nabla_y \hat{v} \quad \text{weakly in } L^p(\Omega \times Y)^{N \times N}. \end{aligned}$$

Then  $u$  belongs to  $W^{2,p}(\Omega)$  and there exists  $\mathbf{u} \in L^p(\Omega; W_{per,0}^{1,p}(Y))$  such that, up to a subsequence,

$$\begin{aligned} \text{if } \frac{\varepsilon}{\delta} &\rightarrow \theta \in [0, +\infty), & \frac{1}{\delta} \mathcal{T}_{\varepsilon, \delta}(\nabla u_{\varepsilon, \delta} + v_{\varepsilon, \delta}) &\rightharpoonup \mathcal{X} + \nabla_y \mathbf{u} + \theta \hat{v} \quad \text{weakly in } L^p(\Omega \times Y)^N, \\ \text{if } \frac{\varepsilon}{\delta} &\rightarrow +\infty, & \hat{v} &= \nabla_y \mathbf{u}. \end{aligned} \quad (\text{B.2.8})$$

*Proof.* Consider the fields  $\mathbf{u}_{\varepsilon,\delta} \in W^{1,p}(\Omega)^N$  and the symmetric matrix  $\mathbf{v}_{\varepsilon,\delta} \in W^{1,p}(\Omega)^{N \times N}$  defined by

$$\begin{aligned} \mathbf{u}_{\varepsilon,\delta} &= (u_{\varepsilon,\delta}, 0, \dots, 0), & (\mathbf{v}_{\varepsilon,\delta})_{11} &= v_{1,\varepsilon}, \\ (\mathbf{v}_{\varepsilon,\delta})_{1i} &= (\mathbf{v}_{\varepsilon,\delta})_{i1} = \frac{1}{2}v_{i,\varepsilon}, & (\mathbf{v}_{\varepsilon,\delta})_{ij} &= 0 \text{ if } (i,j) \in \{2, \dots, N\}^2. \end{aligned}$$

These fields satisfy the assumptions of Lemma B.2.1 and the convergences (B.2.1). Therefore, the results in (B.2.2) give (B.2.8).  $\square$

## C Analytic expressions of effective properties

### C.1 Varying Hexagon

Effective  $c_{2222} =$

$$(81 \cdot \pi^2 \cdot ((91 \cdot (4 \cdot y^2 - 4 \cdot y + 4 \cdot x^2 + 1)^{3/2})/2 - 1938146465057258287 \cdot y + 5963527584791566024 \cdot y \cdot x^2 - 3876292930114518212 \cdot y^2 + 7752585860229035332 \cdot y^3 + 2981763792395782400 \cdot x^2 + 969073232528629280)) / (3746994889972252672 \cdot (100 \cdot x + 3) \cdot (78 \cdot y + 13 \cdot (4 \cdot y^2 - 4 \cdot y + 4 \cdot x^2 + 1)^{3/2} + 240 \cdot y \cdot x^2 - 312 \cdot y^2 + 312 \cdot y^3))$$

### C.2 Varying cross section

For quadratic cross section we obtain for  $c_{2222} =$

$$(9966688830111384174375 \cdot 10^{1/2} \cdot \pi \cdot x^4 \cdot y^4) / (2251799813685248 \cdot (325 \cdot x^4 + 309 \cdot 10^{1/2} \cdot y^4) \cdot ((9 \cdot y)/5 + 27/25))$$

and for  $c_{1111} =$

$$(10751552136042485625 \cdot \pi \cdot y^4 \cdot (127 \cdot 10^{1/2} \cdot x^4 + 1200 \cdot y^4)) / (2251799813685248 \cdot (325 \cdot x^4 + 309 \cdot 10^{1/2} \cdot y^4) \cdot ((9 \cdot y)/5 + 27/25))$$

### C.3 Vertical shift of beams

The value for the shifted beams was simplified by `vpa`.  $c_{2222} =$

$$(1.0 \cdot (z + 0.06) \cdot ((2.0 \cdot (4.4066e31 \cdot z^2 \cdot (2.7511e27 \cdot z^2 + 1.2332e31) - 1.3935e32 \cdot z^2 \cdot (3.6387e32 \cdot z^2 + 1.7611e30))) / (1.0 \cdot (2.7511e27 \cdot z^2 + 1.2332e31)^2 - 10.0 \cdot (3.6387e32 \cdot z^2 + 1.7611e30)^2) + (8.8131e31 \cdot z^2 \cdot (5.5022e27 \cdot z^2 + 2.4663e31) - 2.787e32 \cdot z^2 \cdot (7.2774e32 \cdot z^2 + 3.5223e30)) / (1.0 \cdot (5.5022e27 \cdot z^2 + 2.4663e31)^2 - 10.0 \cdot (7.2774e32 \cdot z^2 + 3.5223e30)^2) - (2.0 \cdot (1.4013e33 \cdot z^2 \cdot (3.6387e34 \cdot z^2 + 1.7611e32) - 4.4314e32 \cdot z^2 \cdot (2.7511e29 \cdot z^2 + 1.2332e33))) / (10.0 \cdot (3.6387e34 \cdot z^2 + 1.7611e32)^2 - 1.0 \cdot (2.7511e29 \cdot z^2 + 1.2332e33)^2) - (2.8361e32 \cdot z^2) / (3.6821e34 \cdot z^2 + 5.7283e32) + (2.4268e - 9 \cdot (3.6196e39 \cdot z^2 + 8.4513e37)) / (2.3013e32 \cdot z^2 + 3.5802e30) + (2.8252e - 19 \cdot (3.1092e49 \cdot z^2 + 7.2596e47)) / (2.3013e32 \cdot z^2 + 3.5802e30) + (0.50894 \cdot (1.3808e33 \cdot z^2 + 3.2239e31)) / (9.2053e33 \cdot z^2 + 1.4321e32) - (4.0 \cdot ((9.0003e44 \cdot z^2 + 6.9894e42) \cdot (1.5001e41 \cdot z^2 + 6.724e44) - 3.1623 \cdot (9.0003e44 \cdot z^2 + 6.9894e42) \cdot (1.984e46 \cdot z^2 + 9.6028e43))) / (10.0 \cdot (1.984e46 \cdot z^2 + 9.6028e43)^2 - (1.5001e41 \cdot z^2 + 6.724e44)^2) + ((2.7511e27 \cdot z^2 + 1.2332e31) \cdot (-1.265e18 \cdot z^4 + 4.4066e31 \cdot z^2) - 3.1623 \cdot (3.6387e32 \cdot z^2 + 1.7611e30) \cdot (-1.265e18 \cdot z^4 + 4.4066e31 \cdot z^2)) / (1.0 \cdot (2.7511e27 \cdot z^2 + 1.2332e31)^2 - 10.0 \cdot (3.6387e32 \cdot z^2 + 1.7611e30)^2))) / (1.188 \cdot z + 0.07128)$$

## C.4 Auxetic material

We present the solution, simplified by `vpa(.,10)`,  $c_{1122} =$

$$\begin{aligned} & (1.0 \cdot (4.34989752 \cdot x^4 - (2.0 \cdot (4.335445455e38 \cdot x^5 - 1.021926429e39 \cdot x^4 + 2.393165891e39 \cdot x^3 - \\ & 4.220741956e39 \cdot x^2 + 2.473582211e39 \cdot x - 4.45244798e39)) / (3.042361441e37 \cdot (x^2 - 0.36)^2 + \\ & 1.2676506e38 \cdot (x^2 - 0.36)^3 - 1.25771222e39 \cdot x^2 - 1.213099031e39) - 4.071504079 \cdot x + 2.0 \cdot \\ & x^2 \cdot (0.434989752 \cdot (0.36 - 1.0 \cdot x^2)^{1/2} \cdot (9.0 - 25.0 \cdot x^2)^{1/2} - 0.7829815537) + (24.42902447 \cdot x \cdot \\ & (25.0 \cdot x^2 - 9.0)) / (125.0 \cdot x^3 + 225.0 \cdot x^2 + 150.0 \cdot x + 387.0) - (0.8699795041 \cdot x^2 \cdot (774.0 \cdot (0.36 - \\ & 1.0 \cdot x^2)^{1/2} \cdot (9.0 - 25.0 \cdot x^2)^{7/2} - 282123.0 \cdot (0.36 - 1.0 \cdot x^2)^{1/2} \cdot (9.0 - 25.0 \cdot x^2)^{1/2} - 196830.0 \cdot x + \\ & 3641355.0 \cdot x^2 + 2022975.0 \cdot x^3 - 13122000.0 \cdot x^4 - 7290000.0 \cdot x^5 + 16706250.0 \cdot x^6 + 9281250.0 \cdot \\ & x^7 + 4218750.0 \cdot x^8 + 2343750.0 \cdot x^9 - 17578125.0 \cdot x^{10} - 9765625.0 \cdot x^{11} + 2187000.0 \cdot x^2 \cdot (0.36 - \\ & 1.0 \cdot x^2)^{1/2} \cdot (9.0 - 25.0 \cdot x^2)^{1/2} + 820125.0 \cdot x^3 \cdot (0.36 - 1.0 \cdot x^2)^{1/2} \cdot (9.0 - 25.0 \cdot x^2)^{1/2} - 5163750.0 \cdot \\ & x^4 \cdot (0.36 - 1.0 \cdot x^2)^{1/2} \cdot (9.0 - 25.0 \cdot x^2)^{1/2} - 1771875.0 \cdot x^5 \cdot (0.36 - 1.0 \cdot x^2)^{1/2} \cdot (9.0 - 25.0 \cdot \\ & x^2)^{1/2} + 2250000.0 \cdot x^6 \cdot (0.36 - 1.0 \cdot x^2)^{1/2} \cdot (9.0 - 25.0 \cdot x^2)^{1/2} + 234375.0 \cdot x^7 \cdot (0.36 - 1.0 \cdot x^2)^{1/2} \cdot \\ & (9.0 - 25.0 \cdot x^2)^{1/2} + 450.0 \cdot x^2 \cdot (0.36 - 1.0 \cdot x^2)^{1/2} \cdot (9.0 - 25.0 \cdot x^2)^{7/2} + 3515625.0 \cdot x^8 \cdot (0.36 - \\ & 1.0 \cdot x^2)^{1/2} \cdot (9.0 - 25.0 \cdot x^2)^{1/2} + 250.0 \cdot x^3 \cdot (0.36 - 1.0 \cdot x^2)^{1/2} \cdot (9.0 - 25.0 \cdot x^2)^{7/2} + 1953125.0 \cdot \\ & x^9 \cdot (0.36 - 1.0 \cdot x^2)^{1/2} \cdot (9.0 - 25.0 \cdot x^2)^{1/2} - 109350.0 \cdot x \cdot (0.36 - 1.0 \cdot x^2)^{1/2} \cdot (9.0 - 25.0 \cdot x^2)^{1/2} + \\ & 300.0 \cdot x \cdot (0.36 - 1.0 \cdot x^2)^{1/2} \cdot (9.0 - 25.0 \cdot x^2)^{7/2} - 354294.0)) / ((25.0 \cdot x^2 - 9.0)^3 \cdot (125.0 \cdot x^3 + \\ & 225.0 \cdot x^2 + 150.0 \cdot x + 387.0)) + (8.143008158 \cdot x \cdot (5.0 \cdot x - 3.0) \cdot (5.0 \cdot x + 3.0)^2) / (125.0 \cdot x^3 + \\ & 225.0 \cdot x^2 + 150.0 \cdot x + 387.0) + 7.328707342)) / (0.0082944 \cdot (0.36 - 1.0 \cdot x^2)^{1/2} + 0.000248832). \end{aligned}$$

Here,  $x = l_{\text{aux}} \cdot \cos(\gamma)$ .

## Bibliography

- [1] G. Allaire and T. Yamada. Optimization of dispersive coefficients in the homogenization of the wave equation in periodic structures. *Numer. Math.*, 140(2):265–326, 2018.
- [2] Martin S. Alnæs, Jan Blechta, Johan Hake, August Johansson, Benjamin Kehlet, Anders Logg, Chris Richardson, Johannes Ring, Marie E. Rognes, and Garth N. Wells. The fenics project version 1.5. *Archive of Numerical Software*, 3(100), 2015.
- [3] Hans Wilhelm Alt. *Lineare Funktionalanalysis*. Springer Berlin Heidelberg, 2012.
- [4] A. Bensoussan, J.-L. Lions, and G. Papanicolaou. *Asymptotic analysis for periodic structures*. AMS Chelsea Publishing, Providence, RI, 2011. Corrected reprint of the 1978 original [MR0503330].
- [5] Dimitri P. Bertsekas. *Nonlinear programming*. Athena Scientific Optimization and Computation Series. Athena Scientific, Belmont, MA, second edition, 1999.
- [6] Dominique Blanchard and Georges Griso. Decomposition of the deformations of a thin shell. asymptotic behavior of the green-st venant’s strain tensor. *Journal of Elasticity*, 101(2):179–205, 2010.
- [7] Kai-Uwe Bletzinger, Manfred Bischoff, and Ekkehard Ramm. A unified approach for shear-locking-free triangular and rectangular shell finite elements. *Computers & Structures*, 75(3):321–334, 2000.
- [8] Rolf Busam and Eberhard Freitag. *Funktionentheorie 1*. Springer-Verlag Berlin Heidelberg, 2006.
- [9] D. Caillerie. Thin elastic and periodic plates. *Math. Methods Appl. Sci.*, 6(2):159–191, 1984.
- [10] CR Calladine. Thin-walled elastic shells analysed by a rayleigh method. *International Journal of Solids and Structures*, 13(6):515–530, 1977.
- [11] P. G. Ciarlet and B. Miara. On the ellipticity of linear shell models. *Z. Angew. Math. Phys.*, 43(2):243–253, 1992.
- [12] Philippe G. Ciarlet. *Mathematical elasticity. Vol. I*, volume 20 of *Studies in Mathematics and its Applications*. North-Holland Publishing Co., Amsterdam, 1988. Three-dimensional elasticity.
- [13] Philippe G. Ciarlet. *Mathematical elasticity. Vol. II*, volume 27 of *Studies in Mathematics and its Applications*. North-Holland Publishing Co., Amsterdam, 1997. Theory of plates.
- [14] Philippe G. Ciarlet. *Mathematical elasticity. Vol. III*, volume 29 of *Studies in Mathematics and its Applications*. North-Holland Publishing Co., Amsterdam, 2000. Theory of shells.



- [15] Doina Cioranescu, Alain Damlamian, and Georges Griso. The periodic unfolding method in homogenization. *SIAM Journal on Mathematical Analysis*, 40(4):1585–1620, 2008.
- [16] Doina Cioranescu, Alain Damlamian, and Georges Griso. *The Periodic Unfolding Method: Theory and Applications to Partial Differential Problems*, volume 3. Springer, 2018.
- [17] Doina Cioranescu and Patrizia Donato. *An introduction to homogenization*, volume 17 of *Oxford Lecture Series in Mathematics and its Applications*. The Clarendon Press, Oxford University Press, New York, 1999.
- [18] E. De Giorgi and S. Spagnolo. Sulla convergenza degli integrali dell’energia per operatori ellittici del secondo ordine. *Boll. Un. Mat. Ital. (4)*, 8:391–411, 1973.
- [19] Wolfram Decker, Gert-Martin Greuel, Gerhard Pfister, and Hans Schönemann. SINGULAR 4-1-2 — A computer algebra system for polynomial computations. <http://www.singular.uni-kl.de>, 2019.
- [20] Lloyd Hamilton Donnell. Stability of thin-walled tubes under torsion. *NACA Tech. Rept. No. 479.*, 1933.
- [21] G. Evans, J. Blackledge, and P. Yardley. *Analytic methods for partial differential equations*. Springer Undergraduate Mathematics Series. Springer-Verlag London, Ltd., London, 2000.
- [22] KE Evans and KL Alderson. Auxetic materials: the positive side of being negative. *Engineering Science & Education Journal*, 9(4):148–154, 2000.
- [23] Gero Friesecke, Richard D. James, and Stefan Müller. A hierarchy of plate models derived from nonlinear elasticity by gamma-convergence. *Arch. Ration. Mech. Anal.*, 180(2):183–236, 2006.
- [24] Christophe Geuzaine and Jean-François Remacle. Gmsh: A 3-d finite element mesh generator with built-in pre-and post-processing facilities. *International journal for numerical methods in engineering*, 79(11):1309–1331, 2009.
- [25] Marius Ghergu, Georges Griso, Houari Mechkour, and Bernadette Miara. Homogenization of thin piezoelectric perforated shells. *ESAIM: Mathematical Modelling and Numerical Analysis*, 41(5):875–895, 2007.
- [26] Gert-Martin Greuel and Gerhard Pfister. *A Singular introduction to commutative algebra*. Springer Science & Business Media, 2012.
- [27] Georges Griso. Decompositions of displacements of thin structures. *Journal de mathématiques pures et appliquées*, 89(2):199–223, 2008.
- [28] Georges Griso, Michael Hauck, and Julia Orlik. Asymptotic Analysis for Periodic Perforated Shells. working paper or preprint, July 2019.
- [29] Georges Griso and Bernadette Miara. Homogenization of periodically heterogeneous thin beams. *Chinese Annals of Mathematics, Series B*, 39:397–426, 2018.
- [30] Georges Griso, Anastasia Migunova, and Julia Orlik. Homogenization via unfolding in periodic layer with contact. *Asymptot. Anal.*, 99(1-2):23–52, 2016.

- [31] Michael Hauck, Axel Klar, and Julia Orlik. Design optimization in periodic structural plates under the constraint of anisotropy. *ZAMM-Journal of Applied Mathematics and Mechanics/Zeitschrift für Angewandte Mathematik und Mechanik*, 97(10):1220–1235, 2017.
- [32] Fish Jacob and Belytschko Ted. *A first course in finite elements*. Wiley, 2007.
- [33] IA Jones. Approximate solutions to the orthotropic pinched cylinder problem. *Composite structures*, 42(1):73–91, 1998.
- [34] WT Koiter. On the mathematical foundation of shell theory. In *Proc. Int. Congr. of Mathematics, Nice*, volume 3, pages 123–130, 1970.
- [35] Prem K. Kythe. *Fundamental Solutions for Differential Operators and Applications*. Birkhäuser, 1996.
- [36] H. Le Dret and A. Raoult. The membrane shell model in nonlinear elasticity: a variational asymptotic derivation. *J. Nonlinear Sci.*, 6(1):59–84, 1996.
- [37] SG Lekhnitskii, SW Tsai, and T Cheron. *Anisotropic plates, 1968*. Gordon and Breach Science Publishers.
- [38] Viktor Levandovskyy. *Non-commutative computer algebra for polynomial algebras: Gröbner bases, applications and implementation*. University of Kaiserslautern, 2005. PhD-Thesis.
- [39] Gui-Rong Liu and Siu Sin Quek. *The finite element method: a practical course*. Butterworth-Heinemann, 2013.
- [40] Matej Mencinger. On groebner bases and their use in solving some practical problems. *Universal Journal of Computational Mathematics*, 1(1):5–14, 2013.
- [41] Ismail Merabet and Serge Nicaise. A penalty method for a linear koiter shell model. *ESAIM: Mathematical Modelling and Numerical Analysis*, 51(5):1783–1803, 2017.
- [42] Bernadette Miara and Vanda Valente. Exact controllability of a Koiter shell by a boundary action. *J. Elasticity*, 52(3):267–287, 1998/99.
- [43] N. I. Muskhelishvili. *Some basic problems of the mathematical theory of elasticity*. Noordhoff International Publishing, Leiden, english edition, 1977. Fundamental equations, plane theory of elasticity, torsion and bending, Translated from the fourth, corrected and augmented Russian edition by J. R. M. Radok.
- [44] PM Naghdi. On the theory of thin elastic shells. *Quarterly of Applied Mathematics*, 14(4):369–380, 1957.
- [45] Stefan Neukamm. *Homogenization, linearization and dimension reduction in elasticity with variational methods*. PhD thesis, Technische Universität München, 2010.
- [46] M. Neuss-Radu. *Mathematical modelling and multiscale analysis of transport processes through membranes [Habilitation thesis]*. University of Heidelberg, 2017.
- [47] Gabriel Nguetseng. A general convergence result for a functional related to the theory of homogenization. *SIAM J. Math. Anal.*, 20(3):608–623, 1989.
- [48] O. A. Oleinik, A. S. Shamaev, and G. A. Yosifian. *Mathematical problems in elasticity and homogenization*, volume 26 of *Studies in Mathematics and its Applications*. North-Holland Publishing Co., Amsterdam, 1992.

- [49] Julia Orlik, Grigory Panasenko, and Vladimir Shiryayev. Optimization of textile-like materials via homogenization and beam approximations. *Multiscale Modeling & Simulation*, 14(2):637–667, 2016.
- [50] G. Panasenko. *Multi-scale Modelling for Structures and Composites*. Springer, 2005.
- [51] Gerhard Pfister. On modular computation of standard basis. *Analele Stiintifice ale Universitatii Ovidius, Mathematical Series XV (1)*, pages 129–137, 2007.
- [52] Jyrki Piila and Juhani Pitkäranta. Energy estimates relating different linear elastic models of a thin cylindrical shell. I. The membrane-dominated case. *SIAM J. Math. Anal.*, 24(1):1–22, 1993.
- [53] Jyrki Piila and Juhani Pitkäranta. Energy estimates relating different linear elastic models of a thin cylindrical shell. II. The case of free boundary. *SIAM J. Math. Anal.*, 26(4):820–849, 1995.
- [54] Enrique Sánchez-Palencia. *Nonhomogeneous media and vibration theory*, volume 127 of *Lecture Notes in Physics*. Springer-Verlag, Berlin-New York, 1980.
- [55] Gurii Nikolaevich Savin. *Stress distribution around holes*. National Aeronautics and Space Administration, 1970.
- [56] J Schwaighofer and HF Microys. Orthotropic cylindrical shells under line load. *Journal of applied Mechanics*, 46(2):356–362, 1979.
- [57] J Schwerdtfeger, F Wein, G Leugering, RF Singer, C Körner, M Stingl, and F Schury. Design of auxetic structures via mathematical optimization. *Advanced materials*, 23(22-23):2650–2654, 2011.
- [58] Vladimir Shiryayev. *Modeling and design optimization of textile-like materials via homogenization and one-dimensional models of elasticity*. Technische Universität Kaiserslautern, 2015.
- [59] Stephen P Timoshenko and Sergius Woinowsky-Krieger. *Theory of plates and shells*. McGraw-hill, 1959.
- [60] Luis Trabucho and JM Viano. Mathematical modelling of rods. *Handbook of numerical analysis*, 4:487–974, 1996.
- [61] Eduard Ventsel and Theodor Krauthammer. *Thin plates and shells: theory: analysis, and applications*. CRC press, 2001.
- [62] Shao Wen Yuan. Thin cylindrical shells subjected to concentrated loads. *Quarterly of Applied Mathematics*, 4(1):13–26, 1946.

# Curriculum Vitae

## Deutsch:

1997 - 2001	Grundschule, Weselberg
2001 - 2010	Abitur, Sickingen-Gymnasium, Landstuhl
2010 - 2014	Bachelor of Science, Mathematik, Technische Universität Kaiserslautern (TUK)
08.2012 - 12.2012	Auslandssemester, Lunds Tekniska Högskola (LTH), Schweden
11.2013 -	Hilfswissenschaftler am Fraunhofer-Institut für Techno- und Wirtschaftsmathematik ITWM
2014 - 2016	Master of Science, Mathematics International, Technische Universität Kaiserslautern (TUK)
02.2015 - 07.2015	Auslandssemester, Technische Universiteit Eindhoven (TU/e), Niederlande
2016 - 2019	Doktorand am Fraunhofer-Institut für Techno- und Wirtschaftsmathematik ITWM

## English:

1997 - 2001	Elementary school, Weselberg
2001 - 2010	High-school, Sickingen-Gymnasium, Landstuhl
2010 - 2014	Bachelor of Science, Mathematics Technische Universität Kaiserslautern (TUK)
08.2012 - 12.2012	Semester abroad, Lunds Tekniska Högskola (LTH), Sweden
11.2013 -	Research assistant at Fraunhofer-Institut für Techno- und Wirtschaftsmathematik ITWM
2014-2016	Master of Science, Mathematics International, Technische Universität Kaiserslautern (TUK)
02.2015 - 07.2015	Semester abroad, Technische Universiteit Eindhoven (TU/e), Netherlands
2016 - 2019	PhD student at Fraunhofer-Institut für Techno- und Wirtschaftsmathematik ITWM

The core of this thesis lies in the task of structural optimization of periodic perforated cylindrical shells under a given point load. The problem is divided into three subcategories: Asymptotic analysis, macroscopic model and optimization. In this work we show a qualitative derivation, together with an algorithm for calculating the effective properties. We start with a decomposition of the applied displacements. Using the Unfolding-Rescaling operator we can decouple the two small parameters. The homogenization on beam-like structures is executed numerically and symbolically. The effective properties depend solely on the periodicity cell. We calculate the analytical solution of the limit equation. The solution is determined via a Fourier transformation and series. Moreover, this function depends on the effective properties. It is possible to represent the displacements w.r.t. certain design variables. This allows performing optimization with simple methods. We use a steepest descent method to minimize the resulting displacement. This yields the optimal configuration w.r.t. our admissible design space. Applied industrial problems can thus be effectively solved.

ISBN 978-3-8396-1569-0



FRAUNHOFER VERLAG